THE EQUIVALENT SOURCE METHOD FOR ELECTROMAGNETIC SCATTERING ANALYSIS AND ITS GEOPHYSICAL APPLICATION

A. P. ANNAN

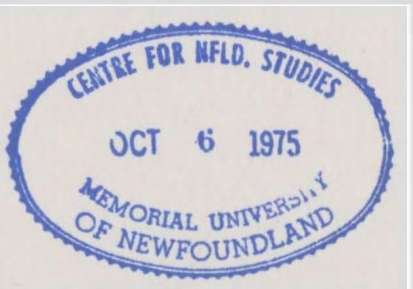
CENTRE FOR NFLD. STUDIES
OCT 6 1975
MEMORIAL UNIVERSITY
OF NEWFOUNDLAND

THE EQUIVALENT SOURCE METHOD
FOR
ELECTROMAGNETIC SCATTERING ANALYSIS
AND
ITS GEOPHYSICAL APPLICATION

by


A. P. ANNAN

Submitted in partial fulfilment of

the requirements for the Doctor of Philosophy degree,

Memorial University of Newfoundland.

January 31, 1974

This thesis has been examined and approved by:

INTERNAL MEMBERS:

M. G. Rochester

M. G. Rochester
Professor of Physics

P D P Smith

P. D. P. Smith
Associate Professor of Physics

EXTERNAL MEMBER:

Theodore A. Madden

T. Madden
Professor of Geophysics
Massachusetts Institute of Technology
Cambridge, Mass., U.S.A.

3 May 1974

DATE

ABSTRACT

The electromagnetic response of magnetically and electrically inhomogeneous media whose geometries are not amenable to conventional partial differential equation analysis are most readily analysed in an integral equation framework. The equivalent source concept of Green's theory affords a generalized manner of formulating static and time-varying electromagnetic problems; material property inhomogeneities are replaced by equivalent source distributions which satisfy a Fredholm integral equation of the second kind.

For static field problems, the equivalent source method represents conductivity, permittivity and permeability variations in terms of current source, charge and "magnetic pole" density distributions. In this form, the problems have analogous mathematical forms and the equivalent source satisfies a scalar Fredholm equation. The formalism is readily related to the static field methods used in applied geophysics.

The time-varying equivalent source formulation represents material property variations in terms of electric and magnetic current densities which satisfy a pair of coupled vector Fredholm equations. Analysis of the integral operators shows that the scattering operator is bimodal for many geophysical problems. This result leads to the analysis of scattering problems in terms of generalized eigenfunctions. The bimodal nature of the scattering operator often leads to highly ill-conditioned matrices when numerical methods are applied to geophysical problems.

Approximate parametric solution methods of solving the time-varying electric scattering problem are considered. Approximation of the solution by a general functional form and applying minimum criteria reduce the integral equations to matrix equations. The least squares method is applied analysing magnetotelluric responses of 2-dimensional structures and the Galerkin formalism is used to find the eigenfunctions for a thin plate in a whole space. The results are compared with other available numerical and experimental results and assessments of the methods are given.

ACKNOWLEDGEMENTS

During the course of this thesis project, which has been conducted at three different institutions since its inception, I have received the advice and assistance of numerous people. First, I wish to thank Dr. J.A. Wright who has managed to supervise me during this project even over distances of thousands of miles and still remain a source of constant encouragement. I also wish to thank Dr. R.D. Murphy whose help in untangling computational difficulties at the start of this project was invaluable.

The support and encouragement of Dr. D.W. Strangway during the later stages of this project while I have been employed on the Surface Electrical Properties experiment project is greatly appreciated. During the period at the University of Toronto, discussions of electromagnetic problems and computational analysis with Drs. G.F. West, J. LaJoie, Y. Lamontagne and R.D. Watts have been valuable in giving alternate viewpoints of some very complex problems.

I particularly wish to thank my wife Judi for her support through various stages of this work such as the all night computing binges, the seven day work weeks, and all the other trials and tribulations of being married to a graduate student. Her understanding and encouragement were what made the work bearable.

I wish to thank Mrs. J. Kean for her assistance in typing the early drafts of this manuscript and Miss V. Melnyk who typed the final version of the manuscript. I also wish to acknowledge the financial support received from the National Research Council of Canada during part of this work.

TABLE OF CONTENTS

LIST OF TABLES

LIST OF FIGURES

TABLE OF BASIC SYMBOLS

$\overline{E}$ - electric field intensity

$\overline{D}$ - electric displacement field

$\overline{B}$ - magnetic flux density

$\overline{H}$ - magnetic field intensity

$\overline{J}$ - electric current

$\overline{J}_s$ - impressed or source electric current

j - $\sqrt{-1}$

ω - angular frequency

$\hat{n}$ - unit normal to a surface

$\wedge$ - unit vector

$*$ - complex conjugate

T - transpose

$\dagger$ - adjoint

V - volume of integration

S - surface of V

A - area of integration

C - contour of integration

With the above exceptions all symbols are defined in the text. Any ambiguities should easily be resolved from the context. The rationalized MKS system of units is used throughout the text.

CHAPTER 1

1-1 Introduction

The solution of electromagnetic scattering problems has become a subject of increasing interest in the fields of applied physics and engineering with the advent of sophisticated computers in the past two decades. Previously, the solutions of electromagnetic scattering problems were limited to those which could be solved analytically. In recent years, many numerical solutions of various electromagnetic problems have been published. These problems have been solved primarily from two viewpoints; one is that of the electrical engineer concerned with radio-wave transmission and antenna design; the other is that of the geophysicist concerned with studying the electromagnetic response of the Earth or the Moon or a portion thereof in order to determine its electrical properties. While the basic equations to be solved are quite similar, the two viewpoints and the derived results are very distinct.

In the electrical engineering field, the primary concern is the response of highly conductive bodies in free-space. These bodies are assumed to be sufficiently conductive that they can be treated as perfect conductors. In some instances, the behaviour of insulating bodies is of interest. In both cases the scattering body has dimensions of the order of the free-space wavelength. If the scattering body is to be used as an antenna, the directionality of its radiation pattern is of prime interest. If a body is internally stimulated electrically, in what manner does it radiate electromagnetic waves? In reverse, if the body is excited by an externally generated field how effective is it in transmitting this stimulus to a sensor attached to the body? In this situation the body is an active element of a radio wave transmission system. If the scattering body is viewed as a disturbing object in a radio transmission system, then

the absorption and re-radiation of energy by the body and minimization of its effect on the transmission system is the primary concern. In one instance the body is an active element of the system and in the other it is a passive disturbance to the system.

From the geophysical viewpoint the scattering body is a passive but unknown element in a system. In some instances, the body is stimulated with a known input and its response is measured. In other cases, the system input is unknown but the total of the input and the system response is measured. The objective is to establish the electric and magnetic properties of the body from observation of its electromagnetic response. If the electromagnetic response of a structure can be computed theoretically, its response can be used as a basis for interpretation of an experimental response; this step is known as the inverse problem. In general, the real system is far more complex than the system whose response can be computed theoretically. As a result, one can only make inferences about the gross structure of the real system. The inverse problem is by no means a trivial one and its complexity is really appreciated only after attempting to interpret real system responses. Additional features of the geophysical scattering problem are that measurements are made over spatial scales much smaller than the free-space wavelength and the scattering bodies are conductors with finite conductivity and are usually embedded in a conductive medium. These features make the geophysical problem quite different from the electrical engineering problem.

1-2 Thesis Objective and Outline

This thesis project was primarily concerned with the geophysical aspect of electromagnetic scattering. Within this context, the thesis project had two basic objectives. The first was the development of a unified mathematical framework from which a wide variety of complex electric, magnetic and electromagnetic problems could be analyzed; the second objective was the development and testing of approximate numerical methods for solving these problems in an economical manner.

The thesis is split into two units; one associated with each of the two objectives. In chapter two, the equivalent source method is developed for static and time-varying electromagnetic problems and chapters three and four are devoted to discussion of particular results which can be derived from the formulation developed in chapter two. Chapters five, six, and seven are devoted to the approximate solution of some time-varying electromagnetic problems using variational methods. The numerical results are compared with experimental data and other numerical solutions which were available. The numerical results are also used to demonstrate some of the theoretical developments given in chapter four. The contents of chapter two through seven are summarized in chapter eight.

Before delving into the detailed mathematical formalism of the equivalent source method, a brief review of the geophysical appliation of static electric and magnetic fields and time-varying electromagnetic fields will be given. In addition, a short summary of the development of solutions to geophysical scattering problems helps provide an insight into the type of time-varying electromagnetic problem encountered in geophysical analysis.

1-3 Background

(i) Applied Geophysics

The analysis of electric and magnetic fields generated by or associated with electric and magnetic properties of the Earth's crust is a subject of great interest to the applied geophysicist. The applications break into three basic categories; one based on the time-varying electromagnetic response of the Earth; one based on the Earth's response to static conduction currents; and one based on the Earth's static magnetic field and its disturbance by the presence of local magnetic inhomogeneities. The three types are schematically illustrated in Fig. 1-1.

Geophysical survey techniques are, by and large, designed to detect lateral variations in the electric and magnetic properties of the upper kilometer or so of the Earth's crust. These variations are associated with changes in geological material and structures, and in some instances, indicate the presence of mineral deposits which have economic importance. A survey system consists of an electromagnetic field source and field detection device, or, in some instances, a field detection unit only. This system is then transported across a region of geological interest with measurements being made at discrete spatial intervals or continuously. If the system properties are not varied during this traverse, the fluctuation in the system response can be used to infer lateral variations in the Earth's properties which influence the system response.

The time-varying electromagnetic systems are units which respond primarily to the electrical conductivity and dielectric properties and, to a lesser extent, to the magnetic properties (since magnetic property effects are quite small relative to electrical effects) of the Earth. In most environments, the Earth's conductive response swamps the dielectric behaviour since the time variations must be in the audio or subaudio frequency range in order to overcome skindepth effects. In almost all

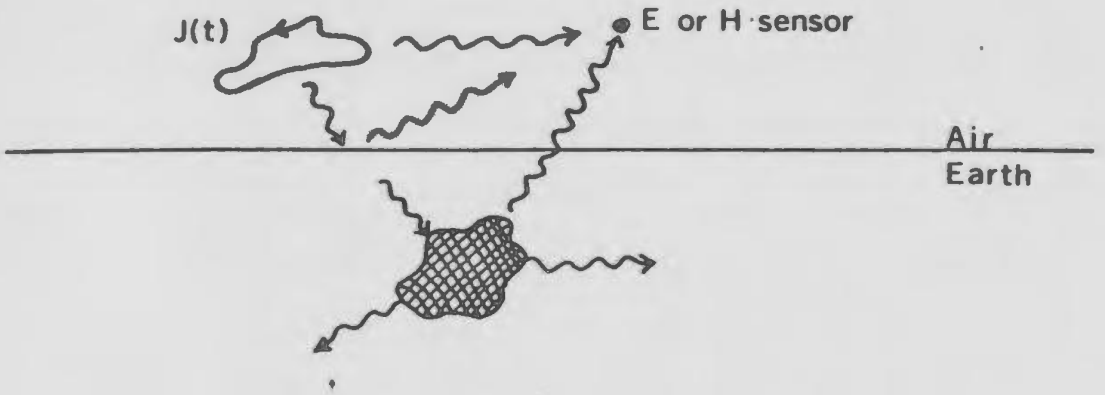

(a) Time-varying electromagnetic system

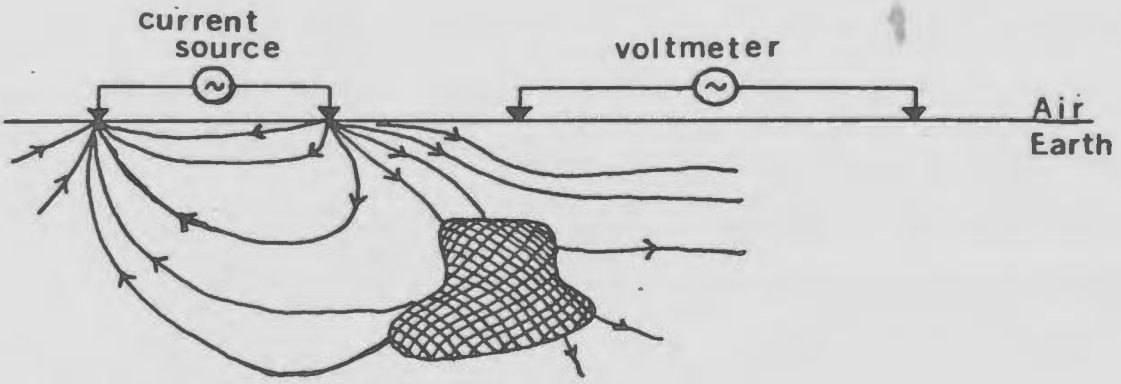

(b) Static conduction system

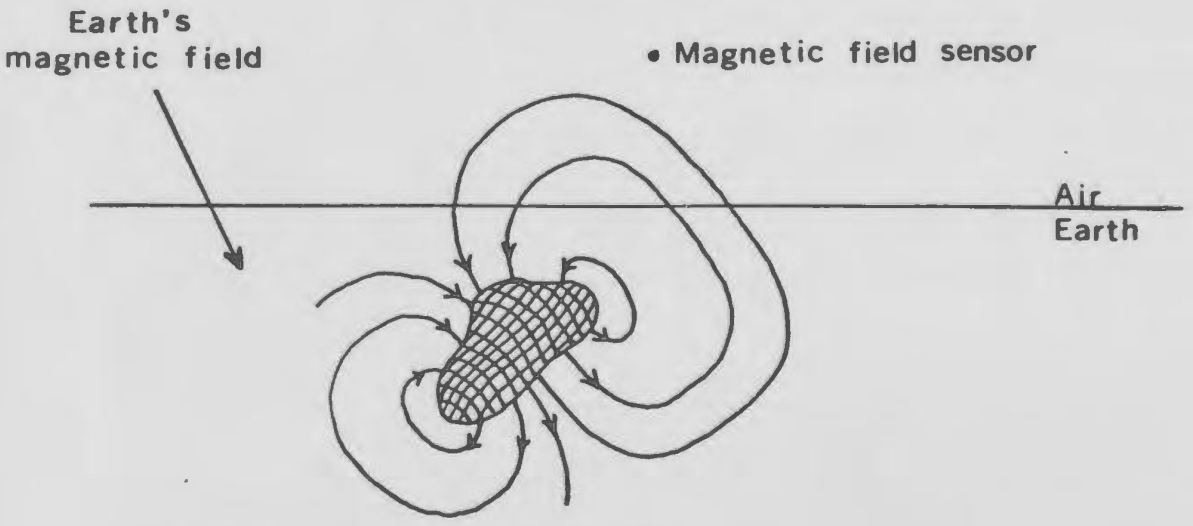

(c) Static magnetic system

FIG 1-1

applications, therefore, an electromagnetic system is used to detect variations in electrical conductivity.

The static conduction system uses a source of direct current which is connected to the Earth at two or more points, and measures the electric field generated at the Earth's surface as shown in Fig. 1-1 (b). The variation of electrical conductivity in the vicinity of the probes influences the surface electric field. These methods are known as resistivity surveys and are used to map lateral variations in the near surface conductivity.

Magnetic surveys measure the magnetic field at or above the Earth's surface. The magnetic field is composed of the ambient Earth's magnetic field plus disturbances due to remnant or intrinsic magnetization carried by the near surface material or by changes in the material permeability. Permeability changes cause distortion of the primary field. Lateral variations in the static magnetic field reflect the magnetic properties of the underlying structure.

In some instances, the material properties versus depth are of more interest than their lateral variation. This is particularly true for some electromagnetic and resistivity survey methods. In these applications, the properties of the survey system are varied, and the Earth's response as a function of a system parameter is measured. In a time-varying electromagnetic system, the excitation frequency might be varied while in a resistivity survey, the electrode separations might be changed.

In order to interpret this data, the response of models of the geological structure are computed and compared with the real data either manually or automatically by computer. The ability to solve the forward problem for the theoretical response is therefore essential for solution of the inverse problem.

(ii) Solution of Electromagnetic Problems

The solution of time-varying electromagnetic problems in geophysics has been studied by numerous researchers. The inherent property of electromagnetic scattering problems is that they invariably require numerical analysis at some stage in order to obtain useful results. Scattering problems fall into two categories; those for which analytic solutions can be derived and those which must be solved numerically.

Scattering problems which have analytic solutions are structures which have very simple geometrical shapes such as those with spherical, cylindrical or planar symmetry or in some instances simple material properties such as perfect conductivity. While closed forms for the solutions can be derived, the solutions are invariably given in terms of a sum or integral over the eigenfunctions of the system which is not usually expressible in terms of elementary functions. As an example, the response of two adjoining halfspaces for excitation by a point dipole source of arbitrary type (electric or magnetic dipole) can be expressed in terms of a Fourier integral which cannot be evaluated analytically.

All other scattering problems have the property that either the geometry or material property behaviour is not compatible with formulating and solving the problems using conventional methods of partial differential equation analysis. The major problem in geophysical studies is the geometrical problem. For all but the simplest of geometries, the equations governing the response cannot be reduced by separation of the variables. The eigenfunctions of the system are functions of more than one geometrical variable and are unknown. The only practical way out is a numerical solution of the governing equation.

Before the advent of advanced computers, solution of geophysical problems was primarily confined to obtaining the response of spherical layered or plane layered structures with each layer having homogeneous

electrical properties, or slight variations of these basic models. The spherical model was used to simulate the entire Earth while the plane layered model was used to simulate small scale features where curvature of the Earth is negligible. Once a closed form solution was derived, the emphasis was on finding approximate forms of the solution for special cases of the general model which were useful for calculating the response. No attempt is made to summarize all the results in these topics since excellent discussions of these subjects are given by Wait (1962, 1970) and Ward (1967).

When computers became available for number crunching, the result was a two-fold change in emphasis. First the computer permitted numerical evaluation of integrals, sums and special functions required by the analytical solutions. Secondly, the analytic stage of analysis can be totally circumvented by numerically solving the governing equation from the beginning. This second result is particularly important since it meant solutions to problems intractable by analytic methods could be obtained.

The geophysical problems solved in this manner can be summarized as 2 and 2½-dimensional models. The basis of this classification is depicted in Fig. 1-2 where the cross section of inhomogeneity embedded in a whole space is shown in Fig. 1-2 (a). If this cross section is extended into the third dimension in a particular fashion, the electromagnetic response of the system is considerably simplified. A true 2-dimensional model is one where the structure does not vary in the third dimension as in Fig. 1-2 (b). The body extends to infinity in both directions and no property varies as a function of the third dimension. Other extensions into the third dimension are shown in Fig. 1-2 (c) and (d). In (c), the cross section (a) is revolved about an axis of symmetry producing a cylindrically symmetric structure. In (d), the structure does not extend into the third dimension and is an infinitesimally thin sheet or plate model. These latter two models are

(a) Possible structure cross-section

(b) Plan view at "true" 2D model

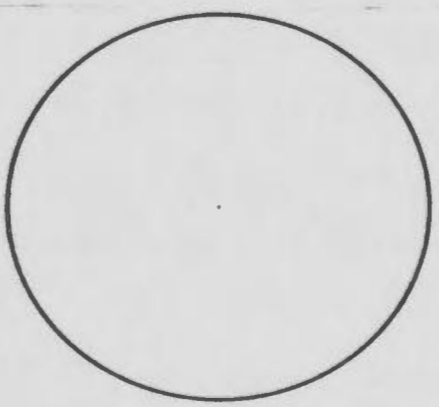

(c) Plan view of a round model ($2\frac{1}{2}$D)

(d) Plan view of a plate model ($2\frac{1}{2}$ D)

Fig. 1-2

termed 2½-dimensional problems in that the structures are 3-dimensional but the response can be formulated as a function of two dimensions by taking advantage of the special geometry of the bodies.

The numerical computation of the response of such models has been carried out by several people over the past six years. The response of two dimensional structures has been given by Swift (1967, 1971), Wright (1969) and Jones and Price (1969), using a finite difference (or equivalent type of discretization) method to solve the governing partial differential equation. All these analyses were primarily concerned with determination of the magnetotelluric response of lateral variations in conductivity in a half-space at very low frequencies with excitation by a plane wave vertically incident on the surface of the half-space from a free-space medium. Following initial solution of the governing differential equation numerically, the 2-dimensional problems were reformulated as integral equations (or differential-integral equations). Solutions to the 2-dimensional problem using integral equation formulation are given by Parry and Ward (1971) and Hohmann (1971). The response of circular and rectangular plates which require an integral equation formulation are given by Greenfield (1971) and Lamontagne (1971). The magnetotelluric response of round structures in a conductive half-space is given by Watts (1972) who worked the problem by discretization of the governing partial differential equation.

In all instances the approach to solving the problems was that of reducing the governing equation to a finite set of linear equations by sampling the fields at a finite set of points. The field between the samples was implicitly assumed or explicitly stated and the discretized governing equation was forced to hold at the sample points. In the preceding works, the number of linear equations, N, ranged from several tens to around one thousand and required direct or indirect inversion of matrices of dimension N x N. The solution of linear equations of large dimension is the most

difficult and expensive step in the analysis. Since geophysical applications require the response for many parameter combinations, it is desirable that the number of equations, N, be as small as possible. This problem is the main drawback in the analysis of full three dimensional problems, since the solution to a vector equation results in $N = 3\ M^3$ equations where M is the average number of points sampled in each of the three spatial dimensions.

CHAPTER 2

The Equivalent Source Method for Electromagnetic Problems

2-1 Green's Function Theory and the Equivalent Source Concept

The theory of Green's functions and the equivalent source concept are the fundamental building blocks in the following analysis. This section is directed to a brief summary of Green's function theory and the equivalent source method. For a more detailed discussion of the subject, the reader is referred to Morse and Feshbach (1953).

A Green's function summarizes all the information about a given system into a single function which can then be used to describe the response of the system to an arbitrary input. In physical problems, the behaviour of a system is usually characterized most easily in the form of a differential equation. For a given input $\mathcal{F}$, a system which is characterized by the differential operator $\mathcal{D}$, yields the differential equation

$$\mathcal{D}(u) = \mathcal{F} \qquad 2\text{-}1$$

where u is the system output. Additional constraints are imposed on u when a region of existence V is defined such that u satisfies 2-1 within V and is subject to constraints (boundary conditions) at the surface S of V .

The solution of 2-1 is expressed in terms of the system Green's function by

$$u(P) = \int_V \mathcal{G}(P,Q)\, \mathcal{O}(Q)\, dQ \qquad 2\text{-}2$$

where

$$\mathcal{O}(Q) = \mathcal{F}(Q) + \mathcal{T}(s)\,\delta(S,Q) + \mathcal{U}(s)\,\delta'(S,Q)$$

In 2-2 , P and Q represent the coordinates of the observation point and source point, S denotes a point on the surface S of V , G(P,Q) is the homogeneous Green's function

and $\mathcal{J}(S)\ \delta(S,Q)$ and $\mathcal{M}(S)\ \delta'(S,Q)$ are equivalent surface sources which arise when the boundary conditions on S are inhomogeneous. $\delta(S, Q)$ and $\delta'(S, Q)$ are the Dirac delta function and its derivative. The appropriate dimensions and one or more derivatives w.r.t. one or more dimensions are implied in the notation.

The Green's function satisfies the equation

$$\mathcal{D}_p(\mathcal{G}(P,Q)) = \delta(P,Q) \qquad 2\text{-}3$$

where $\mathcal{D}_p$ implies differentiation w.r.t. the P coordinates and $\mathcal{G}(P, Q)$ is subject to homogeneous boundary conditions on S.

In many physical problems, one is faced with the need to solve an equation similar in form to 2-1 with the added constraint that

$$\mathcal{D}(\mathcal{U}(P)) = \mathcal{F}(P) \qquad P \in V \qquad P \notin V' \qquad 2\text{-}4$$

$$\mathcal{D}(\mathcal{U}(P)) + \mathcal{Q}(\mathcal{U}(P)) = \mathcal{F}(P) \qquad P \in V, V' \qquad 2\text{-}5$$

where V' is a subregion of V. It is possible (on the assumption of linear operators) to re-express the effect of the operator $\mathcal{Q}$ in terms of an equivalent source distribution in the original system V. This reformatting of the problem is called the equivalent source method.

First, the system response $\mathcal{U}$ is split into two parts

$$\mathcal{U} = \mathcal{U}_0 + \mathcal{U}_1 \qquad 2\text{-}6$$

where $\mathcal{U}_0$ is the solution of 2-4 and 2-5 when $\mathcal{Q}$ is a null operator ($\mathcal{Q} = 0$). Thus

$$\mathcal{D}(\mathcal{U}_0(P)) = \mathcal{F}(P) \qquad 2\text{-}7$$

If $\mathcal{Q}$ is not a null operator, 2-5 becomes

$$\mathcal{D}(\mathcal{U}_1(P)) = -\mathcal{Q}(\mathcal{U}_0 + \mathcal{U}_1) \qquad 2\text{-}8$$

The equivalent source $\mathcal{E}$ is defined as

$$\mathcal{E} = -\mathcal{Q}(\mathcal{U}_0 + \mathcal{U}_1) \qquad 2\text{-}9$$

and u_0 and u_1 can be expressed using 2-2 as

$$u_0(P) = \int_V \mathcal{G}(P,Q)\,\Theta(Q)\,dQ \qquad 2\text{-}10$$

$$u_1(P) = \int_V \mathcal{G}(P,Q)\,\mathcal{E}(Q)\,dQ \qquad 2\text{-}11$$

Upon combining 2-9 and 2-11 , $\mathcal{E}$ satisfies the integral equation

$$\mathcal{E}(P) = -\mathcal{L}(u_0(P)) - \mathcal{L}\int_{V'} \mathcal{G}(P,Q)\,\mathcal{E}(Q)\,dQ \qquad 2\text{-}12$$

in V' and $\mathcal{E}(P) = 0$ at all points where $\mathcal{L} = 0$ (i.e. $P \notin V'$).

In summary, the equivalent source method yields the following results.

(1) The effect of a perturbation (large or small) on a system can be expressed in the form of an equivalent source in the undisturbed system if the undisturbed system Green's function is known.

(2) The effect of the disturbance at any point P in V is determined solely by the convolution of the undisturbed system Green's function with the equivalent source distribution which exists only in the region V' where the anamalous disturbance occurs.

(3) The equivalent source satisfies a Fredholm integral equation of the second kind within V' and is zero outside this region.

The equivalent source method and integral equation approach become important techniques when the problem at hand has to be solved numerically. The solution for $\mathcal{E}$ in region V' has to be found rather than the solution for u_1 in region V which is usually much larger. In addition, boundary conditions on $\mathcal{E}$ and u_1 are already contained in the integral equation.

2-2 Basic Equations of Electromagnetic Theory

The solution of an electromagnetic problem in a continuum requires obtaining a solution to Maxwell's equations combined with the appropriate set of constitutive equations which describe the electromagnetic properties of the medium. In this section the basic equations are summarized, using the rationalized MKS system of units.

Maxwell's equations control the behaviour of the electromagnetic fields. In differential form these equations are

$$\bar{\nabla} \times \bar{E} = -\frac{\partial \bar{B}}{\partial t} \qquad 2\text{-}13 \qquad\qquad \bar{\nabla} \times \bar{H} = \bar{J} + \frac{\partial \bar{D}}{\partial t} \qquad 2\text{-}14$$

$$\bar{\nabla} \cdot \bar{D} = q \qquad 2\text{-}15 \qquad\qquad \bar{\nabla} \cdot \bar{B} = 0 \qquad 2\text{-}16$$

In conjunction with Maxwell's equations, the constitutive equations which specify the relationships of the electromagnetic fields are required in order to fully specify the problem. The constitutive equations fall into 3 classes; dielectric, magnetic and conductive. These three classes are briefly summarized below. More detailed discussions can be found in Jackson (1962), Reitz and Milford (1960) Landau and Lifshitz (1960).

The dielectric constitutive equations are

$$\bar{D} = \epsilon_0 \bar{E} + \bar{P} \qquad 2\text{-}17 \qquad\qquad \bar{P} = \psi_e \bar{E} + \bar{P}_I \qquad 2\text{-}18$$

$$\bar{D} = \epsilon \bar{E} + \bar{P}_I \qquad 2\text{-}19 \qquad\qquad \epsilon = \epsilon_0 (1 + \frac{\psi_e}{\epsilon_0}) = K_e \epsilon_0 \qquad 2\text{-}20$$

where $\bar{P}$ is the electric dipole moment density and ϵ_0 is the free space permittivity. $\bar{P}$ can be split into two parts; one induced by an applied electric field denoted by $\psi_e \bar{E}$, where ψ_e is the electric susceptibility, and the other is an intrinsic dipolar distribution $\bar{P}_I$. Equations 2-17 and 2-18 can be combined into a single equation 2-19 using a general permittivity given by 2-20. The ratio ϵ/ϵ_0 is known as the dielectric constant K_e.

The magnetic constitutive equations are

$$\bar{B} = \mu_o (\bar{H} + \bar{M}) \qquad 2\text{-}21 \qquad\qquad \bar{M} = \chi_m \bar{H} + \bar{M}_I \qquad 2\text{-}22$$

$$\bar{B} = \mu \bar{H} + \mu_o \bar{M}_I \qquad 2\text{-}23 \qquad\qquad \mu = \mu_o(1+\chi_m) = K_m \mu_o \qquad 2\text{-}24$$

and closely follow the dielectric equations. Here $\bar{M}$ is the magnetic dipole moment density and μ_o is the free space permeability. $\bar{M}$ can be split into two parts; one induced by an applied field $\chi_m \bar{H}$, where χ_m is the magnetic susceptibility, and the other an impressed or source magnetization $\bar{M}_I$. In static field geophysical applications, $\bar{M}_I$ is the intrinsic or remanent magnetization of a material; in time-varying applications, $\bar{M}_I$ is used to describe magnetic field sources which in turn give rise to the concept of "magnetic" currents. Combining equations 2-21 and 2-22 yields 2-23 where μ is the generalized permeability given in 2-24. The ratio μ/μ_o is the relative permeability K_m.

The conductive constitutive relationship is simply Ohm's law

$$\bar{J}_c = \sigma \bar{E} \qquad\qquad \bar{J} = \bar{J}_s + \bar{J}_c \qquad 2\text{-}25$$

where σ is the conductivity. Equations 2-17 through 2-25 suffice to describe the electromagnetic properties of any linear, isotropic medium, When the material properties K_e, K_m, σ and the source terms $\bar{P}_I$, $\bar{M}_I$, $\bar{J}_s$, and q are given, an electromagnetic problem is totally specified.

2-3 Equivalent Source Formulation

(i) Time Invariant Problems

For an electromagnetic problem where the fields are stationary in time, the electric and magnetic fields are no longer coupled in Maxwell's equations. Since this particular type of problem is encountered often in applied physics, the application of the equivalent source method to these problems is discussed as a separate topic.

The time invariant problems fall into three groups; dielectric electrostatic problems, magnetostatic problems, and static electric conduction problems. Since these three types of problems are analogous (the same mathematical equations describe the response), the general mathematical problem will be set up. The reduction of the three types of problems to identical form is shown in Table 2-1. The only point to be noted is the separation of $\bar{H}$ in the magnetostatic problem into $\bar{H}_J$, the field generated by static current flow and $\bar{H}_M$ the field due to magnetic property effects. Splitting off $\bar{H}_M$ and examining the equation for $\bar{\nabla} \times \bar{H}_M$ reduces the magnetic problem to the same form as the electric problems; any field due to current flow can be incorporated into the excitation or source term.

Using the equations listed at the bottom of Table 2-1, the equivalent source method is formulated in the following manner. K is an arbitrary function of position. The problem is to find the fields when K is a somewhat complicated function. The first step is to split K into two parts;

$$K = K_b + K_a \qquad 2\text{-}26$$

where K_b is the "homogeneous" or background material property and K_a is an anomalous variation superimposed on the background K_b. The choice of K_b is explained later.

From the equation

$$\bar{\nabla} \times \bar{\mathcal{H}} = 0 \qquad 2\text{-}27$$

TABLE 2-1

Equations for Static Field Problems

Dielectric Electrostatic Equations

$$\bar{\nabla} \times \bar{E} = 0 \qquad \bar{D} = \epsilon \bar{E} + \bar{P}_I$$

$$\bar{\nabla} \cdot \bar{D} = q$$

Magnetostatic Equations

$$\bar{H}_T = \bar{H}_M + \bar{H}_J \qquad \bar{\nabla} \times \bar{H}_J = \bar{J}$$

$$\bar{\nabla} \times \bar{H}_M = 0 \qquad \bar{B} = \mu \bar{H}_T + \mu_0 \bar{M}_I$$

$$\bar{\nabla} \cdot \bar{B} = 0$$

Static Conduction Equations

$$\bar{\nabla} \times \bar{E} = 0 \qquad \bar{J} = \sigma \bar{E} + \bar{J}_s$$

$$\bar{\nabla} \cdot \bar{J} = 0$$

General Form of Static Field Equations

$$\bar{\nabla} \times \bar{\mathcal{F}} = 0 \qquad \bar{F} = K \bar{\mathcal{F}} + \bar{C}$$

$$\bar{\nabla} \cdot \bar{F} = \mathcal{Q}$$

it is possible to express the response of the system in terms of a scalar potential Φ with

$$\mathcal{E} = -\nabla \Phi \qquad 2\text{-}28$$

$\mathcal{E}$ and Φ are now split into "homogeneous" or background and anomalous components

$$\mathcal{E} = \mathcal{E}_o + \mathcal{E}_a \qquad 2\text{-}29 \qquad\qquad \Phi = \Phi_o + \Phi_a \qquad 2\text{-}30$$

$$\mathcal{E}_o = -\nabla \Phi_o \qquad 2\text{-}31 \qquad\qquad \mathcal{E}_a = -\nabla \Phi_a \qquad 2\text{-}32$$

where $\mathcal{E}_a$ and Φ_a vanish when K_a is zero. Setting K_a to zero yields the equation

$$\nabla^2 \Phi_o + \frac{\nabla \Phi_o \cdot \nabla K_b}{K_b} = -\frac{\mathcal{Q} + \nabla \cdot \bar{C}}{K_b} \qquad 2\text{-}33$$

for Φ_o. This is the point where the choice of K_b becomes important. K_b must be chosen such that equation 2-33 can be solved to find Φ_o in analytic form. In general the form of K_b must be one where K_b has a different but constant value within different spatial volumes (i.e. K_b being plane-stratified is an example). In addition, the spatial volumes must be separated by a set of surfaces which permit separation of Laplace's equation and the boundary conditions on $\mathcal{E}$. This choice of K_b reduces equation 2-33 to

$$\nabla^2 \Phi_o = -\frac{\mathcal{Q} + \nabla \cdot \bar{C}}{K_b} \qquad 2\text{-}34$$

in each region. Invoking the boundary conditions (i.e. tangential $\bar{E}$ and $\bar{H}$, normal $\bar{J}$, $\bar{B}$, and $\bar{D}$ must be continuous) the Green's function for the background medium can be found. As a result

$$\Phi_o(r) = \int_V \left\{\frac{\mathcal{Q} - \nabla \cdot \bar{C}}{K_b}\right\} g(r,r')\, d^3r' \qquad 2\text{-}35$$

where $g(r,r')$ is the Green's function. For example, if the background is a wholespace with a constant value for K_b, $g(r,r')$ is just

$$g(r,r') = \frac{1}{4\pi R} \qquad R = |\bar{r} - \bar{r}'| \qquad 2\text{-}36$$

The effect of the anomalous part of the material can be expressed in terms of ρ_e where

$$\nabla^2 \Phi_a = -\frac{\rho_e}{K_b} \qquad 2\text{-}37$$

$$\rho_e(r) = \rho_0(r) + \frac{K_b \bar{\nabla} K_a}{(K_b + K_a)} \cdot \bar{\nabla} \int_V \frac{\rho_e(r')}{K_b} g(rr')\, d^3r' \qquad 2\text{-}38$$

$$\rho_0(r) = \frac{(\bar{\nabla}\cdot\bar{C} - \rho) K_a + K_b \bar{\nabla} K_a \cdot \bar{\nabla} \Phi_0}{(K_b + K_a)} \qquad 2\text{-}39$$

The equivalent source distribution satisfies the Fredholm integral equation 2-38 where ρ_0 is the excitation or source term for ρ_e. The appropriate form for ρ_0 for each physical problem is given in Table 2-2. The particular forms in Table 2-2 give ρ_0 in terms of the exciting fields $\bar{E}_0$ and $\bar{H}_0^T = \bar{H}_0^M + \bar{H}_J$. (Note the inclusion of $\bar{H}_J$ in the magnetic case). In physical terms, ρ_e corresponds to a charge density distribution in a dielectric problem, a magnetic pole density distribution in the magnetic case and a current source density in the static conduction problem.

The preceding set of equations summarize the equivalent source formulation for static problems. The derivation has been done in a very general manner and has a wide range of application. The application to static field problems in applied geophysics is briefly outlined in chapter three.

TABLE 2-2

Excitation Terms for the Static Equivalent Source Problems

Dielectric Problem

$$q_0 = \frac{\epsilon_a (\bar{\nabla}\cdot\bar{P}_I - q) - \epsilon_b \bar{\nabla}\epsilon_a \cdot \bar{E}_0}{(\epsilon_b + \epsilon_a)}$$

$$\bar{E}_0 = -\bar{\nabla}\Phi_0$$

Magnetic Problem

$$q_0 = \frac{(\mu_a \bar{\nabla}\cdot\mu_0\bar{M}_I - \mu_b \bar{\nabla}\mu_a \cdot \bar{H}_0^I)}{(\mu_b + \mu_a)}$$

$$\bar{H}_0^I = \bar{H}_0^M + \bar{H}_J = -\bar{\nabla}\Phi_0 + \bar{H}_J$$

Conduction Problem

$$q_0 = \frac{(\sigma_a \bar{\nabla}\cdot\bar{J}_s - \sigma_b \bar{\nabla}\sigma_a \cdot \bar{E}_0)}{(\sigma_b + \sigma_a)}$$

$$\bar{E}_0 = -\bar{\nabla}\Phi_0$$

(ii) Time-varying Problems

The equivalent source technique for time-varying problems will be analysed in the frequency domain. Defining the Fourier transform pair

$$F(r,t) = \frac{1}{2\pi}\int_{-\infty}^{\infty} F(r,\omega)\, e^{-j\omega t}\, d\omega \qquad 2\text{-}40$$

$$F(r,\omega) = \int_{-\infty}^{\infty} F(r,t)\, e^{j\omega t}\, dt \qquad 2\text{-}41$$

the frequency domain form of Maxwell's equations is

$$\bar{\nabla}\times\bar{E} = j\omega\bar{B} \qquad 2\text{-}42 \qquad\qquad \bar{\nabla}\times\bar{H} = \bar{J}_s + \bar{J}_c - j\omega\bar{D} \qquad 2\text{-}43$$

$$\bar{\nabla}\cdot\bar{D} = q \qquad 2\text{-}44 \qquad\qquad \bar{\nabla}\cdot\bar{B} = 0 \qquad 2\text{-}45$$

where all fields are of the form $F(r,\omega)$

It is most convenient to introduce the complex permittivity notation at this point. The dielectric and conductive constitutive equations are combined by defining a general conduction current

$$J_T = \bar{J}_c - j\omega\bar{D} \qquad 2\text{-}46$$
$$= -j\omega\epsilon\bar{E}$$

where $\epsilon = \epsilon + j\frac{\sigma}{\omega}$ is the complex permittivity. Inserting the constitutive equations into 2-42 and 2-43, yields

$$\bar{\nabla}\times\bar{E} = j\omega\mu\bar{H} + j\omega\mu_0\bar{M}_I \qquad 2\text{-}47 \qquad\qquad \bar{\nabla}\times\bar{H} = \bar{J}_s - j\omega\epsilon\bar{E} - j\omega\bar{P}_I \qquad 2\text{-}48$$

An additional change in notation makes the following analysis simpler; the generalized electric and magnetic currents are defined as

$$\bar{\mathcal{M}} = j\omega\mu_0\bar{M}_I \qquad 2\text{-}49 \qquad\qquad \bar{\mathcal{J}} = \bar{J}_s - j\omega\bar{P}_I \qquad 2\text{-}50$$

As a result 2-47 and 2-48 become

$$\bar{\nabla}\times\bar{E} = j\omega\mu\bar{H} + \bar{\mathcal{M}} \qquad 2\text{-}51 \qquad\qquad \bar{\nabla}\times\bar{H} = -j\omega\epsilon\bar{E} + \bar{\mathcal{J}} \qquad 2\text{-}52$$

The equivalent source formulation begins at this point; the material properties are split into background ϵ_b, μ_b and anomalous components ϵ_a, μ_a

$$\mu = \mu_b + \mu_a \qquad 2\text{-}53 \qquad \epsilon = \epsilon_b + \epsilon_a \qquad 2\text{-}54$$

Next the equivalent current distributions are defined as

$$\bar{\mathcal{M}}_e = j\omega\mu_a \bar{H} \qquad 2\text{-}55 \qquad \bar{J}_e = -j\omega\epsilon_a \bar{E} \qquad 2\text{-}56$$

Taking the curl of equations 2-51 and 2-52 and using the definitions 2-53 through 2-56 yields

$$\bar{\nabla}\times\bar{\nabla}\times\bar{E} - k_b^2\bar{E} + j\omega\bar{H}\times\bar{\nabla}\mu_b = \bar{\nabla}\times(\bar{\mathcal{M}}+\bar{\mathcal{M}}_e) + j\omega\mu_b(\bar{J}+\bar{J}_e) \qquad 2\text{-}57$$

$$\bar{\nabla}\times\bar{\nabla}\times\bar{H} - k_b^2\bar{H} - j\omega\bar{E}\times\bar{\nabla}\epsilon_b = \bar{\nabla}\times(\bar{J}+\bar{J}_e) - j\omega\epsilon_b(\bar{\mathcal{M}}+\bar{\mathcal{M}}_e) \qquad 2\text{-}58$$

where $k_b = \omega(\epsilon_b\mu_b)^{1/2}$ is the background propagation constant.

As in the static problem, the background material properties are chosen such that the Green's dyadic can be evaluated. The distribution of material properties in the background medium is limited to regions of constant property value which are separated by surfaces which permit separation of the governing differential equation and the boundary conditions on the electric and magnetic fields. The fields are now split into background and anomalous components.

$$\bar{E} = \bar{E}_o + \bar{E}_a \qquad 2\text{-}59 \qquad \bar{H} = \bar{H}_o + \bar{H}_a \qquad 2\text{-}60$$

Defining the operator

$$O_b = \bar{\nabla}\times\bar{\nabla}\times - k_b^2\tilde{I} \qquad 2\text{-}61$$

2-59 and 2-60 combine with 2-57 and 2-58 to give

$$O_b(\bar{E}_o) = \bar{\nabla}\times\bar{\mathcal{M}} + j\omega\mu_b\bar{J} \qquad 2\text{-}62 \qquad O_b(\bar{E}_a) = \bar{\nabla}\times\bar{\mathcal{M}}_e + j\omega\mu_b\bar{J}_e \qquad 2\text{-}63$$

$$O_b(\bar{H}_o) = \bar{\nabla}\times\bar{J} - j\omega\epsilon_b\bar{\mathcal{M}} \qquad 2\text{-}64 \qquad O_b(\bar{H}_a) = \bar{\nabla}\times\bar{J}_e - j\omega\epsilon_b\bar{\mathcal{M}}_e \qquad 2\text{-}65$$

where the anomalous fields $\bar{E}_a$ and $\bar{H}_a$ are totally determined by the equivalent currents $\bar{J}_e$ and $\bar{M}_e$.

On the assumption that ϵ_b and μ_b have been chosen such that the Green's dyadic for 2-61 can be derived, a set of four dyadics $({}^{E}_{J}\tilde{\Psi}, {}^{E}_{M}\tilde{\Psi}, {}^{H}_{J}\tilde{\Psi}, {}^{H}_{M}\tilde{\Psi})$ can be defined. The superscripts E and H indicate the dyadic is an electric or magnetic field dyadic and the subscripts J and M denote the excitation to be electric or magnetic currents. These dyadics are not all independent; the interrelation of the dyadics is given in part 1 of Appendix A.

Combining the dyadics with 2-62 through 2-65 yields;

$$\bar{E}_b = \int_V {}^{E}_{M}\tilde{\Psi} \cdot \bar{M}\, dV + \int_V {}^{E}_{J}\tilde{\Psi} \cdot j\omega\mu_b \bar{J}\, dV \qquad 2\text{-}66$$

$$\bar{H}_b = \int_V {}^{H}_{J}\tilde{\Psi} \cdot \bar{J}\, dV + \int_V {}^{H}_{M}\tilde{\Psi} \cdot (-j\omega\epsilon_b) \bar{M}\, dV \qquad 2\text{-}67$$

$$\bar{E}_a = \int_V {}^{E}_{M}\tilde{\Psi} \cdot \bar{M}_e\, dV + \int_V {}^{E}_{J}\tilde{\Psi} \cdot j\omega\mu_b \bar{J}_e\, dV \qquad 2\text{-}68$$

$$\bar{H}_a = \int_V {}^{H}_{J}\tilde{\Psi} \cdot \bar{J}_e\, dV + \int_V {}^{H}_{M}\tilde{\Psi} \cdot (-j\omega\epsilon_b) \bar{M}_e\, dV \qquad 2\text{-}69$$

Returning to the definitions of the equivalent currents $\bar{J}_e$ and $\bar{M}_e$, it becomes apparent that the equivalent currents satisfy the coupled pair of vector integral equations

$$\bar{J}_e = -j\omega\epsilon_a \bar{E}_b + \omega^2\epsilon_a\mu_b \int_V {}^{E}_{J}\tilde{\Psi} \cdot \bar{J}_e\, dV - j\omega\epsilon_a \int {}^{E}_{M}\tilde{\Psi} \cdot \bar{M}_e\, dV \qquad 2\text{-}70$$

$$\bar{M}_e = j\omega\mu_a \bar{H}_b + \omega^2\epsilon_b\mu_a \int_V {}^{H}_{M}\tilde{\Psi} \cdot \bar{M}_e\, dV + j\omega\mu_a \int {}^{H}_{J}\tilde{\Psi} \cdot \bar{J}_e\, dV \qquad 2\text{-}71$$

When either the anomalous permittivity or permeability is zero, the problem reduces to a single vector integral equation in either $\bar{J}_e$ or $\bar{M}_e$.

2-4 Summary

The general formulation of the equivalent source method for electromagnetic problems is now complete. The analysis of electromagnetic problems in a continuum with a complicated distribution of material properties is reduced to finding an equivalent source distribution in a medium with a simple distribution of electrical and magnetic properties. The problem is solved once the integral equation for the equivalent source has been solved; however, the solving of the integral equations involved is not a trivial matter. In any problem of interest the integral equation must be solved by a numerical method. The numerical solution of the integral equations by variational methods which yield approximate solutions is treated in detail in chapters five, six, and seven.

CHAPTER 3

STATIC FIELD APPLICATIONS

3-1 Static Field Methods in Geophysics

The resistivity and magnetic survey methods are both based on the measurement of static electric and magnetic fields. The interpretation of data collected by these methods is usually one of postulating and theoretically computing the response of a given model and comparing the response with the data.

The equivalent source appraoch permits the formulation of the equations for a wide variety of models which are difficult to analyse otherwise. From chapter 2, the fundamental integral equation has the form

$$q(r) = q_0(r) + \frac{\bar{\nabla}\eta}{1+\eta} \cdot \bar{\nabla} \int_v g(r,r')\, q(r')\, d^3r' \qquad 3\text{-}1$$

where η is a material property ratio, q and q_0 are charge, current source or magnetic pole distributions depending on the particular problem. To formulate the response of an arbitrary body, only η , the excitation field (which enters through q_0) and the appropriate Green's function have to be specified. The problem is reduced to solving equation 3-1.

The magnetic and electrostatic response are formulated by the same equation. The analysis of the solution of 3-1 differs for the two types of problems. For magnetic problems η is the permeability contrast ratio and in most applications it is considerably less than unity. For electrical conduction problems, η is a conductivity contrast ratio which, in most situations, is considerably greater than unity.

The solution of 3-1 is given for a spherical model in a whole-space in order to demonstrate the equivalent source method. This model is useful in demonstrating the features of magnetic and conduction response discussed later in the chapter.

3-2 Response of a Sphere

A sphere of anomalous material property embedded in an otherwise homogeneous whole-space can be described by the material property equation

$$\eta = \eta_d \, h(a-r) \qquad 3\text{-}2$$

where a is the radius of the sphere, η_d is the ratio of the difference in material property of the sphere from background to the background value and $h(r)$ is the Heaviside step function. For example, a body with conductivity σ_1 in a whole-space of conductivity σ_b would have

$$\eta_d = \frac{\sigma_1 - \sigma_b}{\sigma_b} \qquad 3\text{-}3$$

The center of the sphere is taken as the origin of a spherical polar coordinate system (r, θ, φ).

Using equation 3-2

$$\frac{\bar{\nabla}\eta}{1+\eta} = - \frac{\eta_d \, \delta(a-r) \, \hat{r}}{1+\eta_d} \qquad 3\text{-}4$$

where $\hat{r}$ is the (radial) unit vector. The exciting source q_0 generally has the form

$$q_0(r) = \frac{\bar{\nabla}\eta}{1+\eta} \cdot \bar{\mathcal{F}} \qquad 3\text{-}5$$

where $\bar{\mathcal{F}}$ is a vector field. The equivalent source for the sphere must be a surface distribution since it must have a delta function behaviour at the surface of the sphere. The appropriate Green's function for the problem is that for the scalar Poisson equation in a whole-space which is given in Appendix F.

$$g(r, r') = \frac{1}{4\pi R} \qquad 3\text{-}6$$

Since q is a surface distribution on a sphere it can be expanded in spherical harmonics

$$q(r, \theta, \varphi) = \delta(a-r) \sum_{n,m} c_n^m \, Y_n^m(\theta, \varphi) \qquad 3\text{-}7$$

where

$$Y_n^m(\theta,\varphi) = \left\{ \frac{2n+1}{4\pi} \frac{(n-|m|)!}{(n+|m|)!} \right\}^{1/2} P_n^{|m|}(\cos\theta)\, e^{im\varphi} \qquad 3\text{–}8$$

and P_n^m is the associated Legendre polynomial of degree n and order m

Using the generating function for Legendre polynomials and addition theorem for spherical harmonics

$$\frac{\partial}{\partial r} g(r,r') = -\frac{1}{a^2} \sum_{l=0}^{\infty} \frac{(l+1)}{(2l+1)} \sum_{k=-l}^{l} Y_l^k(\theta,\varphi)\, Y_l^{k*}(\theta,\varphi) \qquad 3\text{–}9$$

on the surface $|r| = |r'| = a$.

From the orthogonality property of spherical harmonics

$$\frac{\hat{r}\cdot\bar{\nabla}}{4\pi} \iiint \frac{\sigma(r')}{|\bar{r}-\bar{r}'|} d^3r' = -\sum_{n=0}^{\infty} \frac{(n+1)}{(2n+1)} \sum_{m=-n}^{n} c_n^m\, Y_n^m(\theta,\varphi) \qquad r=a \quad 3\text{–}10$$

Substituting into 3-1 reduces the integral equation to

$$\sum_{n=0}^{\infty} \sum_{m=-n}^{n} c_n^m \left(1 - \frac{m_d}{1+m_d} \frac{(n+1)}{(2n+1)}\right) Y_n^m(\theta,\varphi) = -\frac{m_d}{1+m_d}\, \hat{r}\cdot\bar{\mathcal{A}}\Big|_{r=a} \qquad 3\text{–}11$$

By expanding the source term in spherical harmonics

$$\hat{r}\cdot\bar{\mathcal{A}} = \sum_{n=0}^{\infty} \sum_{m=-n}^{n} d_n^m\, Y_n^m(\theta,\varphi) \qquad r=a \qquad 3\text{–}12$$

the c_n^m are solved for and are

$$c_n^m = -\left\{ \frac{\alpha\, d_n^m}{1-\alpha\left(\frac{n+1}{2n+1}\right)} \right\} \qquad 3\text{–}13$$

where $\alpha = m_d/(1+m_d)$

The anomalous fields associated with σ are described in terms of the gradient of a scalar potential. The scalar potential is given by

$$\Phi = \iiint \sigma(r')\, g(r,r')\, d^3r' \qquad 3\text{–}14$$

The spherical harmonic expansion of Φ for the sphere is

$$\Phi = \frac{a^2}{r} \sum_{n=0}^{\infty} \left(\frac{a}{r}\right)^n \sum_{m=-n}^{n} \frac{c_n^m Y_n^m(\theta,\varphi)}{(2n+1)} \qquad r \geq a$$

3-15

$$= a \sum_{n=0}^{\infty} \left(\frac{r}{a}\right)^n \sum_{m=-n}^{n} \frac{c_n^m Y_n^m(\theta,\varphi)}{(2n+1)} \qquad r \leq a$$

The response of the sphere for a spatially invariant exciting field is commonly discussed. Appropriately orienting the coordinates

$$\hat{r} \cdot \bar{H} = \frac{|\bar{H}|}{N_1^0} Y_1^0(\theta,\varphi) \qquad 3\text{-}16$$

where N_1^0 is the normalizing factor for the Y_1^0 spherical harmonic. Then

$$d_1^0 = \frac{|\bar{H}|}{N_1^0} \qquad 3\text{-}17$$

and all other d_n^m are zero.

The anomalous potential is

$$\Phi = \frac{c_1^0}{3} \frac{a^3}{r^2} Y_1^0(\theta,\varphi) \qquad r \geq a$$

$$= \frac{c_1^0}{3} r \, Y_1^0(\theta,\varphi) \qquad r \leq a \qquad 3\text{-}18$$

which is the usual expression for a sphere in a constant field (Jackson 1962)).

The analytic solution of equation 3-1 for a sphere is possible due to the fact the problem can be solved by the conventional boundary value problem method of separation of variables. In general the geometry is more irregular and the eigenfunctions are not known. As a result, approximate numerical methods must be used to solve the integral equation.

3-3 Magnetic Methods

The magnetic survey method detects regions of high permeability and possible remanent magnetization. The basic model for interpretation is the response of a body of anomalous permeability and remanent magnetization

embedded in a whole-space with free-space magnetic properties. The body is placed in a uniform magnetic field equivalent in amplitude and direction to that of the Earth. For most purposes, the dimensions of the body are sufficiently small that the Earth's internally generated field can be assumed spatially invariant over the region of the body.

The magnetic survey measures the total magnetic field at a point or a component of it. The field is composed of two parts; that of the Earth and that due to the presence of an anomalous body

$$\bar{H} = \bar{H}_o + \bar{H}_a \qquad 3\text{-}19$$

For interpretation purposes, $\bar{H}_a$ is computed for a postulated model and compared with the observed $\bar{H}_a$.

Using the equivalent source approach, solving for $\bar{H}_a$ is reduced to solving for an equivalent magnetic pole distribution. From chapter 2,

$$\bar{H}_a = -\bar{\nabla}\Phi_a \qquad 3\text{-}20$$

and

$$\Phi_a = \iiint g(r,r')\,\varphi(r')\,d^3r' \qquad 3\text{-}21$$

where φ is an equivalent magnetic pole density distribution. φ is given by the integral equation 3-1 where η is the susceptibility χ_m. The primary source term is

$$\varphi_o(r) = \frac{(\chi_m \bar{\nabla}\cdot\mu_o\bar{M}_r)}{(1+\chi_m)} - \frac{\mu_o\bar{H}_o\cdot\bar{\nabla}\chi_m}{(1+\chi_m)} \qquad 3\text{-}22$$

where $\bar{M}_r$ is the remanent magnetization.

One of the commonly used assumptions in computing magnetic anomalies is to neglect demagnetization effects. The integral equation 3-1 can be used to demonstrate why this is a good approximation. For a given model, the integral equation for φ can be written

$$\varphi = \varphi_o + \alpha\,\mathcal{A}(\varphi) \qquad 3\text{-}23$$

where α is a material property factor and $\mathcal{A}$ is a geometrical function containing the integral term of equation 3-1. α has the form

$$\alpha = \frac{\chi_m^p}{1+\chi_m^p} \qquad 3\text{-}24$$

where χ_m^p is the maximum value χ in the problem. The integral equation 3-23 can be solved by the successive approximation method. Taking successive approximations to

$$\begin{aligned} q &= q_0 \\ q &= q_0 + q_1 \\ &\vdots \\ q &= q_0 + q_1 + q_2 \cdots\cdots \end{aligned} \qquad 3\text{-}25$$

and substituting into 3-23 yields

$$\begin{aligned} q_1 &= \alpha\, \mathcal{A}(q_0) \\ q_2 &= \alpha\, \mathcal{A}(q_1) = \alpha^2\, \mathcal{A}(\mathcal{A}(q_0)) \\ &\vdots \\ q_n &= \alpha^n\, \mathcal{A}_n(q_0) \end{aligned} \qquad 3\text{-}26$$

where $\mathcal{A}_n$ is the n^{th} application of $\mathcal{A}$ to q_0.

In general $\mathcal{A}$ is different for every point in the body. On physical grounds q must be finite and the series expansion must converge. Since $\alpha<1$, the geometrical factor $\mathcal{A}$ must be unity or less at all points. The spherical model is an excellent example of this result. The $\mathcal{A}$ for a given spherical harmonic is independent of position. From equation 3-13 the coefficient C_n^m is proportional to

$$\frac{1}{1-\alpha\left(\frac{n+1}{2n+1}\right)} \qquad 3\text{-}27$$

The successive approximation solution is given by expanding 3-27 in a geometrical series

$$\frac{1}{1-\alpha\left(\frac{n+1}{2n+1}\right)} = \sum_{s=0}^{\infty} \alpha^s \left(\frac{n+1}{2n+1}\right)^s \qquad 3\text{-}28$$

The geometrical factor is just

$$\frac{n+1}{2n+1} \qquad 3\text{-}29$$

In general, the higher the irregularity of the geometry in a localized region the closer to one the geometrical factor will be. In a cube, for example, α would be closer to unity in the corners than in the central part of one of the faces.

The convergence rate of the successive approximation methods is primarily controlled by the material property factor. For most geophysical problems, the susceptibility is seldom greater than 10^{-2} and often less than 10^{-3}. Thus $\alpha < 10^{-2}$ and the first term of the series is more than adequate to specify the response of the body.

For a model where demagnetization effects are negligible,

$$q \simeq \chi_m \bar{\nabla} \cdot \mu_0 \bar{M}_I - \mu_0 \bar{H}_0 \cdot \bar{\nabla} \chi_m \qquad 3\text{-}30$$

and there is no need to solve the integral equation. The specification of M_I, $\bar{H}_0$ and χ_m automatically specifies q and therefore $\bar{H}_a$.

For problems where demagnetization effects are not small, the integral equation 3-1 must be solved. With the exception of a few special geometries, the solution must be found approximately or by numerical methods. In either case, the response of an arbitrary body can be quickly formulated with the equivalent source method. The Green's functions which are required are the 2 and 3-dimensional Green's function for the scalar Poisson equation. The two dimensional Green's function is useful for solving models with sufficiently long strike lengths that they may be considered infinite in one dimension.

3-4 Resistivity Methods

The resistivity method is used to detect and delineate electrical

conductivity variations in the outer kilometer of the Earth's crust. As mentioned in chapter 1, the method is one of passing electrical current directly through the Earth and measuring the potential difference between different points at the Earth's surface. The voltage at the detector can be thought of being composed of two parts; one due to the current flow from the generator through the background Earth, $\mathcal{V}_o$, and one due to the disturbing influence of different conductivity zones in the region, $\mathcal{V}_a$.

$$\mathcal{V} = \mathcal{V}_o + \mathcal{V}_a \qquad 3\text{-}31$$

The interpretation of resistivity and induced polarization surveys is based on the postulation and computed response of a given model. The anomalous field is compared with the theoretical response to interpret the data.

The equivalent source method has been successfully applied to resistivity problems by Dieter, Paterson and Grant (1969) who computed the response of ellipsoidal conductors in a conducting half-space. The integral equation used by Dieter et al can be derived from the general equations for static conduction problems given in chapter 2.

For an ellipsoidal body of conductivity σ_1 embedded in a conducting half-space with conductivity σ_o the conductivity as a function of position is

$$\sigma = \sigma_o + \sigma_d \, h(f(r)) \qquad 3\text{-}32$$

where $\sigma_d = \sigma_1 - \sigma_o$ and

$$f(r) = 1 - \left(\left(\frac{x_1 - x_1^\circ}{a_1} \right)^2 + \left(\frac{x_2 - x_2^\circ}{a_2} \right)^2 + \left(\frac{x_3 - x_3^\circ}{a_3} \right)^2 \right)^{1/2} \qquad 3\text{-}33$$

Setting $f(r)$ to zero defines the surface of the ellipsoid. The conductivity gradient factor is

$$- \frac{\sigma_d}{\sigma_o + \sigma_d} \, \delta(f(r)) \, \hat{n} \qquad 3\text{-}34$$

where $\hat{n} = -\bar{\nabla} f(r)$ is the outward normal at the surface of the body. The equivalent source is a surface distribution. The η factor of equation 3-1 is σ_d/σ_o.

By defining the equivalent surface current source distribution

$$g(r) = \mathcal{J}(r)\,\delta(f(r)) \qquad 3\text{-}35$$

and substituting into equation 3-1, the integral equation for $\mathcal{J}$ on the surface of the ellipsoid becomes

$$\mathcal{J}(r) = \mathcal{J}_o(r) - \frac{\sigma_d}{\sigma_o+\sigma_d}\,\hat{n}\cdot\bar{\nabla}\iint g(r,r')\,\mathcal{J}(r')\,d^2r' \qquad 3\text{-}36$$

where

$$\mathcal{J}_o(r) = \frac{\sigma_d}{\sigma_o+\sigma_d}\,\hat{n}\cdot\bar{E}_o(r) \qquad 3\text{-}37$$

$\bar{E}_o$ is the electric field associated with an external current in the background medium and has the form

$$\bar{E}_o(r) = -\bar{\nabla}\Phi_o \qquad 3\text{-}38$$

where Φ_o is the potential associated with the external source.

The appropriate Green's function for the problem, as given in Appendix F, is that for the scalar Poisson equation in a half-space with a Neumann boundary condition at the surface

$$g(r,r') = \frac{1}{4\pi}\left[\frac{1}{R} + \frac{1}{R_1}\right] \qquad 3\text{-}39$$

where

$$R = \left(\sum_{i=1}^{3}(x_i - x_i')^2\right)^{1/2}$$

$$R_1 = \left(\sum_{i=1}^{2}(x_i - x_i')^2 + (x_3 + x_3')^2\right)^{1/2} \qquad 3\text{-}40$$

Regrouping equation 3-36, yields

$$\frac{\sigma_1}{\sigma_1-\sigma_o}\,\mathcal{J}(r) = -\hat{n}\cdot\bar{\nabla}\Phi_o - \hat{n}\cdot\bar{\nabla}\iint g(r,r')\,\mathcal{J}(r')\,d^2r' \qquad 3\text{-}41$$

which is the same as that used by Dieter et al.

Unlike the magnetic problems, the material property contrast is usually large, with contrasts of the order $\eta \sim 10^3$ not uncommon. As a result the feedback from the integral term of 3-41 is not negligible and the successive approximation solution would be slowly convergent. For a conduction problem, the integral equation must be solved in most instances.

The only approximation that can be applied in these problems is neglect of the second term in the Green's function. The Earth's surface interacts with the anomalous body and is equivalent to placing an image source at an equal height above the boundary and considering the response of two interacting bodies in a wholespace. This effect is introduced by the $1/R_1$ term in the Green's function. If the body is buried sufficiently deep in the Earth in comparison to its lateral dimensions, R/R_1, is much less than one and

$$g(r,r') \simeq \frac{1}{4\pi R} \qquad 3\text{-}42$$

For example, the response of a deeply buried sphere excited by a uniform electric field as shown in Fig. 3-1, can be obtained directly from the results of section 3-2. In the x_1-x_3 plane through the center of the sphere, the anomalous potential at the Earth's surface is

$$\Phi_a = -\left(\frac{\sigma_1 - \sigma_0}{\sigma_1 + 2\sigma_0}\right) \frac{2|\bar{E}_0| a^3 x_1}{(x_1^2 + d^2)^{3/2}} \qquad 3\text{-}43$$

which is the result given by Grant and West (1965, pg. 425)

The general response of a conductor in conducting half-space must be found by numerical methods. The integral equation 3-1 can be solved by a least squares method (see chapter five) as used by Dieter et al or the problem can be analysed by digitizing $\mathcal{S}$.

In practice slow time varying currents are commonly used in place of direct currents. The interpretation is still based on the static field

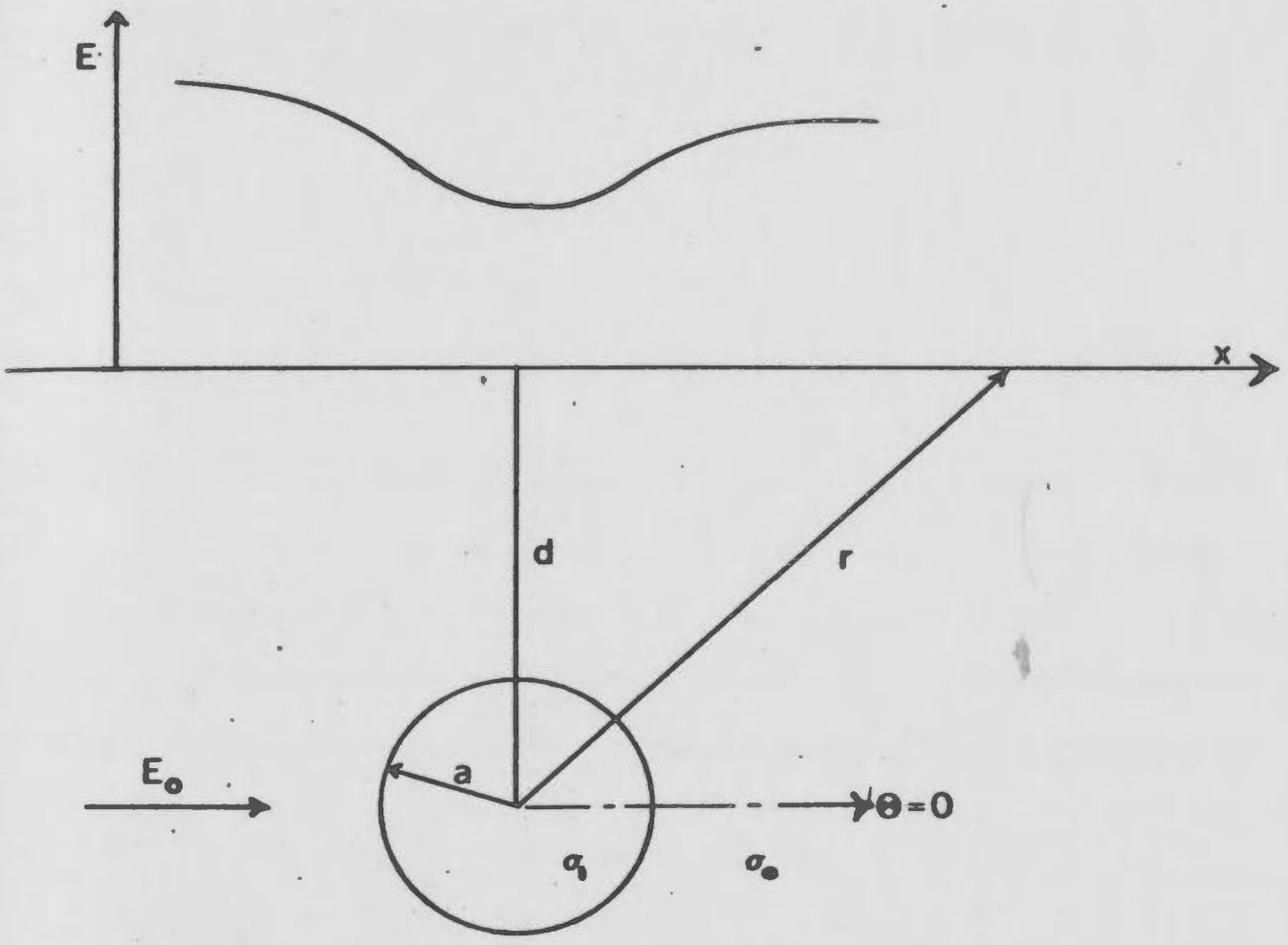

FIG 3-1 Electrostatic response of a deeply buried sphere in a uniform field

equations since the time varying field effects are small. The induced polarization method is a product of using time varying currents for resistivity surveys. Bulk earth materials exhibit frequency dependent electrical properties below a few Hertz. This anomalous behaviour is known as the induced polarization or overvoltage effect. (J.R. Wait, 1959). Since some bulk earth materials, such as disseminated sulphide ore bodies, show much higher induced polarization effects than the host material surrounding them, the induced polarization method can be used to detect and delineate localized concentrations of these materials. The computation of induced polarization responses are made directly from the theoretical resistivity response. As a result the equivalent source method is applicable to computing the induced polarization response as well as the resistivity response of theoretical models.

3-5 Summary

The treatment of static field problems encountered in geophysical methods can be readily treated using the equivalent source method. The generality and flexibility of the method make it a powerful method for analysing problems not as yet solved. Neglect of demagnetization effects yields a very simple and straightforward method of solving magnetic problems. The resistivity analysis of section 3-4 can readily be generalized to the case of the body buried in a conductively layered half-space by changing the Green's function. A thin conducting surface layer representative of a conductive overburden can be incorporated in this manner.

CHAPTER 4

THEORY OF INTEGRAL EQUATIONS IN ELECTROMAGNETIC SCATTERING PROBLEMS

4-1 Basic Scattering Equation

This chapter is devoted to a study of the mathematical nature of the integral equations encountered in electromagnetic scattering problems. The effect of a scattering body in an electromagnetic system, for which the electromagnetic Green's dyadic can be evaluated, may be expressed in terms of equivalent electric and magnetic current systems as shown in chapter 2. The equivalent currents satisfy a pair of coupled vector Fredholm equations. In the majority of scattering problems, the scattering is due to the electrical properties of the scattering body; the magnetic properties are almost identical to those of the background media in most instances. In order to illustrate the properties of the integral equations encountered, the particular problem of scattering by an electric scatterer in a homogeneous whole-space is discussed in detail in this chapter. The analysis of a scatterer in a more complicated system does not differ markedly from the whole-space problem; the basic difference is the addition of a homogeneous term to the whole-space dyadic. This result can be seen from the form of the Green's dyadic for a plane stratified medium derived in Appendix A; similar derivations can be made for background media which have cylindrical or spherical stratification.

The integral equation for the equivalent current describing an electric scatterer is developed from the general equation 2-70. The scatterer is located in a whole-space and occupies a volume V bounded by a surface S. In geophysical analysis, conductivity is more commonly used than permittivity; as a consequence, a complex conductivity notation is adopted here in place of the complex permittivity used in chapter 2. The scatterer has a complex

conductivity difference $\sigma_a = -j\omega\epsilon_a$ where ϵ_a is the complex permittivity difference. The background whole-space has complex conductivity $\sigma_b = -j\omega\epsilon_b$. The permeability of the scatterer and the background medium are taken as the free-space permeability. Since there are no variations in magnetic properties, the scatterer is replaced by an equivalent electric current density $\bar{J}_e$, which satisfies the integral equation

$$\frac{\bar{J}_e(r)}{\sigma_a} = \bar{E}_o(r) + j\omega\mu_o \int_V {}^{\epsilon}_{J}\tilde{\mathcal{G}}(r,r') \cdot \bar{J}_e(r') d^3r' \qquad 4\text{-}1$$

From Appendix A, ${}^{\epsilon}_{J}\tilde{\mathcal{G}}$ is given by

$${}^{\epsilon}_{J}\tilde{\mathcal{G}}(r,r') = \left[\tilde{I} + \frac{\bar{\nabla}\bar{\nabla}}{k_b^2} \right] g(r,r') \qquad 4\text{-}2$$

where

$$g(r,r') = \frac{e^{jk_b R}}{4\pi R}$$

$$k_b^2 = \omega^2 \epsilon_b \mu_o = j\omega\sigma_b\mu_o$$

A format which is more compact and physically simpler to understand is now introduced. The integral term of 4-1 may be re-expressed as

$$j\omega\mu_o \int_V {}^{\epsilon}_{J}\tilde{\mathcal{G}}(r,r') \cdot \bar{J}_e(r') d^3r' = \mathcal{L}(\bar{J}_e) + \mathcal{C}(\bar{J}_e) \qquad 4\text{-}3$$

where

$$\mathcal{L}(\bar{J}_e) = j\omega\mu_o \int_V g(r,r')\, \bar{J}_e(r')\, d^3r' \qquad 4\text{-}4$$

and

$$\mathcal{C}(\bar{J}_e) = \frac{\bar{\nabla}\bar{\nabla}}{\sigma_b} \int_V g(r,r')\, \bar{J}_e(r')\, d^3r' \qquad 4\text{-}5$$

A more intuitively obvious form for $\mathcal{C}$ is obtained with the aid of the

divergence theorem, namely

$$\mathcal{C}(\bar{J}_e) = \frac{\bar{\nabla}}{\sigma_b} \int_V \{\bar{\nabla}' \cdot \bar{J}_e(r')\}\, g(r,r')\, d^3r' \qquad 4\text{-}6$$

where $\bar{\nabla} \cdot \bar{J}_e$ is the total divergence of $\bar{J}_e$ defined as

$$\bar{\nabla} \cdot \bar{J}_e = \bar{\nabla} \cdot \bar{J}_e - \bar{J}_e \cdot \hat{n}\, \delta(s) \qquad 4\text{-}7$$

Equation 4-1 can now be written as

$$\frac{\bar{J}_e}{\sigma_a} - \mathcal{L}(\bar{J}_e) - \mathcal{C}(\bar{J}_e) = \bar{E}_o \qquad 4\text{-}8$$

In this form the equation is analogous to the simple RLC circuit equation

$$\left(R - j\omega L - \frac{1}{j\omega C}\right) I = V \qquad 4\text{-}9$$

The three terms on the left of 4-8 may be interpreted as follows. The first term represents the ohmic electric field generated by $\bar{J}_e$ due to variations in the conductivity from σ_b (i.e. $\sigma_a = \sigma - \sigma_b$). The second represents the electric field generated inductively by the time variations of $\bar{J}_e$. The last term is analogous to the capacitive term of 4-9. When the background medium is an insulator, this term is the capacitive effect of the body. When the background is not an insulator, this term represents the conductive channelling effect of the scattering body. (In the case of magnetic property variations which are not included in this example, this term would represent the demagnetization effect.) In all instances, this term represents the generalization of the static field response discussed in chapter 3 to the time-varying case. For this electric scatterer, the static equation of the last chapter is obtained by multiplying 4-1 by σ_a, taking the divergence of the equation, setting $q = \bar{\nabla} \cdot \bar{J}_e$ in a conductive problem ($q = -j\omega \bar{\nabla} \cdot \bar{J}_e$ in a dielectric problem) and taking the limit as $\omega \to 0$. An analogous derivation can be made for magnetic problems.

In the following discussions, the first term of 4-8 will be referred

to as the ohmic term while $\mathcal{L}(\bar{J}_e)$ and $\mathcal{G}(\bar{J}_e)$ will be called the inductive and depolarization terms. The associated integral operators defined by 4-4 and 4-5 will be termed the induction and depolarization operators. In many cases, it is convenient to refer to the combination of the three terms as the total impedance operator and denote it by

$$\mathcal{Z} = \frac{1}{\sigma_a} - \mathcal{L}(\ ) - \mathcal{G}(\ ) \qquad 4\text{-}10$$

One other combination of $\mathcal{L}$ and $\mathcal{G}$ which is useful to note is that the anomalous or scattered field is given

$$\bar{E}_a = \mathcal{L}(\bar{J}_e) + \mathcal{G}(\bar{J}_e) \qquad 4\text{-}11$$

Before continuing further with the scattering problem, some of the mathematical properties of the induction and depolarization operators are examined. These properties make the discussion of the nature of the equivalent current $\bar{J}_e$ somewhat easier to understand in a general context.

4-2 Induction and Depolarization Operators: Mathematical Properties

The induction and depolarization operators are in essence convolution integrals. The equivalent current is convolved with the background Green's function or dyadic. The elements of the Green's dyadic are built from solutions to a Helmholtz equation of the form

$$(\nabla^2 + k_b^2)\, g(r,r') = -\delta(|\bar{r}-\bar{r}'|) \qquad 4\text{-}12$$

The solution $g(r, r')$ exhibits a pole or branch point singularity when $|\bar{r}-\bar{r}'| \to 0$ and has an essential singularity as $|r-r'| \to \infty$. The exact form depends on the number of spatial dimensions involved (i.e. 1, 2, or 3).

The operation of general interest takes the form

$$\mathcal{A}(f) = \int_V g(r,r')\, f(r')\, d^3r' \qquad 4\text{-}13$$

where f is a function belonging to G, the complex Hilbert space of functions in V. The operator $\mathcal{A}$ is a "definite operator". The term "definite operator" is used to imply that there exists no subset of functions in G for which $\mathcal{A}$

is a null operator. In more specific terms the following definition is adopted.

Definition: An operator $\mathcal{A}$, which has the operational space V, is termed definite (or complete) if $\mathcal{A}(f) \neq 0$ for all $f \neq 0$ where f is any functional belonging to G, the complex Hilbert space of functions in V.

The operator $\mathcal{A}$ has this property as can be demonstrated simply by taking $f = \delta(r)$, the Dirac delta function, which has its support located at a single point in V. (The definite property is actually implicit from equation 4-10). An additional feature of $\mathcal{A}$ is that the kernel $g(r, r')$ is a quadratically integrable kernel when V is a finite dimensioned volume (Morse and Feshbach (1953)).

The inductive and depolarization operators are vector operators composed of terms of the form 4-13. Denoting the components of $\bar{J}_e$ by (J_1, J_2, J_3) where J_i are scalar functions belonging to G, the induction operator has the property that it is a definite operator for any vector function in the vector Hilbert space of functions in region V.

The depolarization operator is almost identical to the induction operator; it differs, however, in that it contains the total divergence operator

$$\mathcal{C}(\bar{J}_e) = + \frac{\bar{\nabla}}{\sigma_b} \mathcal{A}(\bar{\nabla} \cdot \bar{J}_e) \qquad 4\text{-}14$$

The additional operation of $\bar{\nabla}\cdot$ inside $\mathcal{A}$ has the property that it makes $\mathcal{C}$ an indefinite or incomplete operator. For all sets (J_1, J_2, J_3) such that $\bar{\nabla} \cdot \bar{J}_e \equiv 0$, $\mathcal{C}$ is a null operator. A current flow for which $\bar{\nabla} \cdot \bar{J}_e \equiv 0$ is termed a solenoidal current flow for the region V from this point on.

While more detailed analysis of the mathematical properties of $\mathcal{K}$ and $\mathcal{C}$ could be given, the essential features of these operators are summarized above and permit continuation of the analysis of the electromagnetic scattering problem.

4-3 Dimensional Analysis

The impedance operator $\mathcal{Z}$ is composed of three terms. In order to weigh the importance of the individual terms, an estimate of their magnitudes is a useful parameter to have available. $\bar{J}_e$ is assumed to be bounded with a finite maximum of J in V. This assumption is valid provided σ_a remains finite and the source of E_o is external to V or is distributed with finite amplitude within V.

In order to obtain an estimate of the magnitude of $\mathcal{L}$ and $\mathcal{C}$ the magnitude of $\mathcal{U}(f)$ where f = 1 in V is derived. If A is the characteristic length of volume V, then

$$\mathcal{U}(f) = \int_V g(r r')\, d^3r' < \frac{A^2}{4\pi} \int_0^1 \int_0^{2\pi} \int_0^{\pi} r \sin\theta \, dr \, d\theta \, d\varphi = A^2 \qquad 4\text{-}15$$

Taking the divergence operator to have a magnitude of the order

$$|\nabla| \sim \frac{1}{A} \qquad 4\text{-}16$$

the terms in $\mathcal{Z}(\bar{J}_e)$ become

$$\left| \frac{\bar{J}_e}{\sigma_a} \right| \sim \frac{J}{|\sigma_a|_{min}} \quad \text{volt/m.} \qquad 4\text{-}17$$

$$|\mathcal{L}(J_e)| \sim \omega \mu_o A^2 J \quad \text{volt/m.} \qquad 4\text{-}18$$

$$|\mathcal{C}(J_e)| \sim \frac{J}{\sigma_b} \quad \text{volt/m.} \qquad 4\text{-}19$$

where $|\sigma_a|_{min}$ is the minimum absolute value of σ_a attained in V. The order of magnitude of $\mathcal{Z}$ now depends on the form of $\bar{J}_e$. From the discussion of the last section $\mathcal{C}$ is a null operator for all solenoidal current flows in V. As a result two distinct impedance estimates can be given for Z. For J_e solenoidal

$$|\mathcal{Z}| = Z_1 \sim \frac{1}{|\sigma_a|_{min}} - j\omega\mu_o A^2 \quad \text{ohm-m.} \qquad 4\text{-}20$$

and for J_e not solenoidal,

$$|\mathbb{Z}| = Z_2 \sim \frac{1}{|\sigma_a|_{min}} - j\omega\mu_o A^2 - \frac{1}{\sigma_b} \qquad 4\text{-}21$$

The appearance of two characteristic impedances is not surprising; it just reflects the fact that a vector field can be expressed in two parts, namely, its longitudinal and transverse components. The bimodal characteristic of $\mathbb{Z}$ accounts for the whole subject of magnetic induction. For spatial dimensions small on a wavelength scale, the coupling between conductive bodies and/or current systems embedded in an insulator are described as inductive. The capacitive or conductive effects can be ignored in such a system provided only the magnetic fields associated with currents are observed. The reason for this is that the solenoidal currents see a very low impedance when σ_b/σ_a and $\omega\mu A^2\sigma_b$ are small while the non-solenoidal currents see a relatively high impedance. Since the magnetic fields are primarily determined by the solenoidal currents which may be several orders of magnitude larger than the non-solenoidal currents, only solenoidal currents need to be considered in determining the response. The impedances as a function of body dimension vary much like those of simple RL and RC series circuits as a function of frequency.

4-4 Eigenfunction Analysis

The method of characterizing an operator and understanding its response is to analyse the operator in terms of its eigenfunctions and eigenvalues. The electromagnetic scattering problem is characterized by the equation

$$\mathbb{Z}(\bar{J}_e) = \bar{E}_o \qquad 4\text{-}22$$

where $\mathbb{Z}$ is a complex symmetric operator (non-Hermitian). The general eigenfunction equation associated with 4-22 is

$$\mathbb{Z}(\bar{I}_n) = \lambda_n \mathbb{W}(\bar{I}_n) \qquad 4\text{-}23$$

where W is a real positive-definite symmetric weighting operator, $\bar{I}_n$ is an eigenfunction of $\mathcal{Z}$ with weight W and λ_n is the associated eigenvalue. Since $\mathcal{Z}$ has a quadratically integrable kernel for V finite, $\mathcal{Z}$ is characterized by a denumerable but infinite set of eigencurrents and eigenvalues. (Morse and Feshbach, (1953)). In simplistic terms, this means the eigenfunctions are analogous in application to those of a Fourier expansion (i.e. series) on a finite interval as opposed to those of a Fourier expansion (i.e. integral) on a infinite interval.

The unweighted eigenfunction problem is

$$\mathcal{Z}(\bar{I}_n) = \lambda_n \bar{I}_n \qquad 4\text{-}24$$

Since $\mathcal{Z}$ is non-Hermitian, $\mathcal{Z}$ is not self-adjoint. The adjoint operator to $\mathcal{Z}$ denoted by $\mathcal{Z}^\dagger$ has the property that

$$\mathcal{Z}^\dagger = \mathcal{Z}^* \qquad 4\text{-}25$$

The adjoint eigenfunction problem is

$$\mathcal{Z}^\dagger(\bar{I}_n^\dagger) = \lambda_n^* \bar{I}_n^\dagger \qquad 4\text{-}26$$

where $\bar{I}_n^\dagger$ are the eigenfunctions of the adjoint operator. From 4-23, the adjoint eigenfunctions are just the complex conjugates of $\bar{I}_n$.

$$\bar{I}_n^\dagger = I_n^* \qquad 4\text{-}27$$

Defining the inner product of two vectors in V as

$$(\bar{A}, \bar{B}) = \int_V \bar{A} \cdot \bar{B}\, dV \qquad 4\text{-}28$$

the properties of $\mathcal{Z}$, $\mathcal{Z}^\dagger$ and the eigenfunctions are summarized by

$$(\bar{I}_n, \bar{I}_m) = \delta_{nm} \qquad 4\text{-}29$$

$$(\bar{I}_n, \mathcal{Z}(\bar{I}_m)) = \lambda_n \delta_{nm} \qquad 4\text{-}30$$

$$(\bar{I}_n^\dagger, \mathcal{Z}^\dagger(\bar{I}_m^\dagger)) = \lambda_n \delta_{nm} \qquad 4\text{-}31$$

Adopting the Dirac bra-ket notation, the inverse of $\mathbb{Z}$ is given by

$$\mathbb{Z}^{-1} = \frac{|I_n\rangle\langle I_n|}{\lambda_n} \qquad 4\text{-}32$$

A useful variation on this approach is the extension of a concept discussed by Harrington and Mautz (1971) in their analysis of scattering from perfectly conducting bodies. In their analysis, an appropriate weighting operator was chosen, such that the I_n are real; the eigencurrents are equiphase over the entire body. The impedance operator $\mathbb{Z}$ is split into its real and imaginary parts $\mathbb{R}$ and X.

$$\mathbb{Z} = \mathbb{R} + j X \qquad 4\text{-}33$$

The real part of $\mathbb{Z}$ corresponds to the sum of the ohmic resistance and radiation resistance. The imaginary term, X corresponds to the reactive impedance associated with capacitive and inductive effects. $\mathbb{R}$ is a positive definite, real symmetric operator and X is a real symmetric operator. Both operators have an associated set of real eigenvalues and real eigenfunctions.

The choice of $W = R$ in 4-23 results in a weighted eigenfunction problem which has a set of real eigenfunctions. In the Dirac bra-ket notation, equation 4-23 becomes (vector bars have been dropped for compactness)

$$\mathbb{R}|I_n\rangle + j X|I_n\rangle = \lambda_n \mathbb{R}|I_n\rangle \qquad 4\text{-}34$$

or

$$j X|I_n\rangle = (\lambda_n - 1)\mathbb{R}|I_n\rangle$$

Denoting the eigenfunctions of $\mathbb{R}$ by s_n and the eigenvalues by r_n, the following results hold

$$\langle s_n | s_m \rangle = \delta_{nm} \qquad 4\text{-}35$$

$$\langle s_n | \mathbb{R} | s_m \rangle = r_n \delta_{nm} \qquad 4\text{-}36$$

Equation 4-32 is expanded in terms of the s_i's as

$$j\,|s_p\rangle\langle s_p|\,X\,|s_i\rangle\langle s_i|\,I_n\rangle = (\lambda_n - 1)\,|s_p\rangle\, r_p\,\delta_{pi}\,\langle s_i|\,I_n\rangle \qquad 4\text{-}37$$

Next the operator P and its inverse P^{-1} are defined as

$$P = |s_i\rangle\, r_i^{-1/2}\,\delta_{in}\,\langle s_n| \qquad 4\text{-}38$$

$$P^{-1} = |s_i\rangle\, r_i^{1/2}\,\delta_{in}\,\langle s_n| \qquad 4\text{-}39$$

P and its inverse are real positive definite operators by virtue of the fact that R is a positive definite operator which makes the $r_i > 0$. With the following definitions

$$|I_n'\rangle = P^{-1}\,|I_n\rangle \qquad 4\text{-}40$$

$$X' = P\,X\,P \qquad 4\text{-}41$$

equation 4-37 becomes

$$j\,X'|I_n'\rangle = (\lambda_n - 1)\,|I_n'\rangle \qquad 4\text{-}42$$

which is a new unweighted eigenfunction problem. The new operator X' is real and symmetric; therefore, it has real eigenvalues and eigenfunctions. This implies that

$$\lambda_n - 1 = j\,\beta_n \qquad 4\text{-}43$$

where β_n and I_n' are real. Equation 4-40 then reduces to

$$X'|I_n'\rangle = \beta_n\,|I_n'\rangle \qquad 4\text{-}44$$

Thus the use of the weighting function M = R yields a set of real eigencurrents and

$$Z\,|I_n\rangle = (1 + j\beta_n)\,|I_n\rangle \qquad 4\text{-}45$$

where β_n is an eigenvalue of the modified reactance matrix X'. The eigencurrents are given in terms of the eigenfunctions of X' by

$$|I_n\rangle = P\,|I_n'\rangle \qquad 4\text{-}46$$

4-5 Complex Power Balance

When the equivalent source method is applied to formulate an electromagnetic scattering problem, the re-distribution of energy or power can be expressed in a simple manner which can be readily interpreted. The analysis for the electric scatterer discussed in the previous sections of this chapter is presented here to demonstrate the interpretation of the energy-power redistribution.

The total power in the system is

$$P = \iiint_{V_\infty} \left\{ \bar{J}_o^* \cdot \bar{E}_o + \bar{J}_o^* \cdot \bar{E}_a + \bar{J}_e^* \cdot \bar{E}_o + \bar{J}_e^* \cdot \bar{E}_a \right\} dV \qquad 4\text{-}47$$

$$= P_1 + P_2 + P_3 + P_4$$

where $\bar{J}_o$ is the excitation current driving $\bar{E}_o$. The first term P_1 represents the power associated with the primary source field, E_o; the second, represents power associated with the interaction of $\bar{J}_o$ with the backscattered field of the scatterer, $\bar{E}_a$; the third term represents the power flow into scattering body from the primary field, $\bar{E}_o$; the fourth term represents the power contained in the scattered field of the body in the absence of any external field. In general, the interaction of the scatterer with the source current is negligible. In most treatises on scattering, the interaction of the scattered field with the source is implicitly assumed to be negligible. When interaction of the source-scatterer is negligible, $\bar{J}_o$ and $\bar{E}_o$ are independent of the scattered field $\bar{E}_a$ and the first term of 4-45 P_1 is constant. The power redistribution due the presence of the scatterer is given by

$$\Delta P = P_2 + P_3 + P_4 \qquad 4\text{-}48$$

In the problems solved in chapter 6 and 7, the source fields $\bar{J}_o$ and $\bar{E}_o$ are assumed independent of the backscattered fields.

The power associated with the equivalent current, $\bar{J}_e$, is described

primarily by the term P_4. From equations 4-10 , 4-11 and 4-22

$$P_4 = \frac{(\bar{J}_e^*, \bar{J}_e)}{\sigma_a} - (\bar{J}_e^*, \Sigma(\bar{J}_e)) \qquad 4\text{-}49$$

$$= \frac{(\bar{J}_e^*, \bar{J}_e)}{\sigma_a} - (\bar{J}_e^*, \bar{E}_o)$$

In this form P_4 is the difference between the power ohmically dissipated and/or stored in the anomalous region and that extracted from the primary field $\bar{E}_o$.

The redistribution of power associated with P_4 is explored in more detail with the aid of Poynting's theorem. P_4 is split into its intrinsic components by

$$P_4 = (\bar{J}_e^*, \bar{E}_a)$$

$$= \iiint_{V\infty} \left\{ \bar{\nabla} \times \bar{H}_a^* - \sigma_b^* \bar{E}_a^* \right\} \cdot \bar{E}_a \, dV \qquad 4\text{-}50$$

$$= \iiint_{V\infty} \left\{ -\bar{\nabla} \cdot (E_a \times H_a^*) + j\omega\mu_o \bar{H}_a \cdot \bar{H}_a^* - \sigma_o \bar{E}_a \cdot \bar{E}_a^* \right\} dV$$

Rewriting the complex background conductivity in terms of the real conductivity and permitivity $\sigma_b = \sigma_b' - j\omega\epsilon_b$

$$P_4 = \iiint_{V\infty} \left\{ -\bar{\nabla} \cdot (\bar{E}_a \times \bar{H}_a^*) + j\omega\mu_o \bar{H}_a \cdot \bar{H}_a^* - j\omega\epsilon_b \bar{E}_a \cdot \bar{E}_a^* - \sigma_b' \bar{E}_a \cdot \bar{E}_a^* \right\} dV \qquad 4\text{-}51$$

The terms of P_4 have simple physical interpretations; the first term is just the divergence of the Poynting vector and represents the power re-radiated by the scatterer; the second and third term represent the time-varying generalization of the magneto-and electrostatic power storage; the fourth term is the ohmic dissipation of power in the background medium.

4-6 Summary

The preceding analysis has been aimed at pointing out some of the general features of the solutions of scattering problems. The results are concerned specifically with electric scatterers; analogous results can be readily derived

for magnetic scatterers. Many of the general features of $\bar{J}_e$ derived here will appear specifically when numerical solutions to some scattering problems are analysed in chapters six and seven.

CHAPTER 5

Variational Methods for the Approximate Numerical Solution of Integral Equations

5-1 Background

In many instances, the mathematical formulation of a physical problem results in an integral equation either because it is the only way the problem can be expressed or because it is most conveniently expressed in this manner. The geometry of the problem is invariably one which is not amenable to analytic solution by conventional methods. A closed form solution for the eigenfunctions of the system is not attainable; as a result, some form of numerical method of solving the equations must be found. The following analysis is devoted to the variational approach of numerically solving integral equations; the emphasis is placed on the nature of the techniques and discussion of the more esoteric theory of integral equations is kept to a minimum.

The general integral equation of interest has the form

$$a\,\mathcal{U}(P) + \int_V \mathcal{K}(P,Q)\,\mathcal{U}(Q)\,dV = \mathcal{F}(P) \qquad 5\text{-}1$$

where $\mathcal{U}$ and $\mathcal{F}$ can be either scalar or vector, real or complex fields in one or more dimensions. a is a scalar constant. When a is 0, the integral equation is termed an equation of the first kind; when $a \neq 0$, it is called an equation of the second kind. $\mathcal{K}$ is the kernel of the integral equation which can be scalar or tensor and real or complex. The integration is over the region denoted by V which includes all the region of existence of $\mathcal{U}$. P and Q are point coordinates in one or more dimensions. When V is independent of the coordinates P, the equation is a Fredholm integral equation; when V is a function of P, it is called a Volterra

integral equation. General discussions on the theory of integral equations are given in Morse and Feshbach (1953) and Green (1969). Some analyses related to the numerical problems are given by Mikhlin (1964) and Kopal (1961).

5-2 Numerical Problem and Notation

The problem at hand is to find $\mathcal{U}$ given $\mathcal{J}$. From a numerical computation standpoint, the integral equation, which corresponds to an infinite set of linear equations in an infinite set of unknowns, must be reduced to a finite set of N equations in N unknowns where N can be made sufficiently small to make solution tractable by computer. The numerical problem is to find a satisfactory approximation to $\mathcal{U}$ which is denoted by $\mathcal{U}_N$ and is characterized by N unknown parameters. $\mathcal{U}_N$ is subject to the constraint that the deviation of $\mathcal{U}_N$ from the true $\mathcal{U}$, obtained by some error estimator, be sufficiently small and at the same time make N as small as possible.

The method of solution most commonly used and most easily implemented is to digitize $\mathcal{U}$ at N points in V; the integral is then converted to a sum and the error criterion applied is that

$$\left| a\,\mathcal{U}_N(P_i) + \sum_{r=1}^{N} \mathcal{K}(P_i, Q_r)\,\mathcal{U}_N(Q_r) - \mathcal{J}(P_i) \right| \equiv 0 \qquad 5\text{-}2$$

at the N discrete points. A more sophisticated version of this technique is to assume some interpolating function between the points and evaluate the integral numerically or analytically if possible and then apply 5-2. While this approach is quite straighforward, it is only feasible in one or two dimensions since, if one assumes n samples per dimension, $N = n^m$ discrete values are needed in m dimensions and N soon becomes unmanageable for economical computation. It is therefore desirable to find an approximation to $\mathcal{U}$ which carries the most information for a given N.

The major difficulty encountered in numerical problems is the estimation

of error. While some problems can be analysed fully and error bounds estimated with reasonable accuracy, most numerical solutions can only be judged satisfactory after the fact, owing to the complexity of the problem. Accuracy of the solution for a given N must be determined by application of the numerical technique to problems with known analytical solutions as a check or by comparison with experimental data.

In the next two sections, the variational or minimization methods called the least squares method and the Galerkin method are considered. In order to formulate these techniques in a compact form, the following suppositions and definitions are given. The kernel of the integral equation is assumed to be quadratically integrable, and the integral operator is assumed to be definite. (Morse and Feshbach, 1953).

First, the equation is rewritten as

$$\mathcal{L}(u) - g = 0 \qquad 5\text{-}3$$

where $\mathcal{L}$ denotes a linear operator which corresponds to the constant plus integral operator in this particular case. Next, the weighted inner product of a pair of functions is defined as

$$(A, B)_W = \int_V A(P)\, B(P)\, W(P)\, dP \qquad 5\text{-}4$$

where W is a positive definite weighting function. (A, B) indicates a unit weighting function is used. Expression 5-4 then corresponds to the inner product used in chapter 4. For vectors this operation implies the vector dot product is taken as well.

5-3 Least Squares Method

The least squares method is based on minimization of the error generated by approximating u by u_N in the governing equation. The approximate solution is defined in terms of N parameters

$$u_N = \mathcal{F}(\alpha_1, \alpha_2 \cdots \alpha_N) \qquad 5\text{-}5$$

The choice of $\mathcal{F}$ is completely arbitrary and is made using all prior knowledge of the behaviour of the true solution u. The only requirements on $\mathcal{F}$ in the following analysis is that u_N be a linear function of the α_i. In general the choice of the approximating function should be one such that as $N \to \infty$ the resulting function will span V. For example, U_N might be an expansion of the form

$$u_N = \sum_{i=0}^{N-1} \alpha_i \varphi_i \qquad 5\text{–}6$$

where φ_i, $i=0,N-1$ are part of a complete set of functions which span the region V. The φ_i could be N terms of a power series expansion or a Fourier series expansion. If u is known to have singular points in V, the approximating function should contain a term which has the same type of singularity but with an unknown magnitude.

Upon substitution of u_N into the governing equation, 5-3 becomes

$$\mathcal{L}(u_N) - g = \Theta \qquad 5\text{–}7$$

where Θ is the error generated at any point in V due to the inadequacy of U_N in approximating the true solution U. The total squared error over the region V is defined as

$$\mathcal{H} = (\Theta, \Theta)_w \qquad 5\text{–}8$$

(If Θ is complex $\mathcal{H} = (\Theta^*, \Theta)_w$). The weighting function is used to bias the error to achieve higher accuracy in regions known to be critical to the true solution u. The optimum solution in the least squares sense for the set of N parameters is given by the N equations

$$\frac{\partial \mathcal{H}}{\partial \alpha_i} \equiv 0 \qquad i = 0, N-1 \qquad 5\text{–}9$$

or the 2 N equations,

$$\frac{\partial \mathcal{H}}{\partial \alpha_i} \equiv 0 \qquad \frac{\partial \mathcal{H}}{\partial \alpha_i^*} = 0 \qquad i = 0, N-1 \qquad 5\text{–}10$$

if the functions are complex.

For the approximate solution form given by equation 5-6, the equations become

$$a_p \, Re(\mathcal{L}_{pq}) - b_p \, Im(\mathcal{L}_{p,q}) = Re(\mathcal{S}_q) \qquad 5\text{-}11$$

$$a_p \, Im(\mathcal{L}_{pq}) + b_p \, Re(\mathcal{L}_{p,q}) = Im(\mathcal{S}_q)$$

where

$$\alpha_i = a_i + j\, b_i$$

$$\mathcal{L}_{pq} = (\mathcal{L}^*(\varphi_p), \mathcal{L}(\varphi_q))_w \qquad 5\text{-}12$$

$$\mathcal{S}_q = (\mathcal{L}^*(\varphi_q), \mathcal{S})_w$$

5-4 Galerkin Method

The Galerkin method or as it is sometimes called the Bobnov-Galerkin method is a generalized form of the Ritz method. In physical problems it corresponds to an energy or power minimization technique. The formulation has many features in common with the least squares method.

An approximate solution is defined in terms of N test or trial functions

$$\mathcal{U}_N = \sum_{i=1}^{N} \alpha_i \varphi_i \qquad 5\text{-}13$$

The φ_i are arbitrary and the choice should be weighted by any prior knowledge of the solution to the problem. The comments given in the least squares section also apply here. In the Galerkin method, the unknown α_i are determined by the requirement that the residual or error,

$$\Theta = \mathcal{L}(\mathcal{U}_N) - \mathcal{S} \qquad 5\text{-}14$$

generated by the approximation, be orthogonal to the trial functions φ_i ; that is

$$(\varphi_i, \Theta) \equiv 0 \qquad 5\text{-}15$$

The condition can be derived by minimization of the function

$$(\mathcal{U}_N, \Theta) \qquad 5\text{-}16$$

w.r.t. α_i which may be interpreted as a minimization of the energy or power associated with the error. In a physical problem such as an electromagnetic scattering problem, $\mathcal{U}$ may be a current density field and the operator $\mathcal{L}(\mathcal{U})$ the electric field associated with $\mathcal{U}$. In this case 5-16 would have the dimensions of power density.

Upon application of this condition to the governing equation, the equation is reduced to N linear equations in the unknown α_i , which have the form

$$\sum_p \alpha_p \left(\varphi_q, \mathcal{L}(\varphi_p) \right) = \left(\varphi_q, \mathcal{G} \right) \qquad 5\text{-}17$$

5-5 Summary

In the two preceding sections two techniques of reducing an integral equation to a set of linear equations by a variational approach have been outlined. There is a close relationship between the Galerkin method and the least squares method. Discussion of the relationship between the two as well as convergence proofs for particular problems are given by Mikhlin (1964). The application of these methods to some geophysical problems is demonstrated in the next two chapters.

CHAPTER 6

SCATTERING FROM TWO-DIMENSIONAL STRUCTURES

6-1 Introduction

The electromagnetic response of 2-dimensional bodies provides a starting point to examine numerically some of the results discussed from the theoretical viewpoint in the previous chapters. The nature of 2-dimensional scattering problems of geophysical interest and the numerical methods used to solve them were briefly reviewed in chapter 1. The problem analysed in this chapter is the response of a 2-dimensional conductive cylinder of rectangular cross-section embedded in a conductive half-space. This model was chosen for two reasons:

(1) The geometry is the most simple and at the same time permits modelling of a wide variety of structures.

(2) Data were available from other numerical solutions and from scale model experiments to provide a check on the computed results.

The response of an infinitely long cylinder embedded in a half-space parallel to the plane of the half-space surface splits into two distinct response types. In the following, these two types are denoted as the TE and TM response. The TE (transverse electric) response implies that the electric field is parallel to all structural boundaries. The TM (transverse magnetic) response implies that the magnetic field is parallel to all structural boundaries. The two types of response are sketched in Fig. 6-1.

The detailed geometry of the model for numerical analysis is shown in Fig. 6-2. The cartesian coordinate system is denoted by (x_1, x_2, x_3) and has the associated unit vectors $\hat{e}_1, \hat{e}_2, \hat{e}_3$. The cylinder strike is in the $\hat{e}_2$ direction. The geometry of the model is parameterized in terms of the factors (a_1, a_3, d), the body half-width, the half-thickness and the depth of burial in the half-space. For numerical computation these geometrical

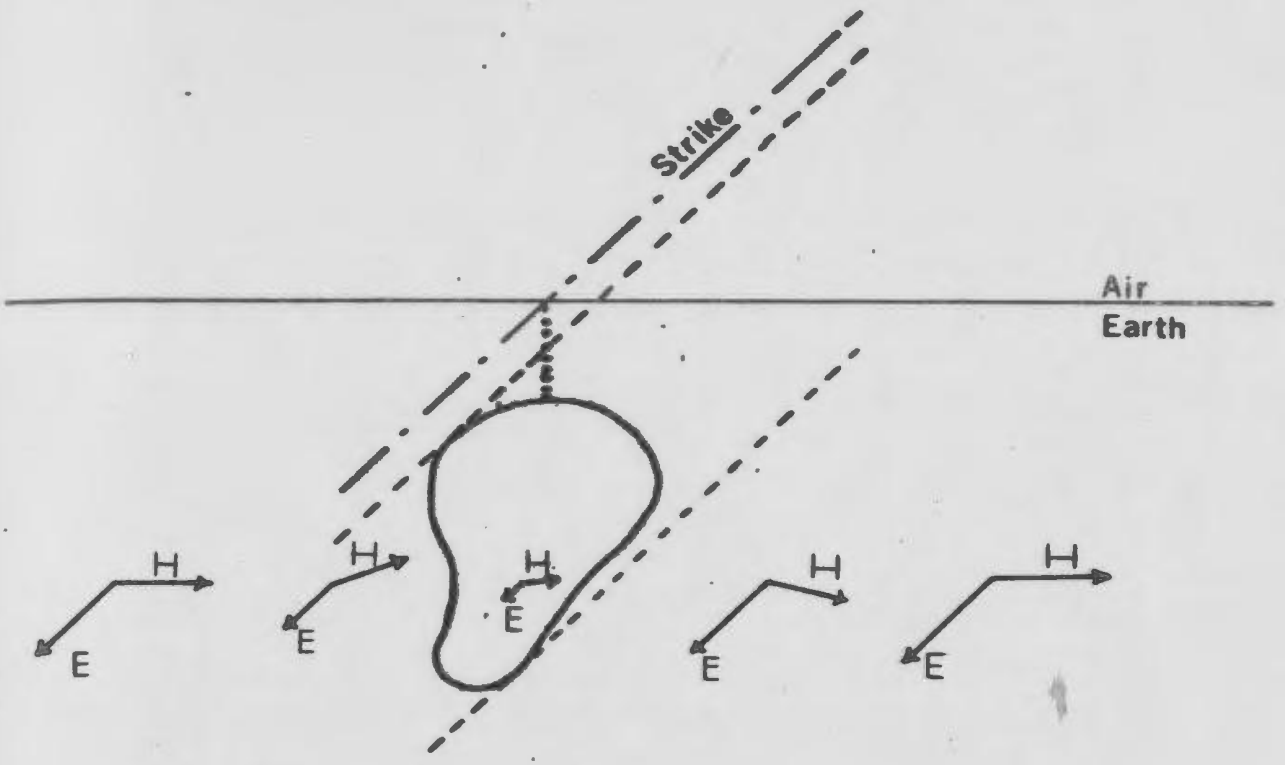

(a) TE 2-Dimensional Structure

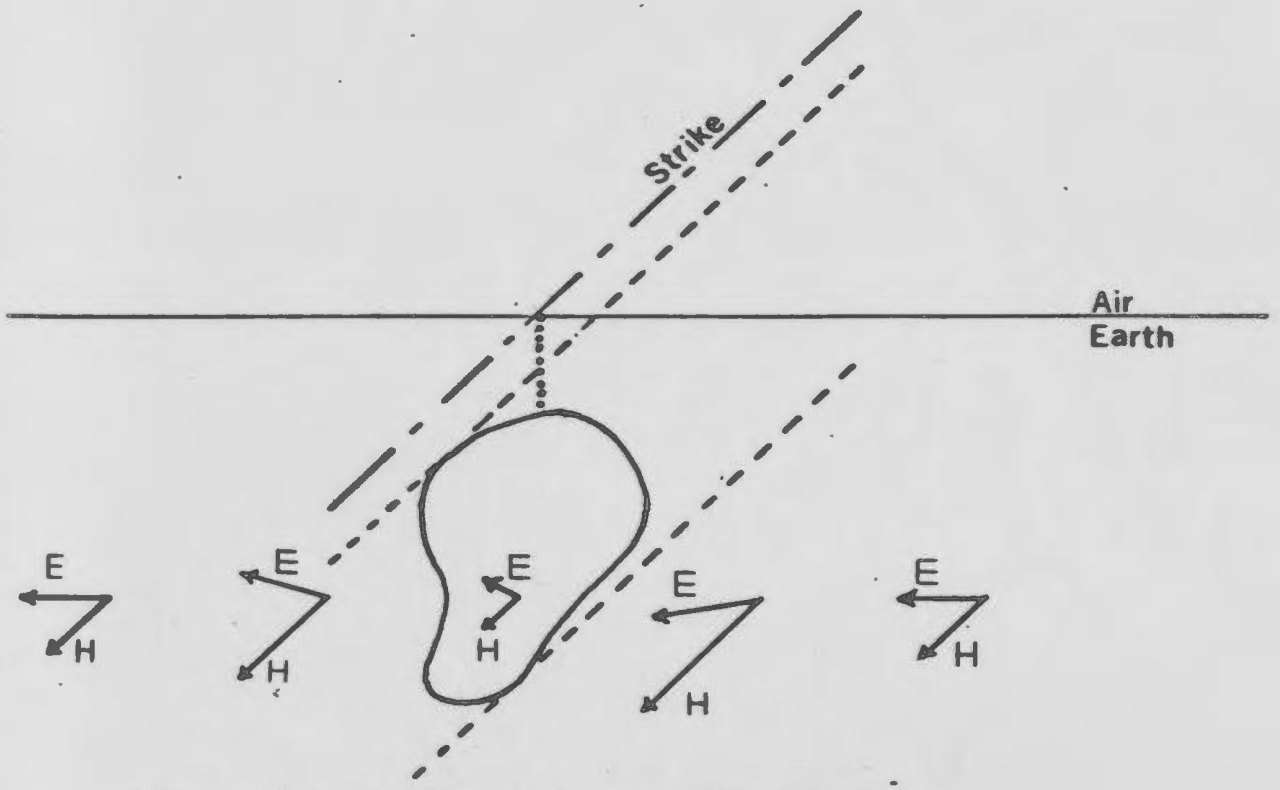

(b) TM 2-Dimensional Structure

FIG 6-1

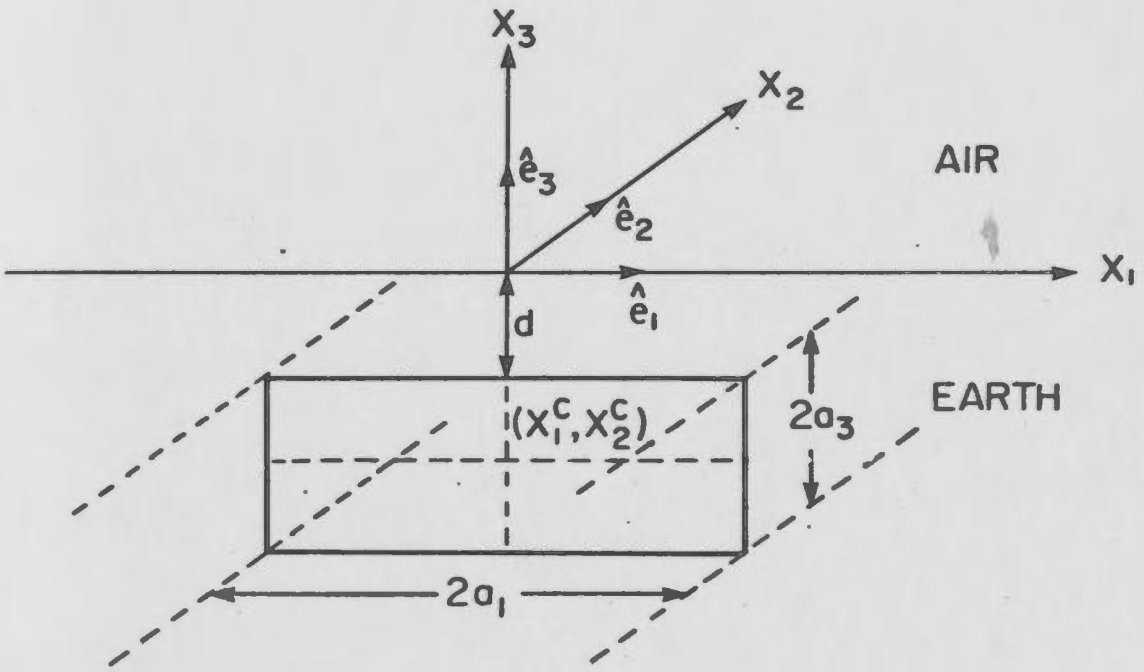

Fig. 6-2 Geometry of 2-dimensional model with a rectangular cross-section

parameters of the structure are normalized against a_1 as follows

$$R = \frac{a_2}{a_1} \qquad 6\text{-}1$$

$$D = \frac{d}{a_1}$$

The body is assumed to have a constant conductivity σ_1 and the background half-space has a conductivity σ_0 . The angular frequency ω is assumed to be sufficiently small that displacement currents are insignificant; there is no need to specify the permittivity of the materials when this assumption is valid. This point is outlined in Appendix C where the evaluation of 2-dimensional Green's function integrals for the conductive earth problem is discussed. The body is assumed to have magnetic properties identical to those of the surrounding half-space. The permeability of the whole system is taken as μ_0 , the free-space permeability.

When displacement currents are negligible, the skindepth of the background medium provides a good base to normalize all lengths. The background skindepth is

$$\delta_0 = \left(\frac{2}{\omega \mu_0 \sigma_0}\right)^{1/2} \qquad 6\text{-}2$$

and a_1 is defined as

$$a_1 = A\,\delta_0 \qquad 6\text{-}3$$

Next, the anomalous conductivity is given by $\sigma_a = \sigma_1 - \sigma_0$ and the body is characterized by the four parameters (A, R, D, σ_a). In the next two sections, the integral equations governing the two response types are derived and the approximate solutions to some typical models are computed using the least squares method discussed in chapter 5.

6-2 TE Response

(i) Integral equation

The TE response of the cylinder is formulated in terms of an equivalent

current $\bar{J}_e$ which has only an $\hat{e}_2$ component. For simplicity, J_e will be used to denote this component. J_e is invariant in the x_2 coordinate and using the 2-dimensional TE Green's function derived in appendix B, J_e satisfies the scalar Fredholm equation

$$\frac{J_e(r)}{\sigma_a} - j\omega\mu_o \int_{-a_1}^{a_1}\int_{-a_3}^{a_3} g(r,r')\, J_e(r')\, d^2r' = E_o(r) \qquad 6\text{-}4$$

where $\bar{E}_o(r)$ is the exciting electric field which also has only an $\hat{e}_2$ component and

$$g(r,r') = L_o(r,r') + L_1(r,r') \qquad 6\text{-}5$$

The explicit forms of L_o and L_1 are given in appendices B and C.

The approximating function for J_e was chosen to be a two dimensional expansion in Chebychev polynomials of the form

$$J_e(r) = \sum_{n=0}^{N}\sum_{m=0}^{M} c_{nm}\; T_n\left(\frac{x_1 - x_1^c}{a_1}\right) T_m\left(\frac{x_2 - x_2^c}{a_3}\right) \qquad 6\text{-}6$$

where $(x_1^c,\ x_3^c)$ are the coordinates of the centre of the cylinder. $T_n(z)$ denotes the Chebychev polynomial of degree n and the first kind. The approximate solution is characterized by a total of $(M + 1)\ (N + 1)$ unknown coefficients. At this point it is convenient to introduce a set of normalized coordinates

$$\xi = \frac{x_1 - x_1^c}{a_1} \qquad \eta = \frac{(x_3 - x_3^c)}{a_3} \qquad 6\text{-}7$$

With the above approximation for J_e, the least squares solution can be formulated. First, the integral coefficient $\mathcal{L}_{nm}$ is defined as

$$\mathcal{L}_{nm} = \int_{-1}^{1}\int_{-1}^{1} T_n(\xi')\, T_m(\eta')\, g(\xi,\xi',\eta,\eta')\, d\xi'd\eta' \qquad 6\text{-}8$$

Substitution of the approximation for J_e into the integral equation yields

$$\sum_{n,m} c_{nm} \left\{ \frac{T_n(\xi) T_m(\eta)}{\sigma_a} - j\omega\mu_o \delta_o^2 A^2 R \mathcal{L}_{nm}(\xi,\eta) \right\} - E_o(\xi,\eta) = \Theta(\xi,\eta) \qquad 6\text{-}9$$

where Θ is the error generated by the approximation of J_e expression 6-6. Since the evaluation of $\mathcal{L}_{nm}$ cannot be carried out analytically, a discrete estimate of the total squared error was used in place of 5-8 and is defined as

$$\mathcal{W}_D = \sum_p \sum_q \Theta^*(\xi_p, \eta_q)\, \Theta(\xi_p, \eta_q) \qquad 6\text{-}10$$

where (ξ_p, η_q) are a discrete set of points in the range $-1 \leq \xi, \eta \leq 1$. For computational purposes, the set of error points (ξ_p, η_q) were chosen as the roots of the Chebychev polynomials $T_p(\xi)$ and $T_Q(\eta)$ where $P, Q > N, M$. This choice was made for two reasons; first, the set of Chebychev polynomials $T_i(x)$ $i = 1, \ldots, (Q-1)$ form a discrete set of orthogonal polynomials on the set of points which are the roots of the Chebychev polynomial $T_Q(x)$; second, the roots of T_Q are unevenly distributed in the interval (-1, 1) with the concentration of roots being most dense near the end points ± 1 and least dense near 0. This in effect biases or weighs the solution in the outer region of the body more heavily than in the central part of the body in the determination of the total squared error $\mathcal{W}_D$. This is compatible with the skindepth effect which results in most of the current flowing near the surface of a good conductor.

The real and imaginary parts of the c_{nm} are denoted by

$$c_{nm} = \alpha_{nm} + j\,\beta_{nm} \qquad 6\text{-}11$$

The impedance operator for an individual element in the expansion is defined as

$$Z_{nm}(\xi,\eta) = \frac{T_n(\xi) T_m(\eta)}{\sigma_a} - j\omega\mu_o \delta_o^2 A^2 R \mathcal{L}_{nm}(\xi,\eta) \qquad 6\text{-}12$$

and the total squared error becomes

$$\mathcal{W}_D = \sum_{p,q} \left(\sum_{nm} c_{nm} Z_{nm} - E_o \right) \left(\sum_{rs} c_{rs}^* Z_{rs}^* - E_o^* \right) \qquad 6\text{-}13$$

Next, $\mathcal{W}_D$ is minimized w.r.t. c_{nm} and c_{nm}^* which yields the set of $2(N + 1)(M + 1)$ linear equations

$$\sum_{nm} \mathcal{K}_{rsnm} \alpha_{nm} - \mathcal{T}_{rsnm} \beta_{nm} = S_{rs}^1 \qquad 6\text{-}14$$

$$\sum_{nm} \mathcal{T}_{rsnm} \alpha_{nm} + \mathcal{K}_{rsnm} \beta_{nm} = S_{rs}^2 \qquad 6\text{-}15$$

where

$$\mathcal{K}_{rsnm} = \text{Real} \sum_{pq} Z_{rs}^* Z_{nm} \qquad 6\text{-}16$$

$$\mathcal{T}_{rsnm} = \text{Imag} \sum_{pq} Z_{rs}^* Z_{nm} \qquad 6\text{-}17$$

$$S_{rs}^1 = \text{Real} \sum_{pq} Z_{rs}^* E_o \qquad 6\text{-}18$$

$$S_{rs}^2 = \text{Imag} \sum_{pq} Z_{rs}^* E_o \qquad 6\text{-}19$$

At this point the first step towards the numerical solution of the integral equation is complete; the integral equation has been reduced to solving a finite set of linear equations in terms of a finite set of unknowns. The steps in the numerical computation are outlined in the next subsection.

(ii) Numerical Solution

The numerical solution of 6-14 and 6-15 consists of three basic steps. The first step in the analysis is the development of a numerical algorithm to evaluate the integrals $\mathcal{L}_{nm}$. The second stage in the analysis is the evaluation of the scattering matrix elements $\mathcal{K}_{rsnm}$ and $\mathcal{T}_{rsnm}$ using the results of the first step. The final step is the inversion of the scattering matrix to find the coefficients for the polynomial expansion of the equivalent current and computation of anomalous fields generated by the equivalent

current.

The model and solution parameters are summarized in Table 6-1 and a flow chart of the numerical analysis is shown in Fig. 6-3. The integrals $\mathcal{L}_{nm}$ are dependent only on the geometry of the anomalous structure and are independent of the anomalous electrical properties. The $\mathcal{L}_{nm}$ were evaluated using the method outlined in appendix D. The coefficients were evaluated at the set of error points (ξ_p, η_q) and were used as data for the generation of the matrix elements. This step of the analysis required specification of the parameters A, R, D, N, M, P, and Q. The Chebychev polynomials were evaluated numerically by using the recursion relationship

$$T_n(x) = 2x\,T_{n-1}(x) - T_{n-2}(x) \qquad 6\text{-}20$$

and the definition of T_0 and T_1

$$T_0(x) = 1 \qquad T_1(x) = x \qquad 6\text{-}21$$

The error points were determined from the property that the roots of the Chebychev polynomial of degree Q are

$$x_i = \cos\left(\frac{(2i-1)\pi}{2Q}\right) \qquad 6\text{-}22$$

All these properties are given in Abramowitz and Stegun (1965).

Next the source field and the anomalous conductivity were specified. The impedance for each element Z_{nm} was computed at each error point using 6-12 and the matrix elements $\mathcal{K}_{rsnm}$ and $\mathcal{T}_{rsnm}$ and the source coefficients S^1_{rs} and S^2_{rs} were computed by summation over the error points as indicated by equations 6-16 through 6-19. The scattering matrix was inverted using a standard Gaussian elimination method. The equivalent current expansion coefficients were then computed for each excitation field.

The polynomial coefficients were used to compute maps of the equivalent current and to evaluate the anomalous fields associated with J_e. The anomalous electric and magnetic fields are given by

Table 6-1 Summary of TE Solution Parameters

Geometrical

A - cylinder half-width in skindepths

κ - thickness to width ratio

D - burial depth to half-width ratio

Electrical

σ_a/σ_o - anomalous conductivity ratio

Numerical Solution

N - maximum polynomial degree in x_1

M - maximum polynomial degree in x_3

P - number of error points in x_1 dimension

Q - number of error points in x_3 dimension

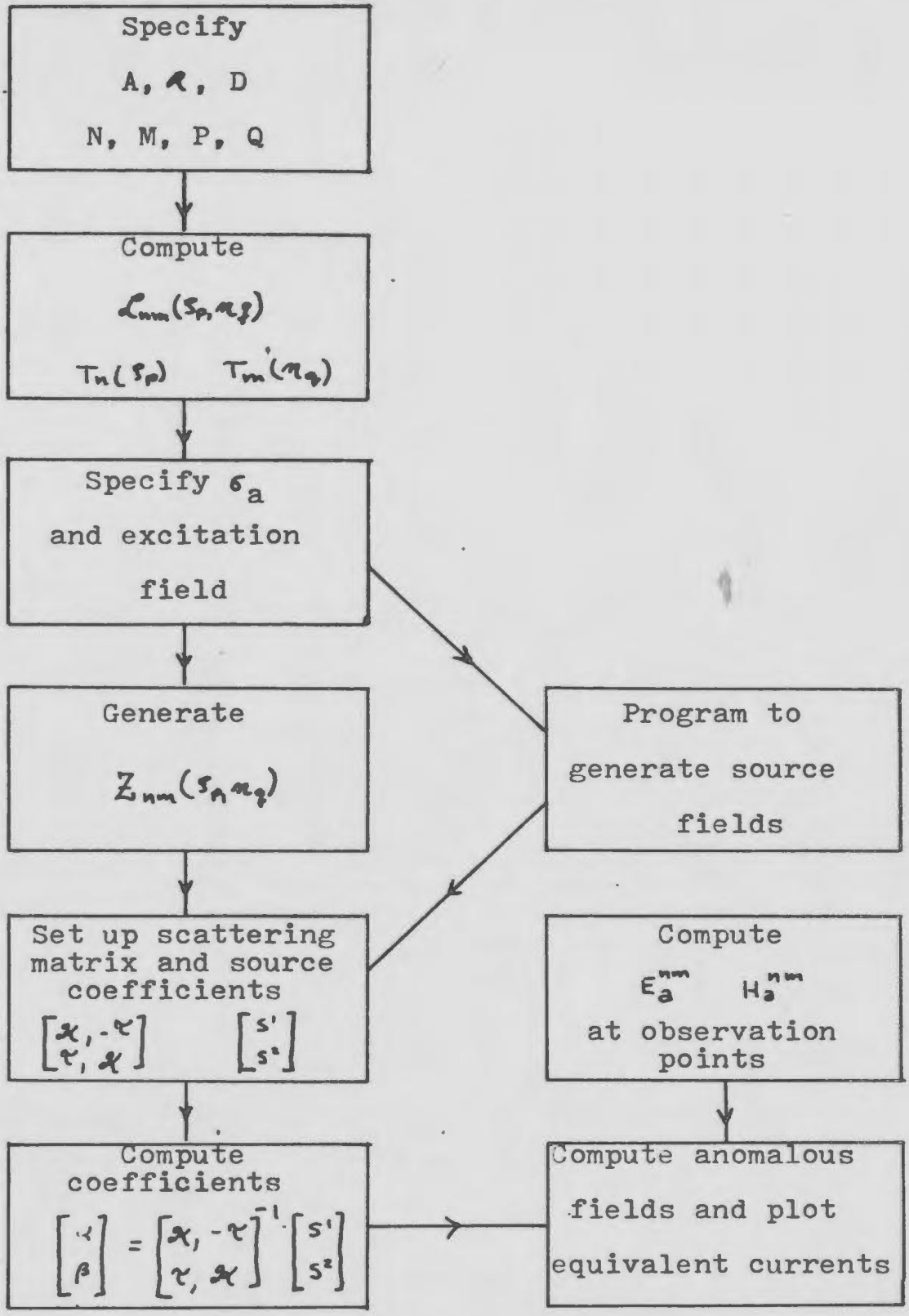

Fig. 6-3 Flow chart of TE Computations

$$E_a = j\omega\mu_0 \int_{-a_1}^{a_1} \int_{-a_3}^{a_3} g(r,r')\, J_e(r')\, dx_1' dx_3' \qquad 6\text{-}23$$

$$\bar{H}_a = \frac{\bar{\nabla} \times (E_a \hat{e}_2)}{j\omega\mu_0} \qquad 6\text{-}24$$

Defining an anomalous field associated with each element in the expansion of J_e, 6-23 and 6-24 become

$$E_a = \sum_{n,m} c_{nm}\, E_a^{nm} \qquad 6\text{-}25$$

$$\bar{H}_a \cdot \hat{e}_1 = \sum_{n,m} c_{nm}\, {}^1H_a^{nm} \qquad 6\text{-}26$$

$$\bar{H}_a \cdot \hat{e}_3 = \sum_{n,m} c_{nm}\, {}^3H_a^{nm} \qquad 6\text{-}27$$

where the coefficients are

$$E_a^{nm}(r) = j\omega\mu_0 \int_{-a_1}^{a_1} \int_{-a_3}^{a_3} g(r,r')\, T_n(s')\, T_m(s')\, dx_1' dx_3' \qquad 6\text{-}28$$

$${}^1H_a^{nm}(r) = -\frac{\partial}{\partial x_3} \int_{-a_1}^{a_1} \int_{-a_3}^{a_3} g(r,r')\, T_n(s')\, T_m(s')\, dx_1' dx_3' \qquad 6\text{-}29$$

$${}^3H_a^{nm}(r) = \frac{\partial}{\partial x_1} \int_{-a_1}^{a_1} \int_{-a_3}^{a_3} g(r,r')\, T_n(s')\, T_m(s')\, dx_1' dx_3' \qquad 6\text{-}30$$

The integral coefficients E_a^{nm} and ${}^1H_a^{nm}$, ${}^3H_a^{nm}$ are independent of the source field and the electrical properties of the body; this information is contained in the C_{nm}. The field coefficients have only to be computed once for a given model geometry.

The computer programs were written to compute the response for any number of source fields and anomalous conductivities for one given model geometry. This maximizes the number of model configurations for a given amount of computer expense, since the numerical quadratures consumed considerately more computer time than any other part of the computations.

As pointed out previously the numerical quadratures have only to be carried out once for a given geometry.

(iii) Numerical Results

The results of computation for a pair of simple models is given in this section. The following results are intended to demonstrate the general nature of the solution method and the computations rather than to give an exhaustive study of the particular models in question. The numerical response is presented in the following format; first, a table of the solution and model parameters accompanied by a sketch of the geometry is given; this is followed by a set of contour maps for the equivalent current; finally some selected anomalous fields are computed and compared with other available results.

TE Model 1

The first TE model was chosen in order that the numerically computed response could be compared with data obtained from a scale model experiment by Farstad (1970). The scale model consisted of a large tank of salt water and a current system which simulated plane-wave excitation (see Farstad 1970). One model studied was the response of a long, thin slab. In terms of the skindepth of the salt solution, the slab had dimensions $a_1 = 0.028\delta_0$, $a_3 = 0.856\delta_0$ and a strike length of $3.58\delta_0$. While the model had a finite strike length, it was sufficiently long that measurements made in the central region of the body should be a reasonable simulation of a 2 dimensional response.

The numerical model chosen to compare with the data is summarized by the list of parameters given in Table 6-2. The conductivity contrast for the scale model was $\sigma_1/\sigma_0 = 36.5$. In the numerical study, a set of three conductivity contrasts of 25, 36.5, 50 were computed in order to show the

Table 6-2 Data for TE Model 1

Geometrical

A = 0.0285

R = 15.0

D = 6.0

Electrical

σ_2/σ_0 = 24.0, 35.5, 49.0

σ_0 = 1 mho/meter

Numerical Solution

N = 2

M = 4

P = 6

Q = 8

Source Types

Plane wave

Sketch of Geometry

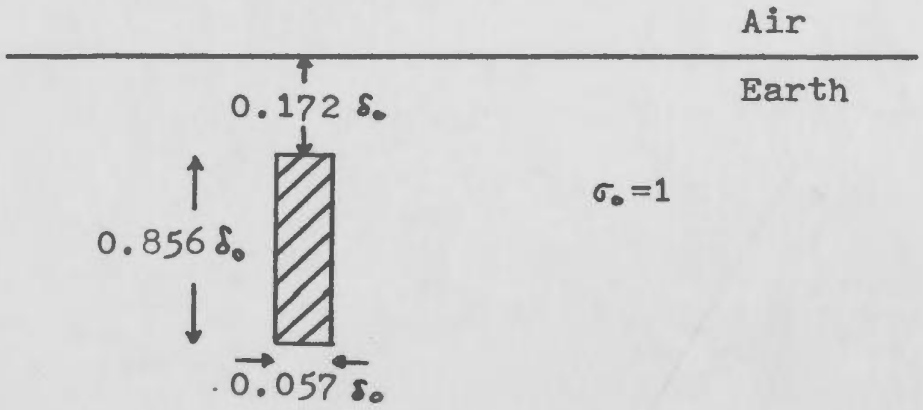

variation of the response with body conductivity. In order to avoid confusion, it should be noted that conductivity contrast and anomalous conductivity contrast are related by

$$\frac{\sigma_1}{\sigma_0} = 1 + \frac{\sigma_a}{\sigma_0} \qquad 6\text{-}31$$

The excitation field is that of a plane wave incident normally on the half-space. The electric field at the surface of the half-space is taken to be 1 volt/m. with a phase of 0 degrees. The electric and magnetic fields as a function of depth in the half-space are then given by

$$\bar{E}_0 = e^{jk_0 x_3}\ \hat{c}_2 \qquad \text{volt/m.} \qquad 6\text{-}32$$

$$\bar{H}_0 = e^{jk_0 x_3}\left(-\left(\frac{\sigma_0}{\omega\mu_0}\right)^{1/2} e^{j\pi/4}\right)\hat{c}_1 \qquad \text{amp/m.} \qquad 6\text{-}33$$

Since $k_0 = (1 + j)/\delta_0$, the fields vary as $e^{(-1+j)x_3/\delta_0}$ with phase rotating through 2π radians and the amplitude decreasing by a factor $e^{-2\pi}$ for $x_3/\delta_0 = 2\pi$. (See Fig. 6-7).

In Fig. 6-4, -5, and -6, contour maps are used to illustrate the equivalent current for the various conductivity contrasts. To keep the maps of J_e uncluttered, the contours were labelled without the 10^n factor. For example, the contour labelled 1.0 in Fig. 6-4 for real J_e implies 1.0×10^1. The power of ten is to be taken from the contour interval (i.e. $0.1 \times \underline{10^1}$). The phase reference for the currents was taken as the electric field at the surface of the half-space. The exciting electric field has a real component which decreases monotonically with depth over the extent of the cylinder; the imaginary component rises and then falls. The primary fields versus depth are shown in Fig. 6-7. The equivalent current depicted in Fig. 6-4 where $\sigma_1/\sigma_0 = 25$, reflects the basic behaviour of the exciting field; however, the field lines are pulled closer to the surface. As the conductivity contrast increases, the constant current lines become more strongly warped upwards

REAL J
CONTOUR INTERVAL IS
0.1E1 AMP/METER²

IMAGINARY J
CONTOUR INTERVAL IS
0.8E0 AMP/METER²

CURRENT MAPS FOR MODEL 1
SOURCE NUMBER 1
CONDUCTIVITY CONTRAST IS 2.50E1

Fig. **6-4**

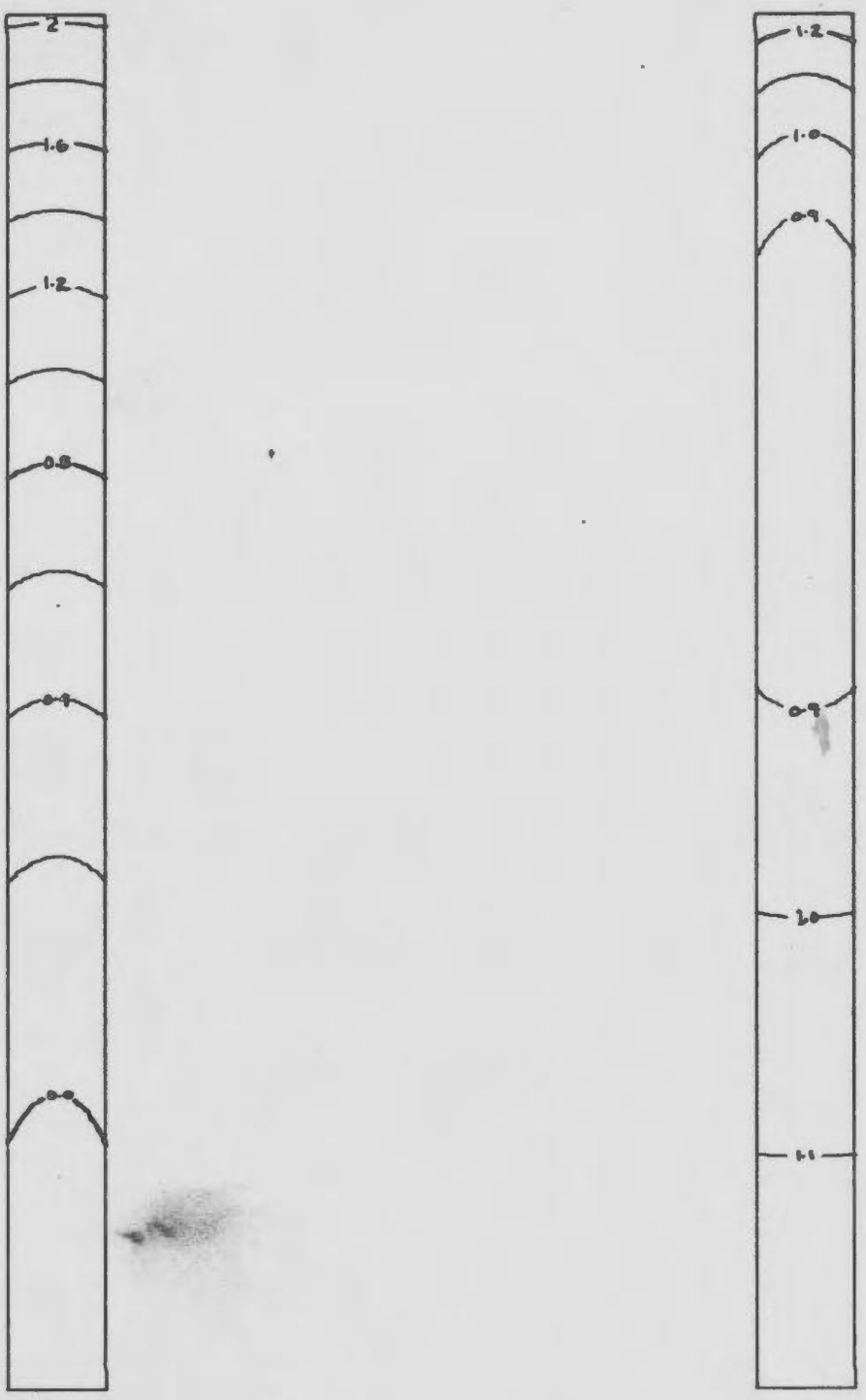

REAL J
CONTOUR INTERVAL IS
0.2E1 AMP/METER^2

IMAGINARY J
CONTOUR INTERVAL IS
0.1E1 AMP/METER^2

CURRENT MAPS FOR MODEL 1
SOURCE NUMBER 1
CONDUCTIVITY CONTRAST IS 3.66E1

Fig. **6-5**

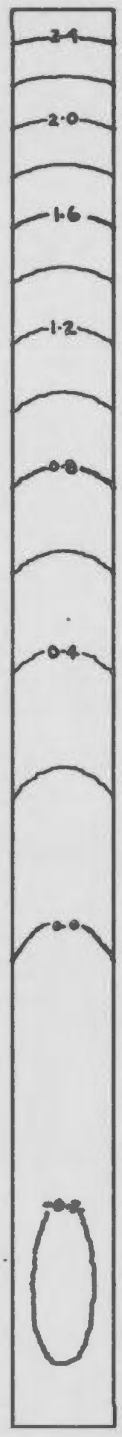

REAL J
CONTOUR INTERVAL IS
0.2E1 AMP/METER^2

IMAGINARY J
CONTOUR INTERVAL IS
0.1E1 AMP/METER^2

CURRENT MAPS FOR MODEL 1
SOURCE NUMBER 1
CONDUCTIVITY CONTRAST IS 5.00E1

Fig. **6-6**

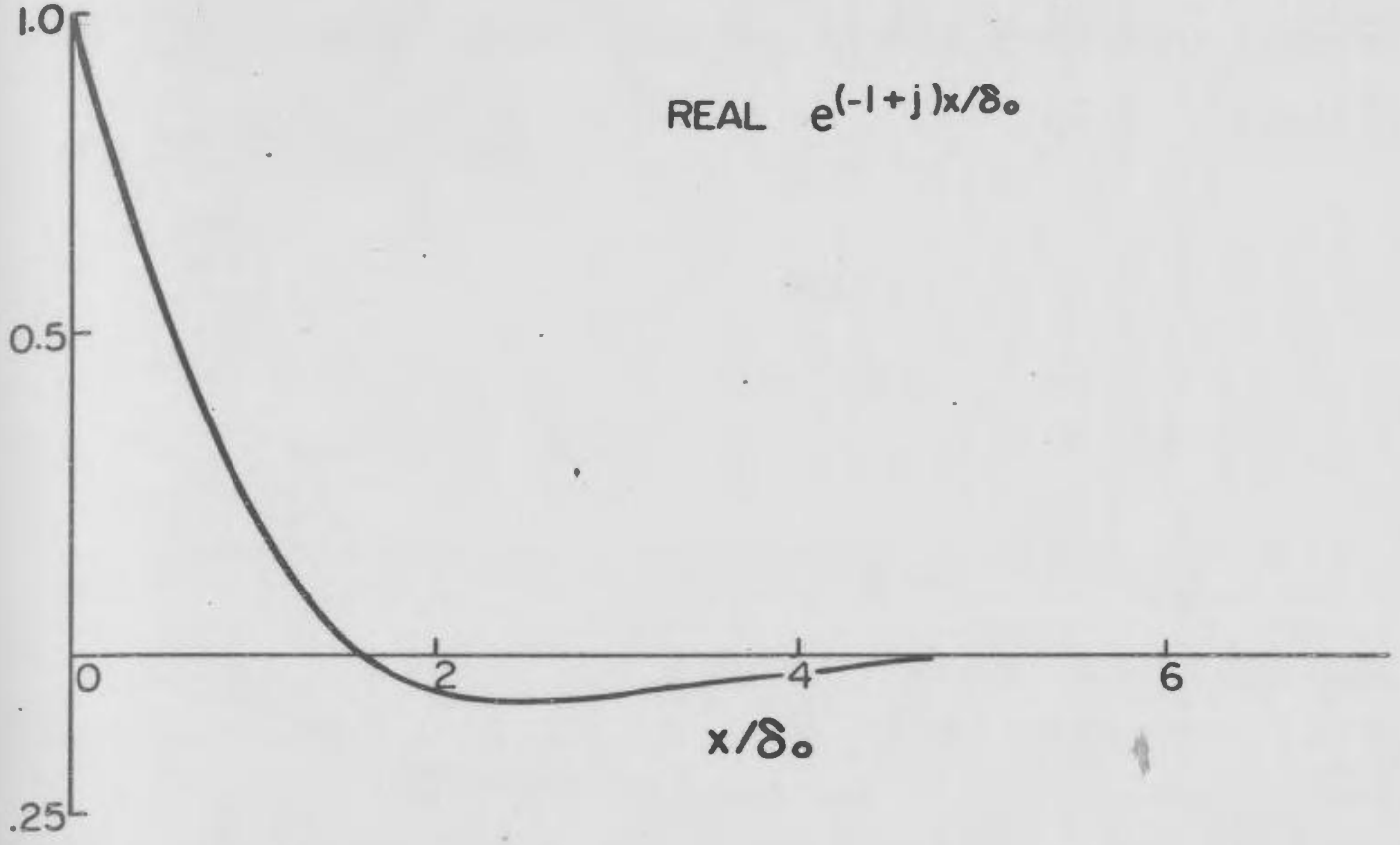

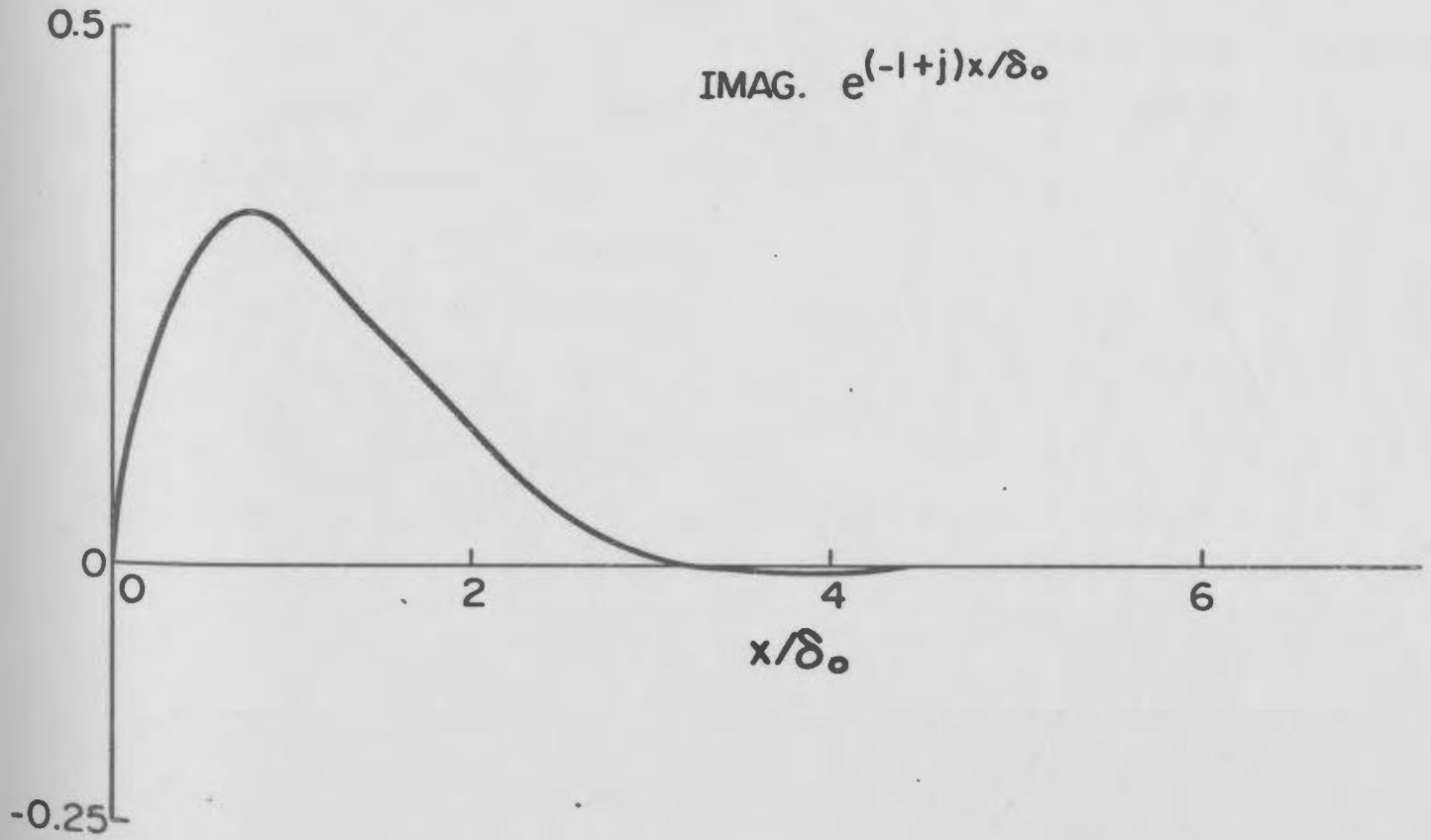

Fig. 6-7 Variation of field strength for a plane wave incident on a conductive half-space

and current flow is being forced towards the outer parts of the body. Since the body is still well below the inductive limit when $\sigma_1/\sigma_0 = 50$, a good percentage of the current still flows in the central region of the body.

Some of the anomalous fields associated with J_e are shown in Fig. 6-9 to 6-10. Fig. 6-9 shows total electric field at the surface of the half-space with

$$E^{N}_{Total} = 1 + \sum c_{nm} E_a^{nm}(x_1, x_3)/E_0 \qquad 6\text{-}34$$

The electric field exhibits a broad minimum which bottoms out directly over the cylinder. The phase of the total electric field exhibits a different behaviour. On the flanks of the body the phase shows a lead of about 3 or 4 degrees; directly over the body the phase lead decreases and for the lower conductivity becomes a lag. The explanation of this behaviour lies in the fact that directly over the body the current near the top of the cylinder, which is also the largest, dominates the secondary field. On the flanks, the anomalous field is generated by the total current flow in the cylinder; the distance to the cylinder is larger and the integral over the cylinder weighs the current contributions more evenly.

The behaviour of E is most easily explained by the phasor diagrams in Fig. 6-8. The analysis gives a gross estimation of the equivalent current and field behaviour (a) for the whole body as an average and (b) for the near surface portion of the body only. While this is somewhat over-simplified synthesis of the response, it does explain the gross features of the anomaly. To some extent, the phase lags due to propagation through the background medium have the effect of making the body look more conductive than it really is since these lags cannot be differentiated from the self-inductive effects which cause a similar lag.

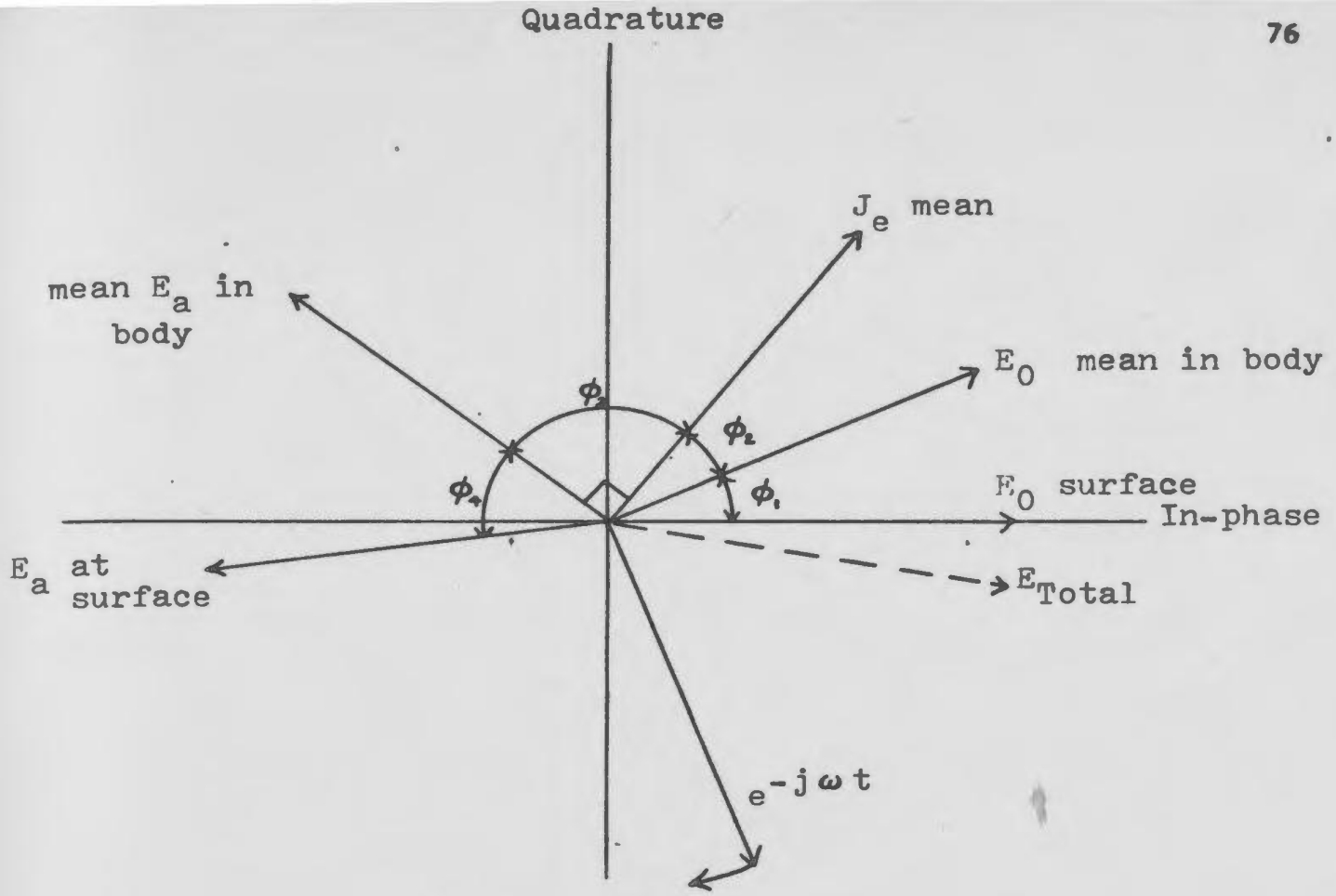

(a) Mean body behaviour

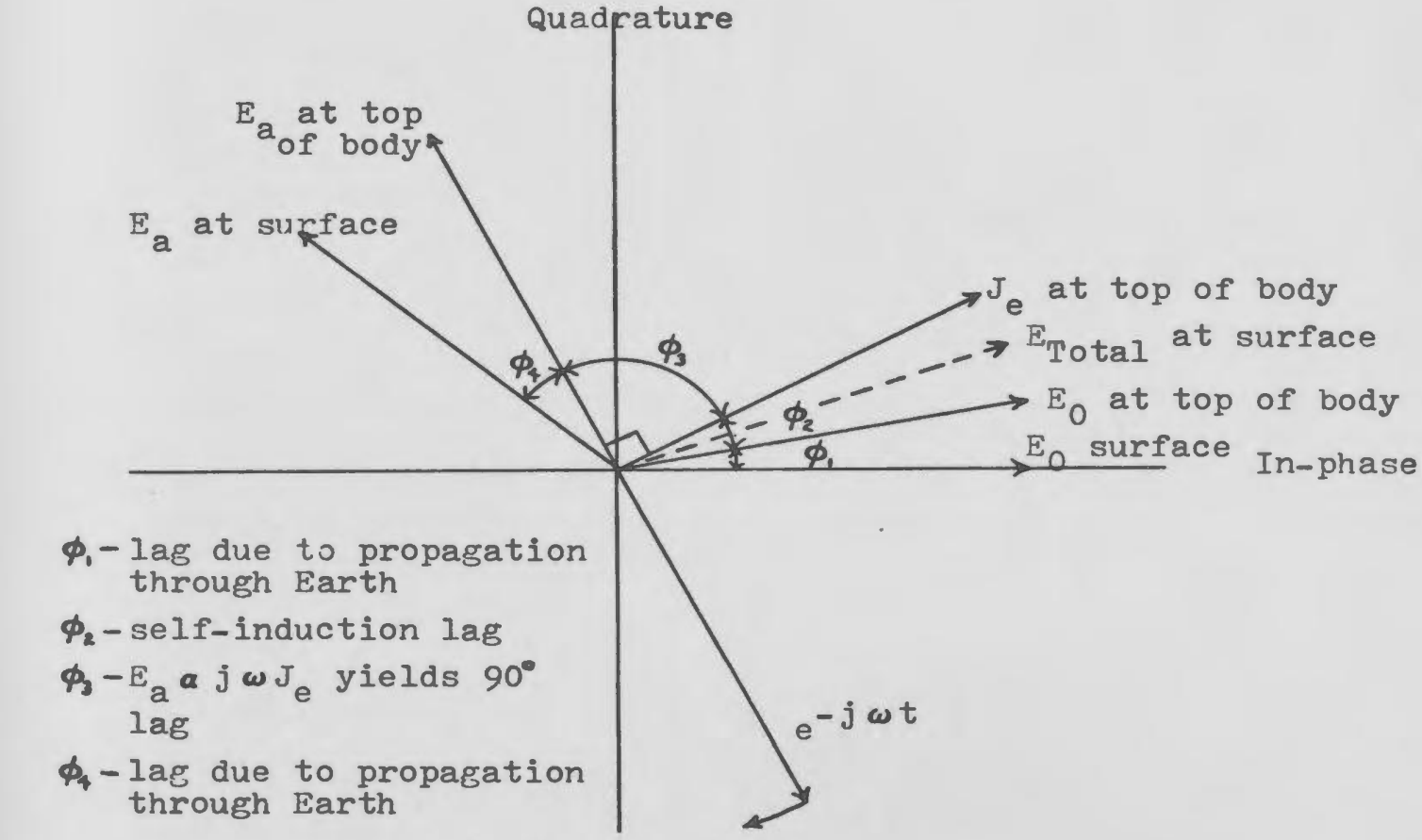

ϕ_1 - lag due to propagation through Earth

ϕ_2 - self-induction lag

ϕ_3 - $E_a \propto j\omega J_e$ yields 90° lag

ϕ_4 - lag due to propagation through Earth

(b) Top of body behaviour

Fig. 6-8 Phasor diagram illustrating physical mechanisms for observed TE anomalies

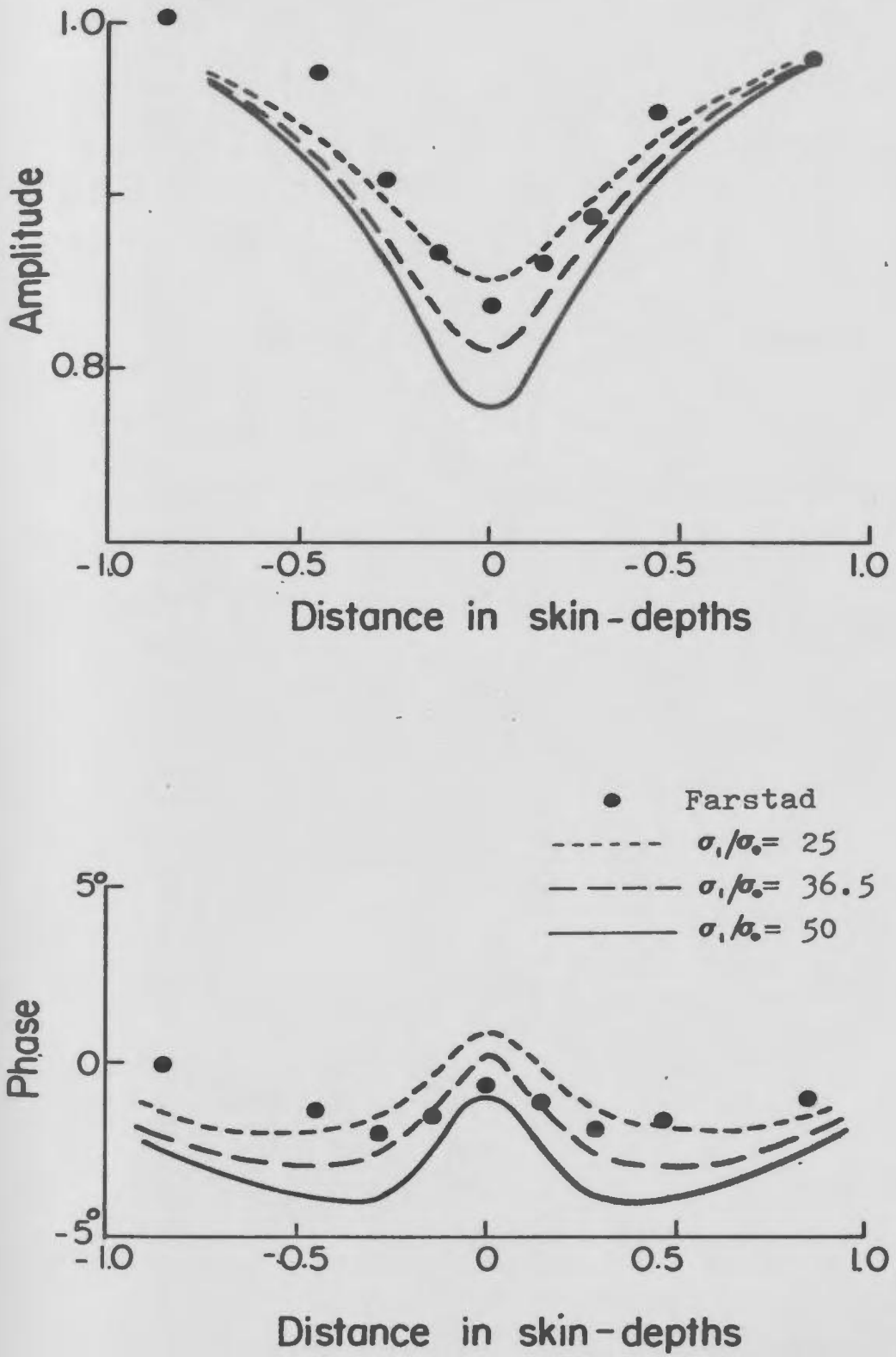

Fig. 6-9 Normalized electric field over TE model #1

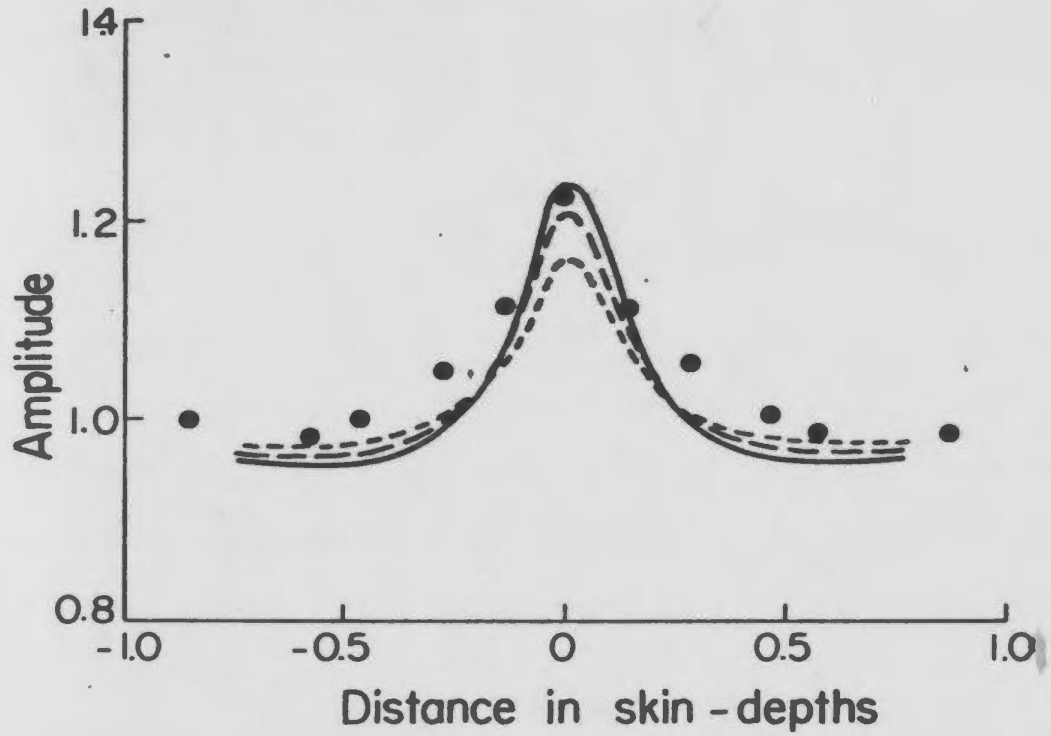

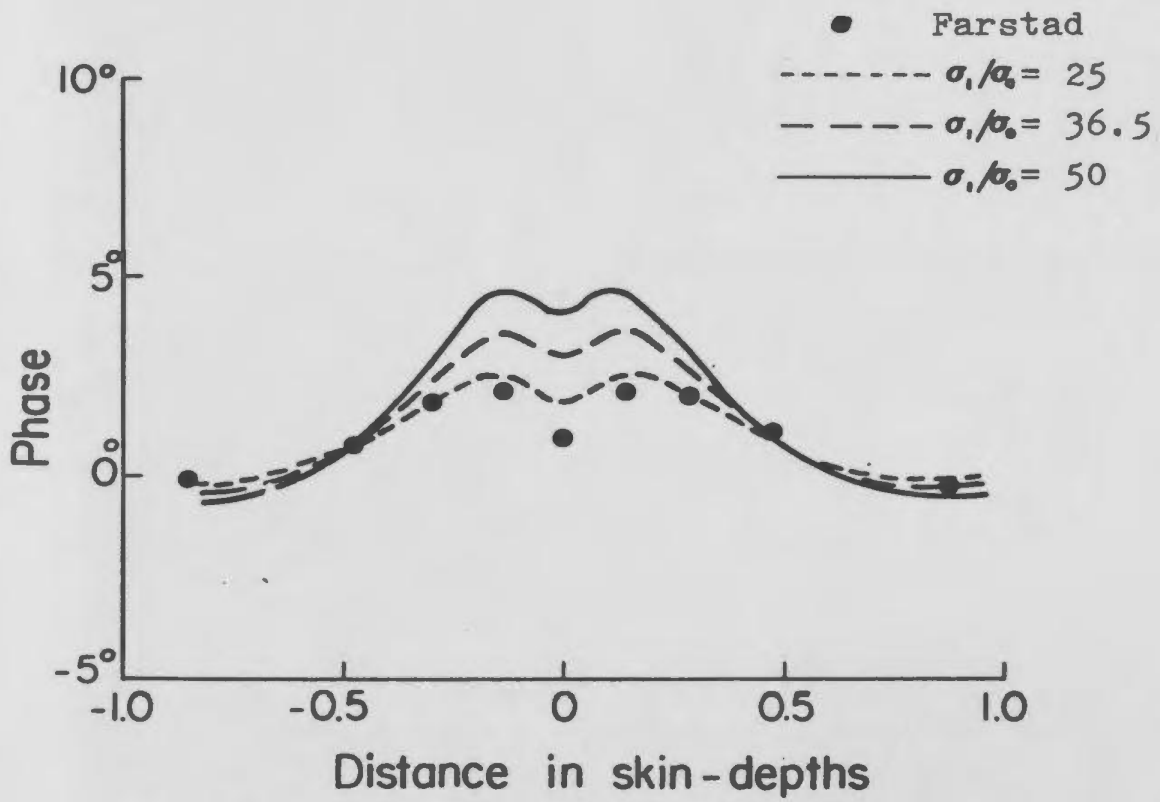

Fig. 6-10 Normalized $\hat{e}_1$ component of magnetic field over TE model #1

In Fig. 6-10, the total H_1 component of the magnetic field at the surface of the half-space is shown. In this diagram, H_1 has been normalized against the primary magnetic field at the surface. The plotted normalized field is

$$'H^N_{Total} = \left\{ 1 + \sum_{n,m} c_{nm}\, 'H^{nm}_a / 'H_o \right\} \qquad 6\text{-}35$$

The total horizontal magnetic field drops below that of the half-space on the flanks of the body and rises to a maximum about 20% above the half-space field directly over the body. The total field lags the primary field except at large lateral distances where it leads slightly. Directly over the body, the field exhibits a dimple in the phase angle and the lag shows a minimum directly over the body. The explanation of this dimple follows that for the electric field behaviour. The current flow at the top of the body strongly influences the anomaly directly over the body. Since the phase of the equivalent current at the top of the body differs from the mean phase of the equivalent current, the phase curve of the anomalous fields shows a fluctuation directly over the body. This fluctuation should be very depth dependent and vanish completely for bodies where the depth of burial makes the distances from any point in the cylinder to the surface more equal. This has been observed experimentally by Farstad (1970).

In Fig. 6-11, the normalized impedance at the surface of the half-space is shown. The normalized impedance is defined as

$$Z_N = \left(\mathcal{E}^N_{Total} \,/\, 'H^N_{Total} \right) = \left(\frac{\mathcal{E}_{total}}{'H_{Total}} \right) \Big/ \left(\frac{\mathcal{E}_o}{'H_o} \right) \qquad 6\text{-}36$$

when $'H_{total}$ and $'H_0$ represent the $\hat{e}_1$ component of $\overline{H}$ only. Aside from normalizing factor Z_N is just the ratio of the curves shown in Fig. 6-9 and 6-10. Z_N shows a smooth variation over the structure dropping to a minimum directly over the body similar in many ways to the electric field

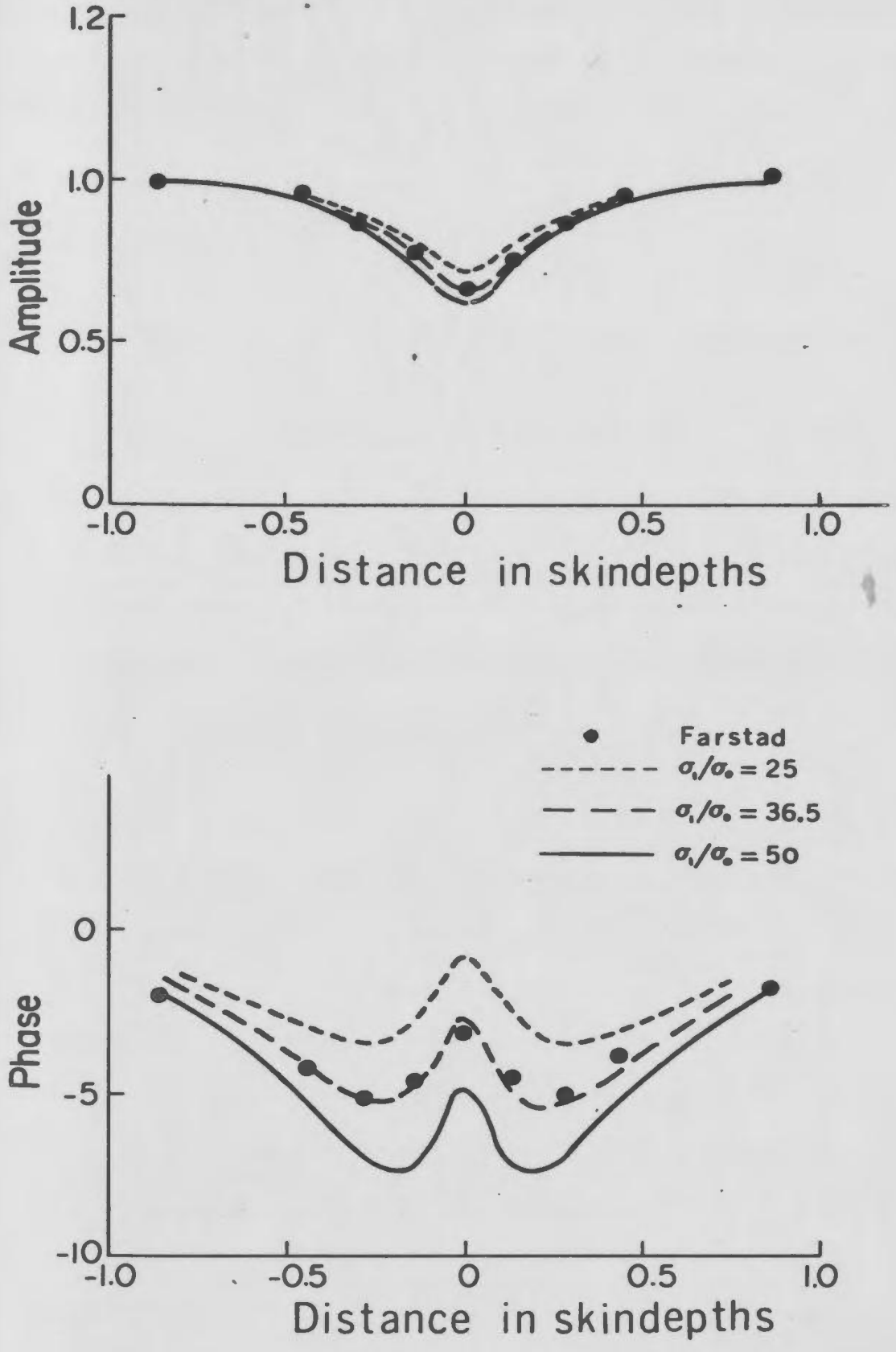

Fig. 6-11 Normalized impedance, Z_N, over TE model #1

variation. The phase shows a lead over most of the spatial range with the dimple directly over the body being even more pronounced. The apparent resistivity ρ_a commonly used in magnetotelluric sounding is given by

$$|\rho_a| = \rho_0 |Z_N|^2 \qquad 6\text{-}37$$

where $\rho_0 = 1/\sigma_0$.

The results of the numerical computation compare favourably with the scale model data collected by Farstad (1970). The experimental data are denoted by •'s on the diagrams in Fig. 6-9, -10, and 11. The amplitudes of the experimental E and H fields do not agree perfectly with the computed data; however, the general shape of the responses is the same. The phase measurements show good agreement in general behaviour but considerable deviations from computed responses occur. The normalized impedance shows much better agreement than the E and H responses.

In general the comparison is encouraging. The deviations between the experimental results and the theoretically computed responses can be rationalized in several ways. The first area in question is the numerical solution. Could some of the approximations be affecting the result? Computational errors were checked by testing the susceptibility of the responses to changes in the numerical computation parameters such as N, M and the accuracy of the numerical integrals. These parameters were found to make little difference to the response. In addition, the programs were checked against other known results (next section of this chapter) and no major discrepancies were found. Another significant factor is the effect of the finite strike length of the body; this effect is difficult to assess quantitatively. Current channelling effects, which saturate very quickly with increasing conductivity contrast, would limit the current in the cylinder to being less than that for an infinitely long body; an under estimation of the electric field anomalies could, therefore, be expected. Another

factor which must be appreciated is the difficulty in designing and constructing a scale model which simulates an idealized structure. The construction of measurement probes which do not significantly alter the system is a difficult task. Whatever the exact cause of the discrepancies in E and H, the effects in the two components oppose each other in computing Z_N since excellent agreement is found for the impedance amplitude and phase.

TE Model 2

This model was chosen in order to compare the least squares method of solution with results obtainned by straight digitization of the integral equation as done by Hohmann (1971) and solutions obtained by finite difference as described by Wright (1969). The model and its parameters are described in Table 6-3. The exciting fields are those of a vertically incident plane wave and of a line source placed on the surface of the half-space one skindepth to the left of center of the body. The equivalent current was computed for various values of σ_1/σ_0 and some of the anomalous fields computed at the surface of the half-space are compared with results obtained by Hohmann and Wright.

The equivalent current for the plane wave source is shown in Fig. 6-12 for a number of σ_1/σ_0 ratios. The equivalent current behaves in a similar manner to that given for model 1. For small conductivity contrasts, $J_e \sim \sigma_a E_0$ and the maps reflect the structure of the exciting field. As the conductivity contrast increases, the self-inductance effects start to take over and the current is forced towards the edges of the cylinder where the inductive impedance is a minimum. The points for maximum concentration of current are the top and bottom of the body. In addition, the relative phase of the current changes from being predominantly in-phase with the

Table 6-3 Data for TE Model 2

Geometrical

A = 0.015

κ = 10.0

D = 3.33

Electrical

σ_2/σ_0 = 4.0, 9.0, 49.0, 99.0, 499.0, 999.0

σ_0 = 1.0 mho/meter

Numerical Solution

N = 4

M = 4

P = 8

Q = 10

Source Types

1. Plane wave
2. Line source

Sketch of Geometry

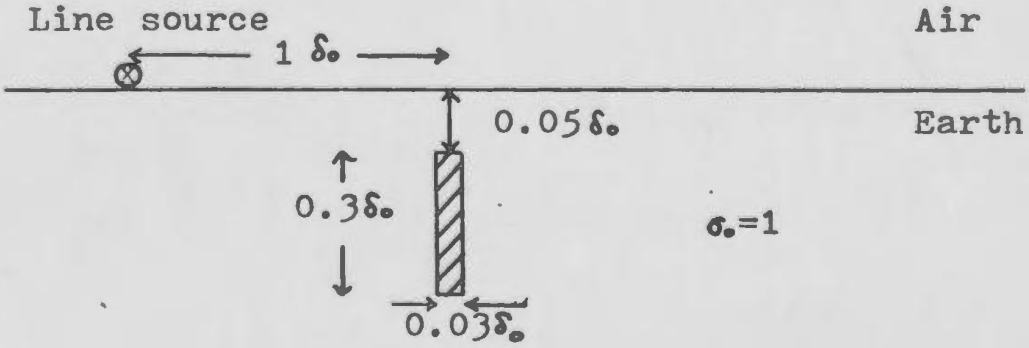

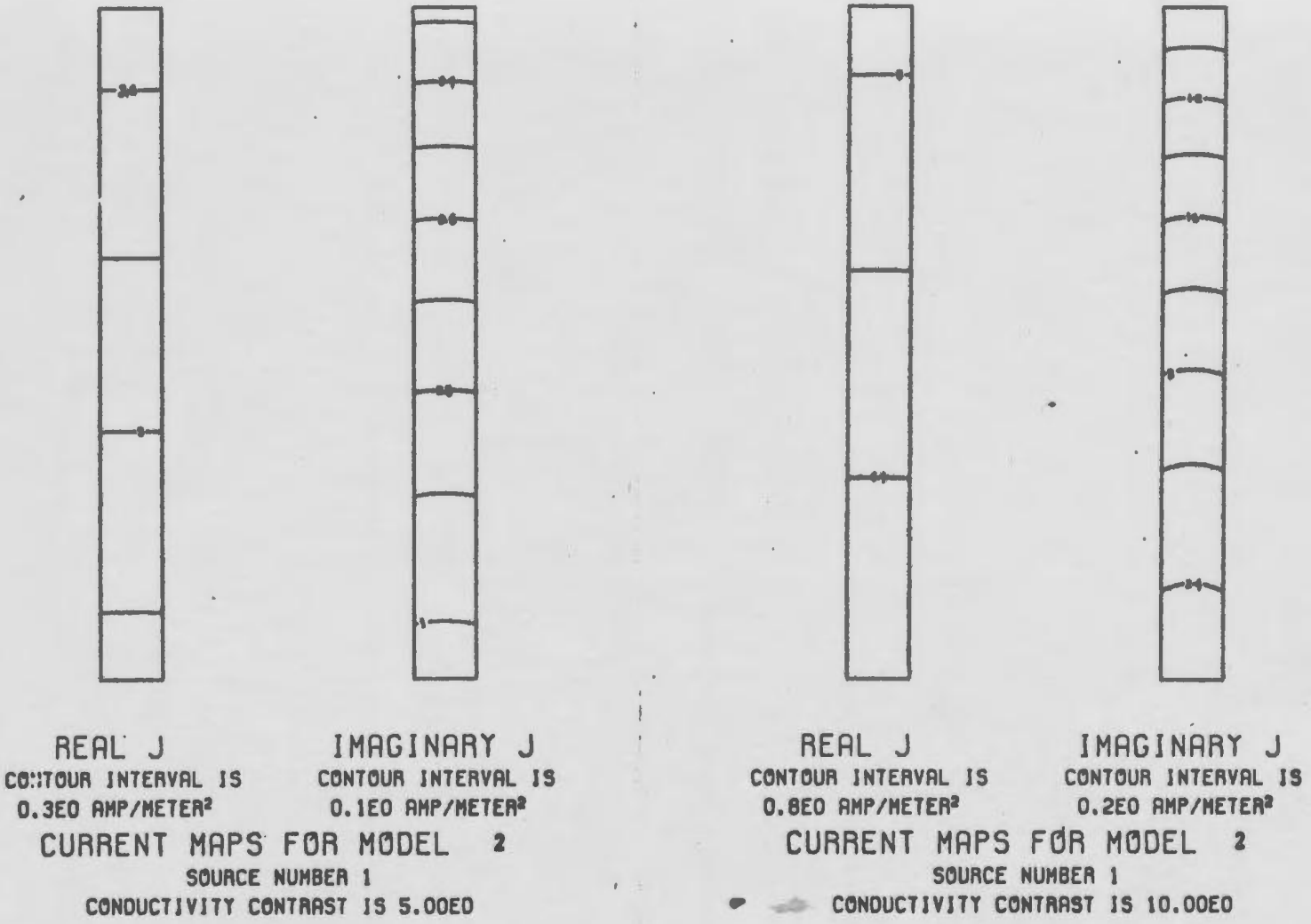

Fig.6-12 Equivalent current for TE model #2 for various conductivities for plane wave excitaion.

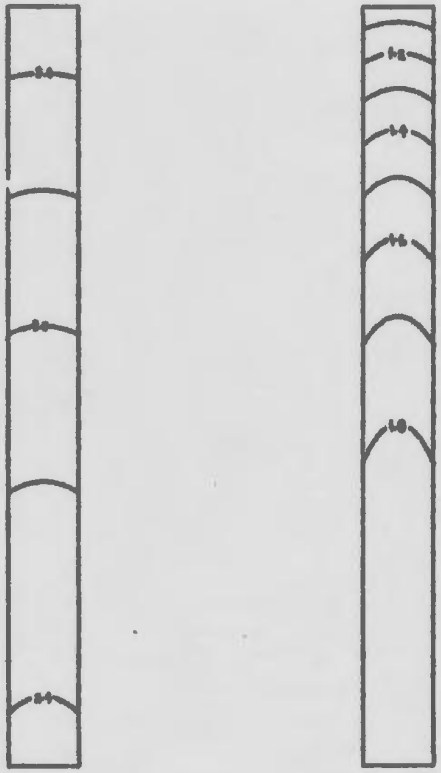

REAL J
CONTOUR INTERVAL IS
0.3E1 AMP/METER²

IMAGINARY J
CONTOUR INTERVAL IS
0.1E1 AMP/METER²

CURRENT MAPS FOR MODEL 2
SOURCE NUMBER 1
CONDUCTIVITY CONTRAST IS 5.00E1

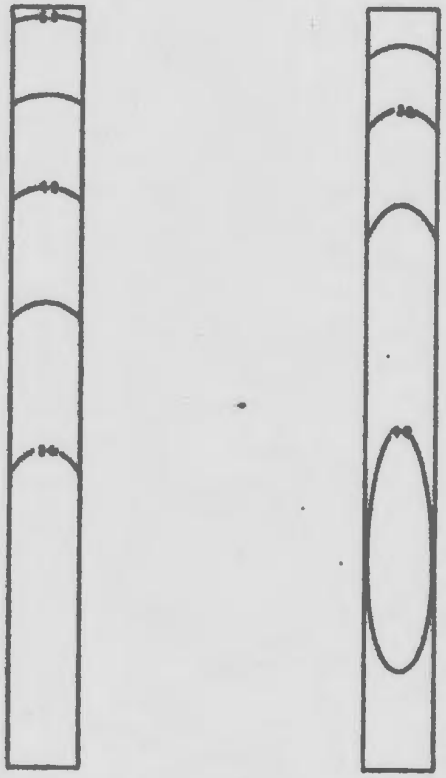

REAL J
CONTOUR INTERVAL IS
0.6E1 AMP/METER²

IMAGINARY J
CONTOUR INTERVAL IS
0.4E1 AMP/METER²

CURRENT MAPS FOR MODEL 2
SOURCE NUMBER 1
CONDUCTIVITY CONTRAST IS 1.00E2

Fig. 6-12 cont'd. Equivalent current for TE model #2 for various conductivities for plane wave excitation

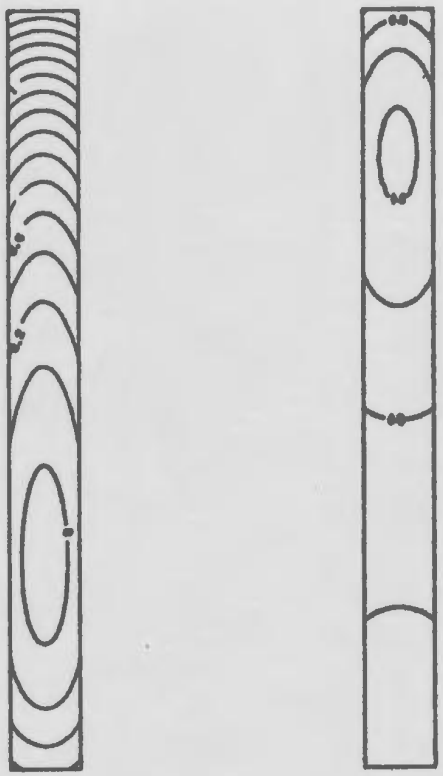

REAL J
CONTOUR INTERVAL IS
0.1E2 AMP/METER²

IMAGINARY J
CONTOUR INTERVAL IS
0.1E2 AMP/METER²

CURRENT MAPS FOR MODEL 2
SOURCE NUMBER 1
CONDUCTIVITY CONTRAST IS 5.00E2

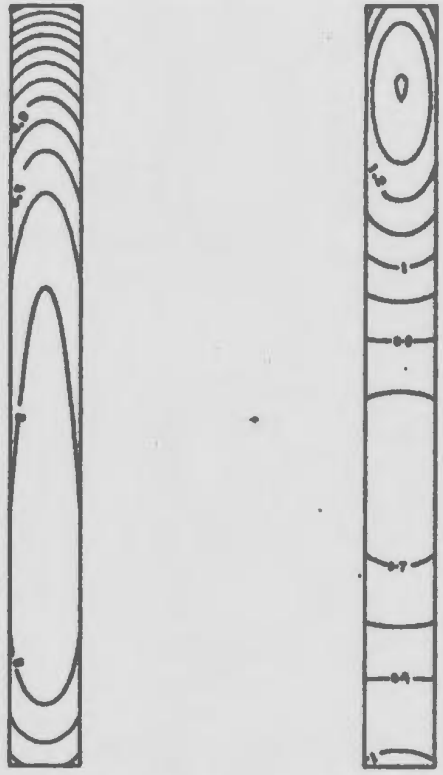

REAL J
CONTOUR INTERVAL IS
0.2E2 AMP/METER²

IMAGINARY J
CONTOUR INTERVAL IS
0.1E2 AMP/METER²

CURRENT MAPS FOR MODEL 2
SOURCE NUMBER 1
CONDUCTIVITY CONTRAST IS 1.00E3

Fig. 6-12 cont'd. Equivalent current for TE model #2 for various conductivities for plane wave excitation.

exciting field to a lag between 45^{o} and 120^{o} at various points in the body.

The normalized impedance over the body at the surface of the half-space is shown in Fig. 6-13 for the various conductivity contrasts. The impedance amplitude shows a deeper and deeper minimum directly over the body as the conductivity contrast increases. For small contrasts, Z_N exhibits a phase lag over the body; this reflects the phase retardation associated with propagation through the background medium. As the conductivity increases, the self-induction effects of the body set in and the mean phase of the equivalent current is significantly altered. This generates a phase lead in Z_N. The proximity of the top of the conductor to the Earth's surface and the fact that the phase of the equivalent current near the top of the conductor is considerably different from the mean phase of J_e results in a dimple in the phase curve similar to that seen for model 1. The x's on the 1000:1 curves denote the response obtained by Wright for the same model. There is very good agreement between the two sets of data. The only discrepancies occur far out on the flanks of the anomaly. These are probably due to edge effects in Wright's finite difference solution.

The J_e response for the line source excitation is shown in Fig. 6-14. The excitation electric field is given by

$$E_o = j\omega\mu_o\left(L_o(r,r_s) + L_1(r,r_s)\right) \quad \text{volt/m.} \qquad 6\text{-}38$$

where $\bar{r}_s$ is the location of the line source. The current in the wire is taken to be 1 amp. The basic behaviour of the equivalent current is much the same as that for the plane wave excitation with the difference being the non-uniform nature of the source field. The current exhibits the same skindepthing effect and attempts to concentrate itself in the upper and lower ends of the cylinder cross-section where the self-inductance is a minimum.

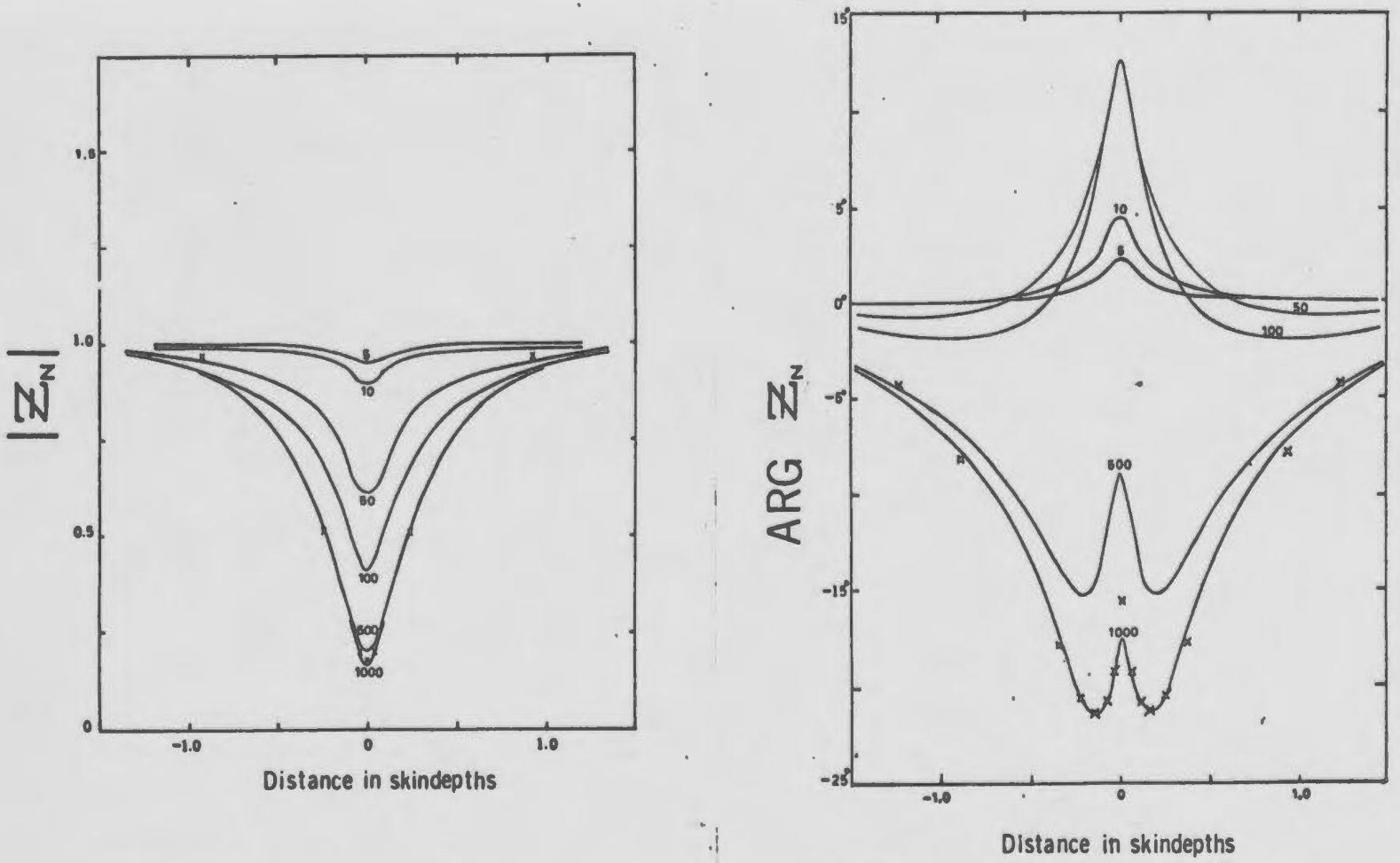

Fig. 6-13 Normalized impedance, Z_N, over TE model #2 for plane wave excitation.

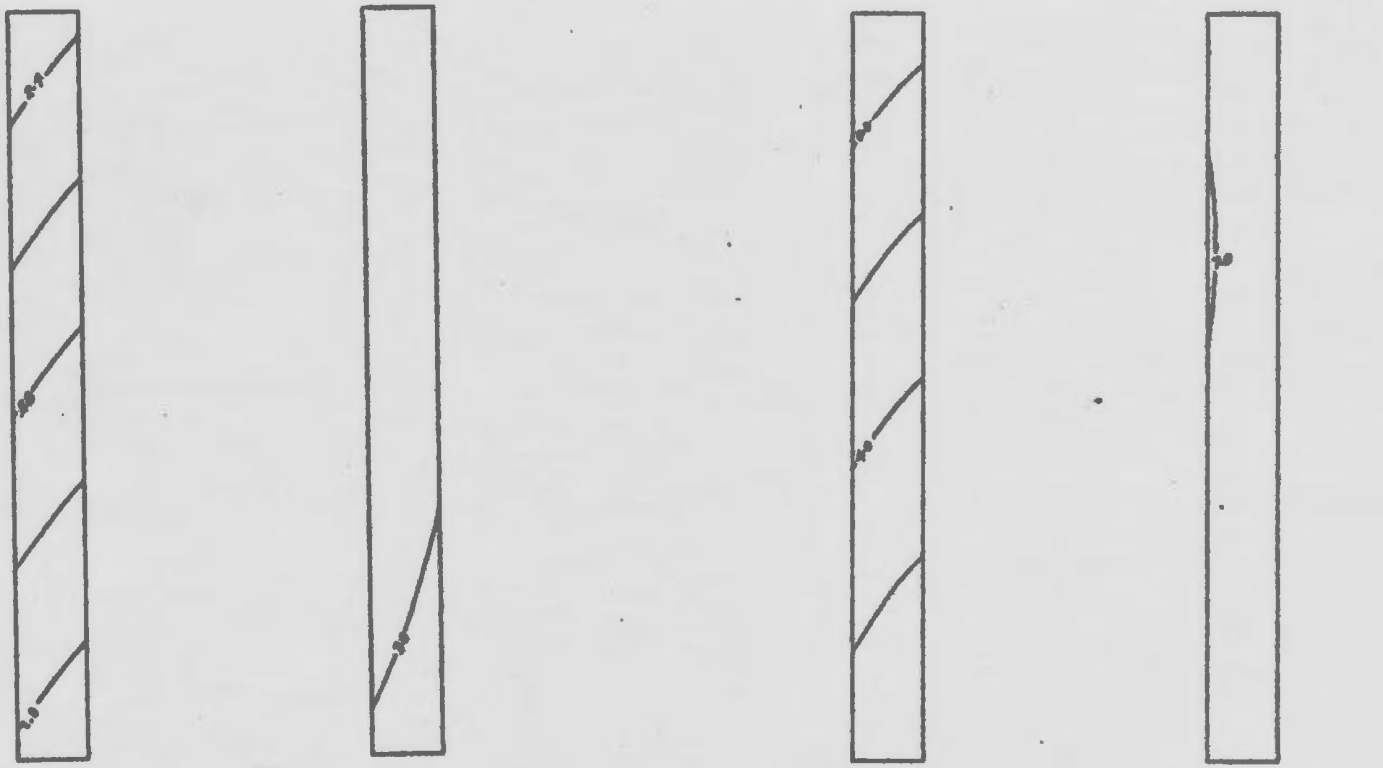

Fig. 6-14 Equivalent current for TE model #2 for various conductivities and line source excitation.

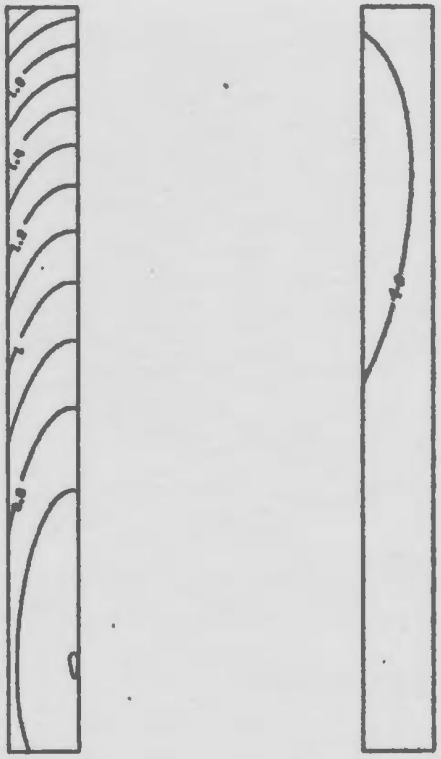

REAL J
CONTOUR INTERVAL IS
0.1E0 AMP/METER²

IMAGINARY J
CONTOUR INTERVAL IS
0.4E0 AMP/METER²

CURRENT MAPS FOR MODEL 2
SOURCE NUMBER 2
CONDUCTIVITY CONTRAST IS 5.00E1

REAL J
CONTOUR INTERVAL IS
0.2E0 AMP/METER²

IMAGINARY J
CONTOUR INTERVAL IS
0.6E0 AMP/METER²

CURRENT MAPS FOR MODEL 2
SOURCE NUMBER 2
CONDUCTIVITY CONTRAST IS 1.00E2

Fig. 6-14 cont'd. Equivalent current for TE model #2 for various conductivities and line source excitation.

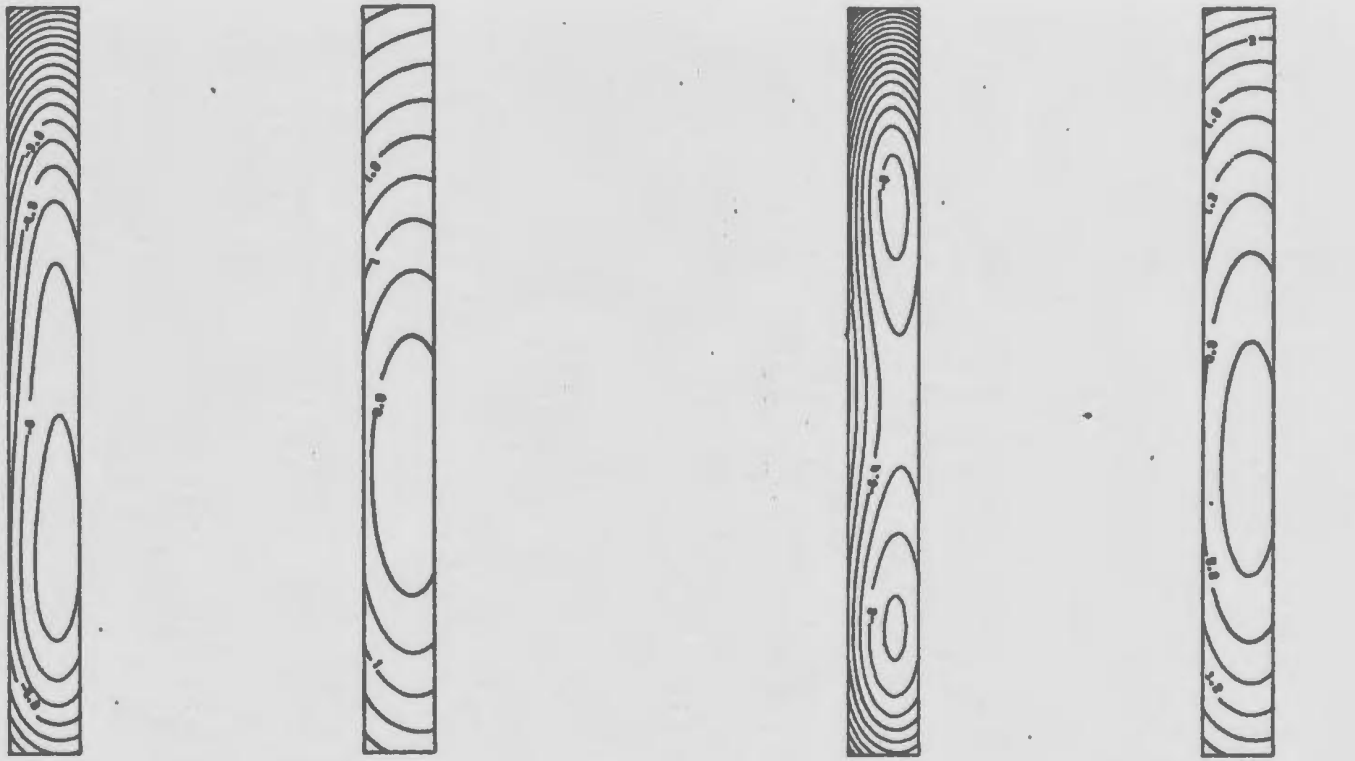

Fig. 6-14 cont'd. Equivalent current for TE model #2 for various conductivities and line source excitation

The magnetic fields at the surface of the half-space were computed on a profile over the body and were normalized by a factor

$$H = \frac{1}{2\pi |\bar{r}-\bar{r}_s|} \qquad 6\text{-}39$$

where $|\bar{r}-\bar{r}_s|$ is the radial distance from the line source. This is the amplitude of the magnetic field about a static line current of 1 amp. Fig. 6-15 shows the horizontal magnetic field as a function of position for various conductivity contrasts. The vertical magnetic fields for the same profile are shown in Fig. 6-16. The curve $\sigma_1/\sigma_0 = 1$ gives the normalized half-space response for both components. The superimposed x, Δ, •, are data obtained numerically by Hohmann (1970). There is extremely good agreement between the two sets of data. The only discrepancies occur in H_x directly over the model; the peak values of H_x obtained by Hohmann are about 2% smaller than those obtained in this study. These variations are most likely due to differences in the numerical solution methods.

(iv) TE Summary

The preceding results indicate the usefulness of the least squares approach to obtaining solutions to the TE integral equation. The data presented is not an exhaustive analysis of these models or of TE models in general and a number of numerical details should be summarized before leaving TE solutions. One feature which was found was that changing the polynomial degree of the approximation to J_e did not significantly alter the response of the preceding models. In fact for TE model 2, the response was computed for (N, M) = (2, 2), (2, 4) and (4, 4). Only for the (2, 2) case and large σ_1/σ_0 ratios was there any detectable difference in the response and this was only about 1 or 2%. For larger bodies the polynomial degree becomes more important but is still not a major factor since the

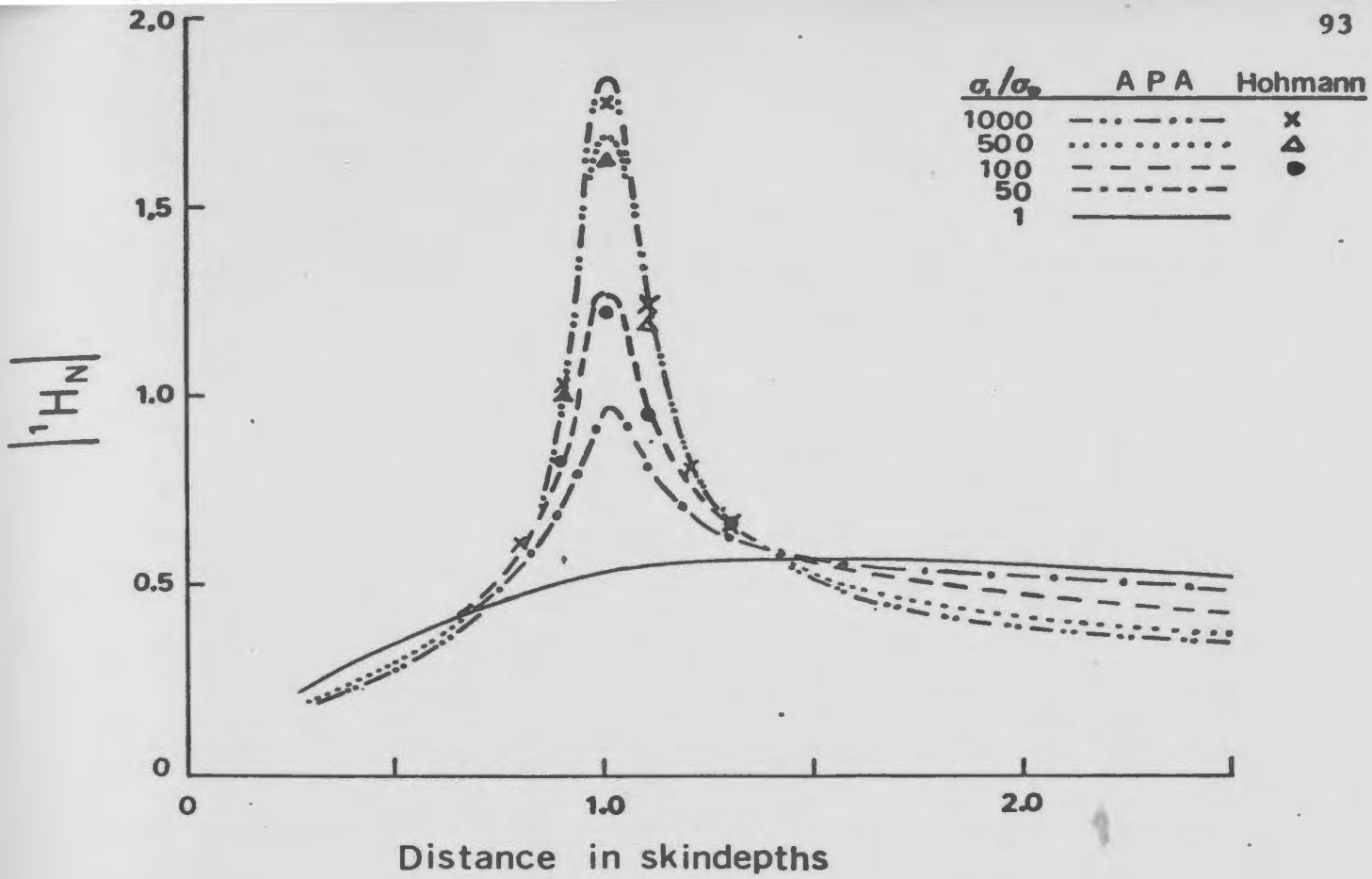

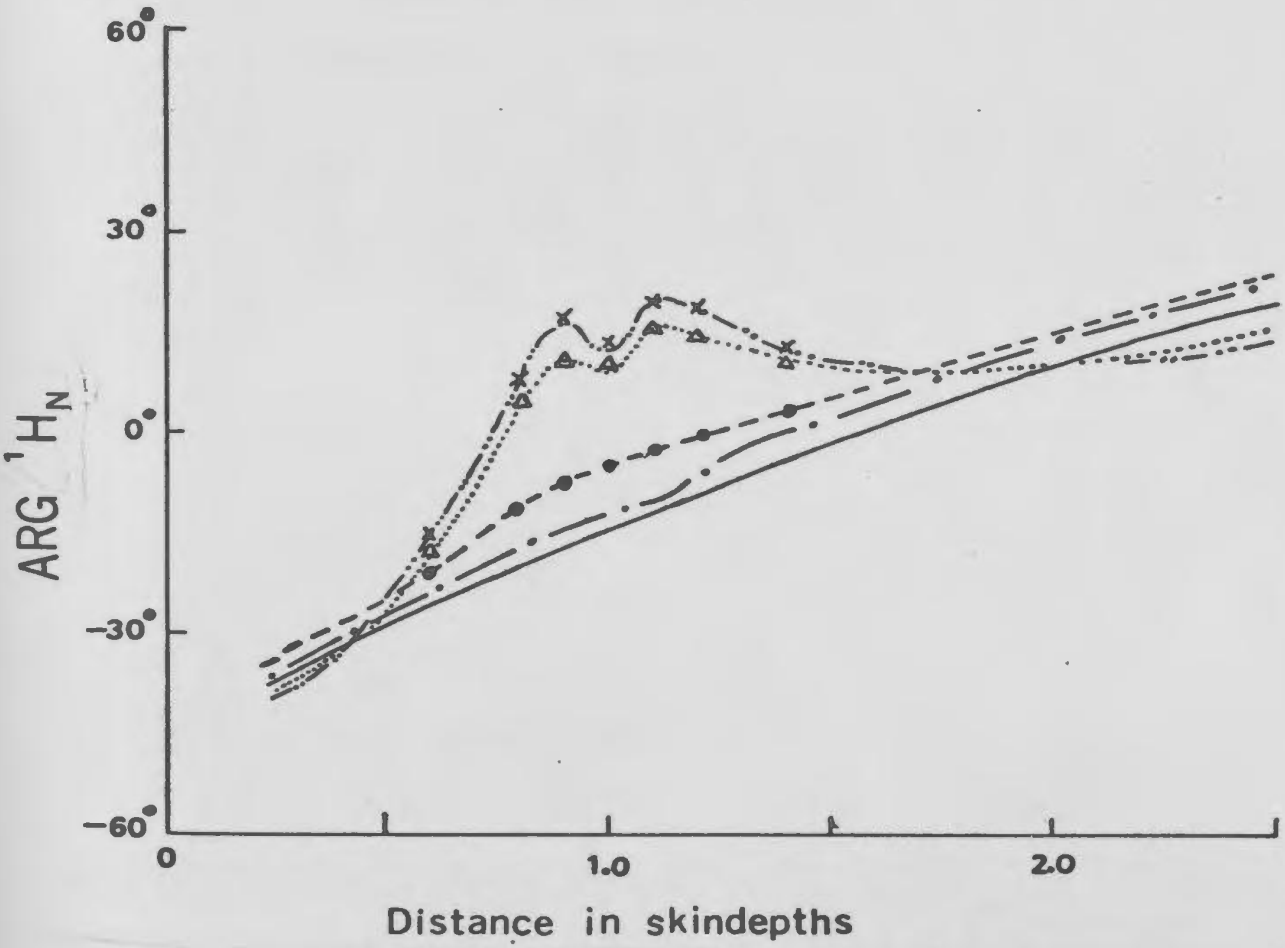

Fig. 6-15 Normalized $\hat{e}_1$ component of magnetic field over TE model #2 for line source excitation vs. distance from line source.

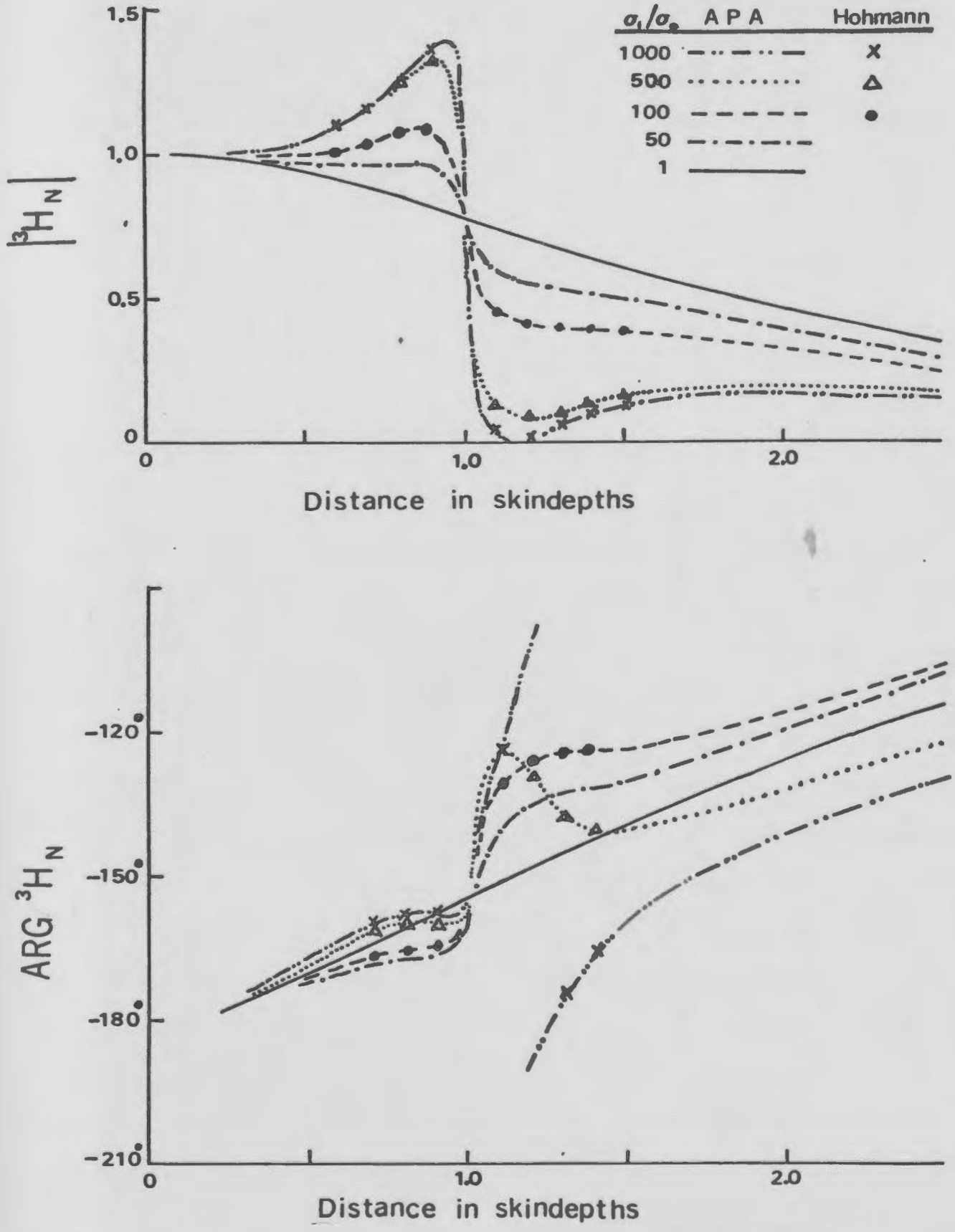

Fig. 6-16 Normalized $\hat{e}_3$ component of the magnetic field over TE model #2 for line source excitation vs. distance form line source.

solution is an approximation in the least squares sense and therefore gives a smoothed version of the true response even when a much higher degree polynomial is required to be representative of every detail of the true solution. Another factor in the solutions which was considered was the accuracy of the numerical integrals; the error tolerance was varied from 1% to 0.1% and again very little variation was noticed in the response. The number of error points in the squared error estimator is also a parameter of the solution which should be mentioned. In general, the number of error points was chosen such that the average number of points gave a mean average spatial separation of less than $0.5\delta_1$. $\delta_1 = (2/\omega\mu_0\sigma_1)^{1/2}$ is the skindepth in the anomalous region. For very small bodies and small σ_1/σ_0 the number of error points was taken to be greater than the number of unknown parameters. The response is not overly dependent on this parameter since the points are spaced in such a manner as to emphasize the dominant part of the solution, namely the current near the surface of the anomalous body. The combination of the facts that the solution is an approximation in the least squares sense and the current is solenoidal results in a highly stable scattering matrix. This accounts for the insensitivity of the response to minor variations of the solution parameters. In the TM response the mixture of the non-solenoidal and solenoidal currents makes the solution considerably more sensitive to these parameters.

The computation time for a model was difficult to judge for general usage since every job run was for a specialized purpose. Opening up the programs and using multiple sources for varying conductivity contrasts in a straight-through production mode would drop the average time per model considerably. The computations of the numerical quadratures were the most expensive part of the analysis; for a given geometrical model, polynomial degree and accuracy of the numerical integrals, all the integrals for a response would require from about 10 seconds to about 60 seconds of CPU

time on an IBM 370-165. The remaining computations consumed less than 5 seconds per 10 source configurations and one conductivity; this factor was controlled mainly by the maximum polynomial degree of the solution. (The maximum core requirements in any stage of the processing were less than 120K bytes or 30K words of memory).

These figures for a single run compare with those required by Wright and Hohmann for the computation of the response for similar models. Hohmann used a grid subdivided into spatial increments of 0.6 δ_1 in most instances. The anomalous electric field was solved for at the discrete set of grid points. In the model 2 discussed here 40 grid-points were used to evaluate the response. The computation time for the solution in this manner was approximately 30 sec. on a CDC 6400 computer per geometry, source and conductivity contrast. The finite difference solution used by Wright required digitization of the host medium and the air or insulating region above the half-space as well as the body itself. The division interval was in general on the order of about 0.25 skindepths in each medium except in local regions near the body where geometrical spreading effects might be significant. Computation time by the finite difference method required about 60 seconds of CPU time on an IBM 370-165.

One point which should be stressed before continuing on to the TM analysis is that the TE response is a pure "inductive" response. The electric fields and currents are parallel to all conductivity variations; as a result, the conductive channelling or depolarization operator is not activated. The TE impedance operator does not exhibit the bimodal feature of the general electric scattering problem discussed in chapter 4. In fact the response is analogous to that of a simple RL series circuit as a function of frequency; at small (ωL/R) the resistive term dominates the response while at large (ωL/R) values the inductive term is the dominant factor in determining the response.

6-3 TM Response

(i) Integral Equation

The TM response of the cylinder is formulated in terms of an equivalent current $\bar{J}_e$ which is a 2-component vector which lies in the plane perpendicular to the strike of the cylinder. The components of $\bar{J}_e$ are denoted by $(J_1, 0, J_3)$ and are assumed independent of the x_2 coordinate. The integral equation for $\bar{J}_e$ is obtained using the 2 dimensional TM Green's dyadic derived in appendix B. The result is the vector Fredholm equation

$$\frac{\bar{J}_e(r)}{\sigma_a} - j\omega\mu_o \int_{-a_1}^{a_1}\int_{-a_3}^{a_3} \tilde{\Psi}(r,r') \cdot \bar{J}_e(r')\, dx_1' dx_3' = \bar{E}_o(r') \qquad 6\text{-}40$$

where $\bar{E}_0$ is the excitation electric field and is also a 2 component vector with components $(E_1, 0, E_3)$. The Green's dyadic is listed in Table 6-4.

Upon regrouping 6-40 and applying Gauss' theorem, the integral equations for the components of $\bar{J}_e$ are

$$\frac{J_1(r)}{\sigma_a} - j\omega\mu_o \int_{-a_1}^{a_1}\int_{-a_3}^{a_3} (L_1 + L_2)\, J_1(r')\, dx_1' dx_3' - \frac{1}{\sigma_o}\frac{\partial \Psi}{\partial x_1} = E_1 \qquad 6\text{-}41$$

$$\frac{J_3(r)}{\sigma_a} - j\omega\mu_o \int_{-a_1}^{a_1}\int_{-a_3}^{a_3} (L_1 - L_2)\, J_3(r')\, dx_1' dx_3' - \frac{1}{\sigma_o}\frac{\partial \Psi}{\partial x_3} = E_3 \qquad 6\text{-}42$$

where

$$\Psi(x_1 x_3) = -\left\{ \int_{-a_1}^{a_1} (L_1 + L_2) J_3(r') \Big|_{x_3' = -a_3}^{x_3' = a_3} dx_1' + \int_{-a_3}^{a_3} (L_1 + L_2) J_1(r') \Big|_{x_1' = -a_1}^{x_1' = a_1} dx_3' \right\} \qquad 6\text{-}43$$

The Ψ term is the conductive channelling term and it involves only surface integrals (line integrals for 2-dimensional structures) when σ_a is constant inside the structure.

The approximate solution for $\bar{J}_e$ was chosen to be a power series expansion. The expansions for J_1 and J_3 have the form

Table 6-4 2 Dimensional TM Green's Dyadic

$$\tilde{\mathcal{G}}(r,r') = \left(\tilde{I}_2 + \frac{\bar{\nabla}_2 \bar{\nabla}_2}{k_0^2} \right) \cdot (\tilde{A} + \tilde{B})$$

$$\bar{\nabla}_2 = \left(\frac{\partial}{\partial x_1} \hat{e}_1 + \frac{\partial}{\partial x_3} \hat{e}_3 \right)$$

$$\tilde{I}_2 = \begin{bmatrix} \hat{e}_1\hat{e}_1 & 0 & 0 \\ 0 & 0 & 0 \\ 0 & 0 & \hat{e}_3\hat{e}_3 \end{bmatrix}$$

$$\tilde{A} = L_1 \begin{bmatrix} \hat{e}_1\hat{e}_1 & 0 & 0 \\ 0 & 0 & 0 \\ 0 & 0 & \hat{e}_3\hat{e}_3 \end{bmatrix}$$

$$\tilde{B} = L_2 \begin{bmatrix} \hat{e}_1\hat{e}_1 & 0 & 0 \\ 0 & 0 & 0 \\ 0 & 0 & \hat{e}_3\hat{e}_3 \end{bmatrix}$$

$$L_1(r,r') = \frac{j}{4} H_0^1(k_0 \rho)$$

$$L_2(r,r') = \frac{j}{4} H_0^1(k_0 \rho_1)$$

$$\rho = \left((x_1 - x_1')^2 + (x_3 - x_3')^2 \right)^{1/2}$$

$$\rho_1 = \left((x_1 - x_1')^2 + (x_2 + x_3')^2 \right)^{1/2}$$

$$J_1 = \sum_{n=0}^{N} \sum_{m=0}^{N} c^1_{nm} \xi^n \eta^m \qquad 6\text{-}44$$

$$J_3 = \sum_{n=0}^{N} \sum_{m=0}^{N} c^3_{nm} \xi^n \eta^m \qquad 6\text{-}45$$

where (ξ, η) are the normalized coordinates

$$\xi = \frac{(x_1 - x_1^c)}{a_1} \qquad \eta = \frac{(x_3 - x_3^c)}{a_3} \qquad 6\text{-}46$$

and the (x_1^c, x_3^c) are the coordinates of the centre of the cylinder. Invoking the fact that $\bar{\nabla} \cdot \bar{J}_e = 0$ inside the cylinder when σ_a is constant, the coefficients of J_1 and J_3 are not all independent and the condition

$$\frac{n+1}{A} c^1_{n+1,m} = - \frac{(m+1)}{RA} c^3_{n,m+1} \qquad 6\text{-}47$$

must be respected. This condition affects all the coefficients except the $c^1_{o,m}$ and $c^3_{n,o}$ terms for which the divergence operator is a null operator. The divergence free condition reduces the number of unknowns required to specify $\bar{J}_e$ and 6-44 and 6-45 can be rewritten as

$$J_1 = \sum_{m=0}^{N} c^1_{om} \eta^m + \sum_{\substack{m=0 \\ n=1}}^{N} c^1_{nm} \xi^n \eta^m \qquad 6\text{-}48$$

$$J_3 = \sum_{n=0}^{N} c^3_{no} \xi^n + \sum_{\substack{n=0 \\ m=1}}^{N} c^1_{m+1,m-1} \left(-R\left(\frac{m+1}{m}\right)\right) \xi^n \eta^m \qquad 6\text{-}49$$

The error vector $\bar{\Theta} = (\Theta_1, o, \Theta_3)$ is defined as the residual when the approximate solution for $\bar{J}_e$ is inserted into the coupled integral equations 6-41 and 6-42. The components of $\bar{\Theta}$ are given by

$$\Theta_1 = c^1_{on} Z^1_{on} + c^1_{nm} Z^2_{nm} + c^3_{no} Z^3_{no} - E_1 \qquad 6\text{-}50$$

$$\Theta_3 = c^1_{on} U^1_{on} + c^1_{nm} U^2_{nm} + c^3_{no} U^3_{no} - E_3 \qquad 6\text{-}51$$

where U^i and Z^i are given in Table 6-5(a) and (b). The subscript summation over the appropriate range is implied.

Table 6-5 (a) TM Impedance Coefficients

$$Z^1_{0,m} = \frac{V^1_{0,m}}{\sigma_a} - j\omega\mu_0 RA^2 (V^2_{0,m} + V^3_{0,m}) - \frac{R}{\sigma_0}(V^4_{0,m} + V^5_{0,m})$$

$$Z^2_{n,m} = \frac{V^1_{n,m}}{\sigma_a} - j\omega\mu_0 RA^2 (V^2_{n,m} + V^3_{n,m}) - \frac{R}{\sigma_0}(V^4_{n,m} + V^5_{n,m})$$

$$+ \frac{1}{\sigma_0} R \frac{n}{m+1} (V^6_{n-1,m+1} + V^7_{n-1,m+1})$$

$$Z^3_{n,0} = -\frac{1}{\sigma_0}(V^6_{n,0} + V^7_{n,0})$$

$$\mathcal{U}^1_{0,m} = -\frac{1}{\sigma_0}(W^6_{0,m} + W^7_{0,m})$$

$$\mathcal{U}^2_{n,m} = \frac{n}{m+1} R \left(-\frac{W^1_{n-1,m+1}}{\sigma_a} + j\omega\mu_0 RA^2 (W^2_{n-1,m+1} + W^3_{n-1,m+1}) \right.$$

$$\left. + \frac{1}{\sigma_0}\frac{1}{R}(W^4_{n-1,m+1} + W^5_{n-1,m+1}) \right) - \frac{1}{\sigma_0}(W^6_{n,m} + W^7_{n,m})$$

$$\mathcal{U}^3_{n,0} = \frac{W^1_{n,0}}{\sigma_a} - j\omega\mu_0 RA^2 (W^2_{n,0} + W^3_{n,0}) - \frac{1}{\sigma_0}\frac{1}{R}(W^4_{n,0} + W^5_{n,0})$$

Table 6-5 (b) TM Impedence Coefficients

$$V^1_{n,m} = \xi^n \eta^m$$

$$V^2_{n,m} = \int_{-1}^{1}\int_{-1}^{1} \xi'^n \eta'^m L_1(\xi,\xi',\eta,\eta')\, d\xi' d\eta'$$

$$V^3_{n,m} = \int_{-1}^{1}\int_{-1}^{1} \xi'^n \eta'^m L_2(\xi,\xi',\eta,\eta')\, d\xi' d\eta'$$

$$V^4_{n,m} = -\frac{\partial}{\partial \xi} \int_{-1}^{1} \xi'^n \eta'^m L_1(\xi,\xi',\eta,\eta')\Big|_{\xi'=-1}^{\xi'=1} d\eta'$$

$$V^5_{n,m} = -\frac{\partial}{\partial \xi} \int_{-1}^{1} \xi'^n \eta'^m L_2(\xi,\xi',\eta,\eta')\Big|_{\xi'=-1}^{\xi'=1} d\eta'$$

$$V^6_{n,m} = -\frac{\partial}{\partial \xi} \int_{-1}^{1} \xi'^n \eta'^m L_1(\xi,\xi',\eta,\eta')\Big|_{\eta'=-1}^{\eta'=1} d\xi'$$

$$V^7_{n,m} = -\frac{\partial}{\partial \xi} \int_{-1}^{1} \xi'^n \eta'^m L_2(\xi,\xi',\eta,\eta')\Big|_{\eta'=-1}^{\eta'=1} d\xi'$$

$$W^1_{n,m} = V^1_{n,m} \qquad W^2_{n,m} = V^2_{n,m} \qquad W^3_{n,m} = -V^3_{n,m}$$

$$W^4_{n,m} = -\frac{\partial}{\partial \eta} \int_{-1}^{1} \xi'^n \eta'^m L_1(\xi,\xi',\eta,\eta')\Big|_{\eta'=-1}^{\eta'=1} d\xi'$$

$$W^5_{n,m} = -\frac{\partial}{\partial \eta} \int_{-1}^{1} \xi'^n \eta'^m L_2(\xi,\xi',\eta,\eta')\Big|_{\eta'=-1}^{\eta'=1} d\xi'$$

$$W^6_{n,m} = -\frac{\partial}{\partial \eta} \int_{-1}^{1} \xi'^n \eta'^m L_1(\xi,\xi',\eta,\eta')\Big|_{\xi'=-1}^{\xi'=1} d\eta'$$

$$W^7_{n,m} = -\frac{\partial}{\partial \eta} \int_{-1}^{1} \xi'^n \eta'^m L_2(\xi,\xi',\eta,\eta')\Big|_{\xi'=-1}^{\xi'=1} d\eta'$$

In an analogous manner to the TE formulation, $\bar{\Theta}$ is evaluated at a discrete set of points (ξ_p, η_q) in the cylinder and a discrete total squared error estimator computed by

$$\mathcal{K}_D = \sum_{pq} \bar{\Theta}^* \cdot \bar{\Theta} \qquad 6\text{-}52$$

The set of error points were chosen as the roots of Chebychev polynomials of degree P and Q.

$$T_p(\xi_p) \equiv 0 \qquad T_Q(\eta_q) \equiv 0 \qquad 6\text{-}53$$

This set of points was chosen since it weighted the error in the corners and at the edges of the cylinder more heavily than that in the central portions of the cylinder; this is in accord with the physical nature of the response.

The coefficients c^i_{nm} are split into real and imaginary parts

$$c^i_{nm} = \alpha^i_{nm} + j\beta^i_{nm} \qquad 6\text{-}54$$

Minimization of the discrete squared error, $\mathcal{K}_D$ w.r.t. α^i_{rs} and β^i_{rs}

$$\frac{\partial \mathcal{K}}{\partial \alpha^i_{rs}} \equiv 0 \qquad \frac{\partial \mathcal{K}_D}{\partial \beta^i_{rs}} \equiv 0 \qquad 6\text{-}55$$

yields a set of linear equations in the set of unknowns $(\alpha^i_{nm}, \beta^i_{nm})$. The resulting coefficient matrix for the set of equations is tabulated in Table 6-6 and is referred to here as the scattering matrix in subsequent discussions. The individual matrix elements are also shown in the table.

(ii) Numerical Solution

The TM response requires considerably more detailed analysis than does the equivalent TE response; the vector nature of the electric fields and currents and the excitation of conductive chanelling effects add to the complexity of the problem. The details of the numerical analysis of the TM response more or less follow those of the TE analysis. The parameters

Table 6-6 TM Least Squares Scattering Matrix and Matrix Element Definitions

$$
\begin{bmatrix}
{}^{1}_{1}\mathcal{R} , -{}^{1}_{1}\mathcal{T} & ; & {}^{1}_{2}\mathcal{R} , -{}^{1}_{2}\mathcal{T} & ; & {}^{1}_{3}\mathcal{R} , -{}^{1}_{3}\mathcal{T} \\
{}^{1}_{1}\mathcal{T} , {}^{1}_{1}\mathcal{R} & ; & {}^{1}_{2}\mathcal{T} , {}^{1}_{2}\mathcal{R} & ; & {}^{1}_{3}\mathcal{T} , {}^{1}_{3}\mathcal{R} \\
\hline
{}^{1}_{2}\mathcal{R}^{T} \quad {}^{1}_{2}\mathcal{T}^{T} & ; & {}^{2}_{2}\mathcal{R} \quad -{}^{2}_{2}\mathcal{T} & ; & {}^{2}_{3}\mathcal{R} \quad -{}^{2}_{3}\mathcal{T} \\
-{}^{1}_{2}\mathcal{T}^{T} \quad {}^{1}_{2}\mathcal{R}^{T} & ; & {}^{2}_{2}\mathcal{T} \quad {}^{2}_{2}\mathcal{R} & ; & {}^{2}_{3}\mathcal{T} \quad {}^{2}_{3}\mathcal{R} \\
\hline
{}^{1}_{3}\mathcal{R}^{T} \quad {}^{1}_{3}\mathcal{T}^{T} & ; & {}^{2}_{3}\mathcal{R}^{T} \quad {}^{2}_{3}\mathcal{T}^{T} & ; & {}^{3}_{3}\mathcal{R} \quad -{}^{3}_{3}\mathcal{T} \\
-{}^{1}_{3}\mathcal{T}^{T} \quad {}^{1}_{3}\mathcal{R}^{T} & ; & -{}^{2}_{3}\mathcal{T}^{T} \quad {}^{2}_{3}\mathcal{R}^{T} & ; & {}^{3}_{3}\mathcal{T} \quad {}^{3}_{3}\mathcal{R}
\end{bmatrix}
\begin{bmatrix}
\alpha^{1}_{om} \\ \beta^{1}_{om} \\ \hline \alpha^{2}_{nm} \\ \beta^{2}_{nm} \\ \hline \alpha^{3}_{no} \\ \beta^{3}_{no}
\end{bmatrix}
=
\begin{bmatrix}
{}^{1}\mathcal{S}^{1}_{os} \\ {}^{1}\mathcal{S}^{2}_{os} \\ \hline {}^{2}\mathcal{S}^{1}_{rs} \\ {}^{2}\mathcal{S}^{2}_{rs} \\ \hline {}^{3}\mathcal{S}^{1}_{no} \\ {}^{3}\mathcal{S}^{2}_{no}
\end{bmatrix}
$$

$$
{}^{i}_{j}\mathcal{R}_{rsnm} = \text{Real} \sum_{pq} \left\{ Z^{i*}_{rs} Z^{j}_{nm} + U^{i*}_{rs} U^{j}_{nm} \right\}
$$

$$
{}^{i}_{j}\mathcal{T}_{rsnm} = \text{Imag} \sum_{pq} \left\{ Z^{i*}_{rs} Z^{j}_{nm} + U^{i*}_{rs} U^{j}_{nm} \right\}
$$

$$
{}^{i}\mathcal{S}^{1}_{rs} = \text{Real} \sum_{pq} \left\{ Z^{i*}_{rs} E_1 + U^{i*}_{rs} E_3 \right\}
$$

$$
{}^{i}\mathcal{S}^{2}_{rs} = \text{Imag} \sum_{pq} \left\{ Z^{i*}_{rs} E_1 + U^{i*}_{rs} E_3 \right\}
$$

characterizing the numerical solution are listed in Table 6-7. The sequence of computations followed that of the flow chart given in Fig. 6-17.

The numerical computations were centered around the numerical integration of the coefficients required to generate the scattering matrix. Following the integration stage, the scattering matrix was generated for a specified conductivity contrast and the inverse of the matrix was computed and used to find $\bar{J}_e$ for excitation by a plane wave vertically incident from the air on the half-space. Plane wave excitation was chosen since the 2 dimensional TM model has little practical use except for the analysis of magnetotelluric responses and obtaining an insight into conductive channelling effects. The final stage of the computations was that of deriving plots of the equivalent current and the anomalous fields at the surface of the half-space. The numerical algorithms were implemented directly from the formulation given in the previous section and little more can be said about the details of the computations. The most important part of the programs, namely the numerical integrations, were carried out following the technique given in Appendix D.

(iii) Numerical Results

The numerical response of a pair of very similar models is discussed in this section and the responses are compared with those computed by Wright's finite difference method. The model parameters are listed in Table 6-8. The two models have identical cross-sections and differ in the fact that one is located at the surface of the half-space while the other is located at a depth of 0.1 δ_o below the surface of the half-space. The computed responses for these models are presented in the following format. First, the equivalent current maps for the given model for different conductivity contrasts are given. These are followed by plots of the

Table 6-7 Table of TM Solution Parameters

Geometrical

A - cylinder half-width in skindepths

$\mathcal{R}$ - thickness to width ratio

D - depth of burial to half-width ratio

Electrical

σ_2/σ_0 - anomalous conductivity ratio

σ_0 - conductivity of background half-space

Numerical Solution

N - maximum polynomial degree in solution

P - number of error points in x_1 dimension

Q - number of error points in x_3 dimension

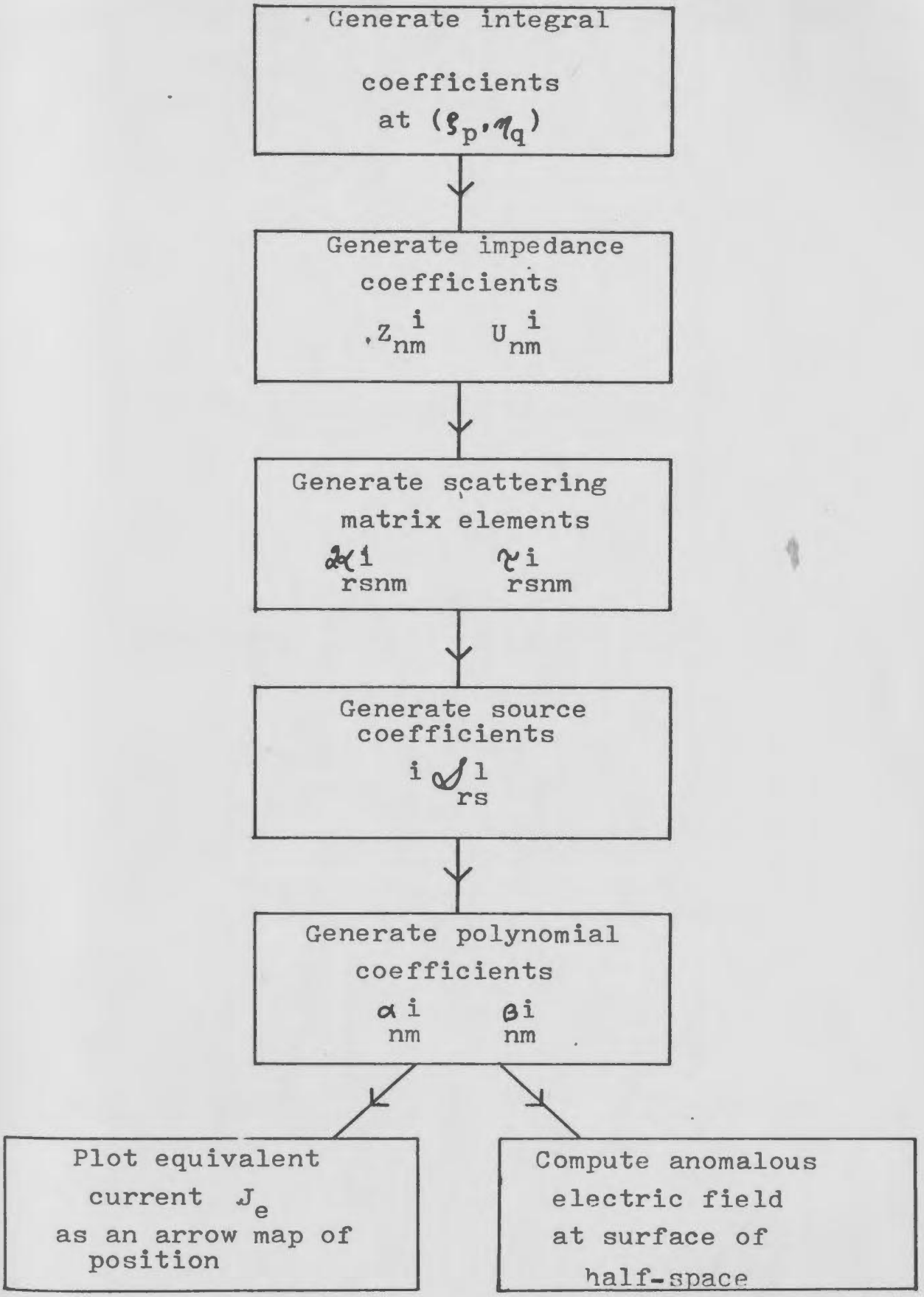

Fig. 6-17 Flow chart of TM computations

Table 6-8 Solution Parameters for TM Model 1 and 2

Geometrical

A = 0.4

$\mathcal{R}$ = 1.0

D = 0.0 and 0.1

Electrical

σ_a/σ_o = 0.5, 4.0, 9.0, 49.0, 99.0

σ_o = 1.0 mho/meter

Numerical Solution

N = 4

P = 8

Q = 8

Sketch of Geometry

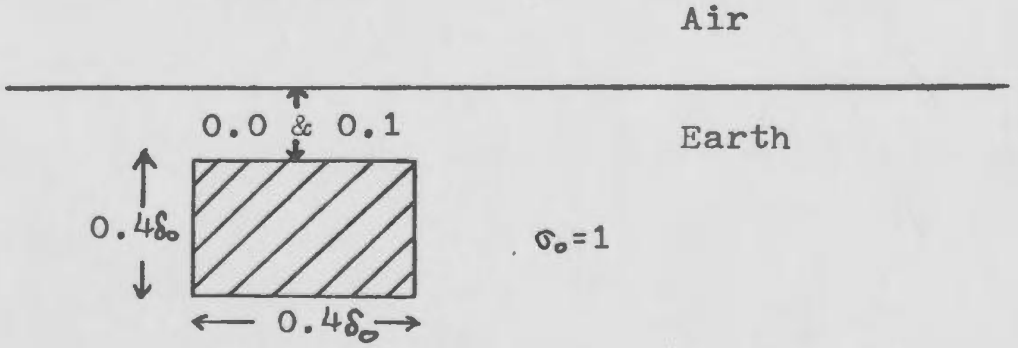

normalized electric field or normalized impedance (the two are equivalent as shown below) at the surface of the half-space.

The anomalous field E_a at the surface of the half-space is given by

$$\bar{E}_a = j\omega\mu_o \int_{-a_1}^{a_1}\int_{-a_3}^{a_3} \tilde{\bar{\mathcal{G}}}(r,r')\cdot\bar{J}_e(r')\,dx_1'dx_3' \qquad 6\text{-}56$$

Denoting the field associated with each individual element of the power series expansion as

$$\bar{E}_{nm}^{k} = j\omega\mu_o \int_{-a_1}^{a_1}\int_{-a_3}^{a_3} \tilde{\bar{\mathcal{G}}}(r,r')\cdot\hat{s}'^{n}\hat{n}'^{m}\hat{e}_k\,dx_1'dx_3' \qquad 6\text{-}57$$

the electric field is given by

$$\bar{E}_a = \sum_{knm} C_{nm}^{k}\ \bar{E}_{nm}^{k} \qquad 6\text{-}58$$

At the surface of the half-space the only component of $\bar{E}$ is the $\hat{e}_1$ component. Both the vertical component of $\bar{E}$ and tangential $\bar{H}$ field (there is no vertical magnetic field by definition of the problem) vanish at the surface of the half-space. This result is discussed in detail in section 4 of Appendix C. This condition is valid for low frequencies and sufficiently high conductivities that displacement currents are negligible. As a result, the normalized impedance ratio defined as

$$Z_N = \left(E^1_{Total}/H^2_{Total}\right)/\left(E^1_o/H^2_o\right) \qquad 6\text{-}59$$

becomes simply

$$Z_N = E^1_{Total}/E^1_o = 1 + \frac{E^1_a}{E^1_o} \qquad 6\text{-}60$$

and is identical to the normalized electric field at the surface of the half-space. The superscripts on E and H denote the components at the fields under consideration.

TM Model 1

The first model considered is a cylinder with a square cross-section of dimension 0.4 δ_o x 0.4 δ_o which is located at the surface of the half-space. The response is computed for a sequence of conductivity contrasts varying from 0.5 to 100. The equivalent current for the various conductivities is shown in Fig. 6-18.

The equivalent current is displayed as a complex vector function of position in the cylinder cross-section. The diagrams are reasonably straight forward and most of the features are self-explanatory. The current components were computed on a grid of points in the cylinder and were transformed to a set of arrows of scaled length and direction. The two maps for each conductivity contrast give the real and imaginary components of $\bar{J}_e$. The relative phase of the currents is given in terms of the electric field of the plane wave at the surface of the half-space in a similar manner to that discussed for the TE resposne. The scale for each map is given by the arrow at the bottom of each map; the current amplitude, in amp/m.^{2}, equivalent to the length of this arrow is marked beneath the arrow.

The equivalent current shows a marked variation as σ_1/σ_o is varied. For σ_1/σ_o = 0.5, the the cylinder is more resistive than the background medium; as a result the equivalent current is the opposite direction to the incident electric field. $\bar{J}_e$ is more or less an image of the exciting electric field (see Fig. 6-7) as a function of depth; near the corners, however, the current channelling effects distort the current from the horizontal. As σ_1/σ_o becomes greater than unity, the equivalent current reverses direction. For σ_1/σ_o = 5.0, the basic variation of $\bar{J}_e$ again reflects the variation of the incident electric field; however, there are significant departures from the planar behaviour of the exciting field. Conductive channelling effects cause the current to be channelled into an

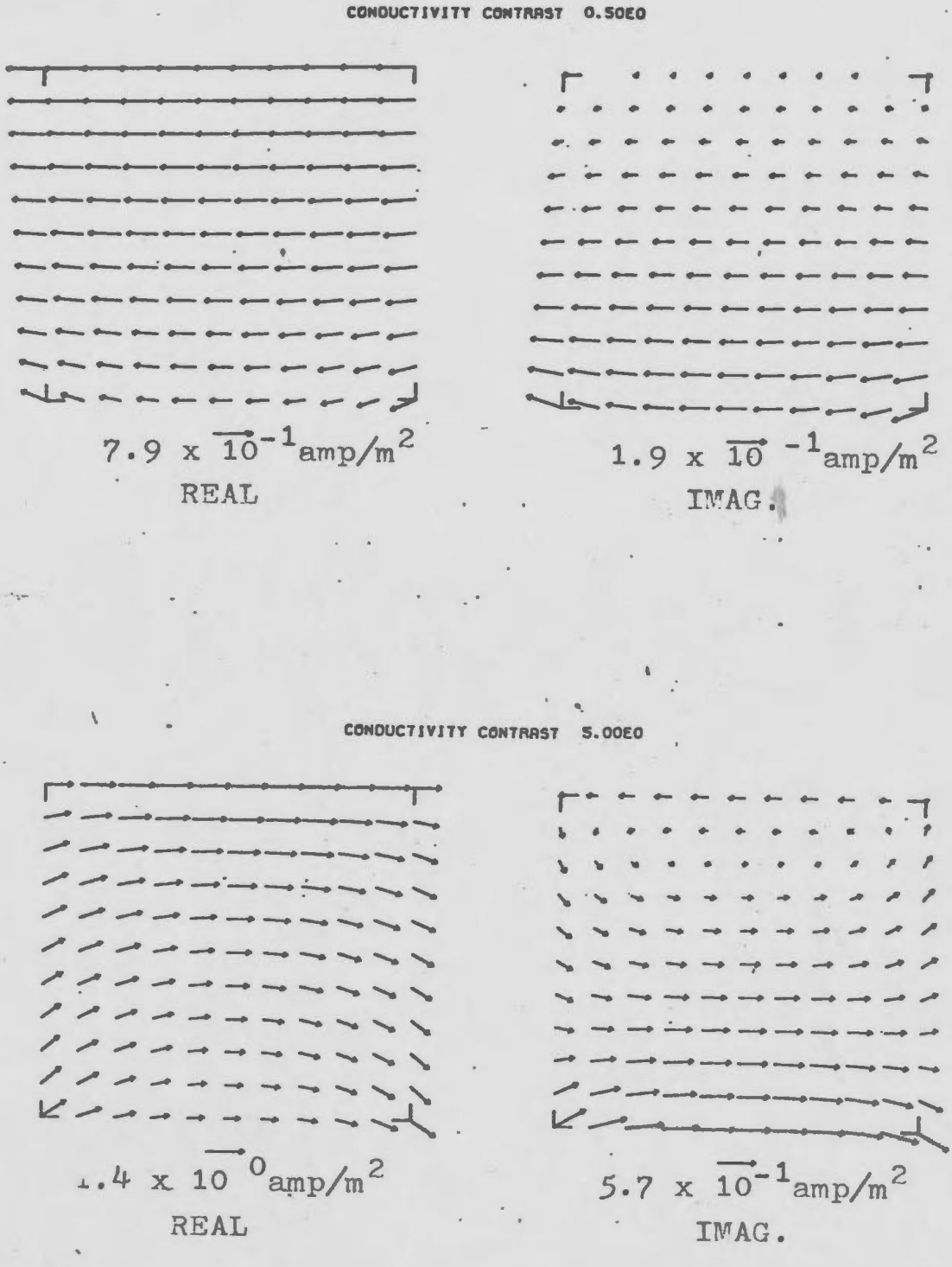

Fig. 6-18 Equivalent current for TM model #1 for various conductivity contrasts.

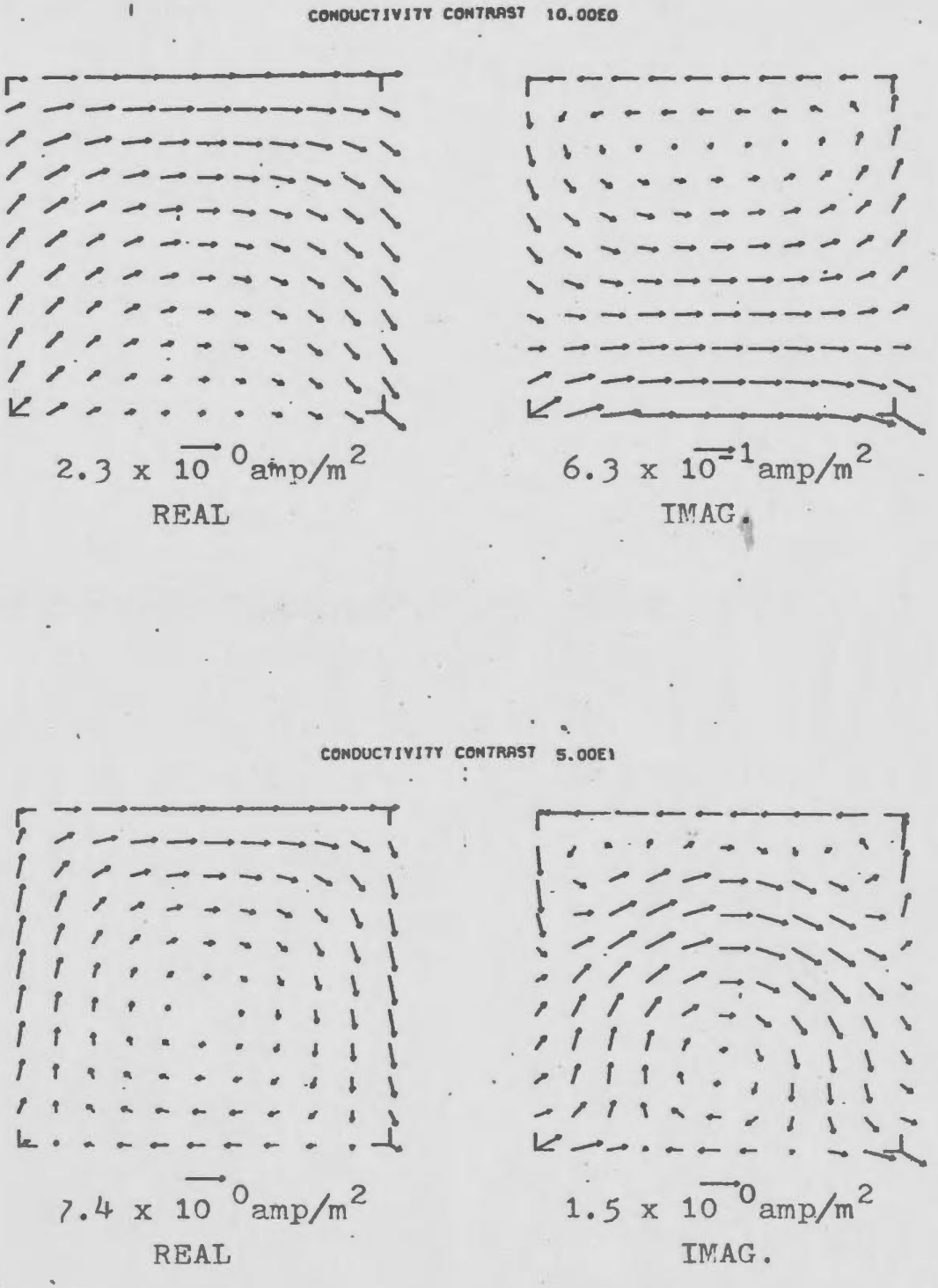

Fig. 6-18 cont'd. Equivalent current for TM model #1 for different conductivities.

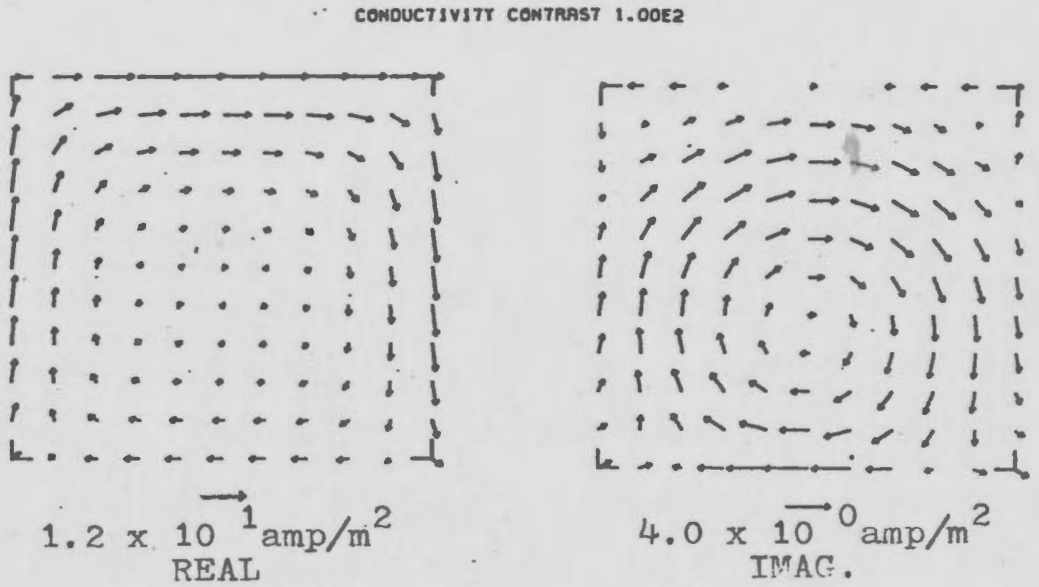

Fig. 6-18 cont'd. Equivalent current for TM model #1 for differnent conductivity contrasts.

out of the cylinder at the lower corners. The self-inductance of the body also exhibits itself by a slight skindepthing effect; for $\sigma_1/\sigma_0 = 5.0$, the body has an internal skindepth $\delta_1 = (\frac{\sigma_1}{\sigma_0})^{1/2}\delta_0 \simeq 2.2\,\delta_0$. The skindepthing effect causes the real current to be pulled towards the top of the cylinder in a curling current flow; this curling of the real current results in a weak but closed eddy current flow being established at the top of the conductor in the imaginary component of $\overline{J}_e$. Increasing σ_1/σ_0 to 10.0, enhances the inductive effects and the eddy pattern in the imaginary component of $\overline{J}_e$ is stronger. One other feature that is beginning to occur is the saturation of the conductive channelling effect; the currents flowing normal to the edges of the cylinder are growing smaller relative to the closed solenoidal current flow which is dominantly parallel to the sides. As the σ_1/σ_0 ratio is increased further, these effects are enhanced; at σ_1/σ_0 equal to 50.0, both the real and imaginary components of $\overline{J}_e$ flows around the cylinder as close to the outer surface as possible and with $\overline{J}_e \cdot \hat{n}$ at the surface small in comparison to the peak current. The imaginary component of $\overline{J}_e$ is much more convoluted showing a small eddy at the top of the cylinder and a larger closed eddy in the lower two thirds of the body which has the opposite sense of flow.

At a 50:1 conductivity contrast the numerical solution is being stretched to its limit; the body is about 2.8 internal skindepths across for this ratio. To emphasise the approximate, but flexible nature, of the least squares solution, the solution for a conductivity contrast of 100:1 is shown for discussion purposes. For $\sigma_1/\sigma_0 = 100.0$, the body is internally four skindepths across. The equivalent current shows an extension of the self-induction effects and saturation of the conductive channelling effects. The closed eddies are much stronger and the real component of $\overline{J}_e$ has been squeezed closer to the cylinder surface. While the numerical solution has limited validity at this conductivity contrast, the solution does exhibit

the type of response to be expected in a gross sense. The least squared error is attained by matching of gross features at the expense of local detail. The consequence of this is more readily seen in the computation of the anomalous fields at the surface of the half-space.

The normalized anomalous electric field at the surface of the half-space for each σ_1/σ_0 ratio is shown in Fig. 6-19 along with results obtained by Wright's finite difference solution method. As pointed out previously the normalized impedance Z_N is equivalent to E'_T/E'_0. For low contrasts, the least squares integral equation solution and the finite difference solution agree within one or two percent; the discrepancies reflect the differences in the numerical solution methods. At $\sigma_1/\sigma_0 = 50.0$, a slight but consistent difference between the two solutions is visible while at a contrast of 100:1, the anomalies directly over the body show only similar trends and the solutions only begin to match at large distances from this cylinder. Here the averaging nature of the least squares method yields the solution at large distances but the local details of the response are incorrect. At large distances from the cylinder the anomalous field is roughly an average of $\bar{J}_e$ over the cylinder and local variations in $\bar{J}_e$ become less important. This smoothing is shown even more clearly by the next TM model discussed.

TM Model 2

As pointed out previously, the second TM model differs from the first only in that the top of the body is located 0.1 δ_0 below the surface of the half-space. (see Table 6- 8) The sequence of equivalent current arrow maps is shown in Fig. 6-20. These diagrams show basically the same behaviour as those for model 1; the main difference is that the current is channelled into the body at all four corners. As the conductivity contrast

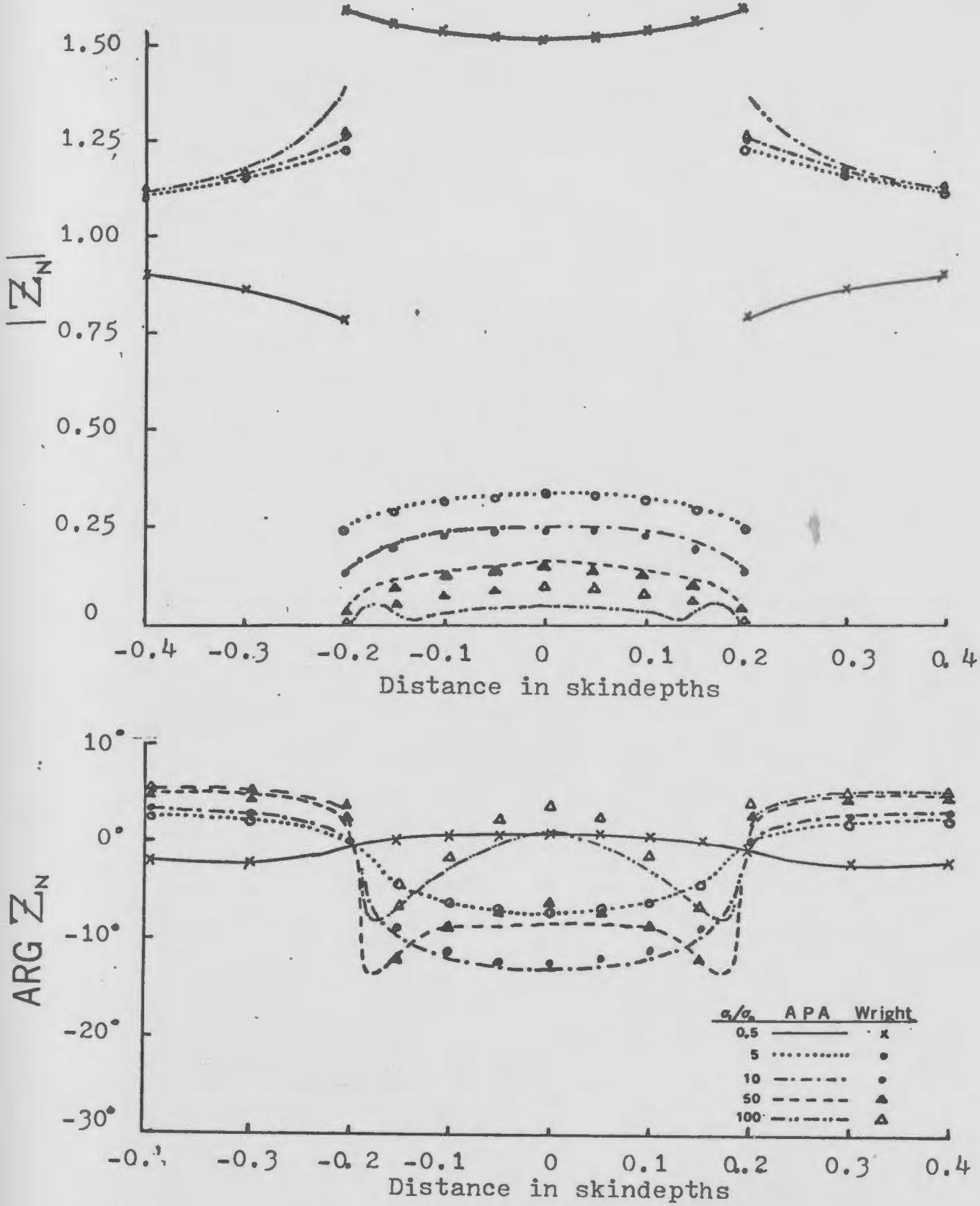

Fig. 6-19 Normalized impedance over TM model #1

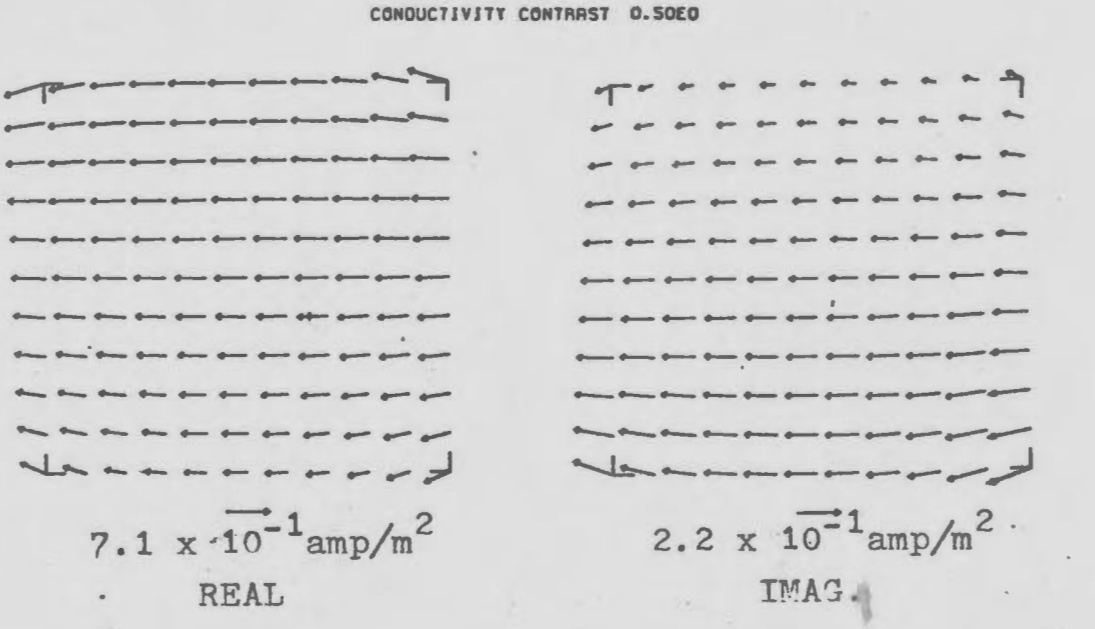

Fig. 6-20 Equivalent current for TM model #2 for different conductivity contrasts.

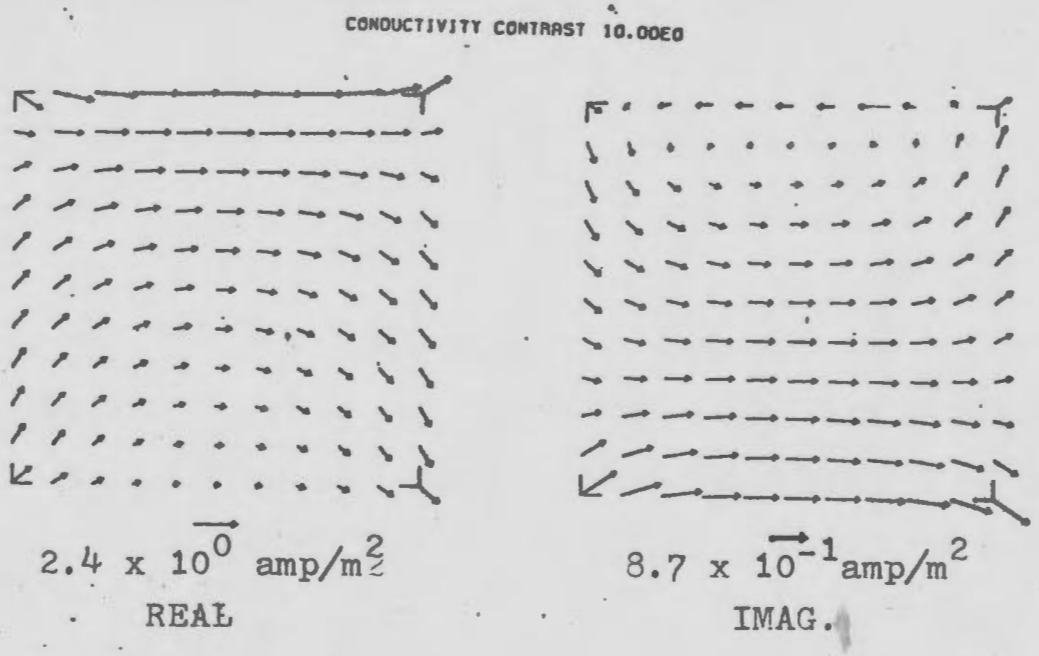

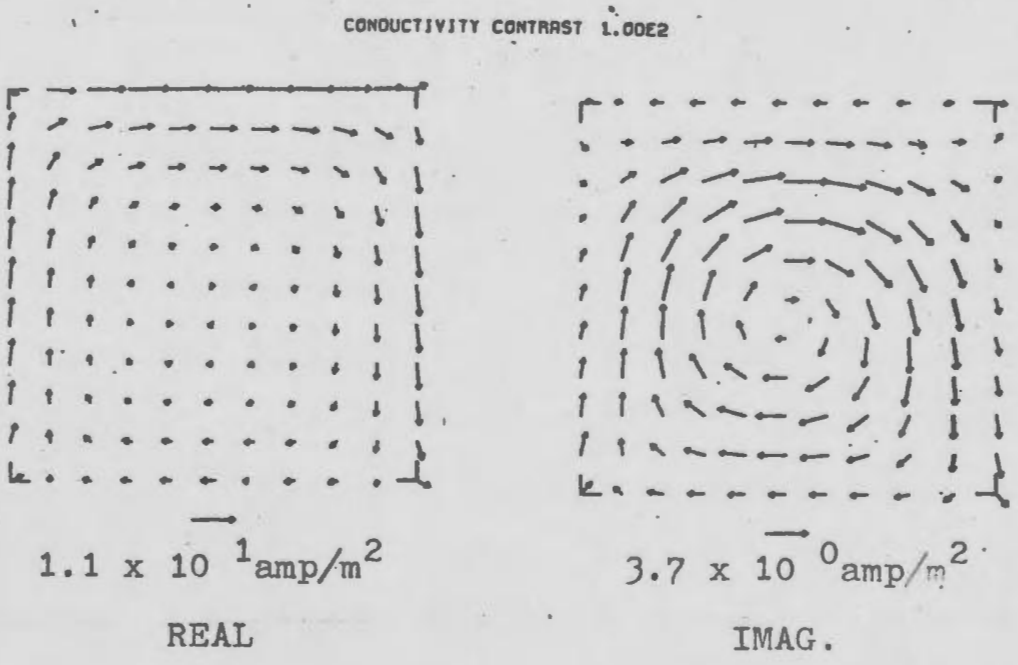

Fig. 6-20 cont'd. Equivalent current for TM model #2 for different conductivity contrasts.

runs from small to large values, the cylinder response runs from the conductive channelling response to the inductive response.

The anomalous fields associated with $\bar{J}_e$ result in the total electric field or normalized impedance profiles given in Fig. 6-21. The discontinuity in the field strength of the last model has now vanished since the model is buried at a finite depth. The burial of the body helps smooth out the localized discrepancies which are a product of the least squares type of solution. As a result, the surface fields are much smoother and much better agreement with Wright's finite difference solution is obtained in this case. With the exception of the points directly over the centre of the body for $\sigma_1/\sigma_0 = 100.0$, the two sets of solutions show differences of only 1 or 2%.

(iv) TM Summary

The preceding models by no means exhaust the possible combinations of parameters which should be examined in order to investigate the least squares solution method and the TM response to their fullest extent. Such a detailed presentation of data is beyond the scope of this thesis project. A number of other models were investigated during this study in order to evaluate in a rough sense the variability and reliability of the least squares method of solution in TM problems. A summary of the general results found during this analysis is given here in order to clarify points not discussed in regard to the two models analysed in detail.

The square cylinder model was run for several other cross-section dimensions which were 0.1, 0.2, and 1.0 δ_0 to a side. The response, aside from minor variations due to geometrical factors, was the same. A surprising result in the initial stages of analysis was the failure of the least squares method to yield good results for small bodies with high conductivity

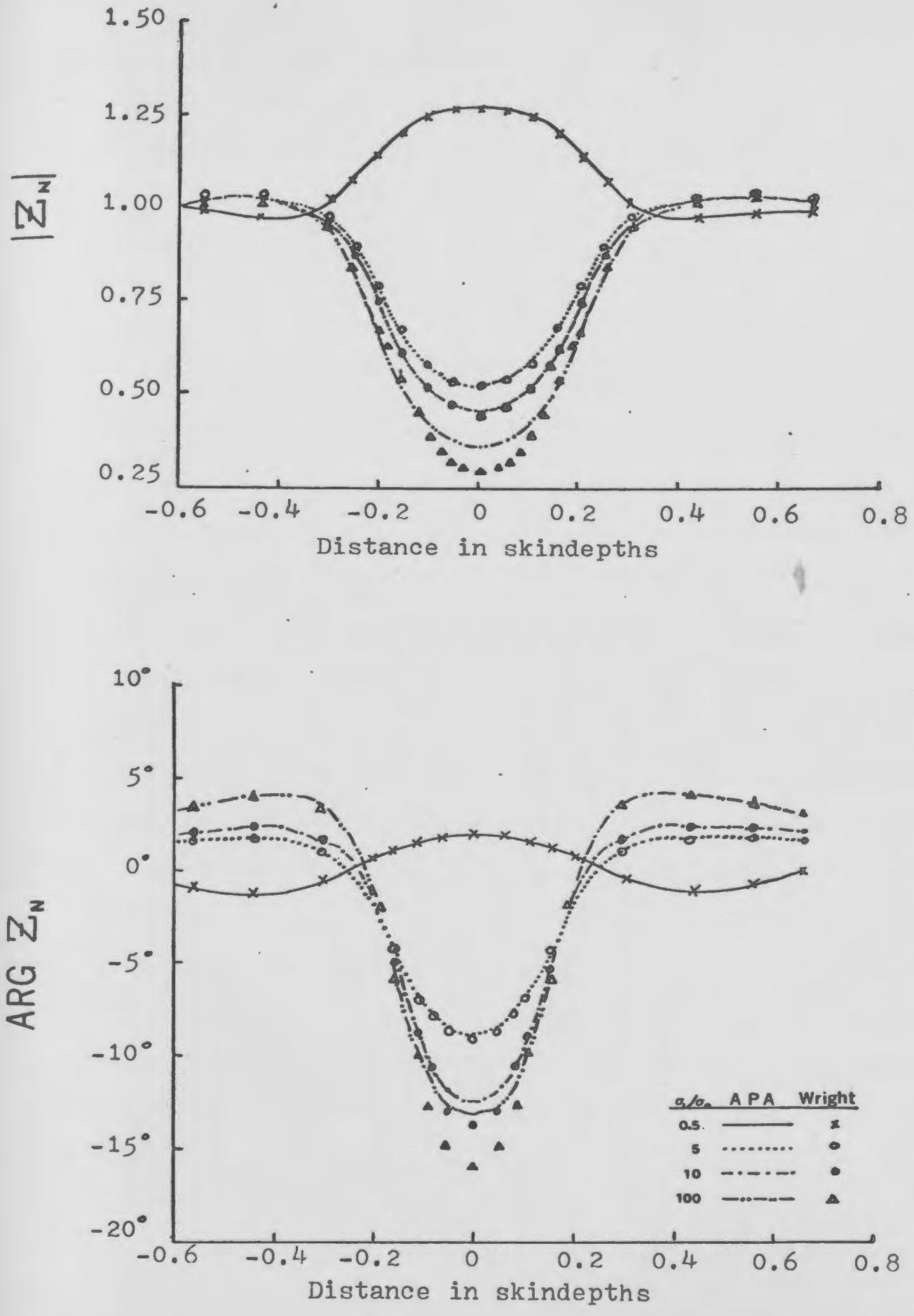

Fig. 6-21 Normalized impedance over TM model #2

contrasts. In general, $\sigma_1 / \sigma_o = 50.$ was the cut off point for reliable results for small bodies. One would anticipate at first glance that skindepthing effects would not become a dominant factor in the response until much higher conductivity contrasts. The reason for the failure at high conductivity contrasts was due to ill-conditioning of the scattering matrix which resulted in gross errors in the numerical inversion of the matrix.

As discussed in a general context in chapter four, the integral operator governing the scattering equivalent current is bimodal and the inductive or solenoidal currents can see a much different impedance than the non-solenoidal currents. For small bodies, the two impedances become highly mismatched when the anomalous complex conductivity of the body is large. In terms of the numerical solution of such a problem, the discrete matrix equation has a coefficient matrix with large differences between various eigenvalues. Since the least squares matrix is proportional to the square of the integral impedance operator, the least squares scattering matrix will have eigenvalues with ratios proportional to the square of the intrinsic impedances of the operator. As a consequence, the matrix becomes very highly ill-conditioned for small bodies with large conductivities. Detailed investigation of the TM scattering matrix and its numerical inverse showed this to be the case for small bodies. While various ways of inverting the matrix were tried, the only way to improve numerical inversion of the matrix was double precision arithmetic on the computer and since it could only afford partial resolution of the problem it was not implemented. Higher accuracy of the arithmetic automatically required higher accuracy in numerical evaluation of the integral coefficients which became impractical from a computer time standpoint. Thus the least squares solution of the TM scattering problem is limited to conductivity contrasts of less than 50:1 for small bodies with a $A \lesssim 0.3\,\delta_o$ being a general rule.

The TM response of larger bodies was more in line with the expected behaviour. The conductivity contrasts which could be modelled accurately depended on the size of the body. The larger the body, the more quickly the internal dimensions in internal skindepths become larger than that which the polynomial degree of the approximate solution could handle accurately. Above a size dependent conductivity contrast, the solution follows the gross behaviour of the true response but departs considerably on the local scale. At large distances from the body where the scattered fields are approximately an average of the anomalous current the least squares response is good to much higher conductivity contrasts. Computations of scattered fields inside or in the proximity of the body will exhibit large deviations from the true solution. While the polynomial degree can be increased and the solution for larger bodies at higher conductivities computed, computational practicalities put a limit to the maximum degree attainable. In the initial part of the study of this problem, polynomial degrees greater than 5 were out of the question because of computer hardware available and the number of computer dollars which could be invested in a particular problem.

Other factors in the numerical solution are the number of error points used in computation of the total squared error and the accuracy of the numerical evaluation of the integral coefficients. The number of error points was not a major factor in the solution. The number of points was taken to be greater than twice the number of unknown polynomial coefficients or such that the average spatial subdivision of the body was about 0.5 internal skindepths. With the exception of small bodies with high conductivities the accuracy of the numerical quadratures was not a significant factor in determining the response. These two factors together with the maximum polynomial degree are the basic factors governing the computer time required for determination of the responses.

The computer time required for the various stages of computation were highly variable, and generally applicable numbers are difficult to give. For the models given here, with a maximum polynomial degree of 4, sixty four error points and numerical integral accuracies better than 0.1% required between 40 to 60 seconds of CPU time on an IBM 370-165. Cutting back on the numerical quadrature accuracy to about a 1% tolerance, dropped this time to about 10 seconds of CPU time. Computation of the scattering matrix and its inverse plus computation of the surface fields required between 10 and 20 seconds of CPU time for the initial run of a given geometrical model and about 5 seconds for each subsequent conductivity contrast. This computation time is compatible with the finite difference method which required about a minute of CPU time per model. For numerous responses at differing conductivity contrasts the least squares method is considerably less expensive. All stages of the computer programs were designed to run in less than 120K bytes or 30K words of memory.

In summary, the least squares solution method as applied to the TM response is a moderately useful technique. There are a number of drawbacks in using this method in general for small highly conductive scatterers where both solenoidal and non-solenoidal currents form the total current flow. These particular bodies result in ill-conditioned matrices. The least squares technique aggravates this ill-conditioning by generating a scattering matrix which is proportional to the square of the general impedance. On the other hand, the least squares solution provides reliable and inexpensive computations of the response in ranges where ill-conditioning is not a problem. For large bodies, it can also provide economical estimates of the response if the body is buried sufficiently deep in the half-space to ensure local discrepancies in the solution are smoothed out by the averaging effect of the integral required to compute the anomalous fields at the surface.

CHAPTER 7

ELECTROMAGNETIC SCATTERING BY A THIN RECTANGULAR SHEET

7-1 Introduction

The electromagnetic response of a thin rectangular sheet is of considerable interest in applied geophysics. Analysis of the thin sheet model provides a quasi-three dimensional structure which can be used to investigate the roles of the inductive and conductive and/or capacitive effects in an electromagnetic scattering problem. The inductive response of a thin conducting sheet in free space has been analysed by Lamontagne and West (1971) for parameters which permit use of the quasi-static assumptions. In this chapter the total response is analysed from the eigencurrent or characteristic mode point of view. The inductive response obtained by Lamontagne and West can be shown to separate out of the solution.

The first step of the analysis will be to derive the equivalent current equations for the thin sheet. These equations are derived from the equations for the response of a rectangular parallelepiped. The thin sheet equations are obtained by letting one dimension of the parallelepiped become infinitesimally small.

7-2 Integral Equations for a Parallelepiped in a Whole-Space

The parallelepiped is illustrated in Fig. 7-1. The parallelepiped resides in a whole-space of complex conductivity σ_o and magnetic permeability μ_o ; the anomalous body has a complex conductivity σ_1 and is taken to have the same magnetic permeability as the background whole-space. The parallelepiped of dimensions $(2a_1, 2a_2, 2a_3)$ is at the center of the cartesian coordinate system (x_1, x_2, x_3) with the associated unit vectors $(\hat{e}_1, \hat{e}_2, \hat{e}_3)$

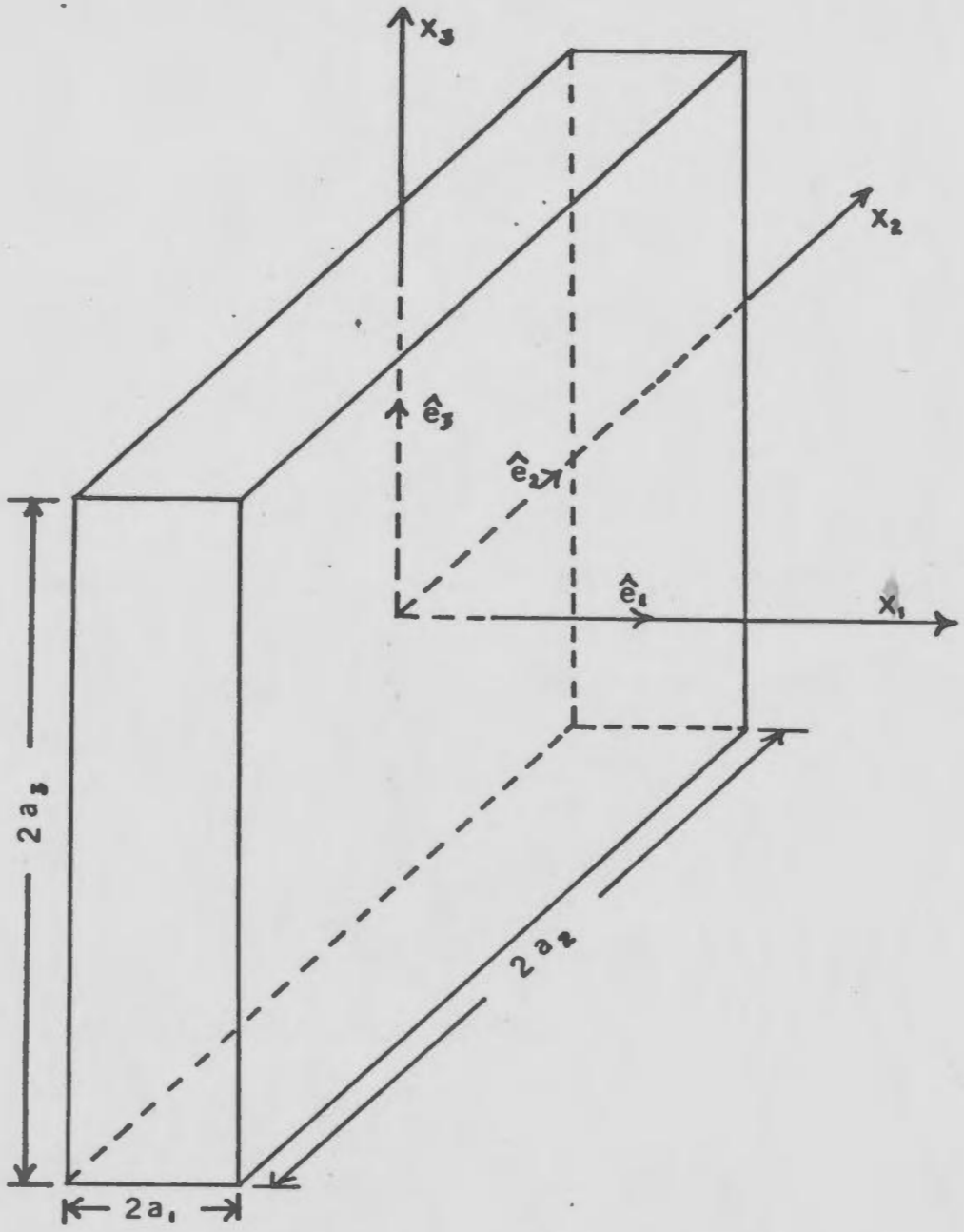

FIG. 7-1 Parallelepiped geometry

The anomalous conductivity is given by

$$\sigma_a = \sigma_D \prod_{i=1}^{3} B(x_i, a_i) \qquad 7\text{-}1$$

where

$$B(x, a) = 1 \qquad |x| \leq a$$
$$= 0 \qquad |x| > a$$

and

$$\sigma_D = \sigma_1 - \sigma_0$$

The equivalent source current $\bar{J}_e$ exists only in the volume, V, where σ_a is non-zero. The integral equation for $\bar{J}_e$ is

$$\bar{J}_e(r) - j\omega\mu_0\sigma_D \int_V \overset{\epsilon}{\underset{J}{\tilde{\mathcal{G}}}}(r,r') \cdot \bar{J}_e(r')\, d^3r' = \sigma_D \bar{E}_0(r) \qquad 7\text{-}2$$

where $\bar{E}_0$ is the external exciting electric field. For a homogeneous whole-space the Green's dyadic $\overset{\epsilon}{\underset{J}{\tilde{\mathcal{G}}}}$ is

$$\overset{\epsilon}{\underset{J}{\tilde{\mathcal{G}}}}(r,r') = \left[\tilde{I} + \frac{\bar{\nabla}\bar{\nabla}}{k_0^2} \right] g(r,r') \qquad 7\text{-}3$$

where

$$g(r,r') = \frac{e^{ik_0|\bar{r}-\bar{r}'|}}{4\pi|\bar{r}-\bar{r}'|}$$

and $k_0 = (j\omega\mu_0\sigma_0)^{1/2}$ is the propagation constant in the background medium.

Substituting for $\overset{\epsilon}{\underset{J}{\tilde{\mathcal{G}}}}$ in 7-2 and dividing through by σ_D yields

$$\frac{\bar{J}_e(r)}{\sigma_D} - j\omega\mu_0 \int_V g(r,r')\, \bar{J}_e(r')\, d^3r' - \frac{\bar{\nabla}}{\sigma_0} \int_S \left(\bar{J}_e(r') \cdot \hat{n}\right) g(r,r')\, d^2r' = \bar{E}_0 \qquad 7\text{-}4$$

where the identities

$$\bar{\nabla} \cdot \int_V g(r,r')\, \bar{J}(r')\, d^3r' = -\int_S \bar{J}(r') \cdot \hat{n}\, g(r,r')\, d^2r' + \int_V g(r,r')\, \bar{\nabla}' \cdot \bar{J}_e(r')\, d^3r' \qquad 7\text{-}5$$

and $\bar{\nabla} \cdot \bar{J}_e \equiv 0$ inside the volume have been used. The terms in 7-4 have a straight forward interpretation as discussed in chapter 4. The sum of these three fields must balance $\bar{E}_0$, the exciting external field.

Equation 7-4 is a set of three coupled integral equations in the

three components of $\bar{J}_e$. While the analysis has been carried out for a rectangular parallelapiped, the equations hold for any shaped body with a constant anomalous conductivity.

7-3 Thin Sheet Equations

The thin sheet equations are derived from 7-4 by letting $a_3 \rightarrow 0$ while the product $\sigma_b a_3$ remains finite. The end product is a surface current on a sheet of zero thickness and infinite conductivity, but which has a finite surface conductivity. This model provides a simulation for real structures which are both geometrically and inductively thin. The geometrically thin constraint requires

$$a_3 \ll a_1 a_2 \qquad 7\text{-}6$$

The inductively thin requirement is

$$|(j\omega\mu_0\sigma_1)^{1/2} a_3| \ll 1 \qquad 7\text{-}7$$

In the limit as $a_3 \rightarrow 0$, the equivalent current must take the form

$$\bar{J}_e(x_1,x_2,x_3) \xrightarrow[a_3 \to 0]{} \bar{K}_e(x_1,x_2)\,\delta(x_3) \qquad 7\text{-}8$$

The surface current $\bar{K}_e$ will be defined in terms of $\bar{J}_e$ by integrating $\bar{J}_e$ over the thickness of the sheet; namely

$$\bar{K}_e(x_1,x_2) = \lim_{a_3 \to 0} \int_{-a_3}^{a_3} J_e(x_1,x_2,x_3)\,dx_3 \qquad 7\text{-}9$$

Performing this integration on each term of 7-4 and dividing by $2a_3$ yields the thin sheet equations. The form of each term in equation 7-4 is shown in Table 7-1. The ohmic and inductive terms can be handled in a straight forward manner.

The capacitive or conductive term is the more difficult term to handle in the limit as $a_3 \rightarrow 0$ since some of the integrals become singular unless $\bar{J}_e$ has particular properties. The reason for this is apparent when the physical nature of the integrals is examined. The surface current

Table 7-1 Parallelapiped to Thin Sheet Transformation

$$\frac{\bar{J}_e(r)}{\sigma_0} \longrightarrow \frac{\bar{K}_e(\rho)}{\sigma_s}$$

$$j\omega\mu_0 \iiint_V \bar{J}_e(r')\, g(r,r')\, d^3r' \longrightarrow j\omega\mu_0 \iint_A \bar{K}_e(\rho')\, g(\rho,\rho')\, d^2\rho'$$

$$\frac{\bar{\nabla}}{\sigma_0} \iint_{S_v} \bar{J}_e(r')\cdot\hat{n}\, g(r,r')\, d^2r' = \sum_{k=1}^{3} \hat{e}_k \frac{\partial}{\partial x_k} \int_{-a_p}^{a_p}\int_{-a_q}^{a_q} J_i(r')\, g(r,r') \Big|_{x_i'=-a_i}^{x_i'=a_i} dx_p' dx_q'$$

$$\longrightarrow -\frac{\bar{\nabla}}{\sigma_0} \iint_A \bar{\nabla}_2' \cdot \bar{K}_e(\rho')\, g(\rho,\rho')\, d^2\rho'$$

$$\sigma_s = 2a_3\sigma_0$$

$$\bar{\rho} = \sum_{i=1}^{2} x_i \hat{e}_i$$

$$\bar{\rho}' = \sum_{i=1}^{2} x_i' \hat{e}_i$$

$$\bar{\nabla}_2 = \sum_{i=1}^{2} \frac{\partial}{\partial x_i} \hat{e}_i$$

component K_3 corresponds to a surface distribution of electric dipoles. For a sheet of zero thickness $\bar{K}_3$ must be identically zero; the current component $\bar{J}_3$ must remain finite as $a_3 \rightarrow 0$. The amount of current flowing through the sheet is determined by the electric field normal to the sheet times the background conductivity; since this current amplitude remains finite as $\sigma_0 \rightarrow \infty$ and $a_3 \rightarrow 0$, $K_3 = 0$. The terms involving K_3 behave much like those for a parallel plate capacitor as the plate separation becomes infinitesimally small. At the point of zero spacing the theoretically capacitance becomes infinite, however, the capacitor actually becomes a short circuit. Thus the thin sheet of zero thickness and finite surface conductivity is invisible to electromagnetic fields which have an electric field which is totally polarized in the $\hat{e}_3$ direction.

Additional constraints on the surface current are that $K_1 \equiv 0$ at $x_1 = \pm a_1$ and $K_2 \equiv 0$ at $x_2 = \pm a_2$. The current flowing perpendicular to the edge of the sheet results in a line charge or line current source/sink around the edge of the sheet. The self-energy of a line charge is infinite. The integrals associated with these line charges which grow in an unbounded manner can be viewed as infinite impedance paths; as a result, the currents in these paths have to vanish.

The overall result for the thin sheet is that it can be characterized by a surface current $\bar{K} = (K_1, K_2, 0)$ which satisfies the integral equation

$$\frac{\bar{K}e(r)}{\sigma_s} - j\omega\mu_0 \iint_A \bar{K}e(r')g(r,r')d^2r' - \frac{\nabla}{\sigma_0}\iint_A \nabla'\cdot\bar{K}_e(r')g(r,r')\,d^2r' = \bar{E}_{0,t} \quad 7\text{-}10$$

with the additional constraint that $\bar{K}_e \cdot n = 0$ where n is the normal at the edge of the sheet in the plane of the sheet and $\bar{E}_{0,t} = (E_1, E_2, 0)$. The third component of $\bar{E}_0$ passes through the sheet as if it did not exist.

7-4 General Thin Sheet Response

(1) Numerical Analysis Formulation

As shown in the last section, the thin sheet problem reduces to one of solving a two dimensional vector Fredholm integral equation. The numerical solution of 7-10 is carried out using the eigencurrent technique discussed in chapter 4. The first step in the analysis follows the Galerkin procedure in which a discrete set of approximating currents is used to reduce 7-10 to a finite dimension matrix equation. The following set of functions were used as the trial functions

$$\varphi^1_{nm} = (1-\xi^2)\, T_n(\xi)\, T_m(\eta) \qquad 7\text{-}11$$

$$\varphi^2_{nm} = (1-\eta^2)\, T_n(\xi)\, T_m(\eta) \qquad 7\text{-}12$$

The arguments ξ and η are dimensionless coordinates defined by

$$\xi = x_1/a_1 \qquad 7\text{-}13 \qquad\qquad \eta = x_2/a_2 \qquad 7\text{-}14$$

thus $-1 \leq \xi, \eta \leq 1$. $T_n(x)$ is the Chebychev polynomial of the first kind and degree n.

Equation 7-10 reduces to a finite set of linear equations by approximating $\overline{K}_e$ by a finite set of 7-11 and 7-12. The approximating set was chosen as

$$K_i = \sum_{n,m} c^i_{nm}\, \varphi^i_{nm} \qquad 7\text{-}15$$

where $n + m \leq N$. The maximum degree of the Chebychev polynomials is N. This leads to a set of $M = (N+1)(N+2)/2$ approximating functions for each K_i or a total of 2M coefficients $c^i_{n,m}$.

From this point on, a matrix formulation of the problem is used. First, the row vector of approximating functions is defined as

$$[\Phi^i] = [\varphi^i_{00}, \varphi^i_{10}, \varphi^i_{01}, \varphi^i_{20}, \varphi^i_{11}, \varphi^i_{02}, \cdots\cdots \varphi^i_{0N}] \qquad 7\text{-}16$$

The functions are grouped in ascending degree n + m = constant. Within

Table 7-2 General Thin Sheet Response: Elements of Galerkin Matrices

$$[F] = \int_{-a_1}^{a_1}\int_{a_2}^{a_2} \begin{bmatrix} [\Phi^1(x_1,x_2)]^T [\Phi^1(x_1,x_2)] & 0 \\ 0 & [\Phi^2(x_1,x_2)]^T [\Phi^2(x_1,x_2)] \end{bmatrix} dx_1 dx_2$$

$$[\mathcal{L}] = \int_{-a_1}^{a_1}\int_{-a_2}^{a_2}\int_{-a_1}^{a_1}\int_{-a_2}^{a_2} g(x_1,x_1',x_2,x_2') \begin{bmatrix} [\Phi^1(x_1,x_2)]^T [\Phi^1(x_1',x_2')] & 0 \\ 0 & [\Phi^2(x_1,x_2)]^T [\Phi^2(x_1',x_2')] \end{bmatrix} dx_1 dx_2 dx_1' dx_2'$$

$$[Q] = \int_{-a_1}^{a_1}\int_{-a_2}^{a_2}\int_{-a_1}^{a_1}\int_{-a_2}^{a_2} g(x_1,x_1',x_2,x_2') \begin{bmatrix} \left[\frac{\partial \Phi^1(x_1,x_2)}{\partial x_1}\right]^T \left[\frac{\partial \Phi^1(x_1',x_2')}{\partial x_1'}\right] & \left[\frac{\partial \Phi^1(x_1,x_2)}{\partial x_1}\right]^T \left[\frac{\partial \Phi^2(x_1',x_2')}{\partial x_2'}\right] \\ \left[\frac{\partial \Phi^2(x_1,x_2)}{\partial x_2}\right]^T \left[\frac{\partial \Phi^1(x_1',x_2')}{\partial x_1'}\right] & \left[\frac{\partial \Phi^2(x_1,x_2)}{\partial x_2}\right]^T \left[\frac{\partial \Phi^2(x_1',x_2')}{\partial x_2'}\right] \end{bmatrix} dx_1 dx_2 dx_1' dx_2'$$

$$[E] = \int_{-a_1}^{a_1}\int_{-a_2}^{a_2} \begin{bmatrix} [\Phi^1(x_1,x_2)]^T E_1(x_1,x_2) \\ [\Phi^2(x_1,x_2)]^T E_2(x_1,x_2) \end{bmatrix} dx_1 dx_2$$

with

$$[Z] = [R] + j[X] \qquad 7\text{-}21$$

where $[R]$ = Real $[Z]$ is the total resistance matrix and $[X]$ = Imag $[Z]$ is the reactance matrix. The resistance matrix contains both the internal ohmic dissipation and the radiation impedance. If the background has a finite conductivity, the radiation impedance, which is the real part of $-j\omega\mu_0[R] - \frac{1}{\sigma_0}[Q]$ corresponds to the ohmic dissipation in the background medium. The reactance matrix describes the energy storage in the internal electric polarization and external "electrostatic" and "magnetostatic" fields.

The weighted eigencurrent problem becomes

$$\{[R] + j[X]\}[I_n] = \lambda_n[R][I_n] \qquad 7\text{-}22$$

The resistance matrix is diagonalized by the unitary transformation $[U]$ which is a matrix comprising the eigenvectors of $[R]$ such that

$$[U]^T[R][U] = [D(r_i)] \qquad 7\text{-}23$$

where $[D(r_i)]$ is a diagonal matrix containing the eigenvalues of $[R]$. As pointed out in chapter 4, λ_n must be of the form $\lambda_n = 1 + j\beta_n$. Defining

$$[X'] = [D^{-1/2}(r_i)][U]^T[X][U][D^{-1/2}(r_i)] \qquad 7\text{-}24$$

and

$$[I_n'] = [D^{1/2}(r_i)][U]^T[I_n] \qquad 7\text{-}25$$

7-22 reduces to the conventional eigenvector problem

$$[X'][I_n'] = \beta_n[I_n'] \qquad 7\text{-}26$$

Diagonalizing $[X']$ with the unitary matrix $[S]$ made up of the eigenvectors of $[X']$

$$[S]^T[X'][S] = [D(\alpha_i)] \qquad 7\text{-}27$$

where α_i are the eigenvalues of $[X']$. The matrix of eigencurrents for 7-21 is then given by

$$[I_n] = [u][D^{-1/2}(r_i)][S] \qquad 7\text{-}28$$

which have the associated eigenvalues

$$\lambda_n = 1 + j\alpha_n$$

The formal inverse to the scattering matrix is given by

$$[Z]^{-1} = [u]\left[D\left(\frac{1}{1+j\alpha_n}\right)\right][u]^T \qquad 7\text{-}29$$

The solution of the original scattering problem is then given by

$$[c] = [u][D^{-1}(1+j\alpha_n)][u]^T[E] \qquad 7\text{-}30$$

At this point the formality of reducing the integral equation to a finite set of linear equations is complete and this permits the approximate representation of the eigenfunctions of the scattering integral operator. In the next section, the eigenfunctions of a particular model are computed numerically in order to demonstrate the type of result to be expected.

(ii) Numerical Results

The approximate eigenfuntions for the model shown in Fig. 7-2 were computed to illustrate some of the ideas developed in chapter 4, with particular emphasis on the bimodal character of $[Z]$. The response is characterized by the parameters listed in Table 7-3 and the particular parameters for the model shown in Fig. 7-2 are listed in Table 7-4. The maximum polynomial degree is 1 and was chosen as small as was reasonable to minimize the amount of data to be presented.

The computations followed the sequence outlined in the flow diagram shown in Fig. 7-3. The first step in the analysis was the computation of the integral coefficient matrices of Table 7-2 which can be expressed in

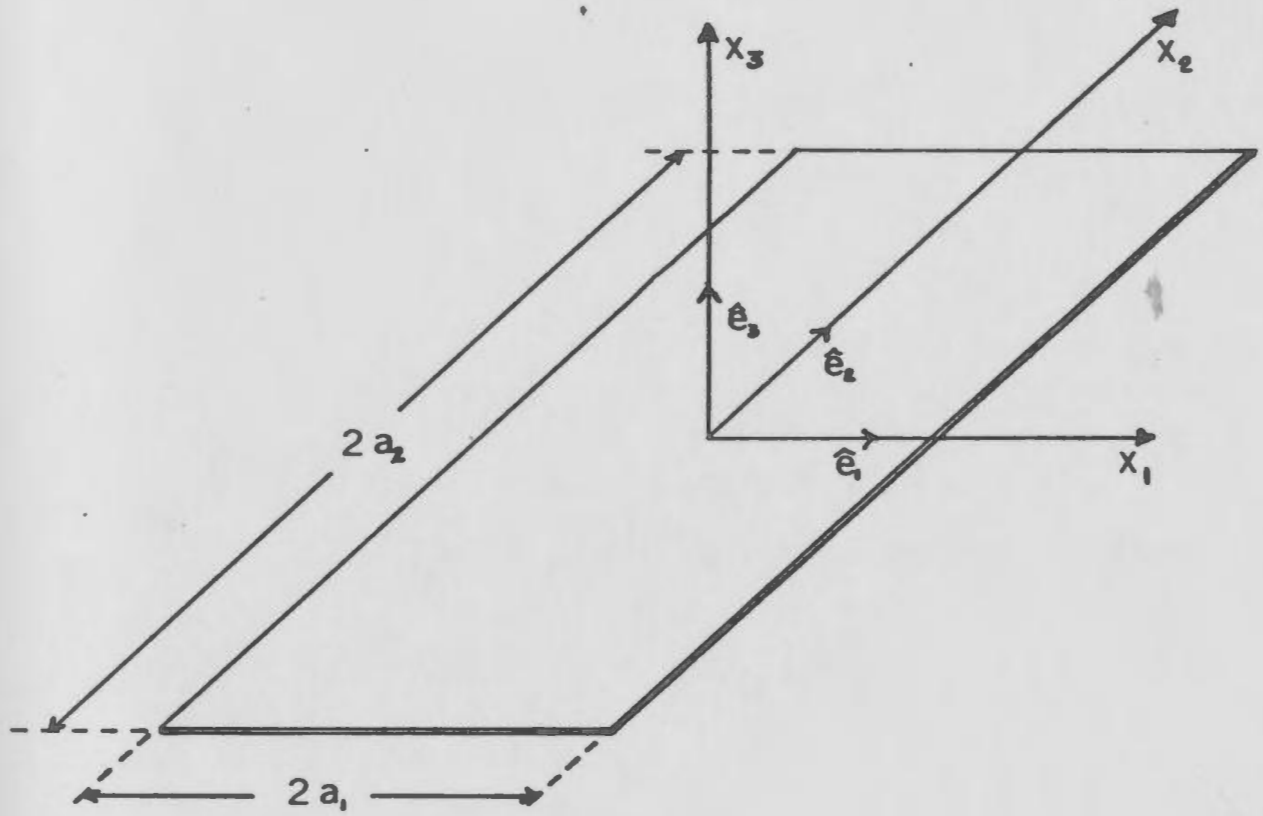

Fig. 7-2 General thin sheet geometry

Table 7-3 General Thin Sheet Governing Parameters

Geometrical

a_1 = Half-length of sheet in meters

$a_2 / a_1 = \mathcal{R}$ = Width to length ratio

Electrical

ω = Angular frequency of excitation rad/sec.

σ_o = Background conductivity

ϵ_o = Background permittivity

σ_s = Sheet anomalous surface conductivity

Numerical Solution Parameters

N = Maximum polynomial degree of approximate solution

Table 7-4 General Thin Sheet: Model Parameters for Computer Analysis

$\omega = 2\pi \times 10^{3}$ rad. / sec.

$\sigma_o = 10^{-3}$ mho / m.

$\epsilon_o = 10^{-9}$ fd. / m.

$\sigma_s = \infty$ mhos

$\mathcal{R} = 0.667$

$a_1 = 300$ m.

$N = 1$

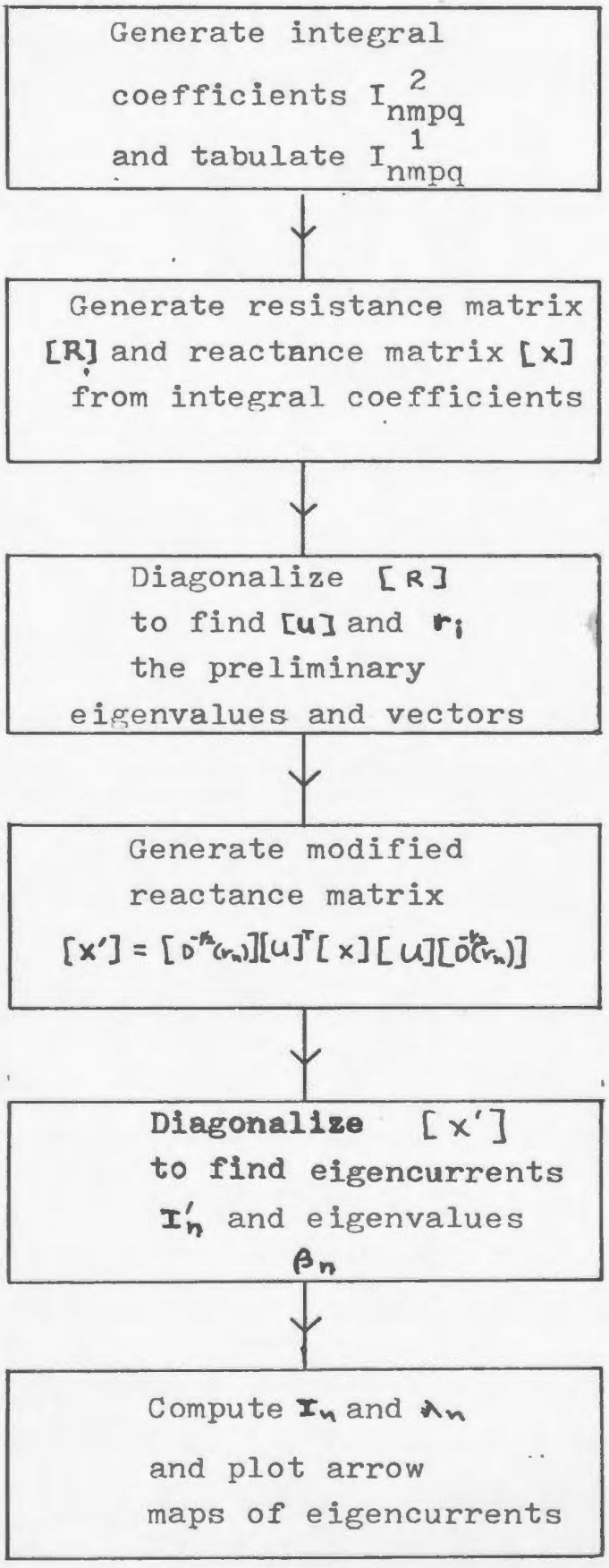

Fig. 7-3 General thin sheet computation flow chart.

terms of the integrals

$$I^{1}_{nmpq} = \int_{-1}^{1}\int T_n(\xi)\, T_m(\eta)\, T_p(\xi)\, T_q(\eta)\, d\xi\, d\eta \qquad 7\text{-}31$$

$$I^{2}_{nmpq} = \int_{-1}^{1}\int \int_{-1}^{1}\int T_n(\xi) T_m(\eta)\, g(\xi,\xi',\eta,\eta')\, T_p(\xi')\, T_q(\eta') d\xi d\eta\, d\xi' d\eta' \qquad 7\text{-}32$$

These integrals of the form 7-32 were computed numerically using a Gaussian scheme as outlined in Appendix D; the integrals of the form 7-31 were computed analytically. The integrals were tabulated and used as data for the programs which generated the $[R]$ and $[X]$ matrices. The resistance matrix was generated and diagnonalized; its eigenvectors and eigenvalues were then used to generate $[X']$ from $[X]$. $[X']$ was diagonalized to yield the eigenvalues λ_i and the eigenvectors of $[Z]$. The diagonalization of the matrices was carried out using a Jacobi iterative scheme.

The resulting eigenvalues of $[R]$ are listed in Table 7-5(a) and the eigenvalues for $\sigma_s \ggg 1$ for $[X']$ are listed in Table 7-5(b). The eigencurrents are shown in Fig. 7-4. The point to be noted here is that the eigenvalue spectrum is split into two distinct sets. Some eigenvalues of $[R]$ are of the order 10^5 larger than the members of the set of eigenvalues. The associated eigencurrents show distinct behaviour depending on which set they belong to. The large eigenvalues are associated with the channelling current flow pattern while the small eigenvalues all belong to the current flow patterns which are predominantly inductive in nature and are characterized by closed current loops or eddies.

This brief set of computations was carried out to show the bimodal nature of $[Z]$. The electrical and geometrical parameters of the sheet were chosen to be typical of those that might be encountered in real geophysical problems. The solution demonstrates that geophysical electromagnetic problems are prone to generation of highly ill-conditioned scattering matrices. The lower the background complex conductivity, and the smaller the body on the

Table 7-5 (a) Eigenvalues of [R] Matrix

Eigencurrent	Eigenvalue
1	1.74×10^{3}
2	1.08×10^{3}
3	7.54×10^{2}
4	6.96×10^{2}
5	3.91×10^{2}
6	2.39×10^{-2}

Table 7-5 (b) Eigenvalues of [X'] Matrix

Eigencurrent	Eigenvalues
1	9.76×10^{-2}
2	7.02×10^{-2}
3	4.00×10^{-2}
4	3.53×10^{-2}
5	2.25×10^{-2}
6	-1.33×10^{1}

Eigencurrent 1

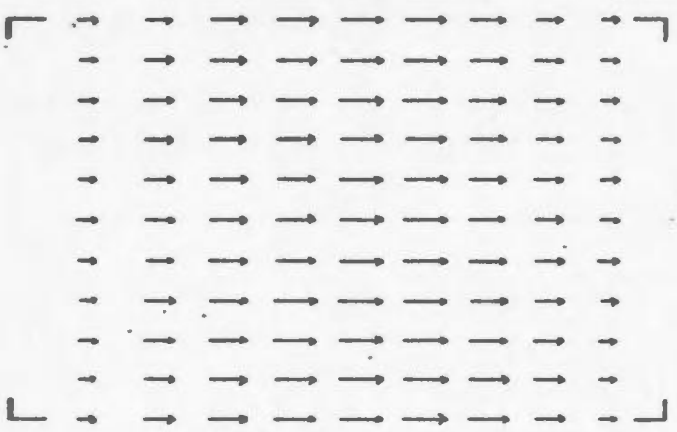

$3.5 \vec{x} 10^{-2}$ amp/m.

Eigencurrent 2

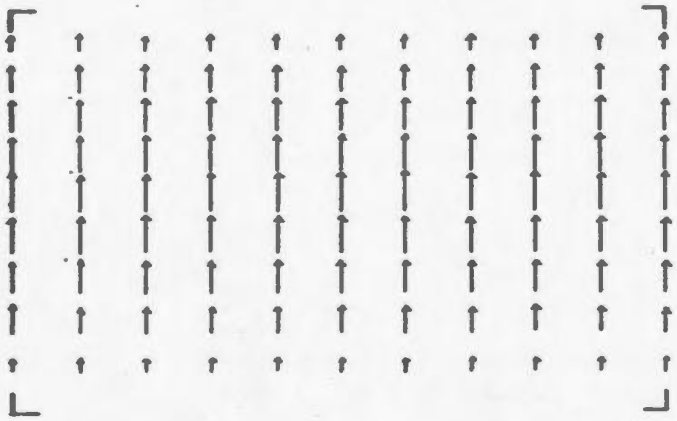

$2.6 \vec{x} 10^{-2}$ amp/m.

Eigencurrent 3

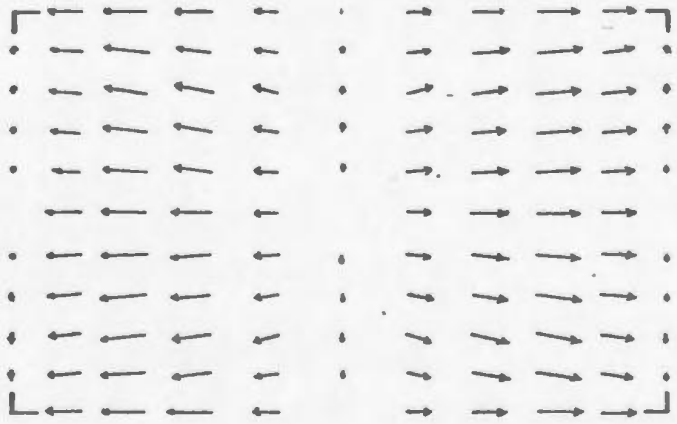

$2.1 \vec{x} 10^{-2}$ amp/m.

Fig. 7-4 Eigencurrents for thin sheet general response.

Eigencurrent 4

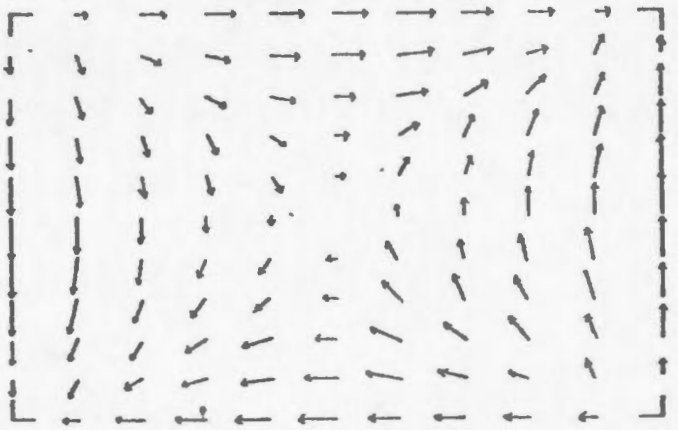

$3.4 \overrightarrow{\times} 10^{-2}$ amp/m.

Eigencurrent 5

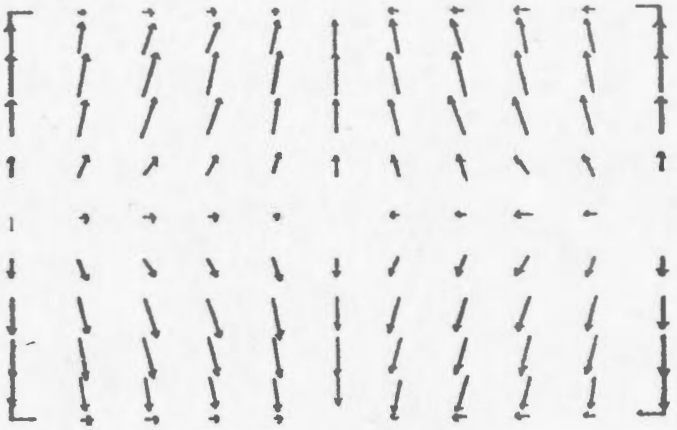

$1.7 \overrightarrow{\times} 10^{-2}$ amp/m.

Eigencurrent 6

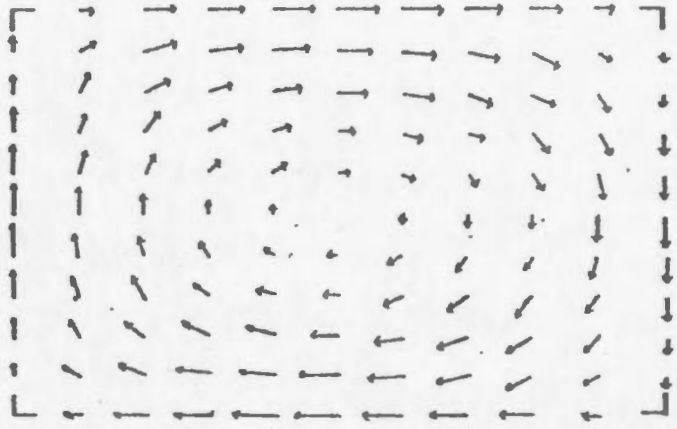

$6.4 \overrightarrow{\times} 10^{0}$ amp/m.

Fig. 7-4 cont'd Eigencurrents for general thin sheet response.

scale of a wavelength in the host medium, the more ill-conditioned the matrix becomes. In the next section, the inductive response of the thin sheet which comes about in this limiting case is discussed.

7-5 The Quasi-static Response

(i) Numerical Formulation

In analysing the response of bodies which are small on the scale of the wavelength in the surrounding medium, the scattering matrix becomes highly ill-conditioned. The surface current for the thin sheet is totally determined by a subset of the eigencurrents. This subset is comprised of the set of currents for which the conductance or capacitance operator is a null operator. Physically this corresponds to the set of currents which are solenoidal for the body, namely

$$\bar{\nabla}\cdot\bar{J}_e \equiv 0 \qquad\qquad J_e\cdot\hat{n} \equiv 0 \qquad\qquad 7\text{-}33$$

These currents are associated with the small eigenvalues of the general impedance operator. In essence, the non-divergence free currents are current limited; these currents complete part of their flow in the external medium. These currents are approximately the same order of magnitude as those in the external medium. The relative magnitude of these currents compared to those in the background medium is determined by the conductive channelling or dielectric polarization effects which are totally geometry dependent and can only enhance the complex current flow by an order of magnitude or so when the sheet conductivity becomes very large. On the other hand the solenoidal currents are limited only by the general self-inductance of the body. As the sheet conductivity becomes very large, these currents increase continually until they reach the inductive limit of the body.

The basic equation for the solenoidal sheet currents is

$$\frac{\bar{K}_s}{\sigma_s} - j\omega\mu_o \iint_A \bar{K}_s(r')\, g(rr')\, d^2r' = \bar{E}_{o,t} \qquad 7\text{-}34$$

with the constraints that

$$\bar{K}_s \cdot \hat{n} \equiv 0 \qquad \bar{\nabla} \cdot \bar{K}_s \equiv 0 \qquad 7\text{-}35$$

Since $\bar{K}_s$ lies in the plane of the sheet and $\bar{K}_s = 0$, $\bar{K}_s$ may be expressed in terms of a scalar potential where

$$\bar{K}_s = \bar{\nabla} \times U \hat{e}_3 = -\hat{e}_3 \times \bar{\nabla} U \qquad 7\text{-}36$$

The condition $\bar{K}_s \cdot \hat{n} = 0$ constrains U to be identically zero on the edge of the sheet.

In the following analysis it is most convenient to take the half-length of the sheet as the unit length. In other words $a_1 = A$ and all dimensions are given in terms of A. The sheet width to length ratio is defined as $R = a_2/a_1 = a_2/A$. . These are the two geometrical parameters which characterize the sheet and are used extensively in the following analysis.

The eigenfunction response for the solenoidal current potentials is formulated following the Galerkin approach. The current potential U is expanded in terms of the trial functions.

$$\varphi_{nm} = (1-\xi^2)(1-\eta^2)\, T_n(\xi)\, T_m(\eta) \qquad 7\text{-}37$$

where

$$U = \sum_{nm} c_{nm}\, \varphi_{nm} \qquad n+m \leq N \qquad 7\text{-}38$$

Following the matrix formalism adopted in the treatment of the total response analysis, $[\Phi]$ is defined as

$$[\Phi] = [\varphi_{00}, \varphi_{10}, \varphi_{01}, \varphi_{20}, \varphi_{11}, \varphi_{02}, \cdots \varphi_{0N}] \qquad 7\text{-}39$$

and the coefficients c_{nm} form a column vector $[C]$ of the same ordering. The total potential can be expressed as the matrix product

$$U = [\Phi][C] \qquad 7\text{-}40$$

Since the test currents are given by

$$\bar{I}_{nm} = \bar{\nabla} \times (\varphi_{nm} \hat{e}_3) \qquad 7\text{-}41$$

the integral equation 7-33 reduces to

$$[Z][C] = \left\{ \frac{1}{\sigma_s}[F] - j\omega\mu_0 \mathcal{R} A^2 [\mathcal{L}] \right\} [C] = -j\omega\mu_0 A [\mathcal{H}] \qquad 7\text{-}42$$

where the $[F]$, $[\mathcal{L}]$, and $[H]$ matrices are given in Table 7-6. In the general case $[L]$ is a complex symmetric matrix and σ_s is also complex. For the particular case of a conductive sheet in free-space for sufficiently low frequencies that the sheet dimensions are only a small fraction of the free-space wavelength, the equation 7-42 simplifies further. With these conditions, the scalar function in the Green's dyadic reduces to

$$g(r,r') \simeq \frac{1}{4\pi|\bar{r}-\bar{r}'|} \qquad 7\text{-}43$$

Thus $[\mathcal{L}]$ and $[F]$ become real, symmetric matrices. The equivalent partitioning of $[Z]$ as used in the last section is now applied to 7-42 and

$$[Z] = [R] + j[X] \qquad 7\text{-}44$$

where

$$[X] = -\omega\mu_0 \mathcal{R} A [\mathcal{L}] \qquad 7\text{-}45$$

$$[R] = \frac{1}{\sigma_s}[F] \qquad 7\text{-}46$$

Solution of the weighted eigenvector problem

$$[Z][C_n] = \lambda_n [R][C_n] \qquad 7\text{-}47$$

results in a particularly useful and elegant solution to the induction equation.

First, the matrix $[F]$ is diagonalized with the resulting eigenvectors defining a finite set of orthogonal functions in two dimensions. The unitary matrix composed of the normalized eigenvectors is defined as $[\mathcal{V}]$ with the property

$$[\mathcal{V}]^T [F] [\mathcal{V}] = [D(f_i)] \qquad 7\text{-}48$$

where $[D(f_i)]$ is the diagonal matrix containing the eigenvalues of $[F]$. Both $[\mathcal{V}]$ and f_i are real and the f_i are positive since $[F]$ is a real,

Table 7-6 Inductive Thin Sheet Response: Elements of Galerkin Matrices

$$[F] = \int_{-a_1}^{a_1}\int_{-a_2}^{a_2}\left\{\left[\frac{\partial\Phi(x_1x_2)}{\partial x_1}\right]^T\left[\frac{\partial\Phi(x_2x_2)}{\partial x_1}\right] + \left[\frac{\partial\Phi(x_1x_2)}{\partial x_2}\right]^T\left[\frac{\partial\Phi(x_1x_2)}{\partial x_2}\right]\right\}dx_1\,dx_2$$

$$[\mathcal{L}] = \frac{1}{4a_1a_2}\int_{-a_1}^{a_1}\int_{-a_2}^{a_2}\int_{-a_1}^{a_1}\int_{-a_2}^{a_2} g(x_1x_1'x_2x_2')\left\{\left[\frac{\partial\Phi(x_1x_2)}{\partial x_1}\right]^T\left[\frac{\partial\Phi(x_1'x_2')}{\partial x_1'}\right] + \left[\frac{\partial\Phi(x_1x_2)}{\partial x_2}\right]^T\left[\frac{\partial\Phi(x_1'x_2')}{\partial x_2'}\right]\right\}dx_1\,dx_2\,dx_1'\,dx_2'$$

$$[\mathcal{H}] = \frac{1}{j\omega\mu 2a_1}\int_{-a_1}^{a_1}\int_{-a_2}^{a_2}\left[\Phi(x_1x_2)\right]^T H_3(x_1x_2)\,dx_1\,dx_2$$

positive definite symmetric matrix. The reactance is transformed to

$$[X'] = [D^{-1/2}(f_i)][\mathcal{V}]^T[X][\mathcal{V}][D^{-1/2}(f_i)] \qquad 7\text{-}49$$

and 7-47 becomes

$$-j\omega\mu_0 R A[X'][C_n'] = (\lambda_n - \frac{1}{\sigma_s})[C_n'] \qquad 7\text{-}50$$

where

$$[C_n'] = [D^{1/2}(f_i)][\mathcal{V}]^T[C_n] \qquad 7\text{-}51$$

Since $[X']$ is real and symmetric, $[C_n']$ and its associated eigenvalues x_n are real and

$$\lambda_n = \frac{1}{\sigma_s} - j\omega\mu_0 R A x_n \qquad 7\text{-}52$$

where

$$[X'][C_n'] = x_n[C_n'] \qquad 7\text{-}53$$

Therefore,

$$[C_n]^T[Z][C_n] = (\frac{1}{\sigma_s} - j\omega\mu_0 R A x_n) \qquad 7\text{-}54$$

where

$$[C_n] = [\mathcal{V}][D^{-1/2}(f_i)][C_n'] \qquad 7\text{-}55$$

The solution of the original equation becomes

$$[C] = [C_n][D(\frac{-j\alpha}{1-j\alpha R x_n})][C_n]^T \frac{[\mathcal{V}]}{A} \qquad 7\text{-}56$$

where $\alpha = \omega\beta = \omega\mu\sigma_s A$ is defined as the response parameter or induction number of the sheet. In the form 7-56, a very simple decomposition of the response has been obtained. For a given geometry, the effects of source, sheet geometry and electrical properties are completely decoupled.

Each individual eigenpotential responds in the same manner as a simple wire loop. The solution can be viewed as the sum over a set of loop responses with the loops having differing inductance to resistance ratios. The current

flowing in a loop in a uniform field H, normal to the loop, has the form (see Appendix E)

$$I(\omega) = \frac{-j\omega\mu H\cdot(\text{Area})}{R_L - j\omega\mu L_L} \qquad 7\text{-}57$$

where R_L and L_L are the self-resistance and inductance of the loop. The analogous form of each term in 7-56 to 7-57 is readily apparent. The eigenvalues x_n are just the L/R ratios of the individual eigenpotentials. The solution for the eigenpotentials for a given geometry, therefore, yields the total frequency and/or time (transient) response in one operation. The impulse response function for the loop is, from Appendix E,

$$I(t) = -\frac{1}{L_L}\,\frac{e^{-t/\tau}}{\tau}\,\mu H\cdot(\text{Area}) \qquad 7\text{-}58$$

The impulse response of the sheet is obtained very simply by replacing the diagonal response parameter matrix with

$$\left[D\left(\frac{-j\alpha}{1-j\alpha R x_n}\right)\right] \rightarrow \left[D\left(-\frac{1}{R x_n}\,\frac{e^{-t/\tau_n}}{\tau_n}\right)\right] \qquad 7\text{-}59$$

where $\tau_n = 1/\beta R x_n$

In future references the duality of the response forms is stressed and the diagonal matrix will be written as $D_n(\alpha)$ or $D_n(t)$ denoting either the frequency response (response versus induction number) or the impulse response.

(ii) Numerical Results

The inductive response of the plate is characterized by the parameters listed in Table 7-7. The intrinsic parameters of the body are R, the width to length ratio, and α, the response parameter or induction number, which characterizes the general sheet self-induction to self-resistance ratio. The numerical solution is characterized by N, the maximum polynomial degree in the solution; this gives a numerical solution parameterized in terms of

Table 7-7 Inductive Plate Response Parameters

Geometrical Parameters

$$\mathcal{R} = a_2 / a_1$$

Electrical Parameters

$$\alpha = \omega \mu_0 \sigma_s \mathcal{R} A$$

= Sheet Response Parameter or Induction Number

Numerical Solution Parameters

N = Maximum Polynomial Degree in Expansion

$(N + 1)(N + 2)/2$ unknowns. The only other parameters in the computations are those which describe the excitation field. These parameters are usually ones which describe the geometry of the source. Any dimensions associated with a source in the following discussion have been implicitly normalized in terms of a_1.

The numerical computations were carried out in the sequence shown in Fig. 7-5. First, the integral coefficients required in Table 7-6 can all be expressed in terms of the integrals

$$\int_{-1}^{1}\int_{-1}^{1}\int_{-1}^{1}\int_{-1}^{1} \varphi_{nm}(\xi,\eta)\, g(\xi,\xi',\eta,\eta')\, \varphi_{pq}(\xi',\eta')\, d\xi\, d\eta\, d\xi'\, d\eta' \qquad 7\text{-}60$$

$$\int_{-1}^{1}\int_{-1}^{1} \varphi_{nm}(\xi,\eta)\ \varphi_{pq}(\xi,\eta)\, d\xi\, d\eta \qquad 7\text{-}61$$

The first set of integrals were evaluated using the Gaussian quadrature scheme for integrals with singular kernels outlined in Appendix D; the second set of integrals were evaluated analytically. In order to complete this first step of the analysis, R and N had to be specified. The integral coefficients were stored and used as data for subsequent computations. In the next step, the [F] matrix was generated from the integral coefficients and then diagonalized. Diagonalization of [F] gives a finite set of 2 dimensional polynomials which are orthogonal with unity weighting on the surface of the sheet. Next, the $[\mathcal{L}]$ matrix was generated and then transformed in accordance with 7-49 to generate the [X'] matrix. [X'] was then diagonalized to yield the basic eigenvectors and eigenvalues of the $[\mathcal{Z}]$ matrix subject to weighting [R]. The generation of [F] and [X'] from 7-60 and 7-61 was facilitated by the relationship for the derivative of Chebychev polynomial, namely

$$\frac{d}{dx}(1-x^2)T_n(x) = -nx\,T_n(x) + n\,T_{n-1}(x) \qquad 7\text{-}62$$

The elements of the scattering matrix were diagonalized using the Jacobi iterative method. The computer program written to diagonalize the matrices was based on a modified version of the algorithm given by Greenstadt (1960).

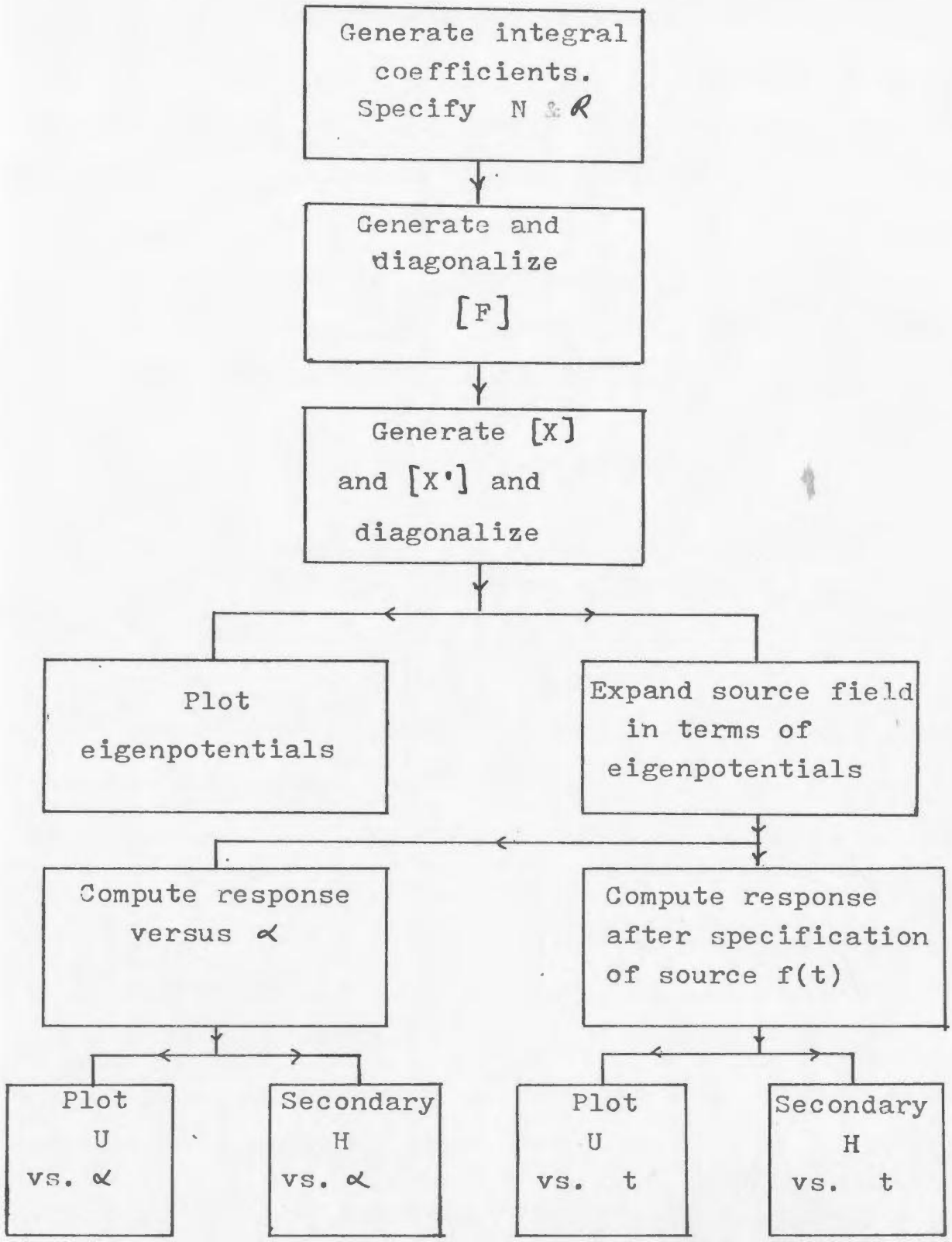

Fig. 7-5 Flow chart of inductive response computations.

At this stage the formal solution of the problem is complete within the limitation that (N + 1) (N + 2)/2 eigenfunctions of maximum polynomial degree N can characterize a system with an infinite sequence of eigenfunctions. The induction eigenpotentials can then be used to express the response of the sheet to arbitrary excitation. The integral coefficients for a given source field, $[\mathcal{H}]$, were evaluated using Gaussian quadrature algorithms similar to those used to evaluate 7-60. Equation 7-56 yields the solution for the equivalent surface current as a function of α (or frequency ω) and/or time. The final step in the analysis is the computation of the anomalous magnetic fields associated with $\overline{K}_e$ which are given by

$$\overline{H}_a(r) = \left\{ -[\Phi]\,\delta(x_3)\hat{e}_3 - \sum_{i=1}^{3} [H_a^i]\,\hat{e}_i \right\} [c] \qquad 7\text{-}63$$

where

$$[H_a^i] = [\, H_{a0}^i(r),\ H_{10}^i(r),\ H_{a1}^i(r),\ H_{20}^i(r) \cdots\cdots\ H_{aN}^i \,]$$

and

$$H_{nm}^i(r) = \frac{\partial^2}{\partial x_i \partial x_3} \int_{-a_1}^{a_1}\int_{-a_3}^{a_3} \frac{\varphi_{nm}(x_1' x_2')}{4\pi R}\, dx_1'\, dx_2'$$

The computer programs were designed to maximize the number of source configurations and response parameter combinations which could be computed for one geometrical model. The reason for this is the same as for the two dimensional computations; the most expensive part of the computation is the numerical quadrature to find the integral coefficients from which the scattering matrices are generated. As a result, a large number of responses can be computed and the amount of information can quickly get out of hand. Since the emphasis here is on the solution method and not on the tabulation of reams of results and type curves, only a limited number of computed results are presented.

The particular model chosen for illustration purposes in the following discussions is shown in Fig. 7-6. This model was chosen since experimental and computed responses for a similar model are given by Lamontagne and

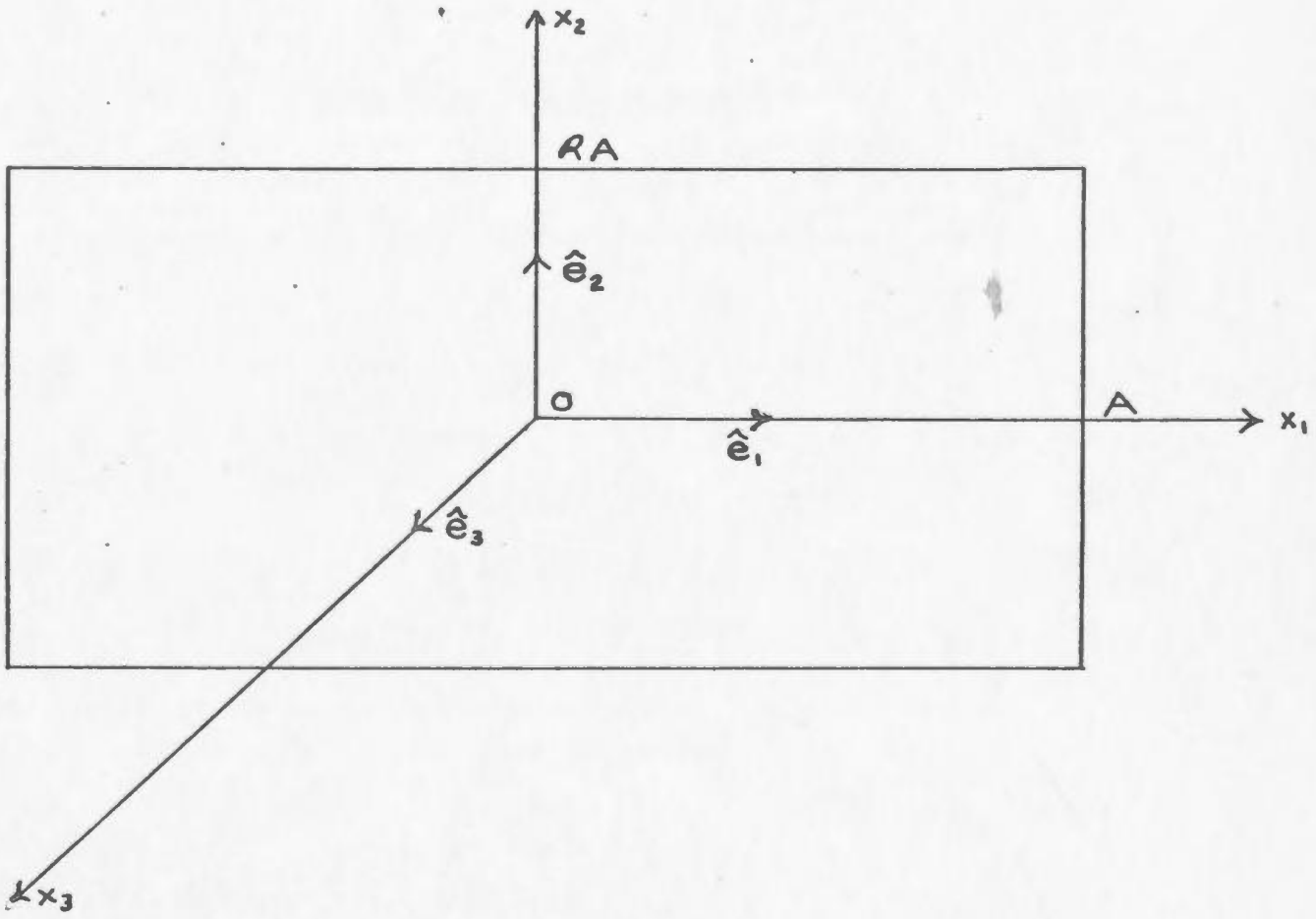

Fig. 7-6 Re-parameterized thin sheet geometry for induction analysis.

West (1971). The sheet has a width to length ratio, $\mathcal{R}$, of 0.5 and the maximum polynomial degree, N, in the approximate solution is 4. The computed results are presented in the same sequence as they appear in the flow chart in Fig. 7-5.

The eigenpotentials generated for this model are shown in Fig. 7-7 With N = 4, there are a total of 15 eigenpotentials. The eigenpotentials are shown in sequence of decreasing x_n. The eigenvalues x_n are listed in Table 7-8. As n the order of the eigenpotential increases the potentials become more and more convoluted; the eigenvalues reflect this behaviour since the self-inductance to self-resistance ratios, which is characterized by x_n, decrease in value. The current flow associated with the individual eigenpotentials can be readily visualized from the contour maps of the potentials since current flow is parallel to the equipotential lines of U_n and is proportional to the gradient of U_n. Examination of the potentials shows that the associated current flow is in the form of rings or eddies and that the surface current is always strongest near the edges of the sheet. The next step is the expansion of some excitation field responses in terms of the eigenpotentials.

TURAM Loop Response

The total response potential U is expressed as a function of α in the frequency domain. The choice of representation in terms of α makes comparison with other results simpler than if the transient response sheet were determined. The transient response can be obtained simply by replacing $[D(\alpha)]$ by $[D(t)]$ in the summation over the eigenpotentials. The first excitation field considered is that of a turam loop shown in Fig. 7-8. This source is equivalent to that used by Lamontagne (1970). The current in the wire loop is taken to be 1 amp. The magnetic field associated with the loop

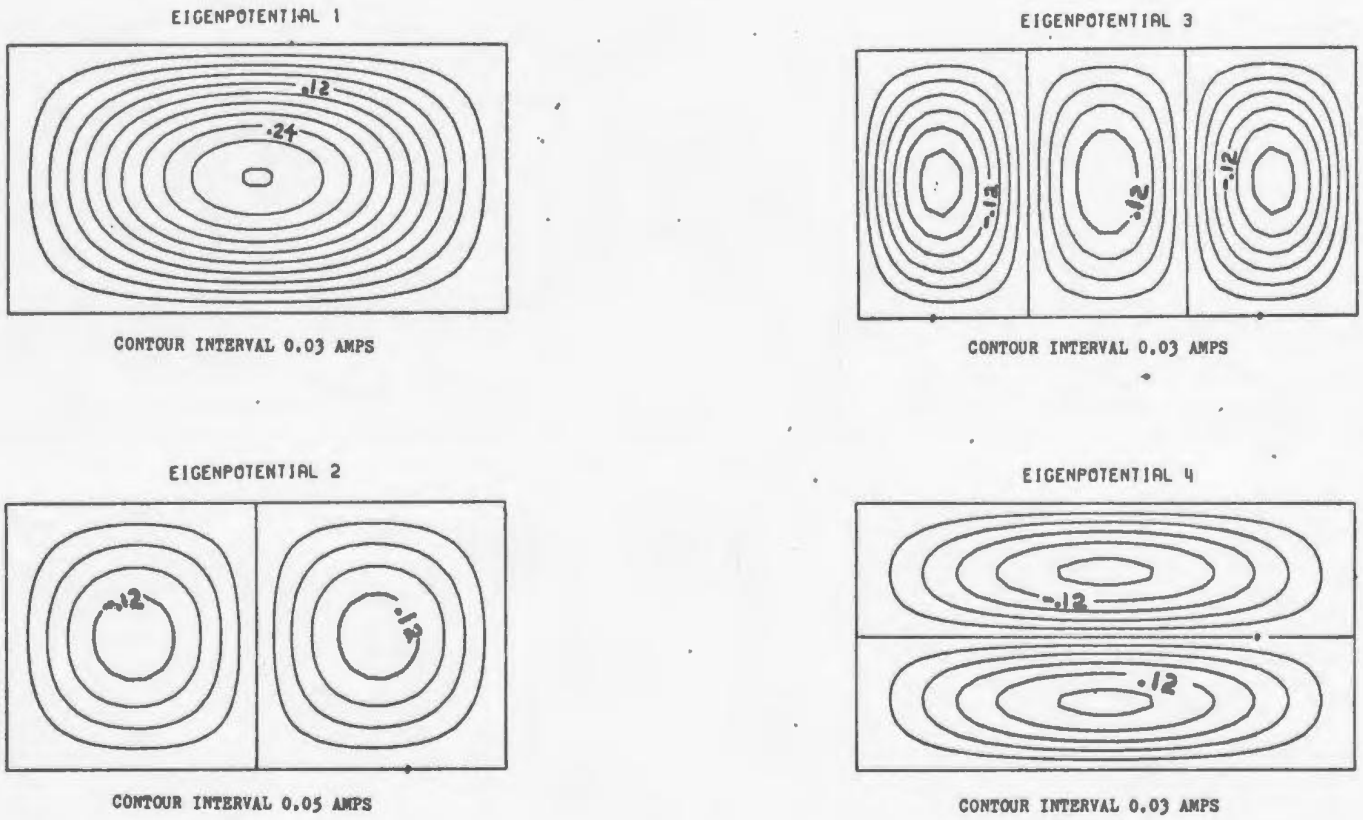

Fig. 7-7 Contour maps of induction eigenpotentials.

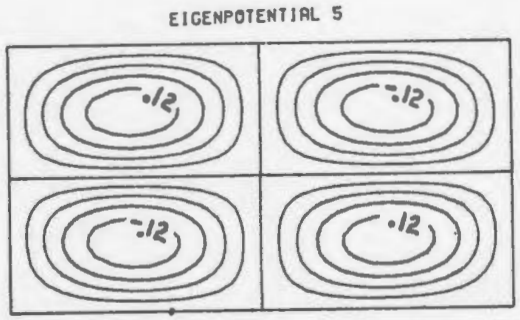

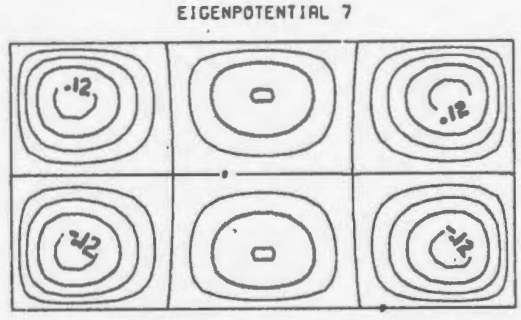

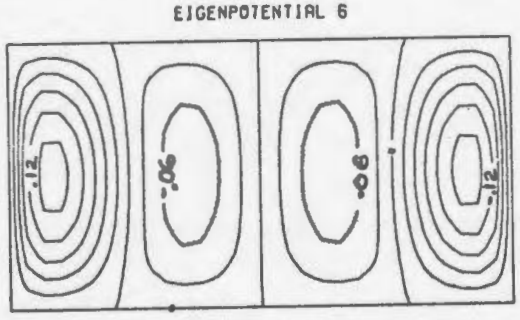

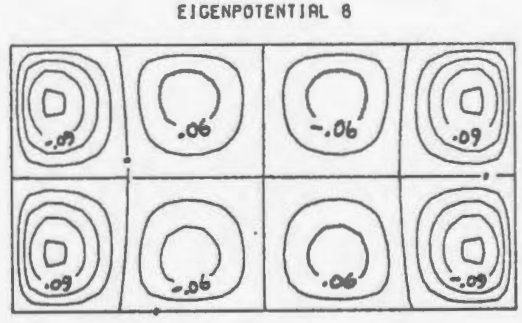

Fig. 7-7 cont'd. Contour maps of induction eigenpotentials.

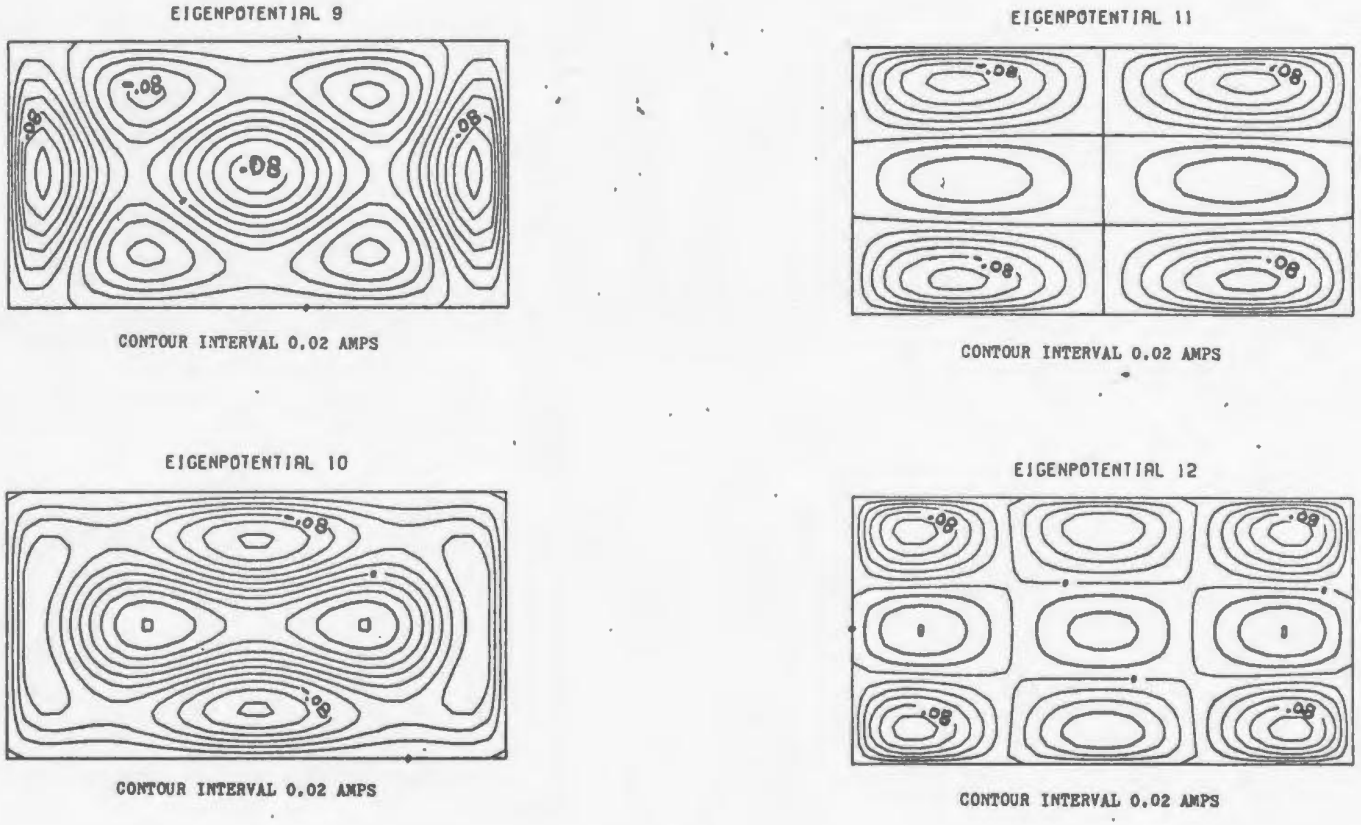

Fig. 7-7 cont'd. Contour maps of induction eigenpotentials.

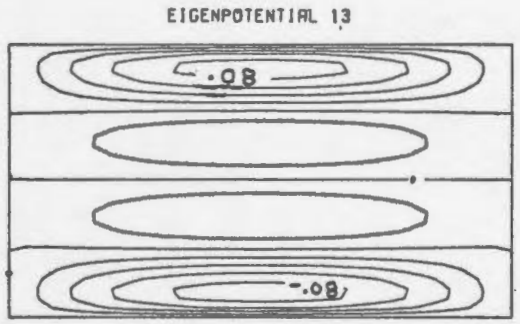

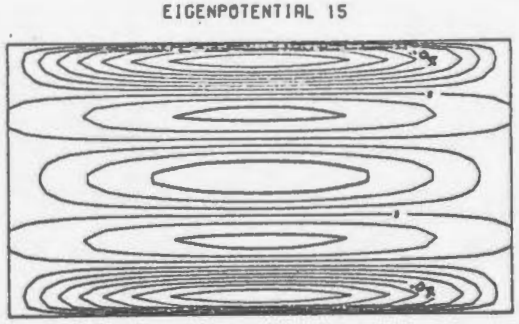

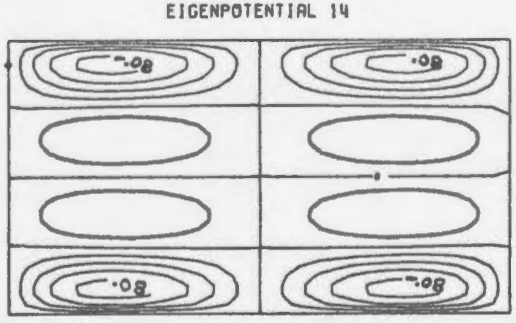

Fig. 7-7 cont'd. Contour maps of induction eigenpotentials.

Table 7-8 Eigenvalues for Inductive Response of Thin Sheet

EIGENFUNCTION	1	EIGENVALUE=	2.328E-01
EIGENFUNCTION	2	EIGENVALUE=	1.970E-01
EIGENFUNCTION	3	EIGENVALUE=	1.552E-01
EIGENFUNCTION	4	EIGENVALUE=	1.331E-01
EIGENFUNCTION	5	EIGENVALUE=	1.242E-01
EIGENFUNCTION	6	EIGENVALUE=	1.129E-01
EIGENFUNCTION	7	EIGENVALUE=	1.036E-01
EIGENFUNCTION	8	EIGENVALUE=	8.975E-02
EIGENFUNCTION	9	EIGENVALUE=	8.772E-02
EIGENFUNCTION	10	EIGENVALUE=	8.600E-02
EIGENFUNCTION	11	EIGENVALUE=	7.488E-02
EIGENFUNCTION	12	EIGENVALUE=	7.262E-02
EIGENFUNCTION	13	EIGENVALUE=	5.526E-02
EIGENFUNCTION	14	EIGENVALUE=	5.479E-02
EIGENFUNCTION	15	EIGENVALUE=	4.141E-02

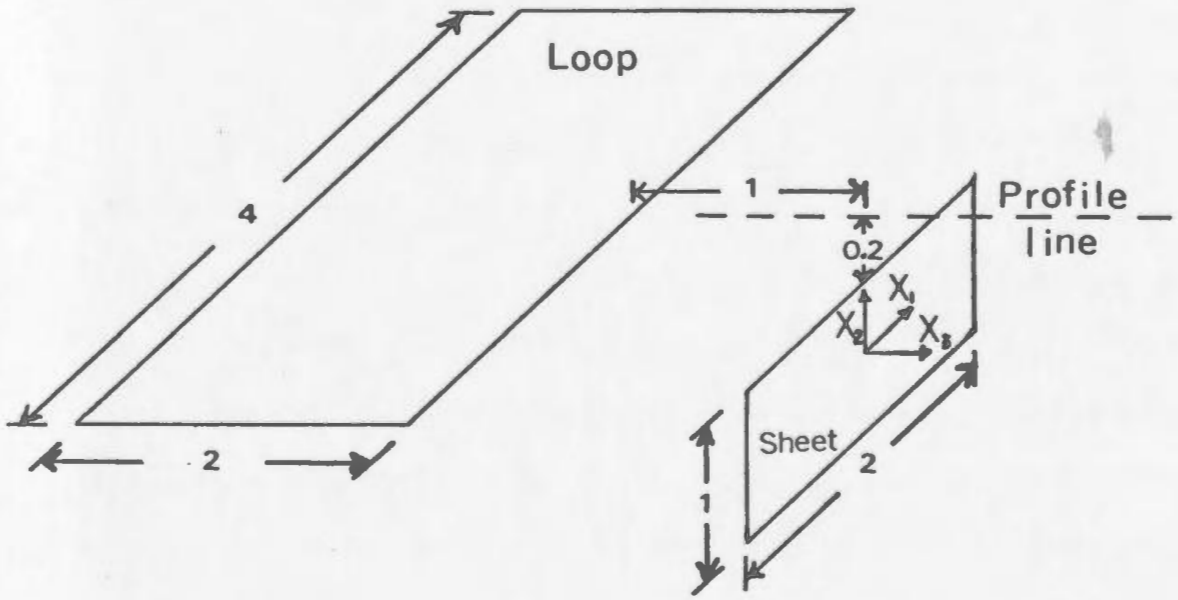

Fig. 7-8 **TURAM** loop and thin sheet configuration

is given by

$$\bar{H}(r) = \sum_{i=1}^{3} \oint \frac{(x_i - x_i')\hat{e}_i \times d\bar{l}}{4\pi R} \qquad 7\text{-}64$$

The total potential for various α ranging from 0.5 to 150 are shown in Fig. 7-9. The potentials display the classic inductive response as a function of α. For small α, the potential is totally quadrature or 90° out of phase with the primary magnetic field. As α increases, the imaginary part of U increases to a maximum and then decreases while the real part of U increases and approaches a limiting value. The response follows that of the simple loop as discussed earlier. For small α, the sheet is of the resistive limit of the response and at large α it has reached the inductive limit. The shape of the in-phase potential remains almost independent of the response parameter, while the imaginary part of U becomes more and more convoluted as α increases. At large α, the imaginary part of the equivalent current is forced out against the edge of the sheet.

The response of U versus α has an interesting interpretation in terms of the various eigenpotentials excited. The dominant mode is the first mode. From the value of x_1, this mode passes through the mid-zone between the resistive and inductive limits for $\alpha \simeq 5$. As α increases beyond this value, more and more of the modes approach their inductive limit; thus at high α, the quadrature component of U is determined by the high order modes which have not been forced to the inductive limit. As a result imaginary U exhibits more complex spatial variations.

The potentials computed by Lamontagne for this model are shown in Fig. 7-10. The two sets of computed potentials compare extremely well. The amplitudes differe by a factor of 4π in normalization. Lamontagne's solution was obtained by discretization of U on a 15 x 15 and 16 x 25 grid and then solving the governing differential-integral equation which he used to describe the response. The good comparison is quite amazing in view of the fact that an

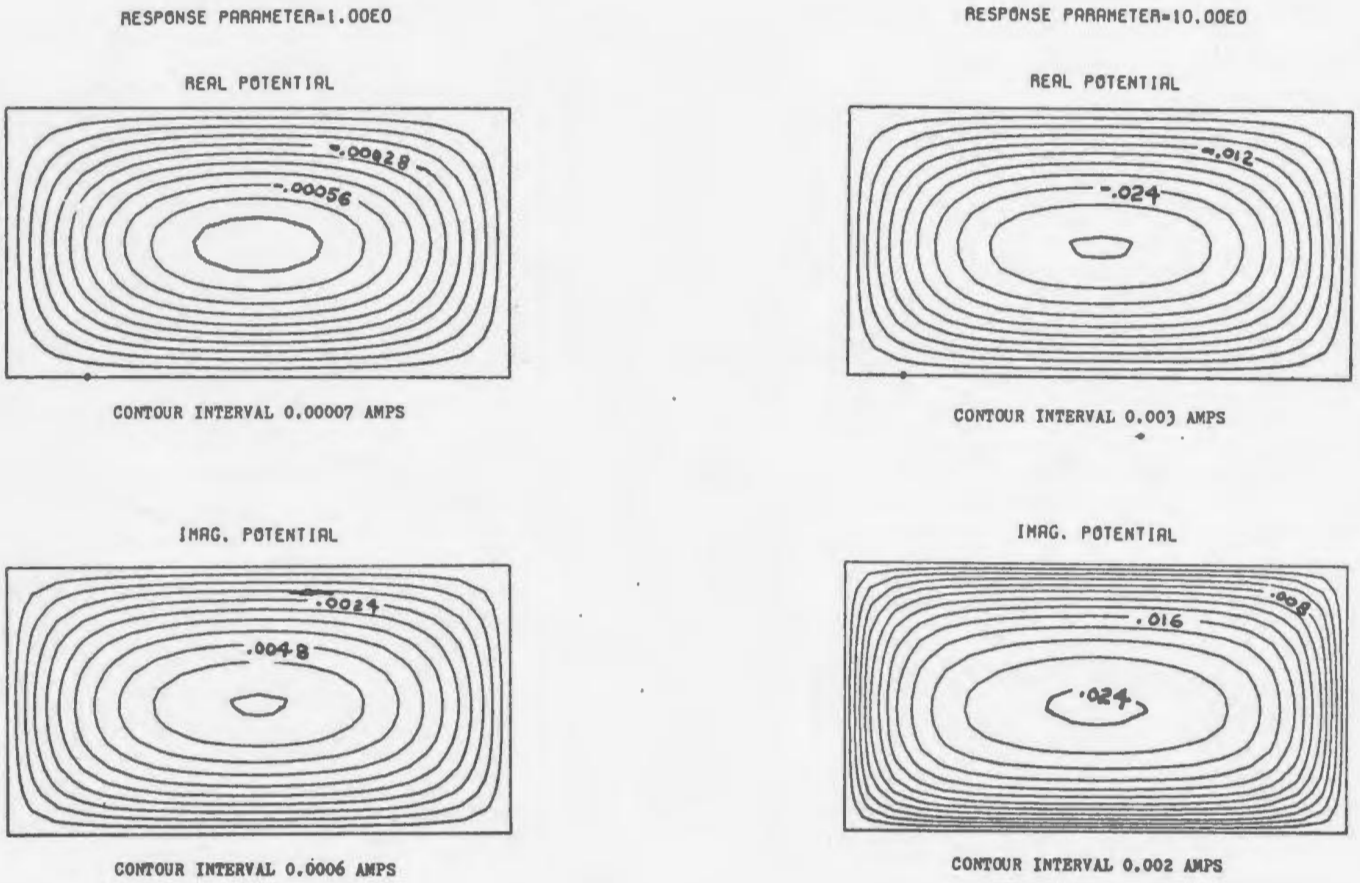

Fig. 7-9 TURAM total potential contour maps for various response parameters.

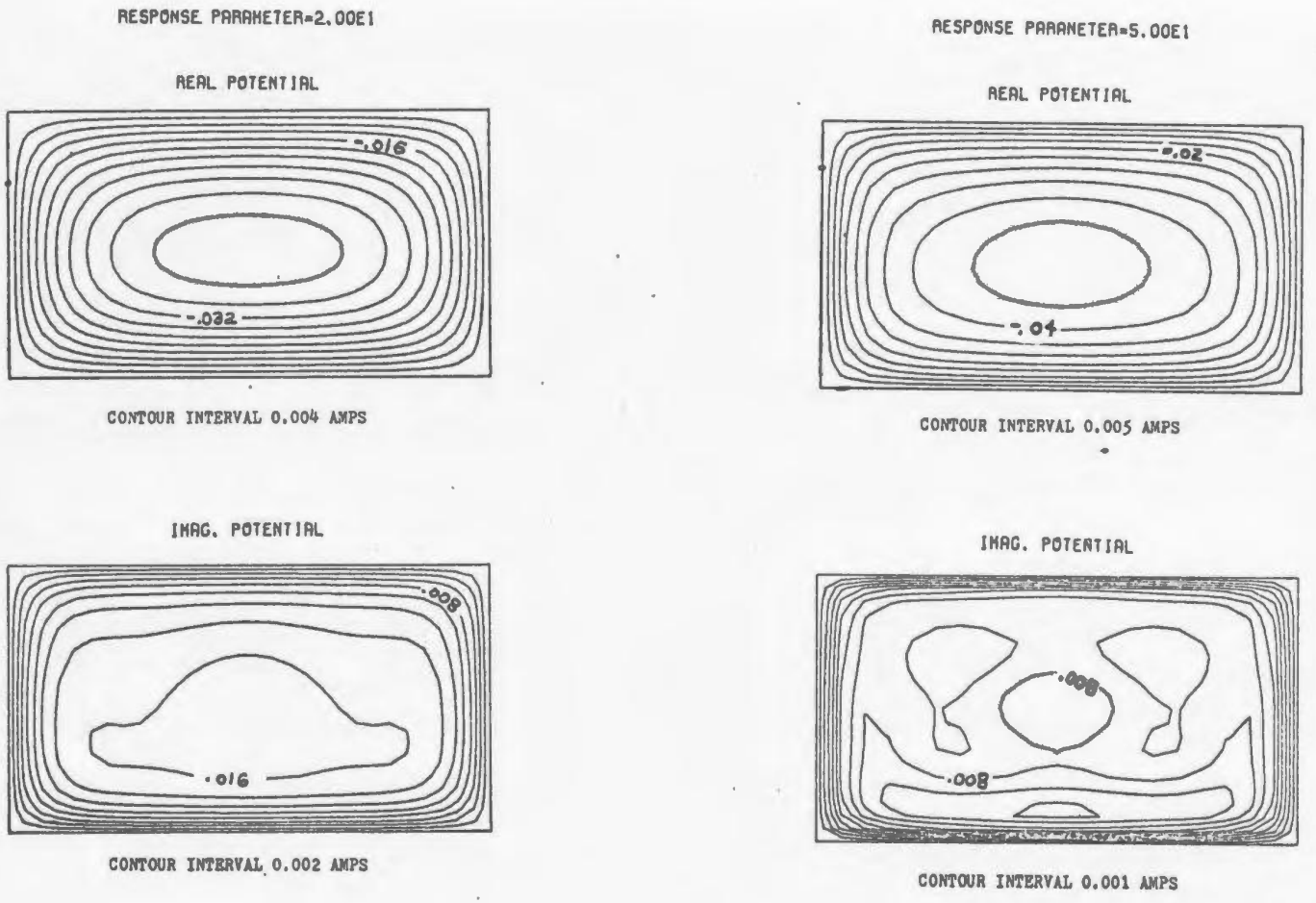

Fig. 7-9 cont'd. TURAM total potential contour maps for various response parameters.

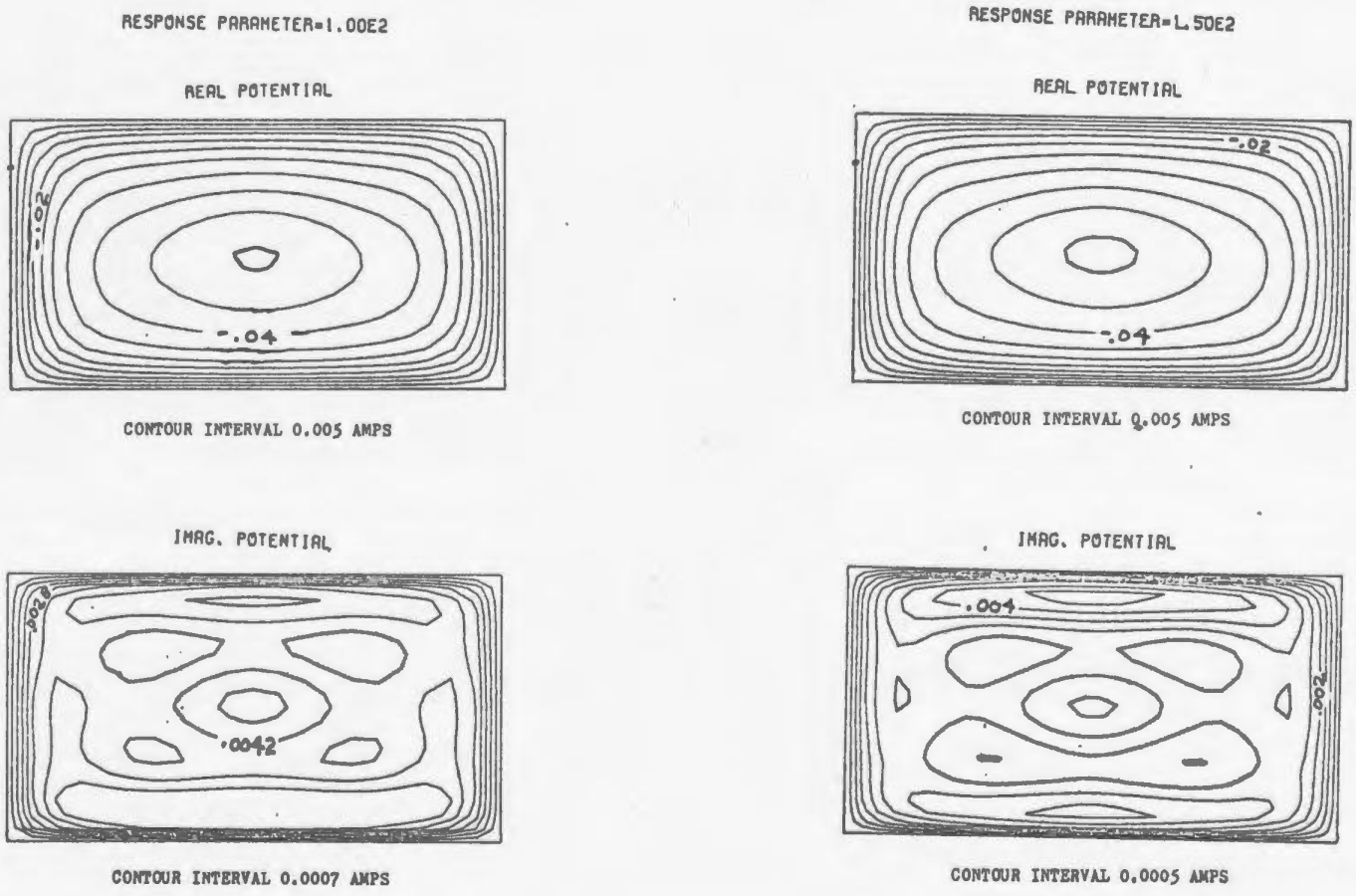

Fig. 7-9 cont'd. TURAM total potential contour maps for various response parameters.

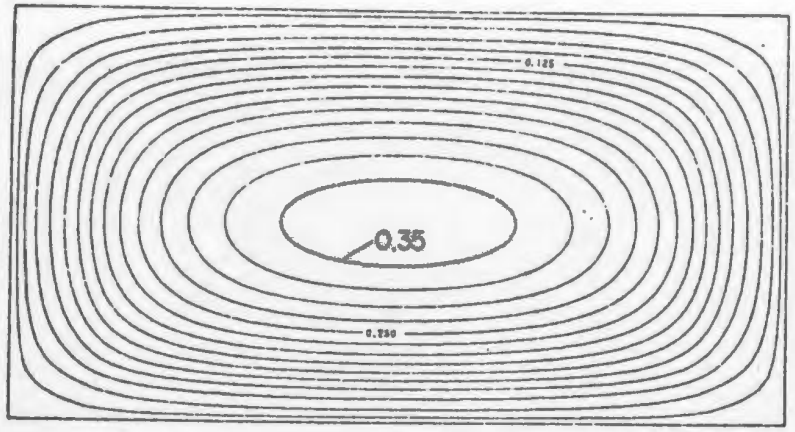

IN-PHASE COMPONENT — INTERVAL = 0.025 AMP.

EDDY CURRENT PATTERN

FOR LOW Q RESPONSE: Q = 1.08

QUADRATURE COMPONENT — INT. = 0.025 AMP.

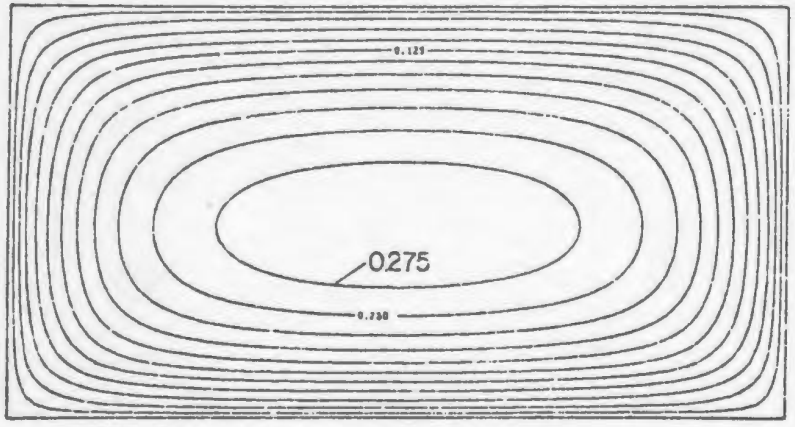

(a)

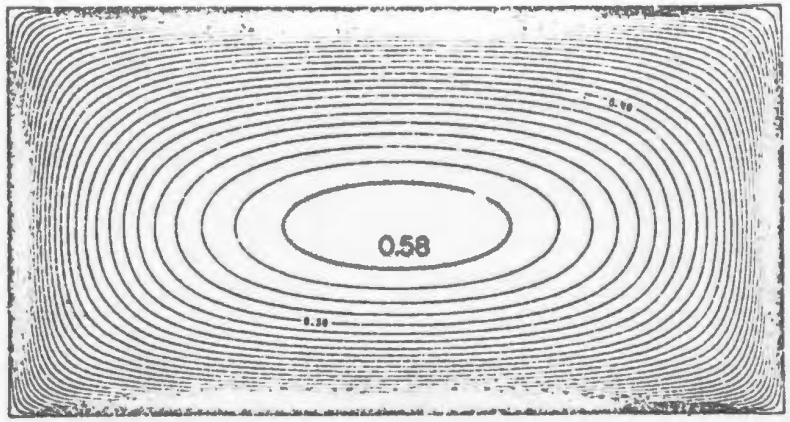

IN-PHASE COMPONENT INTERVAL = 0.02 AMP.

EDDY CURRENT PATTERN

COARSE GRID: $\sigma\mu\omega t\Delta = 5.9$ Q = 10.28

QUADRATURE COMPONENT INTERVAL = 0.004 AMP.

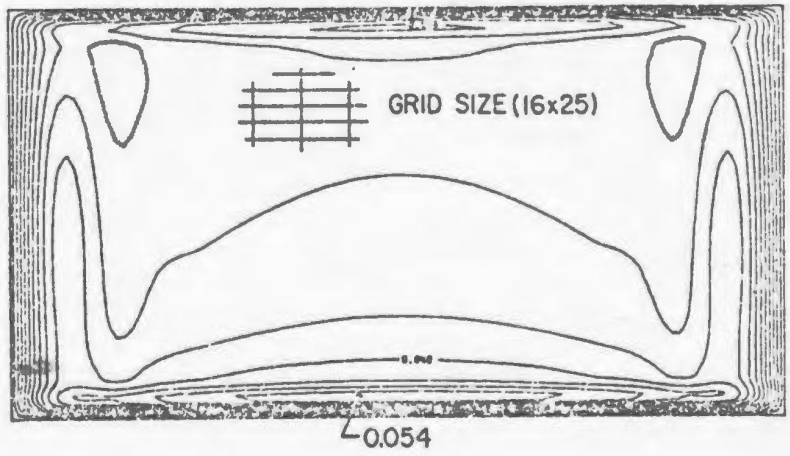

(b)

Fig. 7-10 Total potential contour maps for similar TURAM loop-thin sheet system computed by Lamontagne (1970): (a) α = 9.8; (b) α = 147

order of magnitude fewer unknowns were required to specify the response in the present study.

In Fig. 7-11, the $\hat{e}_z$ component of $\overline{H}$ along the profile line shown in Fig. 7-8 is plotted for a pair of response parameter values. The anomalous field is given as a percentage of the primary excitation field directly over the sheet. (At the point (0., 0.7, 0.) in this case). The solid lines represent data computed using the eigenfunction approach; the dashed lines are from responses computed by Lamontagne (1970) and the x's are experimental data points collected on a scale model. The agreement among the three independent sets of data is remarkably good.

The response of the sheet is summarized in Fig. 7-12 and 7-13. In Fig. 7-12, the peak value of the in-phase and quadrature components of the field on the profile shown in Fig. 7-11 are plotted for various values of α. In Fig. 7-13, the Q of the response, defined as the ratio of peak in-phase to peak quadrature field, is plotted against α. In both diagrams, the solid lines are results tabulated by Lamontagne while the x's indicate results computed for the sequence of response paramters for the total potentials shown in Fig. 7-9. The overall agreement between the two sets of results is again very good. The response obtained with the eigenfunction method departs from Lamontagne's response at large ($\alpha > 100$)) values of α. The in-phase part of the anomaly agrees over the entire range of response parameter whereas the quadrature component falls off more rapidly than that observed experimentally. This behaviour is just a manifestation of the fact that higher order eigenfunctions are required to express the imaginary component of U accurately for large α. Since the exact solution for U would contain an infinite sequence of the true U_n's with eigenvalues ranging from x_1 to $x_n \xrightarrow[n\to\infty]{} 0$, and since the higher order modes are not present in the approximate solution, once α increases beyond $1/x_{15}$, the smallest eigenvalue in the solution, the quadrature component of U should be expected to decrease more

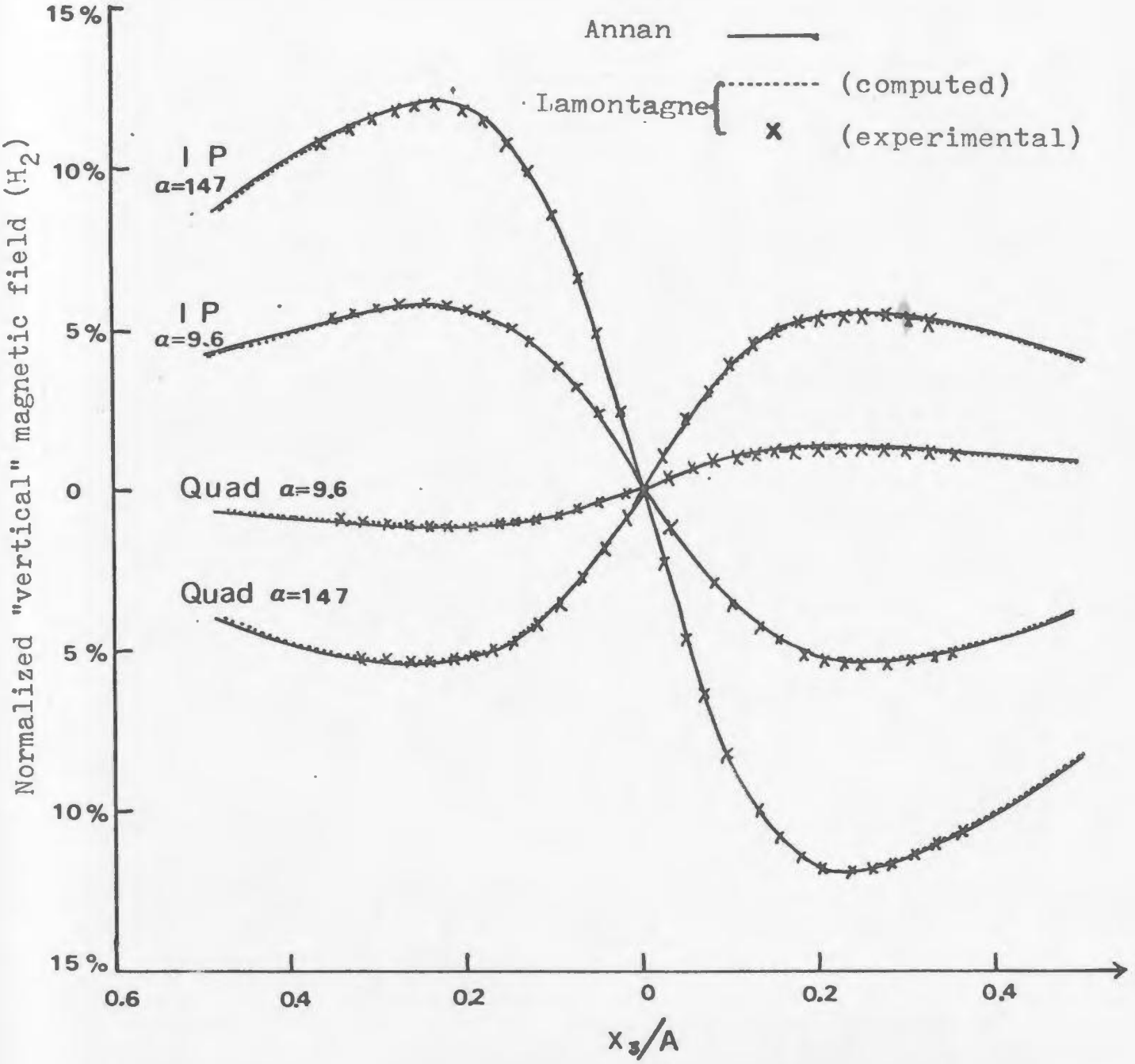

Fig. 7-11 Anomalous "vertical" magnetic field generated by the thin sheet due to excitaion by TURAM loop

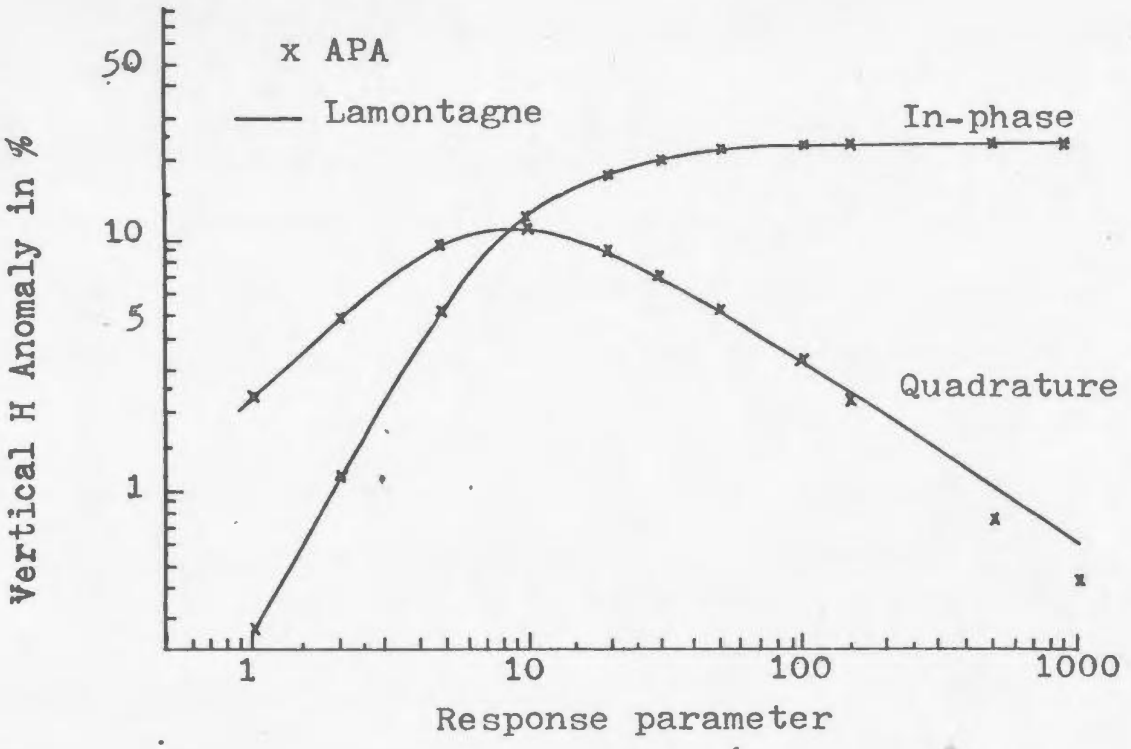

Fig. 7-12 Peak anomalous field versus response parameter compared with results obtained by Lamontagne (1970)

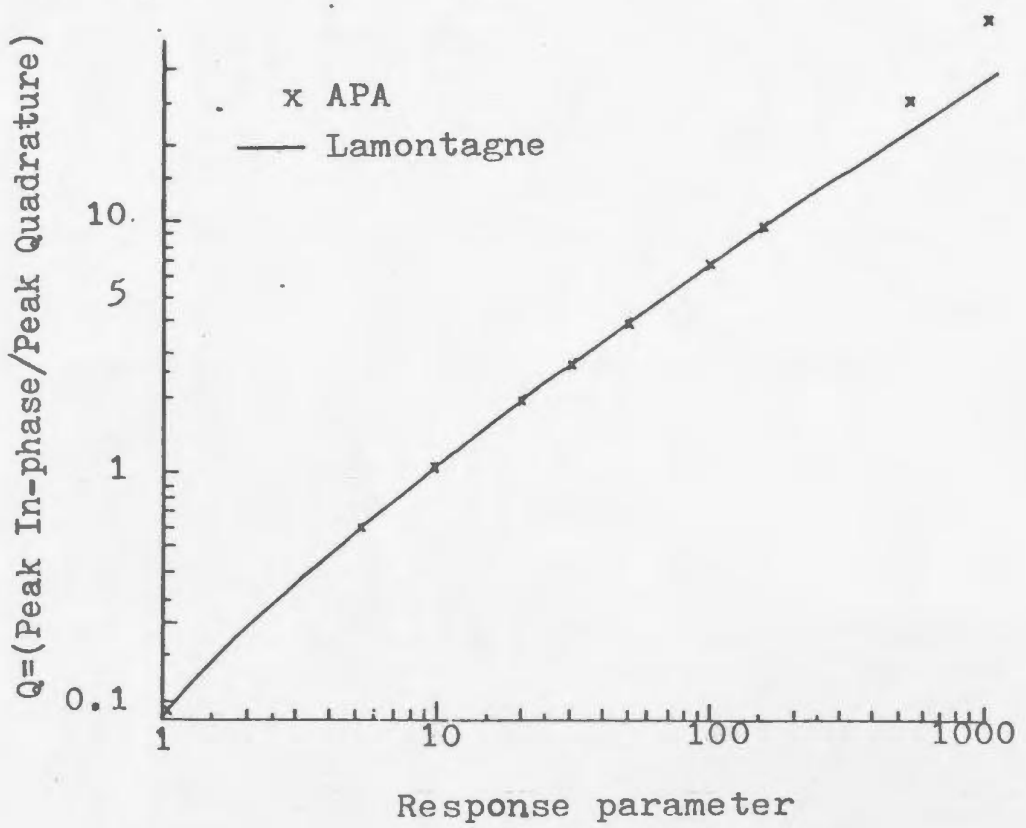

Fig. 7-13 Q of the thin sheet response for TURAM source versus response parameter compared with Lamontagne (1970)

rapidly with α than that of the true solution. Since the failure of the solution occurs only for large α when the response is almost at the inductive limit, the percentage error is quite small since the quadrature component of U is only a small part of the total U. Similar discrepancies at large values of α were found by Lamontagne in his numerical study of the response. The problem was similar to that of the eigenpotential solution; the quadrature component of U varies rapidly at the edge of the sheet and unless U was sampled sufficiently often, the quadrature part of U tended to be underestimated. This resulted in an overestimation of the Q.

Point Magnetic Dipole Excitation

As a further example of the eigenpotential method, the response of the sheet to excitation by a point magnetic dipole is shown in the following section. The magnetic dipole response is useful in simulating various dipole source methods used in applied geophysics. The magnetic field of a point magnetic dipole in the quasi-static zone is given by

$$\bar{H} = \bar{\nabla}\bar{\nabla} \cdot \int \frac{\bar{m}}{4\pi R}\, dV = \bar{\nabla}\left(\hat{m} \cdot \bar{\nabla}\frac{1}{4\pi R}\right) \qquad 7\text{-}65$$

$$\bar{m} = \delta(r)\,\hat{m} \quad \text{amp-m}^2/\text{m}^3$$

The particular source sheet configuration studied in this example is shown in Fig. 7-14. The position of the source relative to the sheet was varied through a sequence of values of c/d in order to demonstrate the source dependance of the response.

Contour maps of the total potential for α = 10 and 50 and the sequence of c/d = 0.25, 1.0, 2.5, 5.0 are shown in Fig. 7-15 and Fig. 7-16. The potential plots show several interesting features. First, the potentials as a function c/d show the dipole couples most strongly with the sheet when $x_3/d \simeq 1$. For $c/d \ll 1$, very little of the dipole field cuts the sheet. For large c/d, the $1/r^3$ fall off of the source field quickly decreases the coupling. Secondly, as the source moves farther from the sheet, the potential

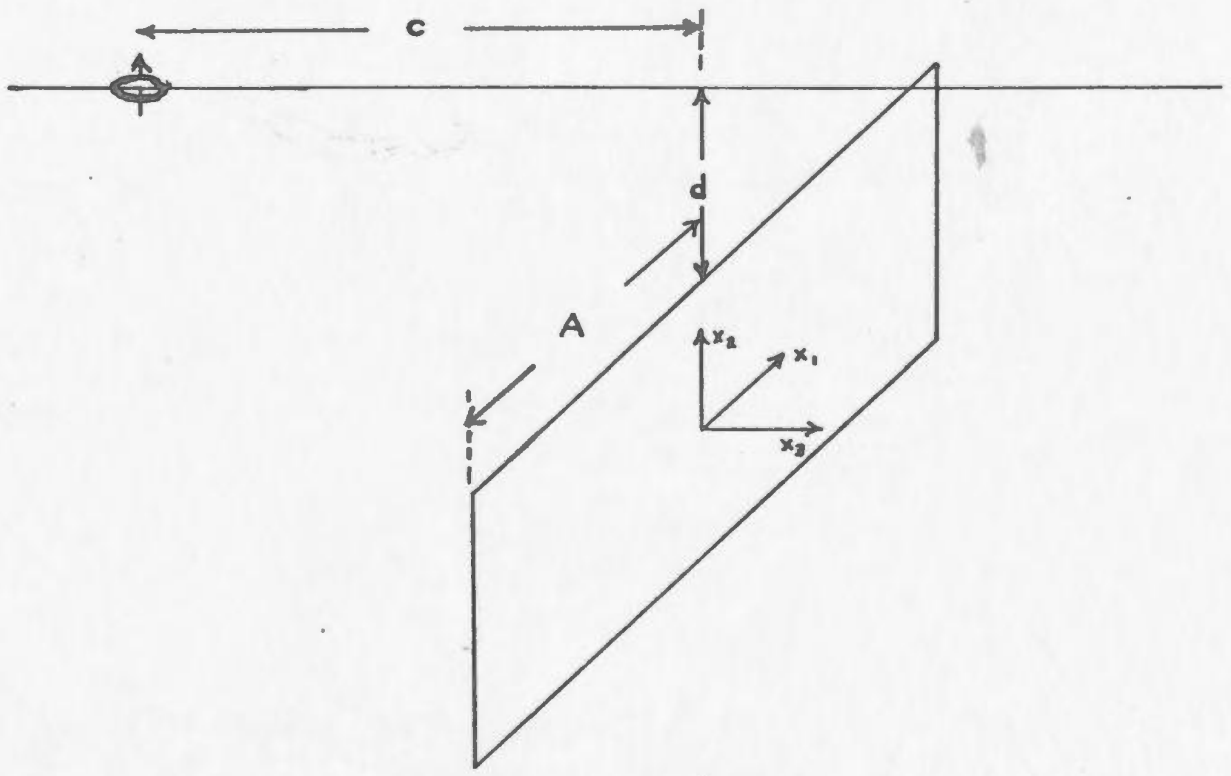

Fig. 7-14 Point magnetic dipole and thin sheet geometry.

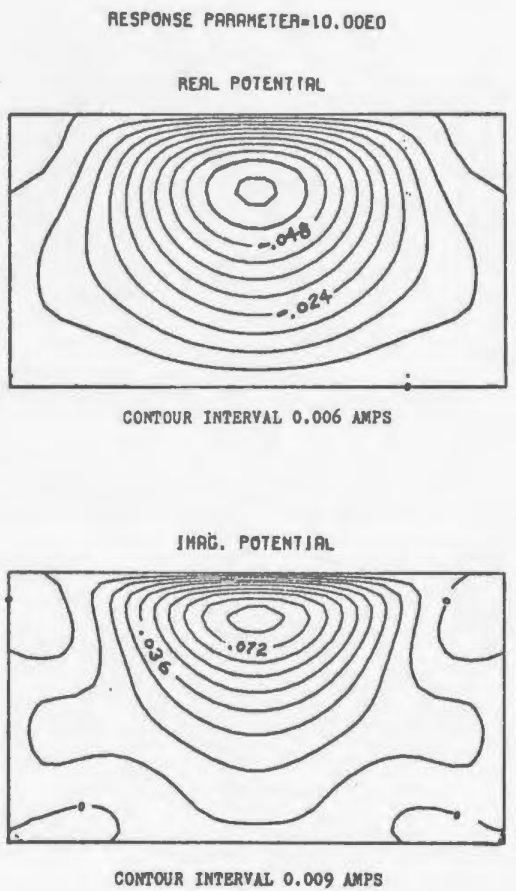

Fig. 7-15 Total potential maps for thin sheet excited by a point magnetic dipole for $\alpha = 10$.

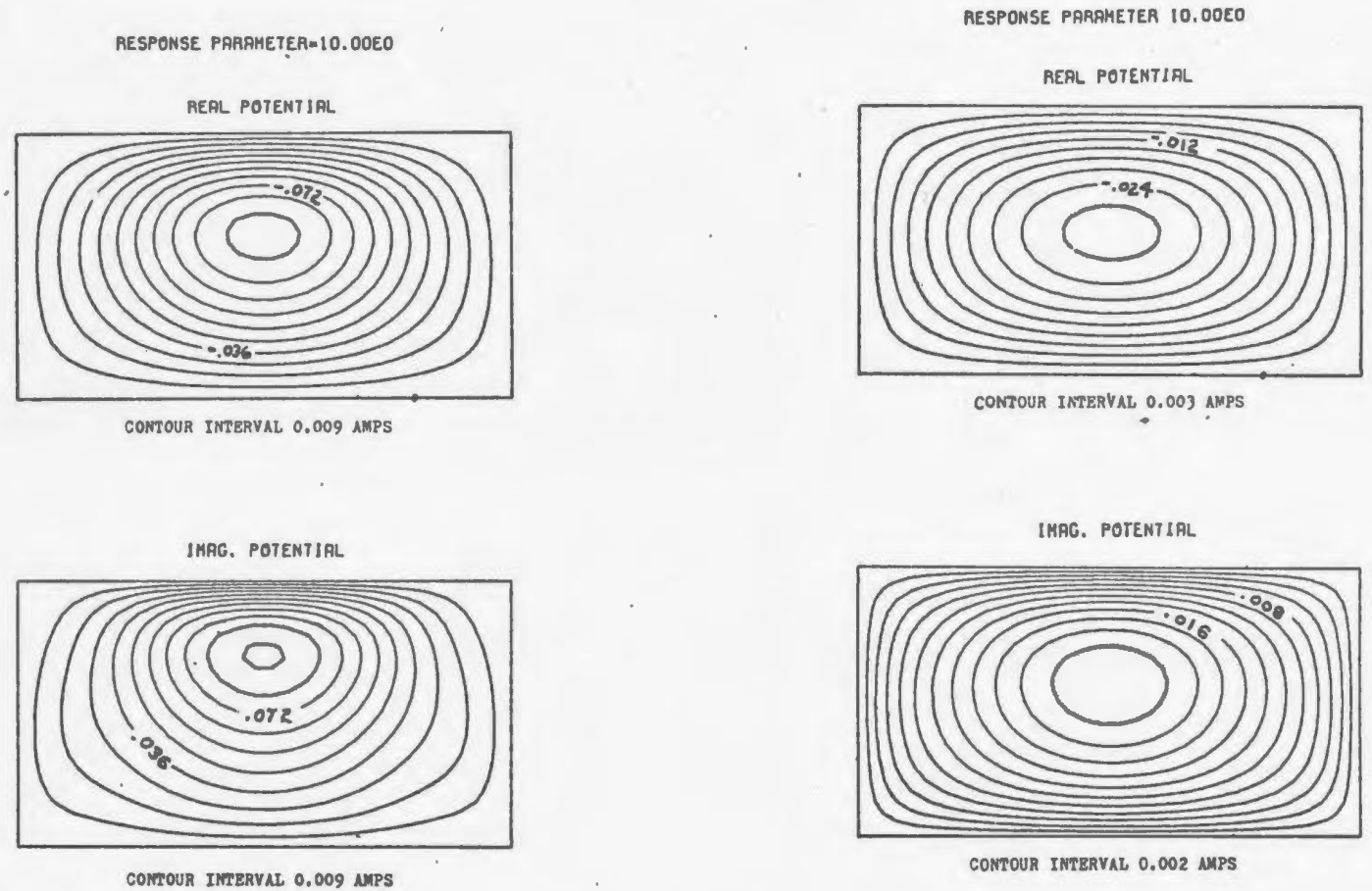

Fig. 7-15 cont'd. Total potential maps for thin sheet excited by a point magnetic dipole for $\alpha = 10$.

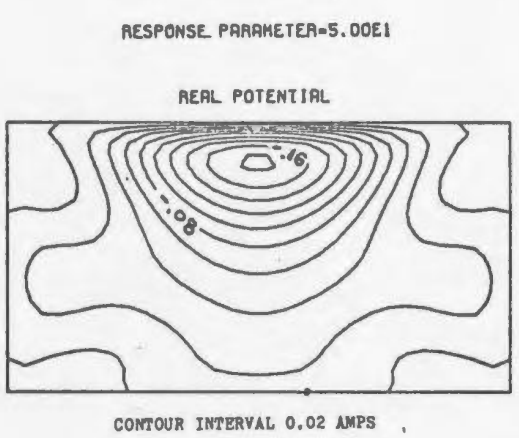

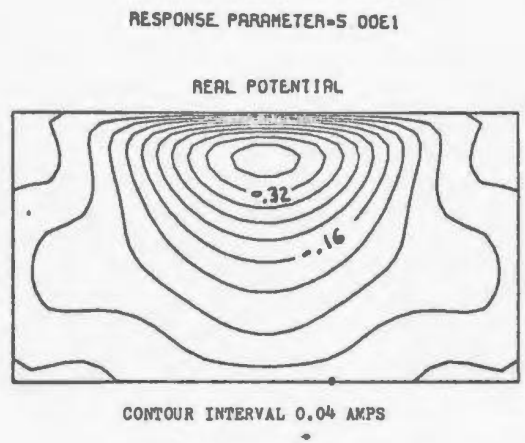

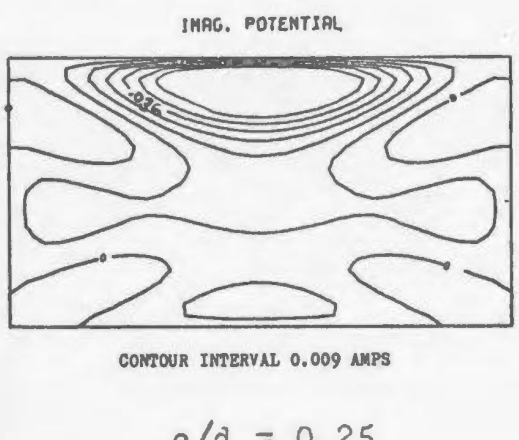

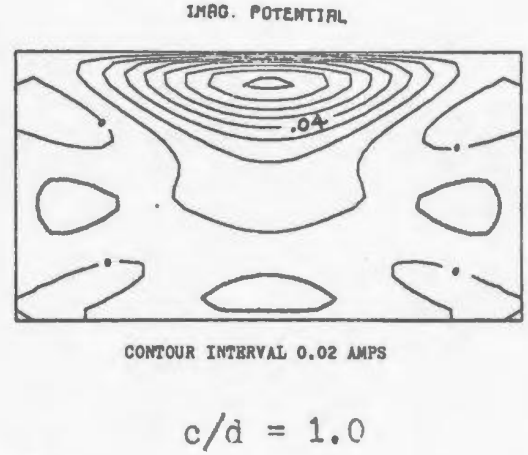

c/d = 0.25

c/d = 1.0

Fig. 7-16 Total potential maps for thin sheet excited by a point magnetic dipole for $\alpha = 50$.

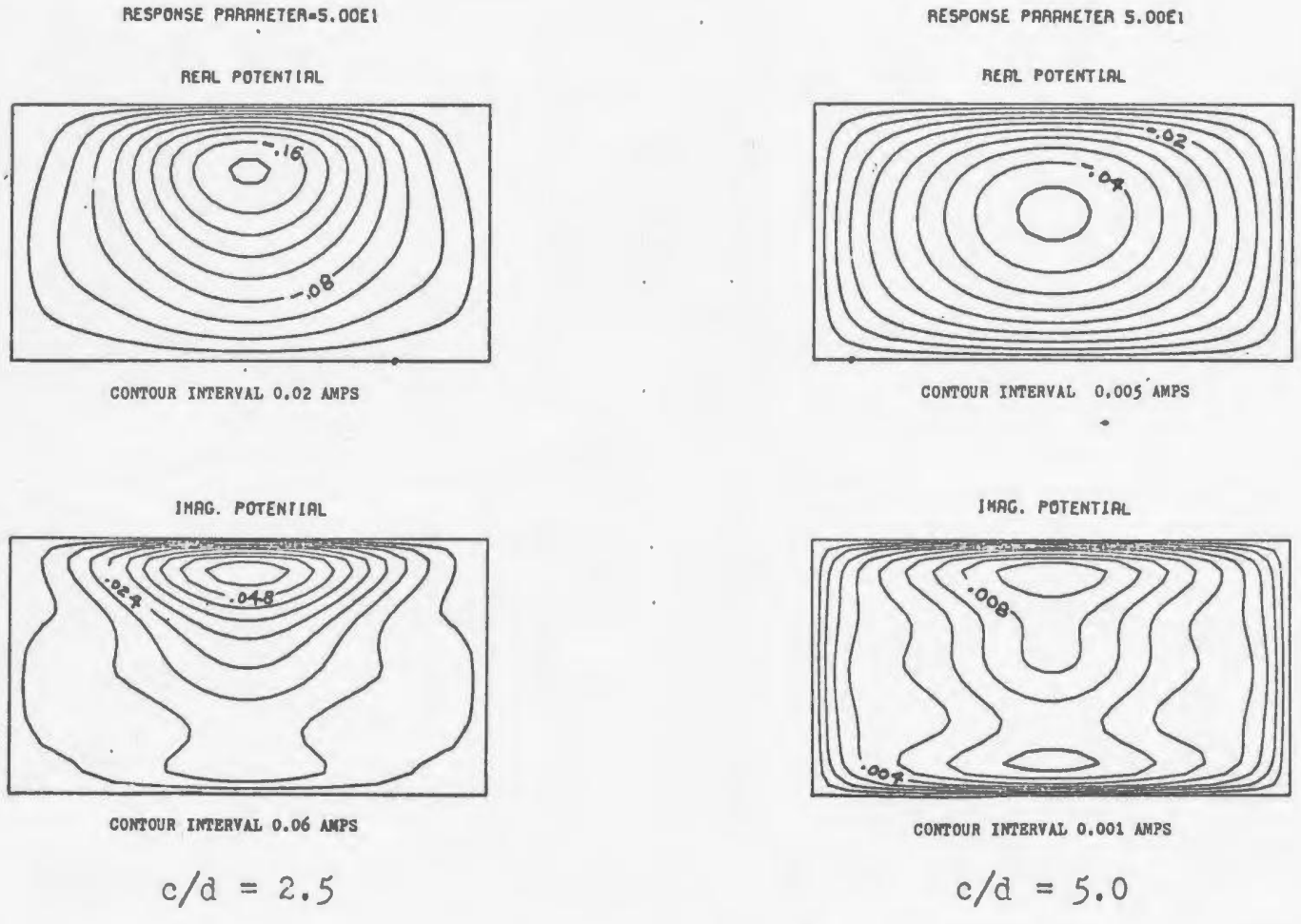

Fig. 7-16 cont'd. Total potential maps for thin sheet excited by a point magnetic dipole for $\alpha = 50$.

becomes more evenly distributed over the sheet reflecting the less abrupt variation of the source field. Associated with this is a change of the relative amplitudes of the real and imaginary part of U. As c/d increases the response moves more towards being in-phase with the exciting field. This is shown more clearly in the next set of figures in which some of the anomalous fields associated with U are plotted. One final comment on the total potential maps concerns the nature of the approximate solution. When the source field is quite localized and the response parameter is large, the potential U shows low amplitude undulations away from the main peak in the potential. This behaviour is a product of the approximate nature of the solution. All the eigenfunctions are of finite polynomial degree and there only a finite number of the possible eigenfunctions. In order to represent a sharp local peak in U, the approximate solution tends to overshoot and exhibit oscillations away from the peak. In the particular examples, the amplitude of these variations is quite small and does not have a major effect on the accuracy of the solution. In cases where the source field is locally very intense, accurate results can only be obtained by using a higher degree polynomial in computing the eigenfunctions. It must be remembered that the technique is an approximate method and that its purpose is to obtain a reasonable approximation to the real solution.

The anomalous magnetic field parallel to the axis of the exciting dipole moment along a profile over the sheet is shown in Fig. 7-17(a) and 7-17(b), for the four values of c/d used in the total potential maps. For each c/d ratio, the field for four response parameters is shown. These demonstrate the response through the swing from resistive to inductive limit. The effect of increasing c/d for fixed α has the effect of moving the response towards the inductive limit. This effect is best illustrated in Fig. 7-18 where the Q ratios versus the various α for varying c/d are plotted. The effect of increasing the s/d translates the Q versus α curve upwards with

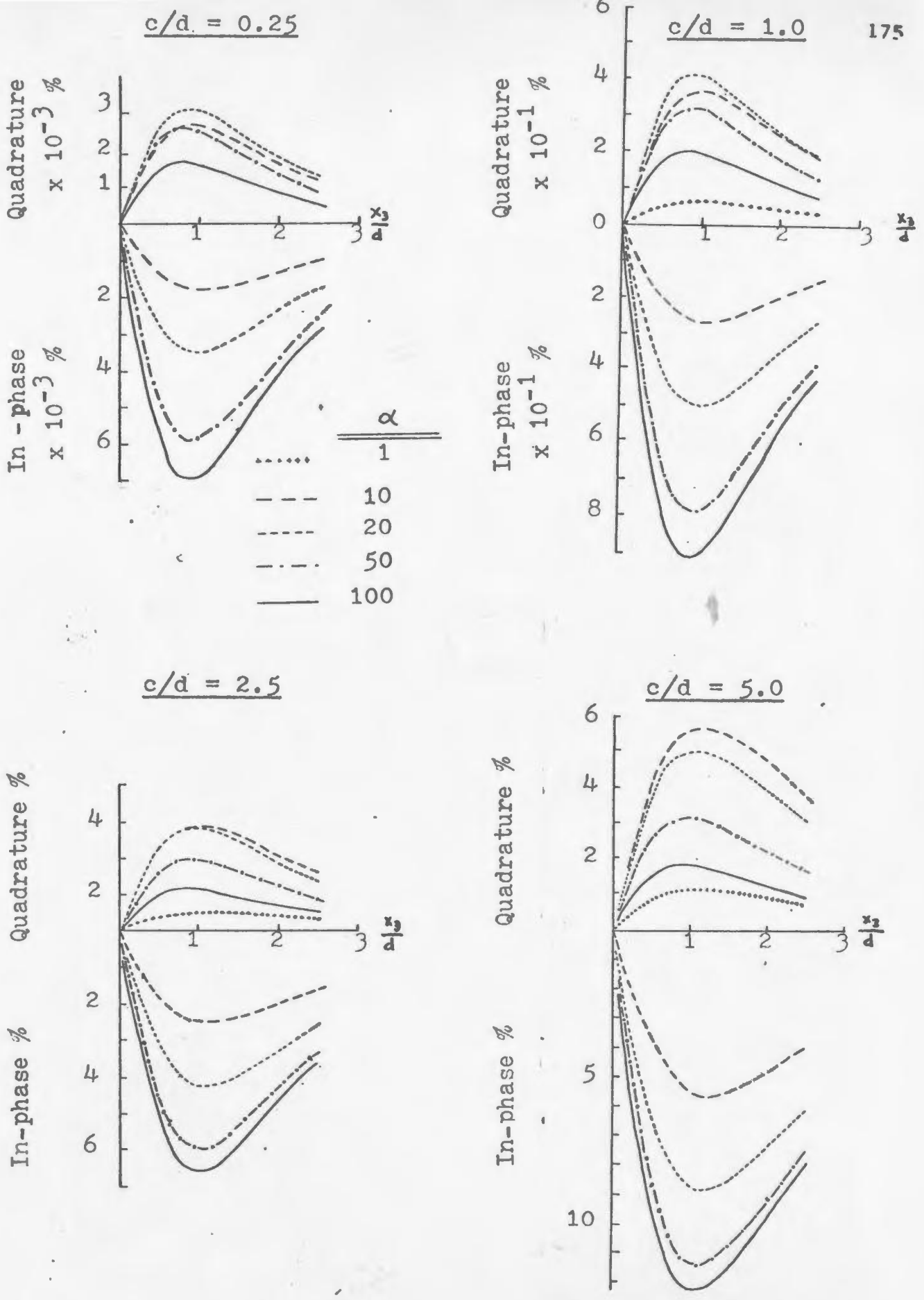

Fig. 7-17 Anomalous "vertical" magnetic field over thin sheet for various positions of the exciting magnetic dipole.

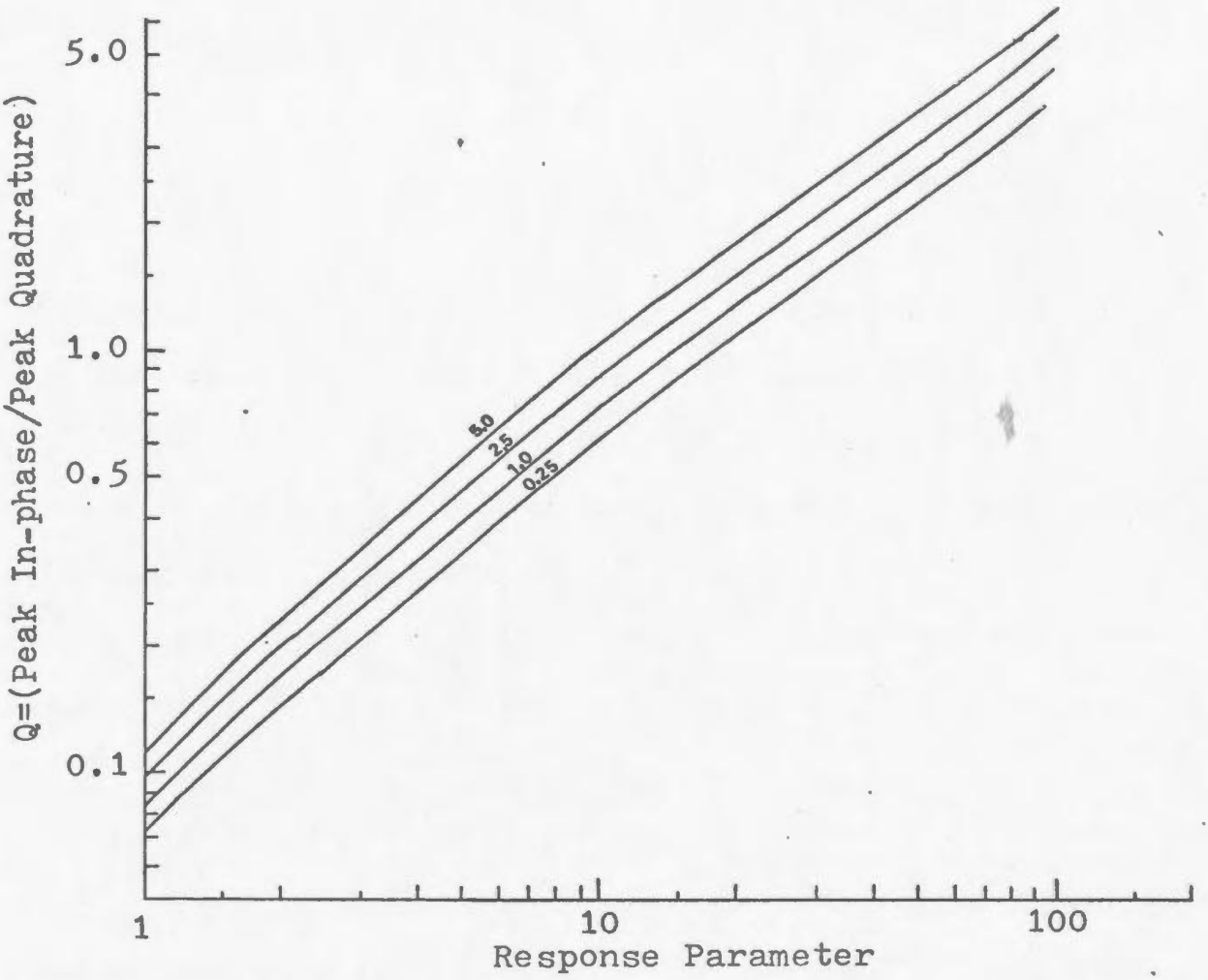

Fig. 7-18 Q versus response parameter α for various positions of exciting magnetic dipole as given by c/d ratios on curves.

no noticeable change in shape.

As a final example, the preceding results are used to generate the response of a horizontal loop survey system over a finite sheet structure. The system is shown in Fig. 7-19. The horizontal loop system consists of two coplanar coils fixed with respect to each other with one coil acting as a source (transmitter, Tx) and the other as a field detection unit (receiver, Rx). Loop-loop electromagnetic systems and their geophysical applications are discussed in more detail by Grant and West (1965) and Ward (1967).

The system response over the sheet is demonstrated in Fig. 7-20 for various coil separations. For s/d small, the system response is similar to that obtained by an airborne system. The body is much farther from the system than the system dimension (i.e. coil separation). For increasing s/d, the response moves towards that of a ground system where the coil separation can be greater than the depth to the body. The responses shown here are typical of those given by Grant and West (1965) for a semi-infinite sheet.

In applied geophysics, it is common to analyse the response for a wide range of solution parameters (in this case s/d, s/A and α). Characteristics of the system response are tabulated and used to make interpretation tables and diagrams. For example, phasor diagrams of peak in-phase and quadrature anomaly for varying response parameter and other system characteristics are commonly used for the interpretation of electromagnetic system data. The horizontal loop system analysed here typifies the results which can be obtained from the formulation of the thin sheet response in terms of the sheet eigenfunctions. Other electromagnetic systems in usage can be analysed in the same manner in both the time and frequency (response parameter) domain. No attempt is made here to analyse all the possibilities since the emphasis is on the development of alternate, economic techniques for analysing

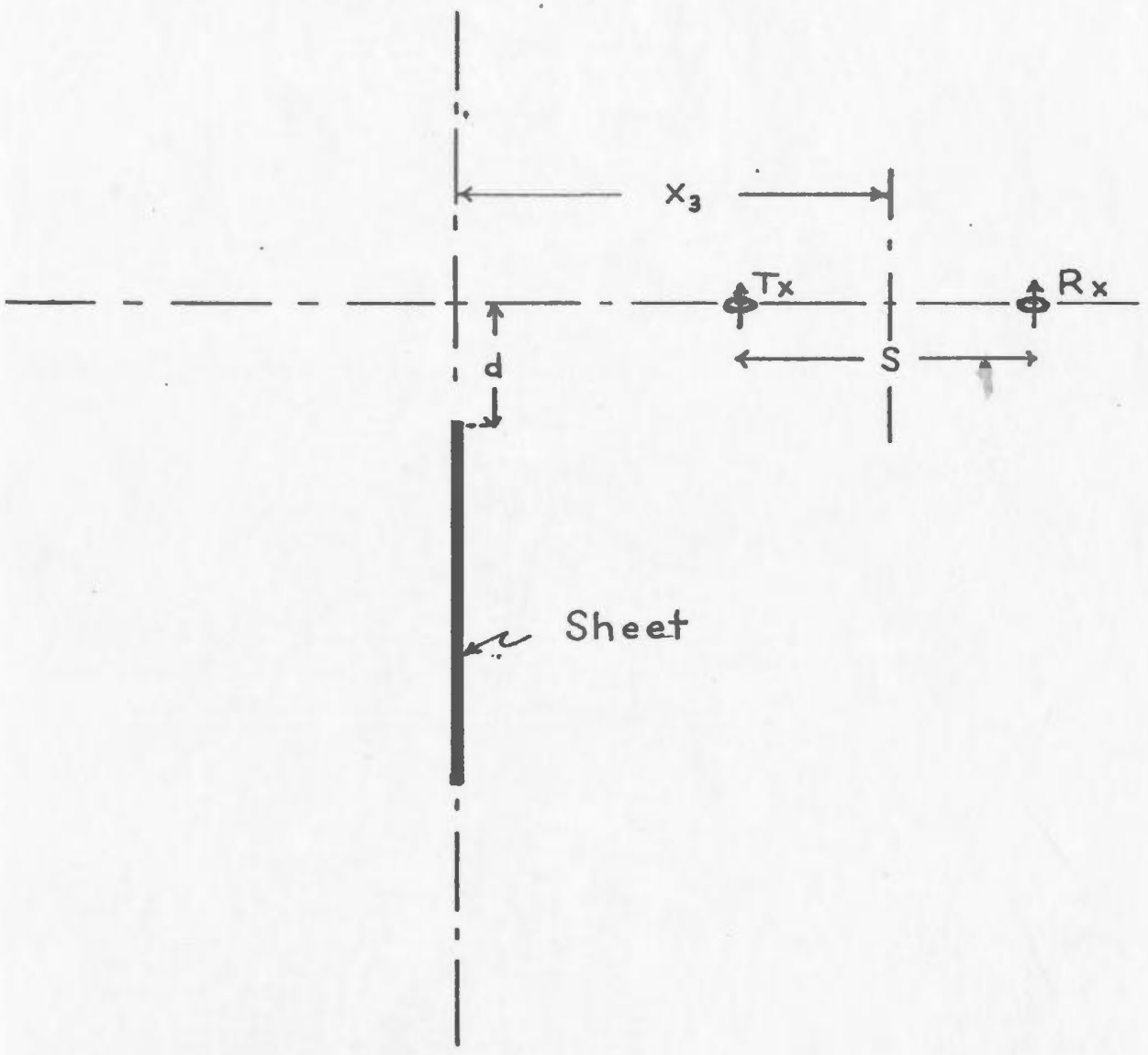

Fig. 7-19 Sketch of a horizontal loop electromagnetic survey system in the thin sheet geometry.

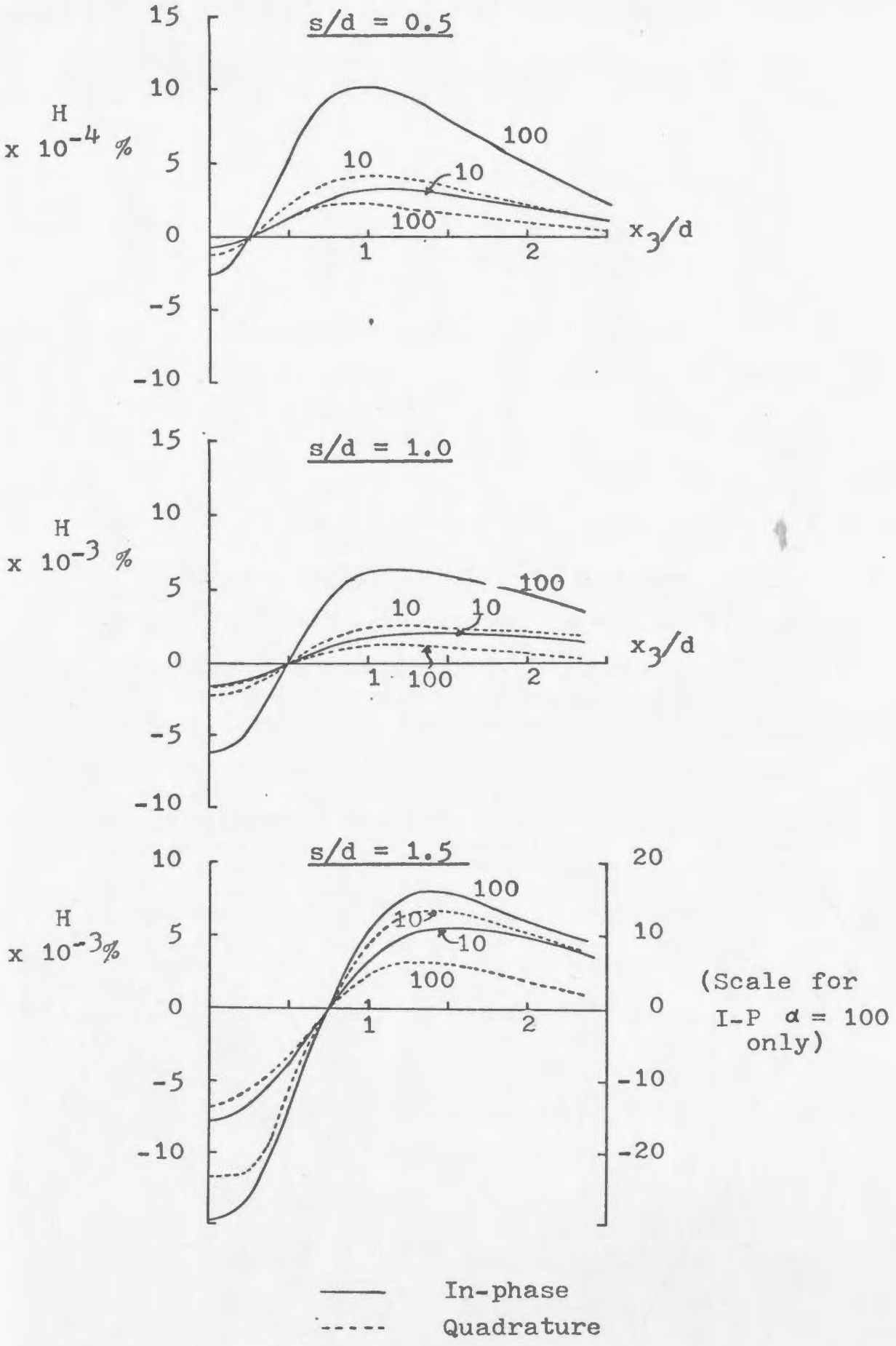

Fig. 7-20 Typical horizontal loop system profiles over the thin sheet for varying coil separations.

geophysical problems and not on tabulating vast amounts of data.

7-6 Summary

The thin sheet response analysed in this chapter typifies the electromagnetic scattering problems encountered in geophysical applications. Once again, the computation techniques have not been considered in detail and the discussions have been kept to the general features of the responses. One of the more important results of the analysis is the usefulness of the Galerkin form of numerical solution. It is more reliable and has a more physical basis then the least squares method used in chapter 6. It is less susceptible to the ill-conditioning of the scattering problem and is more amenable to the analysis of the system eigenfunctions.

The idea of analysing an approximate set of eigenfunctions for the system response also gave very productive results. Although the set of eigenfunctions obtained is not the true set, they do provide a good approximation to the true system. A detailed analysis of this approach to complex mathematical problems is important and should be applied more frequently to geophysical problems. The weighted form of the eigenfunction problem applied here is a natural one for electromagnetic problems. The very simple form of the inductive response eigenfunctions attests to this. Use of the resistance matrix as the weighting operator is very appropriate. It decouples the various factors of the response to a very high degree. The spatial form of the eigenfunctions is independent of the frequency response and electrical properties of the sheet. This result is quite different from the classical solution of boundary value problems in electromagnetics where the spatial form of the eigenfunction is directly linked with the electrical properties of the body. For the inductive sheet response, the evaluation of the eigenfunctions yields the response for all response parameters (and

all times in transient analysis).

One numerical technique which was considered in some detail but not discussed in this chapter was an iterative procedure for pre-whitening the impedance operator for highly ill-conditioned scattering operators. The technique was conceived when the exact manner in which the ill-conditioning arises was discovered. Basically, in matrix terms, the operator is the sum of the resistance (ohmic) matrix, the inductance matrix and the capacitance or channelling matrix. The first two matrices are definite with little variation in their eigenvalues. The channelling operator matrix is added to these other matrices after multiplication by a coefficient which can be very large. Since this matrix is not definite, some of its eigenvalues are zero. From practical computational considerations, these null eigenvalues will not be exactly zero and the large weighting factor multiplying the channelling matrix makes the round off errors the same size as the contributions from the resistive and inductive matrices. The resulting matrix is ill-conditiioned and the small eigenvalues will be those associated with the null eigenvalues of the channelling matrix. (The null eigenvalues are associated with the eigencurrents which are solenoidal). The pre-whitening scheme used the initially determined eigenvalues and eigenfunctions to expand the original matrices and pre-whiten each matrix before it was added to form the total impedance matrix. This procedure can be repeated until the resulting eigenvalues and eigenvectors stabilize. A more complete mathematical analysis of the technique needs to be done before it can be applied extensively but the idea appeared to work quite well in the preliminary tests that were made.

One factor which is important is a brief summary of the computation time and the amount of core required for analysis of the thin sheet problem. As in the 2-dimensional analysis of chapter 6, the most expensive part of the analysis is the numerical quadratures to find the integral coefficients.

The programs for both the total response and the inductive response were similar in structure. The time to generate the total response coefficients was the order of 60 seconds of CPU time on an IBM 370-165. This was for high accuracy integrations and for a polynomial degree of 4. For less accurate integrations this time is reduced by a factor of 3 to 5. A revision of the programs to implement time-reducing alogorithms could save another factor of 2 here. The inductive coefficients took considerably less time since fewer parameters were required and complex arithmetic on the computer which is inefficient could be avoided completely. The time required for the model represented here was about 30 seconds of CPU time and the integrations were conducted at high accuracy. The remaining parts of the computations were very inexpensive with no one step taking more than a few seconds of CPU time. These numbers are for one shot runs. Additional time required for mass productions runs for numerous sources and parameters is of little significance compared to the basic run cost. All programs ran in less than 120K bytes of core and the inductive response programs (except plotting) ran in less than 70K bytes of core.

CHAPTER 8

SUMMARY, CONCLUSIONS, AND RECOMMENDATIONS

8-1 Summary

In the course of this thesis project, numerous aspects of electromagnetic scattering theory were analysed in varying degrees of detail and some of the results of these studies were presented in the preceding chapters. The initial objectives of the study were sufficiently broad that at times it was difficult to confine the work to a particular path of endeavour. In preparing the thesis, however, an attempt was made to develop a comprehensive, coherent statement of the most pertinent results obtained throughout the study. This was somewhat difficult to do since the various stages of analysis did not follow this sequence in their development. As in most research projects, difficulties invariably force one to retrace one's footsteps and pursue an alternate approach or reassess those already taken.

The emphasis throughout the thesis was on the development of a unified formalism to describe the response of electromagnetic scattering problems and the merging of this formalism with variational methods for computing approximate solutions to complicated systems of equations. The first half of the thesis was, therefore, devoted to the theoretical aspects of the formulation of the response while the latter half of the thesis was concerned with the computerized implementation of the approximate varational methods outlined in chapter 5. In the last two chapters where the numerical results were presented, detailed discussions of the computer programs were avoided as much as possible since it was felt that these details would only obscure the points to be made by the computed results.

Overall, a number of important results were found and a good deal of groundwork was laid for the continuation of these ideas into more complex

problems. Some of the major conclusions are summarized in the next section.

8-2 Conclusions

The equivalent source method is a very flexible and efficient technique for formulating the response of scattering structures with quite general electric and magnetic properties. The formulation makes the physical interpretation of the resulting integral equations for the equivalent source distribution very clear. As pointed out in chapter 2, the equivalent source exists only in the region where the anomalous material properties are non-zero. This is particularly important when the system is subjected to a localized disturbance since the equivalent source field has only to be evaluated in that localized region. When contrasted with the finite difference or other numerical methods which operate directly on the governing partial differential equation and force the boundary conditions, there is a considerable saving of work. The major drawback with the application of the equivalent source method is that the Green's function for the background system must be known. In most geophysical problems of interest, however, this is not a major difficulty since it is possible to evaluate the most interesting Green's function analytically or numerically.

A by-product of the equivalent source method is its role in providing a unified approach to the static problems discussed in chapter 3. In addition, the general integral equation formulation makes it possible to study the general properties of the solution without having to solve a number of numerical problems before hand. This is particularly true of the analysis in chapter 4. It is possible to make explicit remarks about the solution of the integral equation and show how these are contained in the integral operators. The bimodal nature of the scattering operator is extremely important when the numerical computation of responses is to be carried out. Since geophysical problems are often strongly bimodal, direct

implementation of a numerical method on the basic integral equation will be exceedingly susceptible to failure. This particular point was emphasised by the TM response discussed in chapter 6 and the thin sheet response in the general case discussed in chapter 7.

The use of approximate solutions based on variational or minimization techniques provide a viable alternative to the commonly used method of digitizing the solution. These techniques are new tools in the analysis of geophysical electromagnetic problems. Both the least squares and the Galerkin techniques yield inexpensive and quite accurate approximate solutions to complex problems when the problems are properly conditioned. From an after-the-fact analysis, the Galerkin method seems to be the better approach; this is particularly true for electromagnetic problems when the scattering matrix is susceptible to ill-conditioning. The reason for this is that the least squares scattering matrix has eigenvalues which are the order of the square of those of the Galerkin formulation. If the eigenvalue spectrum tends to split, resulting in ill-conditioning, the least squares method enhances the ill-conditioning and this is certainly not desirable when the inverse of the matrix is sought by numerical means.

One feature of the variational solution methods is that they attain much higher accuracy than numerical methods which rely on point-by-point solution of the integral equation, when the same number of unknown parameters are used in the solution. This was particularly noticeable in the thin sheet response analysis where the variational method required over an order of magnitude fewer unknowns to solve the same problem as a discrete sample solution method. This vast reduction in the number of unknowns greatly reduces the dimension of the scattering matrix and makes numerical inversion of the scattering matrix more accurate and much less expensive.

The extension of concepts used in solving problems analytically can be

successfully carried over to the domain of numerical analysis. The results of chapter 7 show that determination of multidimensional eigenfunctions is practical and provides much more information about the system response than can be obtained by just solving the system of equations numerous times. This is also an important practical consideration when the cost of computing is a significant factor in determining the number of responses which can be computed. This is invariably the major factor in problems of numerical analysis. In such cases, maximization of knowledge about the system should be striven for. This is exemplified by the use of the shifted eigenvalue approach applied in chapter 7. Formulation in this manner provided the total frequency and/or time response of the thin sheet in one computation. This approach to numerical problems where type curves for a wide variety of input or system parameters are required should be exploited more fully in applied geophysics.

Recommendations for Future Work

While a great deal of time and energy was spent in the development of the results presented in this thesis, there are many areas where more analysis is required. Although this is a common problem in research work, at times it can become discouraging. The subject of electromagnetic theory and scattering in particular is so diverse that there is an inexhaustible (and at times an insurmountable) set of problems to be tackled. The present work has shown that there are some areas which show promise for further research.

A major stumbling block in the initial stages of the thesis work was the problem of solving the integral equations encountered in the equivalent source formulation. While all standard texts on applied mathematics deal with the basic theory of integral equations, the types of equations considered are always those which have particular properties (usually solvable analytically), namely, real, positive definite kernels. While this is fine from

a theoretical point of view, a much more in depth study of integral equation problems, particularly of vector integral equations in multiple dimensions and the numerical solution of integral equations, would be a valuable piece of research.

Another promising research problem is the extension of the Galerkin method and the discrete eigenfunction approach to three dimensional bodies. The acheivement of highly accurate solutions with very few unknowns make the solution of three dimensional problems practical from a computer cost point of view. Combination of this approach with the finite element technique for describing complicated geometrical systems appears to be an area which would yield rewarding results.

The computation of static electric and magnetic responses was not discussed in terms of numerical solutions in the thesis. Application of the equivalent source method to resistivity problems by Dieter et al (1969) showed the feasibility of the method. With the generalized formulation given here, the response of more complex structures with gradational material properties can be formulated. Very simple solutions can be derived in cases where depolarization effects are negligible. Use of the Galerkin method in these problems is another area which bears investigation.

One other topic which seemed quite exciting but which could not be followed up during this project was the application of the equivalent source method in materials with non-linear electric and magnetic properties. By iterating the integral equations obtained from the equivalent source formulation, the behaviour and response of non-linear materials can be investigated. In the static field problems, the equivalent source integral equation can be used to show, by intuition, runaway effects and self-focussing of electric fields or magnetic flux through localized regions.

As pointed out at the beginning of this section, a wide variety of problems in the theory of electromagnetism are wide open for further

investigation. In retrospect, there appear to be many problems which are more interesting than those tackled here; however, this is probably a manifestation of the old adage that the grass is always greener on the other side of the fence.

APPENDIX A

ELECTROMAGNETIC GREEN'S DYADIC IN A PLANE STRATIFIED MEDIUM

A-1 Geometry and Basic Equations

The geometry of the plane layered medium is shown in Fig. 1. The structure is termed an N-layer medium and is composed of N+1 regions which have differing electromagnetic properties separated by N plane parallel boundaries. The Cartesian coordinate system is denoted (X_1, X_2, X_3) and has the associated unit vectors $(\hat{e}_1, \hat{e}_2, \hat{e}_3)$. The medium is stratified in the x coordinate with the N boundaries located at $x_3 = d_i (i = 1, N)$. The permeability and the complex permittivity of each region are denoted by μ_i and ε_i.

The electric and magnetic fields satisfy the differential equations

$$\tilde{\mathcal{O}} \cdot \bar{E} = j\omega\mu \bar{J} + \bar{\nabla} \times \bar{M} \qquad \text{A-1}$$

$$\tilde{\mathcal{O}} \cdot \bar{H} = -j\omega\varepsilon \bar{M} + \bar{\nabla} \times \bar{J} \qquad \text{A-2}$$

where $\tilde{\mathcal{O}} = \bar{\nabla} \times \bar{\nabla} \times \quad - k^2 \tilde{I}$

and $k^2 = \omega^2 \varepsilon \mu$ and $\tilde{I}$ is the unit dyadic. It is most convenient, although somewhat redundant, to define a set of four Green's dyadics in deriving the general Green's function for the system. These dyadics are denoted $({}^{E}_{J}\tilde{G}, {}^{H}_{J}\tilde{G}, {}^{E}_{M}\tilde{G}, {}^{H}_{M}\tilde{G})$ where the superscripts E and H indicate electric or magnetic Green's dyadics and the subscripts J and M denote the excitation to be electric or magnetic currents. The relations

$${}^{E}_{M}\tilde{G} = \frac{\bar{\nabla} \times {}^{H}_{M}\tilde{G}}{-j\omega\varepsilon} = \tilde{Z} \cdot {}^{H}_{M}\tilde{G} \qquad \text{A-3}$$

$${}^{H}_{J}\tilde{G} = \frac{\bar{\nabla} \times {}^{E}_{J}\tilde{G}}{j\omega\mu} = \tilde{Y} \cdot {}^{E}_{J}\tilde{G} \qquad \text{A-4}$$

are readily derived from Maxwell's equations. $\tilde{Z}$ and $\tilde{Y}$ are denoted the impedance and admittance operators.

Interface Depth	Region	Material Properties
$x_3 = d_N$	N	ϵ_N μ_N
	N-1	ϵ_{N-1} μ_{N-1}
$x_3 = d_{N-1}$		
$x_3 = d_{m+1}$		
$x_3 = x_3'$	m	ϵ_m μ_m
$x_3 = d$		
$x_3 = d_2$		
	1	ϵ_1 μ_1
$x_3 = d_1$		
	0	ϵ_0 μ_0

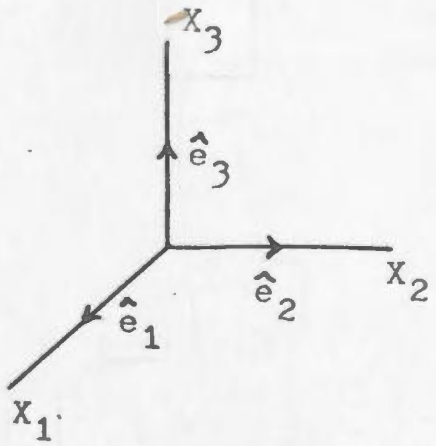

Fig. A-1 Plane Layered Earth Geometry

To define all four dyadics only ${}^{\epsilon}_{J}\tilde{\mathcal{G}}$ and ${}^{\mu}_{M}\tilde{\mathcal{G}}$ have to be found. From the symmetry of the equations, only ${}^{\epsilon}_{J}\tilde{\mathcal{G}}$ need to be derived in detail since the solution for ${}^{\mu}_{M}\tilde{\mathcal{G}}$ can be derived by interchanging the roles of μ and ϵ in the ${}^{\epsilon}_{J}\tilde{\mathcal{G}}$ expression. In the next section, ${}^{\epsilon}_{J}\tilde{\mathcal{G}}$ will be derived in detail.

A-2 Plane Wave Spectrum Analysis

The detailed derivation of ${}^{\epsilon}_{J}\tilde{\mathcal{G}}$ is carried out using the plane wave spectrum concept and a generalized matrix notation. From this point on the subscript J and superscript E on the dyadic will be dropped for compactness of the solution. In matrix notation the dyadic in the i'th region satisfies the equation

$$[\mathcal{O}^i][\mathcal{G}^i] = j\omega\mu_i\,\delta(|\bar{r}-\bar{r}'|)[I]\,\delta_{im} \qquad \text{A-5}$$

The source is taken to be in the m^{th} layer located at r'. The [ ] matrices are listed in Table A-1. $\bar{r} = x_i\hat{e}_i$ denotes the observation point and $\bar{r}' = x_i'\hat{e}_i$ the source point. $\delta(r)$ is the Dirac delta function and δ_{im} the Kronecker delta function.

With the aid of Fourier transform theory, $\tilde{\mathcal{G}}$ can be expressed as a superposition of plane waves

$$\tilde{\mathcal{G}}(r,r') = \frac{1}{4\pi^2}\iint_{-\infty}^{\infty}\tilde{G}(\bar{\lambda}, x_3, x_3')\,e^{j\bar{\lambda}\cdot(\bar{r}-\bar{r}')}\,d\lambda_1 d\lambda_2 \qquad \text{A-6}$$

where $\bar{\lambda} = \lambda_1\hat{e}_1 + \lambda_2\hat{e}_2$. $\tilde{G}$ is the plane wave spectrum amplitude for plane waves having horizontal wave number (λ_1,λ_2). In order to express the plane wave form clearly, a coordinate transformation of the wave number domain is combined with the Fourier transformation. The coordinate transformation is

$$[\hat{e}] = [D][\hat{s}] \qquad \text{A-7}$$

Table A-1 Spatial Form of Matrix Representations

$$\left[\mathcal{O}^i\right] = \begin{bmatrix} -\lambda_2^2 - \lambda_3^2 - k_i^2 , & \partial_1\partial_2 , & \partial_1\partial_3 \\ \partial_2\partial_1 , & -\lambda_1^2 - \lambda_3^2 - k_i^2 , & \partial_2\partial_3 \\ \partial_3\partial_1 , & \partial_3\partial_2 , & -\lambda_1^2 - \lambda_2^2 - k_i^2 \end{bmatrix}$$

$$\left[\mathcal{Y}^i\right] = \begin{bmatrix} \mathcal{Y}_{11}^i , & \mathcal{Y}_{12}^i , & \mathcal{Y}_{13}^i \\ \mathcal{Y}_{21}^i , & \mathcal{Y}_{22}^i , & \mathcal{Y}_{23}^i \\ \mathcal{Y}_{31}^i , & \mathcal{Y}_{32}^i , & \mathcal{Y}_{33}^i \end{bmatrix}$$

$$\left[I\right] = \begin{bmatrix} 1 , & 0 , & 0 \\ 0 , & 1 , & 0 \\ 0 , & 0 , & 1 \end{bmatrix}$$

Definition : $\partial_i = \frac{\partial}{\partial X_i}$

where

$$[D] = \begin{bmatrix} \frac{\lambda_1}{\lambda} & -\frac{\lambda_2}{\lambda} & 0 \\ \frac{\lambda_2}{\lambda} & \frac{\lambda_1}{\lambda} & 0 \\ 0 & 0 & 0 \end{bmatrix} \qquad \text{A-8}$$

and is just an expression of the cylindrical symmetry of the structure. $[\hat{S}]$ are the new unit vectors. The total transformation is then

$$[\mathcal{Y}^i] = \frac{1}{4\pi^2} \iint_{-\infty}^{\infty} [D][G^i][D]^T e^{j\bar{\lambda}\cdot(\bar{r}-\bar{r}')} d\lambda_1 d\lambda_2 \qquad \text{A-9}$$

$$[G^i] = [D]^T \iint_{-\infty}^{\infty} [\mathcal{Y}^i] e^{-j\bar{\lambda}\cdot(\bar{r}-\bar{r}')} dx_1 dx_2 [D] \qquad \text{A-10}$$

where A-9 is the inverse transformation and A-10 is the forward transformation.

Transformation of the differential equation A-5, yields

$$[\Theta^i][G^i] = \mathcal{L}\,\delta(x_3 - x_3')[I]\delta_{im} \qquad \text{A-11}$$

where $\mathcal{L} = j\omega\mu_m$ and $[\Theta^i]$ is the transformed differential operator listed in Table A-2. The solution of A-11 can be written down directly since the differential equations involve x_3 only. The homogeneous solution for A-11 is

$$[G^i] = [{}^{-}c^i \;,\; {}^{+}c^i][\beta^i(x_3)]\begin{bmatrix} {}^{-}a^i \\ {}^{+}a^i \end{bmatrix} \qquad \text{A-12}$$

where $[{}^{\pm}c^m]$ and $[{}^{\pm}a^i]$ are 3 x 3 matrices with $[{}^{\pm}a^i]$ being diagonal. $[\beta^i]$ is a 6 x 6 diagonal matrix. All the matrices are given in detail in Table A- 2. $[{}^{-}c^i]$, the upper half of $[\Theta^i]$ and $[{}^{-}a^i]$ combine to describe plane waves propagating in the negative x_3 direction while the other set describe waves propagating in the positive x_3 direction. To demonstrate this, the explicit forms of some of the components of $[G^i]$ are given here in detail.

$$\hat{s}_1 G^i_{11} \hat{s}_1 + \hat{s}_3 G^i_{31} \hat{s}_1 = \pm a^i \left(\hat{s}_1 e^{\mp \gamma_i x_3} \pm j\frac{\lambda}{\gamma_i}\hat{s}_3 e^{\mp\gamma_i x_3}\right)\left\{e^{j\bar{\lambda}\cdot(\bar{r}-\bar{r}')}\right\}\hat{s}_1 \qquad \text{A-13}$$

$$\hat{s}_2 G^i_{22} \hat{s}_2 = {}^{\pm}a^i\, \hat{s}_2\, e^{\mp\gamma_i x_3}\left\{e^{j\bar{\lambda}\cdot(\bar{r}-\bar{r}')}\right\}\hat{s}_2 \qquad \text{A-14}$$

Table A-2 Wavenumber Domain Matrix Representations

$$\left[G^i\right] = \begin{bmatrix} G_{11} & 0 & G_{13} \\ 0 & G_{22} & 0 \\ G_{31} & 0 & G_{33} \end{bmatrix}$$

$$\left[\mathcal{Q}^i\right] = \begin{bmatrix} -\partial_3^2 + \gamma_i^2 - \lambda^2 & 0 & j\lambda\partial_3 \\ 0 & -\partial_3^2 + \gamma_i^2 & 0 \\ j\lambda\partial_3 & 0 & \gamma_i^2 \end{bmatrix}$$

$$\left[\mp C^i\right] = \begin{bmatrix} 1 & 0 & 1 \\ 0 & 1 & 0 \\ \mp j\frac{\lambda}{\gamma_i} & 0 & \mp j\frac{\lambda}{\gamma_i} \end{bmatrix}$$

$$\left[\mp a^i\right] = \begin{bmatrix} \mp a_{11}^i & 0 & 0 \\ 0 & \mp a_{22}^i & 0 \\ 0 & 0 & \mp a_{33}^i \end{bmatrix}$$

$$\left[\beta^i(x_3)\right] = \begin{bmatrix} e^{\gamma_i x_3} & 0 & 0 & 0 & 0 & 0 \\ 0 & e^{\gamma_i x_3} & 0 & 0 & 0 & 0 \\ 0 & 0 & e^{\gamma_i x_3} & 0 & 0 & 0 \\ 0 & 0 & 0 & e^{-\gamma_i x_3} & 0 & 0 \\ 0 & 0 & 0 & 0 & e^{-\gamma_i x_3} & 0 \\ 0 & 0 & 0 & 0 & 0 & e^{-\gamma_i x_3} \end{bmatrix}$$

Definition :

$$\gamma_i = (\lambda^2 - k_i^2)^{1/2}$$

$$\partial_3 = \frac{\partial}{\partial x_3}$$

The curly bracketed term is inserted from the Fourier transform to explicitly demonstrate the plane wave form of $[G^i]$. Expression A-13 is readily identified with the form of a TM (transverse magnetic) plane wave while A-14 has the form of a TE (transverse electric) plane wave.

To complete the solution, the particular solution of the inhomogeneous equations

$$[O^m][{}^pG^m] = \mathcal{H}_m \delta(x_3 - x_3')[I] \qquad \text{A-15}$$

is required. $[{}^pG^m]$ is given by

$$[{}^pG^m] = [{}^pc^m][{}^p\beta^m(x_3 - x_3')][{}^pa^m] \qquad \text{A-16}$$

where $[{}^pc^m]$, $[{}^p\beta^m$, and $[{}^pa^m]$ are 3 x 3 matrices given in Table A- 3. Above and below the source plane at $x_3 = x_3'$, $[{}^pG^m]$ may be written in a similar form to $[G^i]$, the homogeneous solution, with

$$[{}^{p+}G^m] = [{}^-c^m, {}^+c^m][\beta^m(x_3 - x_3')]\begin{bmatrix} 0 \\ {}^{p+}a^m \end{bmatrix} \qquad \text{A-17}$$

$$[{}^{p-}G^m] = [{}^-c^m, {}^+c^m][\beta^m(x_3 - x_3')]\begin{bmatrix} {}^{p-}a^m \\ 0 \end{bmatrix} \qquad \text{A-18}$$

where $[{}^{p\pm}a^m]$ are given in Table A-3.

At this point, the mathematical form of the $[G^i]$ have been derived with the result that each layer is characterized by 6 unknowns; namely, 3 amplitudes for the upward propagating waves and 3 for the downward travelling waves. In addition, the excitation factors for the various waves are contained in $[{}^pa^m]$. The next step is to solve for the $[{}^\pm a^i]$ in terms of $[{}^pa^m]$. This relation is obtained by invoking the boundary conditions that tangential $\overline{E}$ and $\overline{H}$ be continuous at the boundaries. The interrelation of the $[{}^\pm a^i]$ is compactly expressed using a generalized transmission matrix notation.

Table A-3 Particular Solution Matrix Representations

$$\left[{}^{p}c^{m} \right] = \begin{bmatrix} 1 & 0 & 1 \\ 0 & 1 & 0 \\ j\frac{\lambda}{\gamma_m}\,\mathrm{sgn}(x_3-x_3') & 0 & \left\{ j\frac{\lambda}{\gamma_m} - \frac{2j}{\lambda}\delta(x_3-x_3') \right\} \mathrm{sgn}(x_3-x_3') \end{bmatrix}$$

$$\left[{}^{p}\beta^{m}(x_3-x_3') \right] = \begin{bmatrix} e^{-\gamma_m|x_3-x_3'|} & 0 & 0 \\ 0 & e^{-\gamma_m|x_3-x_3'|} & 0 \\ 0 & 0 & e^{-\gamma_m|x_3-x_3'|} \end{bmatrix}$$

$$\left[{}^{p}a^{m} \right] = j\frac{\omega\mu_m}{2k_m^2} \begin{bmatrix} -\gamma_m & 0 & 0 \\ 0 & \frac{k_m^2}{\gamma_m} & 0 \\ 0 & 0 & -j\lambda\,\mathrm{sgn}(x_3-x_3') \end{bmatrix}$$

$$\left[{}^{p\mp}a^{m} \right] = j\frac{\omega\mu_m}{2k_m^2} \begin{bmatrix} -\gamma_m & 0 & 0 \\ 0 & \frac{k_m^2}{\gamma_m} & 0 \\ 0 & 0 & \pm j\lambda \end{bmatrix}$$

Definition :

$$\mathrm{sgn}(x) = 1 \qquad x \geq 0$$
$$= -1 \qquad x < 0$$

A-3 Transmission Matrices

The boundary conditions of continuity are

$$[\hat{e}_3 \times][\mathcal{E}^i] = [\hat{e}_3 \times][\mathcal{E}^{i\pm1}] \qquad \text{A-19}$$

$$[\hat{e}_3 \times][Y^i][\mathcal{E}^i] = [\hat{e}_3 \times][Y^{i\pm1}][\mathcal{E}^{i\pm1}] \qquad \text{A-20}$$

at $x_3 = d_{i+1}$. The Fourier transformed $[Y^i]$ and $[\hat{e}_3 \times]$ are given in Table A-4. Equations A-19 and 20 yield six equations relating the six $[{}^{\pm}a^i]$ to the six $[{}^{\pm}a^{i\pm1}]$ which may be written

$$[W^i][\beta^i(d_{i+1})]\begin{bmatrix} {}^{-}a^i \\ {}^{+}a^i \end{bmatrix} = [W^{i\pm1}][\beta^{i\pm1}(d_{i+1})]\begin{bmatrix} {}^{-}a^{i\pm1} \\ {}^{+}a^{i\pm1} \end{bmatrix} \qquad \text{A-21}$$

The 6 x 6 matrix $[W^i]$ is given in Table A-4. Given the coefficients in any region, the coefficients can be propagated upward and downward to find all the other coefficients by

$$\begin{bmatrix} {}^{-}a^{i\pm1} \\ {}^{+}a^{i\pm1} \end{bmatrix} = [\beta^{i\pm1}(-d_{i+1})][T_{i\pm1,i}][\beta^i(d_{i+1})]\begin{bmatrix} {}^{-}a^i \\ {}^{+}a^i \end{bmatrix} \qquad \text{A-22}$$

$[T_{i\pm1,i}] = [W^{i\pm1}][W^i]$ is denoted the transmission matrix for the d_{i+1} boundary. The elements of $[T]$ are combinations of the TE and TM Fresnel reflection and transmission coefficients.

A multiple layer transmission matrix, $[U_{pq}]$, can be defined relating the coefficients in regions p and q.

$$[U_{pq}] = [\beta^p(-d_p)][T_{p,p-1}][\beta^{p-1}(d_{p-1}-d_{p-2})]\cdots[T_{q+1,q}][\beta^q(d_{q+1})] \qquad \text{A-23}$$

Here p is assumed greater than q. The analogous form can be derived for p less than q. The sequence of matrices corresponds physically to the reflection and transmission at a boundary, phase shift and attenuation as the wave passes through a layer, reflection and transmission at the next boundary, etc

With this definition of $[U_{pq}]$, the solution for $[{}^{\pm}a^i]$ can be expressed

Table A-4 Boundary Condition Matrix Representations

$$[\hat{e}_3 \times] = \begin{bmatrix} 0 & -1 & 0 \\ 1 & 0 & 1 \\ 0 & 0 & 0 \end{bmatrix}$$

$$[Y^i] = \frac{1}{j\omega\mu_i} \begin{bmatrix} 0 & -\partial_3 & 0 \\ \partial_3 & 0 & -j\lambda \\ 0 & j\lambda & 0 \end{bmatrix}$$

$$[W^i] = \begin{bmatrix} 1 & 0 & 0 & 1 & 0 & 0 \\ 0 & 1 & 0 & 0 & 1 & 0 \\ 0 & 0 & 1 & 0 & 0 & 1 \\ y_i & 0 & 0 & -y_i & 0 & 0 \\ 0 & y_i & 0 & 0 & -y_i & 0 \\ 0 & 0 & y_i & 0 & 0 & -y_i \end{bmatrix}$$

$$[T_{i\pm1,i}] = \begin{bmatrix} \frac{1}{S_{i\pm1,i}} & 0 & 0 & \frac{X_{i\pm1,i}}{S_{i\pm1,i}} & 0 & 0 \\ 0 & \frac{1}{T_{i\pm1,i}} & 0 & 0 & \frac{R_{i\pm1,i}}{T_{i\pm1,i}} & 0 \\ 0 & 0 & \frac{1}{S_{i\pm1,i}} & 0 & 0 & \frac{X_{i\pm1,i}}{S_{i\pm1,i}} \\ \frac{X_{i\pm1,i}}{S_{i\pm1,i}} & 0 & 0 & \frac{1}{S_{i\pm1,i}} & 0 & 0 \\ 0 & \frac{R_{i\pm1,i}}{T_{i\pm1,i}} & 0 & 0 & \frac{1}{T_{i\pm1,i}} & 0 \\ 0 & 0 & \frac{X_{i\pm1,i}}{S_{i\pm1,i}} & 0 & 0 & \frac{1}{S_{i\pm1,i}} \end{bmatrix}$$

Definition :

$y_i = -j\omega\epsilon_i/\gamma_i$	TM mode admittance
$y_i = \gamma_i/j\omega\mu_i$	TE mode admittance
$R_{i\pm1,i} = (y_{i\pm1} - y_i)/(y_{i\pm1} + y_i)$	TE Fresnel reflection coefficient
$X_{i\pm1,i} = (y_{i\pm1} - y_i)/(y_{i\pm1} + y_i)$	TM Fresnel reflection coefficient
$T_{i\pm1,i} = 1 + R_{i\pm1,i}$	TE transmission coefficient
$S_{i\pm1,i} = 1 + X_{i\pm1,i}$	TM transmission coefficient

in terms of $[{}^{p}a^{m}]$. First, the radiation condition requires $[{}^{-}a^{N}] \equiv 0$ and $[{}^{+}a^{0}] \equiv 0$. Then

$$\begin{bmatrix} 0 \\ {}^{+}a^{N} \end{bmatrix} = [U_{Nm}] \left\{ \begin{bmatrix} {}^{-}a^{m} \\ {}^{+}a^{m} \end{bmatrix} + [\beta^{m}(-x_3')] \begin{bmatrix} 0 \\ {}^{p+}a^{m} \end{bmatrix} \right\} \qquad \text{A-24}$$

$$\begin{bmatrix} {}^{-}a^{0} \\ 0 \end{bmatrix} = [U_{0m}] \left\{ \begin{bmatrix} {}^{-}a^{m} \\ {}^{+}a^{m} \end{bmatrix} + [\beta^{m}(-x_3')] \begin{bmatrix} {}^{p-}a^{m} \\ 0 \end{bmatrix} \right\} \qquad \text{A-25}$$

Six equations relating $[{}^{\pm}a^{m}]$ to $[{}^{p}a^{m}]$ can be extracted from A-24 and A-25 and these equations are given by

$$[U_T] \begin{bmatrix} {}^{-}a^{m} \\ {}^{+}a^{m} \end{bmatrix} = [U_p][\beta^{m}(-x_3')] \begin{bmatrix} {}^{p-}a^{m} \\ {}^{p+}a^{m} \end{bmatrix} \qquad \text{A-26}$$

where $[U_T]$ and $[U_p]$ are listed in Table A-5. $[{}^{\pm}_{-}a^{m}]$ are explicitly given by

$$\begin{bmatrix} {}^{-}a^{m} \\ {}^{+}a^{m} \end{bmatrix} = [V][\beta^{m}(-x_3')] \begin{bmatrix} {}^{p-}a^{m} \\ {}^{p+}a^{m} \end{bmatrix} \qquad \text{A-27}$$

The solution matrix $[V]$ is given in Table A-5. The components of $[V]$ are the generalized reflection and transmission coefficients for the structure. Equation A-27 combined with the generalized transmission matrix given in equation A-23 constitute the complete solution for the Green's dyadic. The final stage of analysis is the inverse transform (equation A-10) to obtain the spatical representation,

A-4 Inverse Fourier Transformation

The inverse Fourier transformation to the space domain is the most difficult step of the whole analysis. With the exception of the whole-space problem, the inverse transform cannot be obtained analytically. For special combinations of parameters, approximate analytical solutions can be derived. The integrals encountered for a one layer model with one medium an insulator and the other a good conductor have been studied extensively and summaries of these results are given by Wait (1970), Ward (1967), Banos (1966). The one and two layer models where both media are dielectrics of low loss are discussed by Annan (1970, 1973), Brekhovskikh

Table A-5 Multiple Layer and Total System Transmission Matrices

$$[U_{pq}] = \begin{bmatrix} U_{11}^{pq} & 0 & 0 & U_{14}^{pq} & 0 & 0 \\ 0 & U_{22}^{pq} & 0 & 0 & U_{25}^{pq} & 0 \\ 0 & 0 & U_{33}^{pq} & 0 & 0 & U_{36}^{pq} \\ U_{41}^{pq} & 0 & 0 & U_{44}^{pq} & 0 & 0 \\ 0 & U_{52}^{pq} & 0 & 0 & U_{55}^{pq} & 0 \\ 0 & 0 & U_{63}^{pq} & 0 & 0 & U_{66}^{pq} \end{bmatrix}$$

$$[U_T] = \begin{bmatrix} U_{11}^{Nm} & 0 & 0 & U_{14}^{Nm} & 0 & 0 \\ 0 & U_{22}^{Nm} & 0 & 0 & U_{25}^{Nm} & 0 \\ 0 & 0 & U_{33}^{Nm} & 0 & 0 & U_{36}^{Nm} \\ U_{41}^{Nm} & 0 & 0 & U_{44}^{Nm} & 0 & 0 \\ 0 & U_{52}^{Nm} & 0 & 0 & U_{55}^{Nm} & 0 \\ 0 & 0 & U_{63}^{Nm} & 0 & 0 & U_{66}^{Nm} \end{bmatrix}$$

$$[U_p] \begin{bmatrix} 0 & 0 & 0 & -U_{14}^{Nm} & 0 & 0 \\ 0 & 0 & 0 & 0 & -U_{25}^{Nm} & 0 \\ 0 & 0 & 0 & 0 & 0 & -U_{36}^{Nm} \\ -U_{41}^{om} & 0 & 0 & 0 & 0 & 0 \\ 0 & -U_{52}^{om} & 0 & 0 & 0 & 0 \\ 0 & 0 & -U_{63}^{om} & 0 & 0 & 0 \end{bmatrix}$$

$$[V] = \begin{bmatrix} \frac{U_{14}^{Nm} U_{41}^{om}}{A} & 0 & 0 & -\frac{U_{14}^{Nm} U_{44}^{om}}{A} & 0 & 0 \\ 0 & \frac{U_{25}^{Nm} U_{52}^{om}}{B} & 0 & 0 & -\frac{U_{25}^{Nm} U_{55}^{om}}{B} & 0 \\ 0 & 0 & \frac{U_{36}^{Nm} U_{63}^{om}}{C} & 0 & 0 & -\frac{U_{63}^{Nm} U_{66}^{om}}{C} \\ -\frac{U_{11}^{Nm} U_{41}^{om}}{A} & 0 & 0 & \frac{U_{14}^{Nm} U_{41}^{om}}{A} & 0 & 0 \\ 0 & -\frac{U_{22}^{Nm} U_{52}^{om}}{B} & 0 & 0 & \frac{U_{25}^{Nm} U_{52}^{om}}{B} & 0 \\ 0 & 0 & -\frac{U_{33}^{Nm} U_{63}^{om}}{C} & 0 & 0 & \frac{U_{36}^{Nm} U_{63}^{om}}{C} \end{bmatrix}$$

Definition:

$$A = U_{11}^{Nm} U_{44}^{om} - U_{41}^{om} U_{14}^{Nm}$$

$$B = U_{22}^{Nm} U_{55}^{om} - U_{52}^{om} U_{25}^{Nm}$$

$$C = U_{33}^{Nm} U_{66}^{om} - U_{63}^{om} U_{36}^{Nm}$$

(1960), Ott (1941). For radiation problems, good approximations can be obtained for the integrals (using asymptotic expansions) when all the spatial dimensions of the problem are large compared to the wavelengths in the media. To evaluate the transforms in problems where none of the common approximations can be made, one must resort to numerical integration by computer.

In this section, the whole-space solution, which is just $[{}^{p}G^{m}]$, will be transformed. The spatial dyadic is given by

$$[{}^{p}\mathcal{G}^{m}] = \frac{1}{4\pi^2}\int_{-\infty}^{\infty}\int [D][{}^{p}G^{m}][D]^{T}\, e^{j\bar{\lambda}\cdot(\bar{r}-\bar{r}')}\, d\lambda_1 d\lambda_2 \qquad \text{A-28}$$

The matrix $[D][{}^{p}G^{m}][D]^{T}$ is given in Table A-6. Noting the role of differentiation on a Fourier transform, the matrix can be rewritten in terms of spatial derivatives. The transform becomes

$$[{}^{p}\mathcal{G}^{m}] = j\frac{\omega\mu_m}{k_m^2}[\bar{\nabla}\times\bar{\nabla}\times]\, g(r,r')[I] - j\frac{\omega\mu_m}{k_m^2}\delta(\bar{r}-\bar{r}')[I] \qquad \text{A-29}$$

where the double Fourier transform

$$g(r,r') = \frac{1}{4\pi^2}\int_{-\infty}^{\infty}\int \frac{e^{-\gamma_m|x_3-x_3'|}}{2\gamma_m}\, e^{j\bar{\lambda}\cdot(\bar{r}-\bar{r}')}\, d\lambda_1 d\lambda_2 \qquad \text{A-30}$$

is the well known Sommerfeld integral first evaluated by Sommerfeld in 1909 (see Sommerfeld (1949), Brekhovskikh(1960)). The evaluation of A-30 is given in Appendix C as integral .

$$g(r,r') = \frac{e^{jk_m R}}{4\pi R} \qquad \text{A-31}$$

Inserting $g(r,r')$ into A-29 and noting that

$$\nabla^2 g(r,r') + k_m^2 g(r,r') = -j\omega\mu_m\delta(\bar{r}-\bar{r}') \qquad \text{A-32}$$

the particular solution or Green's dyadic for a whole-space becomes

$${}^{p}\tilde{\mathcal{G}}^{m} = j\omega\mu_m\left\{\tilde{I} + \frac{\bar{\nabla}\bar{\nabla}}{k_m^2}\right\} g(r,r')\,\tilde{I} \qquad \text{A-33}$$

This solution is well known and be be found in any standard text on electromagnetic theory.

Table A-6 Whole-space Matrices Regrouped for Fourier Transformation

$$[D][{}^{p}G^{m}][D]^{T} = \frac{j\omega\mu_m e^{-\gamma_m|x_3-x_3'|}}{2\gamma_m k_m^2}\begin{bmatrix} -\gamma_m^2+\lambda_2^2 & -\lambda_1\lambda_2 & -j\lambda_1\gamma_m\,\mathrm{sgn}(x_3-x_3') \\ -\lambda_1\lambda_2 & -\gamma_m^2+\lambda_1^2 & -j\lambda_2\gamma_m\,\mathrm{sgn}(x_3-x_3') \\ -j\lambda_1\gamma_m\,\mathrm{sgn}(x_3-x_3') & -j\lambda_2\gamma_m\,\mathrm{sgn}(x_3-x_3') & \lambda^2-2\delta(x_3-x_3') \end{bmatrix}$$

$$= \frac{j\omega\mu_m e^{-\gamma_m|x_3-x_3'|}}{2\gamma_m k_m^2}\begin{bmatrix} -\partial_2^2-\partial_3^2 & \partial_1\partial_2 & \partial_1\partial_3 \\ \partial_2\partial_1 & -\partial_1^2-\partial_3^2 & \partial_2\partial_3 \\ \partial_3\partial_1 & \partial_3\partial_2 & -\partial_1^2-\partial_2^2 \end{bmatrix}$$

$$-\frac{j\omega\mu_m e^{-\gamma_m|x_3-x_3'|}}{k_m^2}\,\delta(x_3-x_3')\,e^{-\gamma_m|x_3-x_3'|}\begin{bmatrix} 1 & 0 & 0 \\ 0 & 1 & 0 \\ 0 & 0 & 1 \end{bmatrix}$$

$$\left[\bar{\nabla}\times\bar{\nabla}\times\right] = \begin{bmatrix} -\partial_2^2-\partial_3^2 & \partial_1\partial_2 & \partial_1\partial_3 \\ \partial_2\partial_1 & -\partial_1^2-\partial_3^2 & \partial_2\partial_3 \\ \partial_3\partial_1 & \partial_3\partial_2 & -\partial_1^2-\partial_2^2 \end{bmatrix}$$

Definitions:

$$\mathrm{sgn}(x) = 1 \quad x \geq 0$$
$$= -1 \quad x < 0$$

$$\partial_i = \frac{\partial}{\partial x_i}$$

The additional, homogeneous dyadic which appears when the medium is not a whole-space represents the reflection and refraction of the spherical wave (equation A-32) as it encounters the planar interfaces. Since there is no general method to evaluate the homogeneous dyadic, the analysis of this problem is not considered further here. The evaluation of the integrals required for particular structures considered in the body of the thesis is discussed in Appendix C.

Summary

The preceding development derived the Green's dyadic $\overset{E}{J}\tilde{\Psi}$, and from A-4, $\overset{H}{J}\tilde{\Psi}$ is also defined for an N layered, plane stratified medium. The development of $\overset{H}{M}\tilde{\Psi}$ has not been derived in detail. From the symmetry of equations A-1 through A-4, $\overset{H}{M}\tilde{\Psi}$ can be developed directly from $\overset{E}{J}\tilde{\Psi}$. Interchanging H for E, $-j\omega\varepsilon$ for $j\omega\mu$, and $\overline{m}_s$ for $\overline{J}_s$ in all steps of the derivation yields $\overset{H}{M}\tilde{\Psi}$. In the plane wave spectrum, the roles of the TE and TM waves are interchanged; wherever a TE Fresnel reflection or transmission coefficient appears in $\overset{E}{J}\tilde{\Psi}$, the $\overset{H}{M}\tilde{\Psi}$ will have a TM Fresnel coefficient and vice-versa. $\overset{H}{M}\tilde{\Psi}^P$, the whole-space or inhomogeneous dyadic can be evaluated in the same manner as $\overset{E}{J}\tilde{\Psi}^P$ and is also obtained by analogy with $\overset{E}{J}\tilde{\Psi}^P$. Appendix B develops some particular forms of the Green's dyadic which are useful for applied geophysics analysis.

APPENDIX B

GREENS DYADICS: SPECIAL CASES

The development of the general Green's dyadic in Appendix A is somewhat too general to express the response of simple structures easily. In this appendix, some particular forms of the general dyadic are expressed in a more specific and compact form. This serves two purposes; first, it shows the generality and application of the formulation of Appendix A and secondly, it yields dyadics which can, in some geophysical cases, be evaluated analytically.

The particular cases examined in this section are the general dyadic for a half-space and the particular forms of the half-space dyadic for two-dimensional excitation currents. These two dimensional forms of the dyadics are denoted the TE and TM dyadics. The reason for this becomes apparent after the derivation of the responses. The half-space geometry is shown in Fig. B-1. The dyadic for the lower half-space for a current in the lower half-space is derived.

The inhomogeneous or singular part of the Green's dyadic is the same as that derived in A-33. The homogeneous dyadic accounting for waves reflected from the half-space interface is given by

$$[G^{\circ}] = [{}^{-}C^{\circ}, {}^{+}C^{\circ}][\beta^{\circ}(x_3)]\begin{bmatrix} {}^{-}a^{\circ} \\ {}^{+}a^{\circ} \end{bmatrix} \qquad \text{B-1}$$

in the spatial wave number domain. From A-27

$$\begin{bmatrix} {}^{-}a^{\circ} \\ {}^{+}a^{\circ} \end{bmatrix} = [V][\beta^{\circ}(-x_3')]\begin{bmatrix} {}^{p}{}^{-}a^{\circ} \\ {}^{p}{}^{+}a^{\circ} \end{bmatrix} \qquad \text{B-2}$$

where $[V]$ is given in Table A-5 in terms of $[U_{pq}]$. In this case, the only $[U_{pq}]$ is $[U_{10}]$ which is in turn defined in terms of $[T_{10}]$ which is tabulated in Table A-4. The particular forms of $[T_{10}]$ and $[V]$ are given

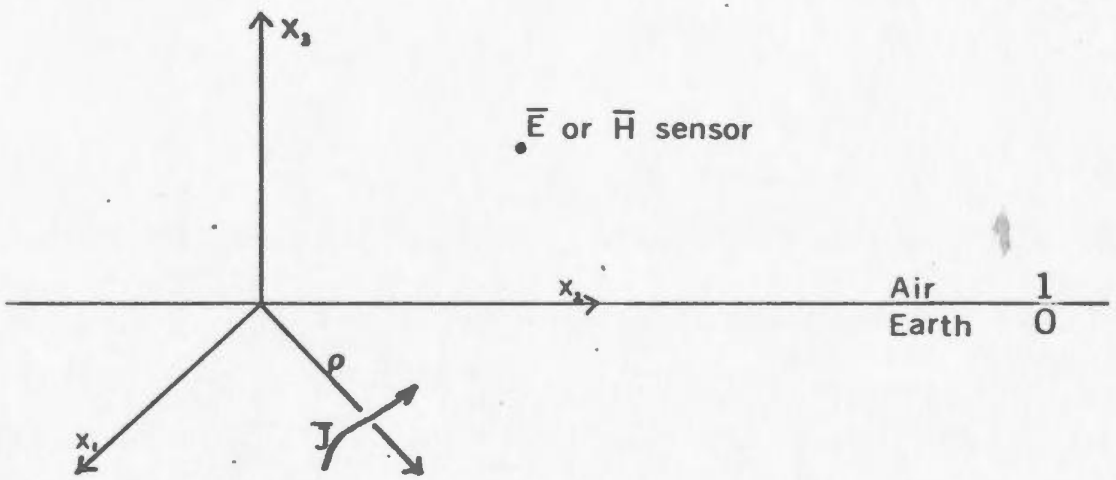

FIG B–1 Half-space geometry

in Table B-1 for the half-space case. The resulting $[{}^{s}a^{o}]$ coefficients and $[G^{o}]$ are listed in Table B-2.

The spatial form of the dyadic in the lower half-space (region 0) is obtained by taking the inverse transformation of B-1 and adding the inhomogeneous part of the Green's dyadic.

$$\tilde{\mathcal{G}}^{o} = {}^{p}\tilde{\mathcal{G}}^{o} + \frac{1}{4\pi^2}\iint_{-\infty}^{\infty} [D][G^{o}][D]^{T} e^{j\bar{\lambda}\cdot(\bar{r}-\bar{r}')} d\lambda_1 d\lambda_2 \qquad \text{B-3}$$

The resulting form of $\tilde{\mathcal{G}}^{o}$ is

$$\tilde{\mathcal{G}}^{o} = j\omega\mu_o \left\{ (\tilde{C}_1 + \tilde{C}_2) + \frac{\bar{\nabla}\bar{\nabla}}{k_o^2} \cdot (\tilde{C}_1 + \tilde{C}_2 + \tilde{C}_3) \right\} \qquad \text{B-4}$$

where the dyadics $\tilde{C}_i, i=1,3$ are listed in Table B-3 and are defined in terms of the integrals L_4, L_5, and L_6 also listed in Table B-3. The approximate evaluation of these integrals in particular geophysical applications is discussed in Appendix C.

The elements of the Green's dyadic are the electric fields associated with the point current

$$\bar{J}_s = \delta(x_1-x_1')\,\delta(x_2-x_2')\,\delta(x_3-x_3')(\hat{e}_1 + \hat{e}_2 + \hat{e}_3) \qquad \text{B-5}$$

Two other particular dyadics which are useful in many applications are those for which $\bar{J}_s$ varies sinusoidally in one spatial dimension. The result is that $\bar{J}_s$ splits into two parts which are denoted TE and TM currents.

$$\bar{J}_s^{TE} = \delta(x_1-x_1')\,\delta(x_3-x_3')\,e^{j\alpha x_2}\hat{e}_2 \qquad \text{B-6}$$

$$\bar{J}_s^{TM} = \delta(x_1-x_1')\,\delta(x_3-x_3')\,e^{j\alpha x_2}(\hat{e}_1 + \hat{e}_3) \qquad \text{B-7}$$

In the wave number domain, $\bar{J}_s^{TE}$ and $\bar{J}_s^{TM}$ become

$$\bar{J}_s^{TE} = \delta(\lambda_2-\alpha)\,\delta(x_3-x_3')\,\hat{e}_2 \qquad \text{B-8}$$

$$\bar{J}_s^{TM} = \delta(\lambda_2-\alpha)\,\delta(x_3-x_3')(\hat{e}_1 + \hat{e}_3) \qquad \text{B-9}$$

In the wavenumber domain, the two homogeneous dyadics denoted $[G_{TM}^{o}]$ and $[G_{TE}^{o}]$ are given in Table B-4 along with the expressions for $[{}^{p}G_{TM}^{o}]$ and

Table B-1 Half-space Earth Transmission Matrices

$$[T_{10}] = \begin{bmatrix} \frac{1}{S_{10}} & 0 & 0 & \frac{X_{10}}{S_{10}} & 0 & 0 \\ 0 & \frac{1}{T_{10}} & 0 & 0 & \frac{R_{10}}{T_{10}} & 0 \\ 0 & 0 & \frac{1}{S_{10}} & 0 & 0 & \frac{X_{10}}{S_{10}} \\ 0 & \frac{R_{10}}{T_{10}} & 0 & \frac{1}{S_{10}} & 0 & 0 \\ 0 & 0 & \frac{X_{10}}{S_{10}} & 0 & \frac{1}{T_{10}} & 0 \\ & & & & 0 & \frac{1}{S_{10}} \end{bmatrix}$$

$$[V] = \begin{bmatrix} 0 & 0 & 0 & X_{01} & 0 & 0 \\ 0 & 0 & 0 & 0 & R_{01} & 0 \\ 0 & 0 & 0 & 0 & 0 & X_{01} \\ 0 & 0 & 0 & 0 & 0 & 0 \\ 0 & 0 & 0 & 0 & 0 & 0 \\ 0 & 0 & 0 & 0 & 0 & 0 \end{bmatrix}$$

Table B-2 Half-space Homogeneous Green's Dyadic in Wavenumber Domain

$$\left[-a^m\right] = \begin{bmatrix} X_{o1}e^{\gamma_o x_3'} & 0 & 0 \\ 0 & R_{o1}e^{\gamma_o x_3'} & \\ 0 & 0 & X_{o1}e^{\gamma_o x_3'} \end{bmatrix} \begin{bmatrix} -\gamma_o & 0 & 0 \\ 0 & \frac{k_o^2}{\gamma_o} & 0 \\ 0 & 0 & -j\lambda \end{bmatrix}$$

$$\left[G^o\right] = \frac{j\omega\mu_o}{2k_o^2} \begin{bmatrix} 1 & 0 & 1 \\ 0 & 1 & 0 \\ -j\frac{\lambda}{\gamma_o} & 0 & -j\frac{\lambda}{\gamma_o} \end{bmatrix} \begin{bmatrix} e^{\gamma_o x_3} & 0 & 0 \\ 0 & e^{\gamma_o x_3} & 0 \\ 0 & 0 & e^{\gamma_o x_3} \end{bmatrix} \left[-a^m\right]$$

$$= \frac{j\omega\mu_o e^{\gamma_o(x_3+x_3')}}{2k_o^2} \begin{bmatrix} -\gamma_o X_{o1} & 0 & -j\lambda X_{o1} \\ 0 & \frac{k_o^2}{\gamma_o} R_{o1} & 0 \\ j\lambda X_{o1} & 0 & -\frac{\lambda^2}{\gamma_o} X_{o1} \end{bmatrix}$$

$$\left[D\right]\left[G^o\right]\left[D^T\right] = \frac{j\omega\mu_o}{2\gamma_o} e^{\gamma_o(x_3+x_3')} \left\{ \begin{bmatrix} R_{o1} & 0 & 0 \\ 0 & R_{o1} & 0 \\ 0 & 0 & -X_{o1} \end{bmatrix} \right.$$

$$\left. + \frac{R_{o1}-X_{o1}}{\lambda^2} \begin{bmatrix} -\lambda_1^2 & -\lambda_1\lambda_2 & 0 \\ -\lambda_1\lambda_2 & -\lambda_2^2 & 0 \\ 0 & 0 & 0 \end{bmatrix} + X_{o1} \begin{bmatrix} -\lambda_1^2 & -\lambda_1\lambda_2 & -j\lambda_1\gamma_o \\ -\lambda_1\lambda_2 & -\lambda_2^2 & -j\lambda_2\gamma_o \\ j\lambda_1\gamma_o & j\lambda_2\gamma_o & -\gamma_o^2 \end{bmatrix} \right\}$$

Table B-3 Sub-dyadics of Half-space Green's Dyadic

$$\tilde{C}_1 = \frac{e^{jk_0|\bar{r}-\bar{r}'|}}{4\pi|\bar{r}-\bar{r}'|}\,\hat{e}_i\hat{e}_p\,\delta_{ip}$$

$$\tilde{C}_2 = L_4\,\hat{e}_1\hat{e}_1 + L_4\,\hat{e}_2\hat{e}_2 - L_5\,\hat{e}_3\hat{e}_3$$

$$\tilde{C}_3 = L_5(\hat{e}_1\hat{e}_1 + \hat{e}_2\hat{e}_2 - \hat{e}_3\hat{e}_3)$$

$$\tilde{C}_4 = L_6(\hat{e}_1\hat{e}_1 + \hat{e}_2\hat{e}_2)$$

$$L_4 = \frac{1}{4\pi^2}\iint_{-\infty}^{\infty} R_{01}\,\frac{e^{\gamma_0(x_3+x_3')}}{2\gamma_0}\,e^{j\bar{\lambda}\cdot|\bar{r}-\bar{r}'|}\,d\lambda_1\,d\lambda_2$$

$$L_5 = \frac{1}{4\pi^2}\iint_{-\infty}^{\infty} X_{01}\,\frac{e^{\gamma_0(x_3+x_3')}}{2\gamma_0}\,e^{j\bar{\lambda}\cdot|\bar{r}-\bar{r}'|}\,d\lambda_1\,d\lambda_2$$

$$L_6 = \frac{1}{4\pi^2}\iint_{-\infty}^{\infty} \frac{(R_{01}-X_{01})}{\lambda^2}\,e^{\gamma_0(x_3+x_3')}\,e^{j\bar{\lambda}\cdot|\bar{r}-\bar{r}'|}\,d\lambda_1\,d\lambda_2$$

Table B-4 Two-dimensional Halfspace Green's Dyadics in Wavenumber Domain

$$\left[D\right]\left[G^{o}_{TE}\right]\left[D^{T}\right] = \frac{j\omega\mu_o}{2\gamma_o} e^{\gamma_o(x_3+x_3')} \delta(\lambda_2-\alpha) \left\{ \begin{bmatrix} 0 & 0 & 0 \\ 0 & R_{01} & 0 \\ 0 & 0 & 0 \end{bmatrix} + \frac{(R_{01}-X_{01})}{\lambda^2} \begin{bmatrix} 0 & -\lambda_1\lambda_2 & 0 \\ 0 & -\lambda_2^2 & 0 \\ 0 & 0 & 0 \end{bmatrix} + X_{01} \begin{bmatrix} 0 & -\lambda_1\lambda_2 & 0 \\ 0 & -\lambda_2^2 & 0 \\ 0 & -j\lambda_2\gamma_o & 0 \end{bmatrix} \right\}$$

$$\left[D\right]\left[G^{o}_{TM}\right]\left[D^{T}\right] = \frac{j\omega\mu_o}{2\gamma_o} e^{\gamma_o(x_3+x_3')} \delta(\lambda_2-\alpha) \left\{ \begin{bmatrix} R_{01} & 0 & 0 \\ 0 & 0 & 0 \\ 0 & 0 & -X_{01} \end{bmatrix} + \frac{(R_{01}-X_{01})}{\lambda^2} \begin{bmatrix} -\lambda_1^2 & 0 & 0 \\ -\lambda_1\lambda_2 & 0 & 0 \\ 0 & 0 & 0 \end{bmatrix} + X_{01} \begin{bmatrix} -\lambda_1^2 & 0 & -j\lambda_1\gamma_o \\ -\lambda_1\lambda_2 & 0 & -j\lambda_2\gamma_o \\ j\lambda_1\gamma_o & 0 & -\gamma_o^2 \end{bmatrix} \right\}$$

$$\left[D\right]\left[{}^{p}G^{o}_{TE}\right]\left[D^{T}\right] = \frac{j\omega\mu_o e^{-\gamma_o|x_3-x_3'|}}{2\gamma_o} \delta(\lambda_2-\alpha) \left\{ \begin{bmatrix} 0 & 0 & 0 \\ 0 & 1 & 0 \\ 0 & 0 & 0 \end{bmatrix} + \frac{1}{k_o^2} \begin{bmatrix} 0 & -\lambda_1\lambda_2 & 0 \\ 0 & -\lambda_2^2 & 0 \\ 0 & \mp j\lambda_2\gamma_o & 0 \end{bmatrix} \right\}$$

$$\left[D\right]\left[{}^{p}G^{o}_{TM}\right]\left[D^{T}\right] = \frac{j\omega\mu_o e^{-\gamma_o|x_3-x_3'|}}{2\gamma_o} \delta(\lambda_2-\alpha) \left\{ \begin{bmatrix} 1 & 0 & 0 \\ 0 & 0 & 0 \\ 0 & 0 & 1 \end{bmatrix} + \frac{1}{k_o^2} \begin{bmatrix} -\lambda_1^2 & 0 & \mp j\lambda_1\gamma_o \\ -\lambda_1\lambda_2 & 0 & \mp j\lambda_2\gamma_o \\ \mp j\lambda_1\gamma_o & 0 & \gamma_o^2 \end{bmatrix} \right\}$$

$[\Gamma G^{e}_{TE}]$ the inhomogeneous dyadics which are derived straight from the full three dimensional case discussed in Table A-6.

A particularly simple form of these dyadics occurs for 0 and is responsible for the TE and TM notation. For $\alpha \equiv 0$, the currents do not vary in the third spatial dimension. These dyadics in this case are the "true" 2 dimensional Green's dyadics; the TE and TM notation is ascribed because the one current system generates only TE waves while the other generates only TM waves. Although this result has been derived for the particular case of a half-space, it is also true for the general N-layer problem. This non-mixing of the two types of waves is just a manifestation of the usual analysis of 2-dimensional structures applied by Swift (1967), Wright (1969) and others analysing two dimensional structures. For the particular case of $\alpha \equiv 0$, the spatial dyadics listed in Table B-5 are expressible in terms of the three integrals L_0 , L_1 , and L_2 . The evaluation of these integrals is outlined in Appendix C for application in the body of the thesis. The integral L_0 is just the Hankel function of zero order and the first kind, $H_0^1(k_0 r)$, which is the usual 2-dimensional Green's function describing cylindrical waves.

Table B-5 Spatial Two-dimensional Green's Dyadics ($\alpha=0$)

$$\tilde{\mathcal{G}}^{\circ}_{TE} = j\omega\mu_0 (L_0 + L_1)\hat{c}_2\hat{e}_2$$

$$\tilde{\mathcal{G}}^{\circ}_{TM} = j\omega\mu_0 (\tilde{C}_5 + \tilde{C}_6) + \frac{\overline{\nabla}\,\overline{\nabla}}{k_0^2} (\tilde{C}_5 + \tilde{C}_6)$$

$$\tilde{C}_5 = L_0 (\hat{e}_1\hat{e}_1 + \hat{e}_3\hat{e}_3)$$

$$\tilde{C}_6 = L_2 (\hat{e}_1\hat{e}_1 - \hat{e}_2\hat{e}_2)$$

$$L_0(x_1 x_3) = \frac{1}{2\pi}\int_{-\infty}^{\infty} \frac{e^{-\gamma_0|x_3 - x_3'|}}{2\gamma_0} e^{j\lambda(x_1 - x_1')}\, d\lambda$$

$$L_1(x_1 x_3) = \frac{1}{2\pi}\int_{-\infty}^{\infty} R_{01}\, \frac{e^{-\gamma_0(x_3 + x_3')}}{2\gamma_0} e^{j\lambda(x_1 - x_1')}\, d\lambda$$

$$L_2(x_1 x_3) = \frac{1}{2\pi}\int_{-\infty}^{\infty} X_{01}\, e^{-\gamma_0(x_3 + x_3')} e^{j\lambda(x_1 - x_1')}\, d\lambda$$

APPENDIX C

INTEGRAL EVALUATION

C-1 General Format

In the process of inverse Fourier transforming the special electromagnetic field dyadics derived in Appendices A and B, a number of integral expressions appeared which required evaluation. These integrals are denoted L_i, $i = 0, 6$, and are listed in Table C-1.

The integrals L_0 and L_3 are standard integrals in the study of radiowave propagation and can be evaluated exactly. The remaining integrals cannot be evaluated analytically except in special cases. By definition of the geometry in Appendix B, both x_3 and x_3' are negative in these integrals.

The physical interpretation of the various integrals is of importance in the subsequent analysis of their evaluation. In all cases, the integrands represent the spectrum of plane waves associated with a point or line source. L_0 and L_3 are the response in a homogeneous whole-space medium. The remaining integrals have the whole-space spectrum weighted by the appropriate Fresnel reflection coefficient and correspond to the plane wave spectrum of the fields reflected from a plane boundary. In other words, each plane wave in the original spectrum is partially reflected from the boundary in accordance with Snell's law and the Fresnel reflection coefficient for the incident plane wave.

C-2 Integral L_0

The integral L_0 is just an integral form of the Hankel function of zero order and the first kind. This is most easily seen by defining

$$\rho^2 = (x_1 - x_1')^2 + (x_3 - x_3')^2 \qquad \text{C-1}$$

Table C-1 Integrals L_i Required for Whole and Half-space Electromagnetic Green's Dyadics

$$L_0 = \frac{1}{2\pi}\int_{-\infty}^{\infty} \frac{e}{2\gamma_0}^{-\gamma_0|x_3-x_3'| + j\lambda(x_1-x_1')}\, d\lambda$$

$$L_1 = \frac{1}{2\pi}\int_{-\infty}^{\infty} R_{01}\, \frac{e}{2\gamma_0}^{\gamma_0(x_3+x_3') + j\lambda(x_1-x_1')}\, d\lambda$$

$$L_2 = \frac{1}{2\pi}\int_{-\infty}^{\infty} X_{01}\, \frac{e}{2\gamma_0}^{\gamma_0(x_3+x_3') + j\lambda(x_1-x_1')}\, d\lambda$$

$$L_3 = \frac{1}{4\pi^2}\iint_{-\infty}^{\infty} \frac{e}{2\gamma_0}^{-\gamma_0|x_3-x_3'| + j(\lambda_1(x_1-x_1') + \lambda_2(x_2-x_2'))}\, d\lambda_1\, d\lambda_2$$

$$L_4 = \frac{1}{4\pi^2}\iint_{-\infty}^{\infty} R_{01}\, \frac{e}{2\gamma_0}^{\gamma_0(x_3+x_3') + j(\lambda_1(x_1-x_1') + \lambda_2(x_2-x_2'))}\, d\lambda_1\, d\lambda_2$$

$$L_5 = \frac{1}{4\pi^2}\iint_{-\infty}^{\infty} X_{01}\, \frac{e}{2\gamma_0}^{\gamma_0(x_3+x_3') + j(\lambda_1(x_1-x_1') + \lambda_2(x_2-x_2'))}\, d\lambda_1\, d\lambda_2$$

$$L_6 = \frac{1}{4\pi^2}\iint_{-\infty}^{\infty} \frac{(R_{01}-X_{01})}{\lambda^2}\, e^{\gamma_0(x_3+x_3') + j(\lambda_1(x_1-x_1') + \lambda_2(x_2-x_2'))}\, d\lambda_1\, d\lambda_2$$

$$x_1 - x_1' = \rho \cos\theta \qquad \text{C-2}$$

$$|x_3 - x_3'| = \rho \sin\theta \qquad \text{C-3}$$

$$\lambda = k_0 \cos\varphi \qquad \text{C-4}$$

$$\gamma_0 = -j\, k_0 \sin\varphi \qquad \text{C-5}$$

Then

$$-\gamma_0|x_3 - x_3'| + j\lambda(x_1 - x_1') = j k_0 \rho \cos(\theta - \varphi) \qquad \text{C-6}$$

and

$$L_0 = \frac{j}{4\pi} \int_{-\pi/2+j\infty}^{\pi/2-j\infty} e^{j k_0 \rho \cos(\varphi-\theta)}\, d\theta \qquad \text{C-7}$$

This integral is a standard form of the Hankel function (Morse and Feshbach, 1953, Pg. 623) and is

$$L_0 = \frac{j}{4} H_0^1(k_0\rho) \qquad \text{C-8}$$

C-3 Integral L_3

The integral L_3 is known as the Sommerfeld integral. Since L_3 is commonly given in the form of a Fourier-Bessel transform, L_3 is modified by transforming the integration variables as follows.

$$\rho^2 = (x_1 - x_1')^2 + (x_2 - x_2')^2 \qquad \text{C-9}$$

$$(x_1 - x_1') = \rho \cos\theta \qquad \text{C-10}$$

$$(x_2 - x_2') = \rho \sin\theta \qquad \text{C-11}$$

$$\lambda^2 = \lambda_1^2 + \lambda_2^2 \qquad \text{C-12}$$

$$\lambda_1 = \lambda \cos\varphi \qquad \text{C-13}$$

$$\lambda_2 = \lambda \sin\varphi \qquad \text{C-14}$$

Now

$$L_3 = \frac{1}{4\pi^2} \int_0^{\infty} \int_0^{2\pi} \frac{e^{-\gamma_0 |x_3 - x_3'| + j\lambda\rho\cos(\varphi-\theta)}}{2\gamma_0} \lambda \, d\lambda \, d\varphi \qquad \text{C-15}$$

$$= \frac{1}{4\pi} \int_0^{\infty} \frac{e^{-\gamma_0 |x_3 - x_3'|}}{\gamma_0} \lambda J_0(\lambda\rho) \, d\lambda$$

where the integral form of the Bessel function of zero order is given by

$$J_0(\lambda\rho) = \frac{1}{\pi} \int_0^{\pi} e^{j\lambda\rho\cos(\varphi-\theta)} \, d\varphi \qquad \text{C-16}$$

(Morse and Feshbach, 1953, Pg. 620). The solution of L_3 is simply the spherical wave

$$L_3 = \frac{e^{jk_0 R}}{4\pi R} \qquad \text{C-17}$$

where $R = (\rho^2 + (x_3 - x_3')^2)^{1/2}$. (Sommerfeld, (1949)).

C-4 Quasistatic Approximations

In geophysical problems, the electromagnetic response of inhomogeneities buried in a conductive half-space is required. The response is observed in the air above the Earth and this is essentially free space. The size of the inhomogeneity and the spatial extent to which observations are made are much less than the free-space wavelength. As a result, the fields in the air, which propagate at the speed of light, may be assumed to reach all points of the observation area instantaneously. In other words the speed of light may be assumed infinite and the propagation constant in the air region is zero. The fields in the air are termed quasistatic. The quasi-static approach is discussed in texts on the subject of electromagnetic methods in geophysics (Grant and West, 1965, Ward, 1967) and has been the key to analysing geophysical E.M. problems.

The electromagnetic fields scattered by an inhomogeneity in the Earth are partially reflected from the earth-air interface back into the Earth

and partially transmitted through the boundary. The reflection coefficients of the boundary appear in the integrands of L_1, L_2, L_4, L_5 and L_6. Combining the quasistatic assumption with the fact that the permeability of bulk earth materials is essentially the free space permeability, the resulting form of the reflection coefficients permit analytic evaluation of most of these integrals. From Appendix A, the TE and TM reflection coefficients are

$$R_{01} = \frac{y_0 - y_1}{y_0 + y_1} \qquad \text{C-18}$$

$$X_{01} = \frac{\gamma_0 - \gamma_1}{\gamma_0 + \gamma_1} \qquad \text{C-19}$$

where $y_0 = \frac{j\gamma_i}{\omega\mu_i}$ and $y_i = \frac{\omega\epsilon_i}{j\gamma_i}$

with $\gamma_i^2 = \lambda^2 - k_i^2$

The subscript 0 denotes the earth region and subscript 1 the air region in this case. Letting $\mu_i = \mu_0$ the free space permeability

$$R_{01} = \frac{(\gamma_0 - \gamma_1)}{(\gamma_0 + \gamma_1)} \qquad \text{C-20}$$

$$X_{01} = \frac{(\epsilon_0\gamma_1 - \epsilon_1\gamma_0)}{(\epsilon_0\gamma_1 + \epsilon_1\gamma_0)} \qquad \text{C-21}$$

Writing out the detailed form of Ro_1 and X_{01} gives

$$R_{01} = \frac{-2k_0^2(1 + k_1^2/k_0^2) - 2\gamma_0\gamma_1}{k_0^2(1 - k_1^2/k_0^2)} \qquad \text{C-22}$$

$$X_{01} = \frac{\epsilon_0^2\lambda^2(1 + \epsilon_1^2/\epsilon_0^2) - \epsilon_1^2 k_0^2(k_1^2/k_0^2 + \epsilon_1^2/\epsilon_0^2) - 2\epsilon_1\gamma_0\gamma_1}{\epsilon_0^2\lambda^2(1 - \epsilon_1^2/\epsilon_0^2) - \epsilon_0^2 k_0^2(k_1^2/k_0^2 - \epsilon_1^2/\epsilon_0^2)} \qquad \text{C-23}$$

These expressions are considerably simplifed when the order of magnitude of the terms k_1^2/k_0^2 and ϵ_1/ϵ_0 (which are the same) are examined.

$$\frac{k_1^2}{k_0^2} = \frac{\omega^2\epsilon_1\mu_0}{\omega^2\epsilon_0\mu_0} = \frac{\epsilon_1}{\epsilon_0} \qquad \text{C-24}$$

For a conductive earth (ϵ are complex permittivities)

$$\epsilon = \epsilon (1 + j \sigma / \omega \epsilon) \qquad \text{C-25}$$

where ϵ is the real permittivity and σ the conductivity. In a real earth environment, $\epsilon < 10^{-9}$ fd/m. and $\sigma > 10^{-3}$ mho/m. are realistic upper and lower limits for the material properties. For frequencies less than 1KHz, the ratio $\sigma/\omega\epsilon > 10^{2}$. In most instances the ratio is $> 10^{4}$. This result indicates that displacement currents in the earth are negligible in comparison to conduction currents and

$$\epsilon \simeq j \frac{\sigma}{\omega} \qquad \text{C-26}$$

A graph of the ratio of displacement currents to conduction is given in Fig. C-1. The ratio ϵ_1 / ϵ_0 becomes $\omega \epsilon_1 / \sigma_0$. By the same arguments $\omega \epsilon_1 / \sigma_0 \sim 10^{-4}$ since the free space permittivity ϵ_1 is 10^{-10} fd./m. . Neglecting terms of the order ϵ_1 / ϵ_0 is the same as assuming an infinite propagation velocity in the air.

The approximate forms for R_{01} and X_{01}, are

$$R_{01} \simeq 1 - \frac{2\lambda^2}{k_0^2} + \frac{2\gamma_0\gamma_1}{k_0^2} \qquad \text{C-21}$$

$$X_{01} \simeq 1 - 2\frac{\epsilon_1}{\epsilon_0}\frac{\gamma_0}{\gamma_1} \simeq 1 \qquad \text{C-28}$$

Since $k_1 \ll 1$ a further approximation is to set

$$\gamma_1 \simeq |\lambda| \qquad \text{C-29}$$

For practical purposes the second term of X_{01} may be neglected. If this is done, the boundary conditions at the air-earth interface for a TM wave propagating upwards in the earth correspond to a perfectly reflecting boundary. The tangential electric field is doubled, the normal electric field is zero (no current flow across the boundary) and the tangential $\overline{H}$ field is zero. In other words, the tangential magnetic field at the boundary does not change in the case of pure TM scattering from an inhomo-

Fig. C-1 Ratio of displacement currents to conduction currents as a function of frequency conductivity ratios. (Hz m./mho)

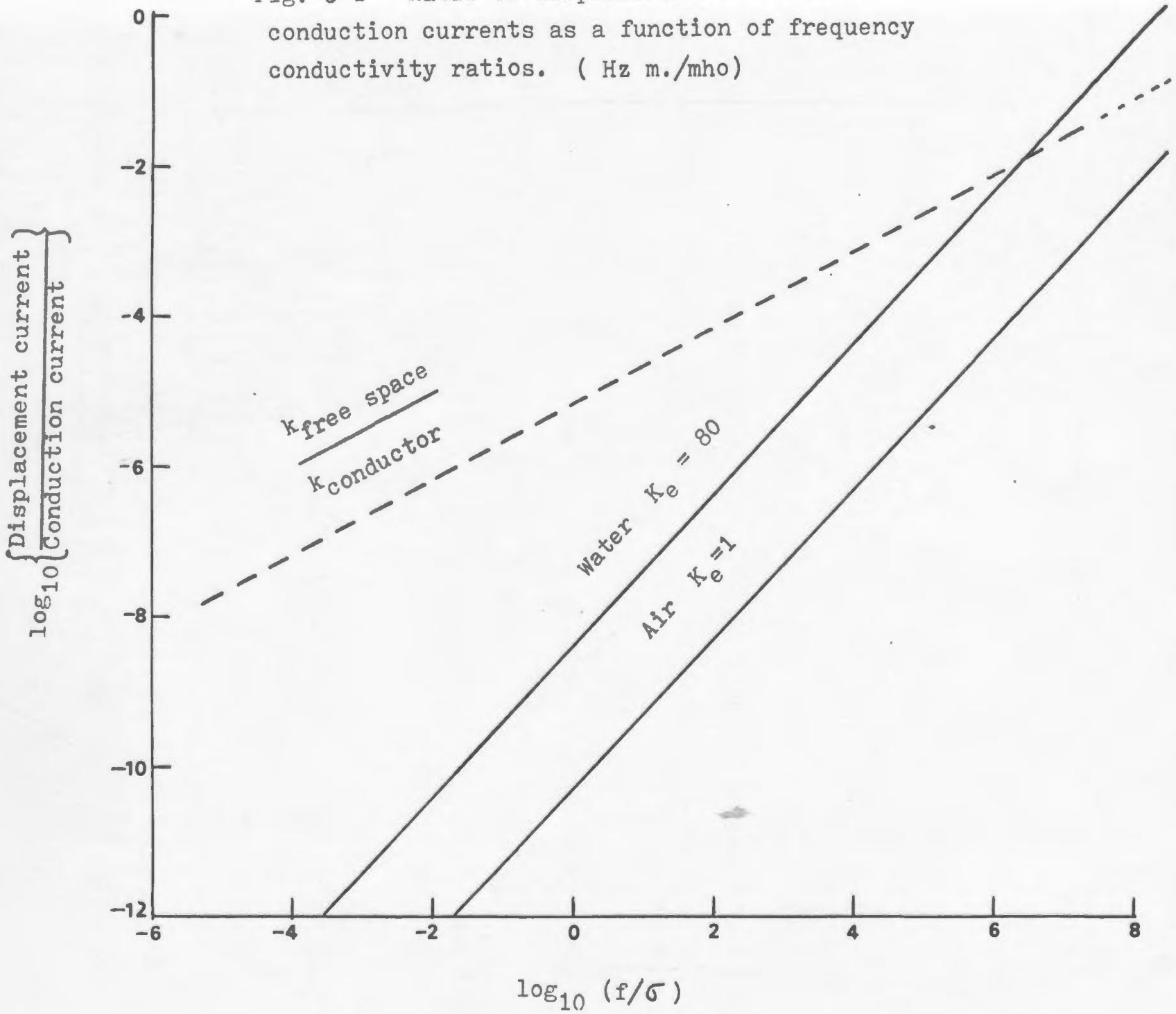

geneity in the earth. This is the boundary condition used by d'Erceville and Kunetz (1962) in the analysis of TM polarization incident on 2 dimensional magnetotelluric structures and adopted by subsequent authors (i.e. Swift (1967), Wright (1970)) in their analysis of the response of 2 dimensional structures to TM waves.

C-5 Integral

In the range where the quasistatic approximations hold,

$$L_1 = \frac{1}{2\pi}\int_{-\infty}^{\infty}\left(1 - \frac{2\lambda^2}{k_0^2} + \frac{2\gamma_0|\lambda|}{k_0^2}\right)\frac{e^{\gamma_0(x_3+x_3') + j\lambda(x_1-x_1')}}{2\gamma_0}\,d\lambda \qquad \text{C-30}$$

can be evaluated analytically when (x_3+x_3') is zero. For all other values of (x_3+x_3'), part of L_1 must be evaluated numerically.

(a) $X_3 + X_3' = 0$

For (x_3+x_3') identically zero, the integral is evaluated in three parts. The first term yields

$$\frac{1}{2\pi}\int_{-\infty}^{\infty}\frac{e^{j\lambda(x_1-x_1')}}{2\gamma_0}\,d\lambda = \frac{j}{4}H_0^1(k_0|x_1-x_1'|) \qquad \text{C-31}$$

The second term is

$$-\frac{1}{2\pi}\int_{-\infty}^{\infty}\frac{e^{j\lambda(x_1-x_1')}}{2\gamma_0}\frac{\lambda^2}{k_0^2}\,d\lambda = \frac{j}{2k_0^2}\frac{\partial^2}{\partial x_1^2}H_0^1(k_0|x_1-x_1'|) \qquad \text{C-32}$$

This term is just the second derivative w.r.t. x_1 of the first term aside from a constant factor.

The last term of L_1 is the one which causes all the difficulty in evaluating L_1. It has the form

$$\frac{1}{2\pi}\int_{-\infty}^{\infty}\frac{|\lambda|}{k_0^2}e^{j\lambda(x_1-x_1')}\,d\lambda \qquad \text{C-33}$$

for $(x_3+x_3')=0$. From Duff and Naylor (1966), the Fourier transform of $|\lambda|$ is

$$\int_{-\infty}^{\infty} |\lambda| e^{j\lambda q} d\lambda = -\frac{2}{q^2} \qquad \text{C-34}$$

and C-40 becomes

$$-\frac{1}{\pi k_0^2} \frac{1}{(x_1 - x_1')^2} \qquad \text{C-35}$$

Thus for $(x_3+x_3') \equiv 0$, L_1 is

$$L_1 = -\frac{j}{4} H_0^1(k_0|x_1-x_1'|) + \frac{j}{2} \frac{H_1^1(k_0|x_1-x_1'|)}{k_0|x_1-x_1'|} - \frac{1}{\pi k_0^2 (x_1-x_1')^2} \qquad \text{C-36}$$

The electric field about a line source of I amps on the surface of a conducting half-space is given by

$$E = j\omega\mu_0 I (L_0 + L_1)_{x_3+x_3' \equiv 0} \qquad \text{C-37}$$

At the surface $x_3+x_3 \equiv 0$,

$$E = j\omega\mu_0 I \left[\frac{j}{2} \frac{H_0^1(k_0|x_1-x_1'|)}{k_0|x_1-x_1'|} - \frac{1}{\pi k_0^2 (x_1-x_1')^2} \right] \qquad \text{C-38}$$

This expression agrees with that given by Wait (1962) when the propagation constant of the air approaches zero.

(b) $X_3 + X_3' \neq 0$

When (x_3+x_3') is not zero, it is more convenient to work with C-30 in a modified form. The reflection coefficient is regrouped to

$$-1 - \frac{2\gamma_0}{k_0^2}(\gamma_0 - |\lambda|) \qquad \text{C-39}$$

and C-30 becomes

$$L_1 = \frac{1}{2\pi} \int_{-\infty}^{\infty} \left\{ -\frac{1}{2\gamma_0} + \frac{1}{k_0^2}(|\lambda| - \gamma_0) \right\} e^{\gamma_0(x_3+x_3') + j\lambda(x_1-x_1')} d\lambda \qquad \text{C-40}$$

The first term is just

$$-\frac{1}{2\pi} \int_{-\infty}^{\infty} \frac{1}{2\gamma_0} e^{\gamma_0(x_3+x_3') + j\lambda(x_1-x_1')} d\lambda = -\frac{j}{4} H_0^1(k\rho_1) \qquad \text{C-41}$$

where $\rho_1^2 = (x_1-x_1')^2 + (x_3+x_3')^2$. This is an image of the original line source reflected at the boundary. The second term in C-40 is denoted

$$\mathcal{U}(x_1-x_1',\ x_3+x_3') = \frac{1}{2\pi k_0^2}\int_{-\infty}^{\infty}(|\lambda|-\gamma_0)\,e^{\gamma_0(x_3+x_3')+j\lambda(x_1-x_1')}\,d\lambda \qquad \text{C-42}$$

This integral is evaluated numerically.

In addition, the derivatives of L_1 w.r.t. x_1 and x_3 are required in the thesis. Thus, a total of three integrals must be numerically evaluated; namely

$$\mathcal{U} \quad ; \quad \mathcal{U}_1 = \frac{\partial \mathcal{U}}{\partial x_1} \quad ; \quad \mathcal{U}_3 = \frac{\partial \mathcal{U}}{\partial x_3} \qquad \text{C-43}$$

The evaluation of $\mathcal{U}$, $\mathcal{U}_1$ and $\mathcal{U}_3$ was carried out in a similar manner to that used by Frischknecht (1967). First the integrals were transformed to Fourier sine and cosine integrals

$$\mathcal{U} = \frac{1}{\pi k_0^2}\int_0^{\infty}(\lambda-\gamma_0)\,e^{\gamma_0(x_3+x_3')}\cos(\lambda(x_1-x_1'))\,d\lambda \qquad \text{C-44}$$

$$\mathcal{U}_1 = -\frac{1}{\pi k_0^2}\int_0^{\infty}\lambda(\lambda-\gamma_0)\,e^{\gamma_0(x_3+x_3')}\sin(\lambda(x_1-x_1'))\,d\lambda \qquad \text{C-45}$$

$$\mathcal{U}_3 = \frac{1}{\pi k_0^2}\int_0^{\infty}\gamma_0(\lambda-\gamma_0)\,e^{\gamma_0(x_3+x_3')}\cos(\lambda(x_1-x_1'))\,d\lambda \qquad \text{C-46}$$

A general program was developed for computing integrals of the form

$$V = \int_0^{\infty} f(\lambda)\,e^{\gamma_0(x_3+x_3')}\begin{matrix}\cos\\ \sin\end{matrix}\left\{\lambda(x_1-x_1')\right\}d\lambda \qquad \text{C-47}$$

The integration interval was divided into two sections such that

$$V = V_0 + \sum_{n=1}^{\infty} V_n \qquad \text{C-48}$$

where

$$V_0 = \int_0^{\lambda_c} f(\lambda)\,e^{\gamma_0(x_3+x_3')}\begin{matrix}\cos\\ \sin\end{matrix}\left\{\lambda(x_1-x_1')\right\}d\lambda \qquad \text{C-49}$$

$$V_n = \int_{\lambda_n}^{\lambda_{n+1}} f(\lambda)\,e^{\gamma_0(x_3+x_3')}\begin{matrix}\cos\\ \sin\end{matrix}\left\{\lambda(x_1-x_1')\right\}d\lambda$$

The integration limits are based on the relative values of x_3+x_3' and x_1-x_1'. When the x_3+x_3' is the dominant factor, λ_c was chosen as the value that makes

$$\left| e^{\gamma_0 (x_3 + x_3')} \right| = e^{-1} \qquad \text{C-50}$$

If this condition held for all values of λ, λ_c was set to zero. The λ_n were taken as

$$\lambda_n = \lambda_c + (n-1)\lambda_c \qquad \text{C-51}$$

For very small $(x_3 + x_3')$, the $(x_1 - x_1')$ controls the behaviour of the integrand. In this case

$$\lambda_c = \begin{cases} \dfrac{\pi}{2(x_1 - x_1')} & \text{cosine integrand} \\ \dfrac{\pi}{(x_1 - x_1')} & \text{sine integrand} \end{cases} \qquad \text{C-52}$$

The λ_n were taken as

$$\lambda_n = \lambda_c + \begin{cases} 2(n-1)\lambda_c & \text{cosine integrand} \\ (n-1)\lambda_c & \text{sine integrand} \end{cases} \qquad \text{C-53}$$

For $(x_3 + x_3')$ dominance, the series for V is rapidly convergent. For $(x_1 - x_1')$ dominance the series is slowly convergent with the signs of the terms alternating. In this case a self-adjusting Euler transform routine was used to force the series to converge. (Hildebrand (1956)). The series was truncated at n = 20 for all cases. The individual terms were evaluated using a Gaussian quadrature routine with an adjustable number of points such that any desired accuracy could be achieved. The functions were then tabulated and used as data in subsequent analysis.

C-6 Integral L_2

In the region where the quasistatic assumption holds

$$L_2 = \frac{1}{2\pi} \int_{-\infty}^{\infty} \left(1 - \frac{2\varepsilon_1}{\varepsilon_0} \frac{\gamma_0}{\gamma_1}\right) \frac{e^{\gamma_0 (x_3 + x_3') + j\lambda (x_1 - x_1')}}{2\gamma_0} \, d\lambda \qquad \text{C-54}$$

The first part of L_z is just

$$\frac{1}{2\pi}\int_{-\infty}^{\infty} \frac{e^{-\gamma_0(x_3+x_3') + j\lambda(x_1-x_1')}}{2\gamma_0}\, d\lambda = \frac{j}{4} H_0^1(k_0\rho) \qquad \text{C-55}$$

where $\rho_1 = \left((x_1-x_1')^2 + (x_3+x_3')^2\right)^{1/2}$

As mentioned in section C-4, the second term is negligible. The term was retained in order to demonstrate that it is small. The second term is

$$I = \frac{1}{\pi}\frac{\varepsilon_1}{\varepsilon_0}\int_{-\infty}^{\infty} \frac{e^{-\gamma_0(x_3+x_3') + j\lambda(x_1-x_1')}}{2\gamma_1}\, d\lambda \qquad \text{C-56}$$

By definition $Re(\gamma_0) \geq 0$ and

$$I \leq \frac{1}{\pi}\frac{\varepsilon_1}{\varepsilon_0}\int_{-\infty}^{\infty} \frac{e^{j\lambda(x_1-x_1')}}{2\gamma_1}\, d\lambda \qquad \text{C-57}$$

$$= \frac{j}{2}\frac{\varepsilon_1}{\varepsilon_0} H_0^1(k_1|x_1-x_1'|)$$

Since k_1 is very small, $k_1|x_1-x_1'| \ll 1$ in the quasistatic range. For small arguments

$$H_0^1(k_1|x_1-x_1'|) \simeq \ln(k_1|x_1-x_1'|) \qquad \text{C-58}$$

Finally

$$I \sim \frac{\sqrt{\varepsilon_1}}{\varepsilon_0}\left\{\sqrt{\varepsilon_1}\ln\sqrt{\varepsilon_1} + \sqrt{\varepsilon_1}\ln\omega\sqrt{\mu_0} + \sqrt{\varepsilon_1}\ln|x_1-x_1'|\right. \qquad \text{C-59}$$

and in the quasistatic limit of $\varepsilon_1 \to 0$, $I \to 0$

The appropriate form for L_z is

$$L_z = \frac{j}{4} H_0^1(k_0\rho_1) \qquad \text{C-60}$$

C-7 Integral L_4

The integral L_4 becomes

$$L_4 = \frac{1}{4\pi^2}\iint_{-\infty}^{\infty}\left(1 - \frac{2\lambda^2}{k_0^2} + \frac{2\gamma_0\gamma_1}{k_0^2}\right)\frac{e^{-\gamma_0(x_3+x_3') + j(\lambda_1(x_1-x_1')+\lambda_2(x_2-x_2'))}}{2\gamma_0}\, d\lambda_1 d\lambda_2 \qquad \text{C-61}$$

using the quasistatic approximation for R_{01}, L_4 is written as a Hankel transform using the type of analysis of section C-3.

$$L_4 = \frac{1}{4\pi}\int_0^\infty \left(1 - \frac{2\lambda^2}{k_0^2} + \frac{2\gamma_0\gamma_1}{k_0^2}\right)\frac{e^{\gamma_0(x_3+x_3')}}{2\gamma_0}\,\lambda J_0(\lambda\rho)\,d\lambda \qquad \text{C-62}$$

where $\rho^2 = (x_1-x_1')^2 + (x_2-x_2')^2$. L_4 is composed of three parts which are evaluated separately. The first term is

$$\frac{1}{4\pi}\int_0^\infty \frac{e^{\gamma_0(x_3+x_3')}}{\gamma_0}\,\lambda J_0(\lambda\rho)\,d\lambda = \frac{e^{jk_0R_1}}{4\pi R_1} \qquad \text{C-63}$$

where $R_1 = (\rho^2 + (x_3+x_3')^2)^{1/2}$.

From Bessel's equation

$$\lambda^2 J_0(\lambda\rho) = -\left(\frac{\partial^2}{\partial\rho^2} + \frac{1}{\rho}\frac{\partial}{\partial\rho}\right)J_0(\lambda\rho) \qquad \text{C-64}$$

The second term of L_4 is given by

$$\frac{2}{k_0^2}\left(\frac{\partial^2}{\partial\rho^2} + \frac{1}{\rho}\frac{\partial}{\partial\rho}\right)\frac{e^{jk_0R_1}}{4\pi R_1} \qquad \text{C-65}$$

The last term of L_4 may be written as

$$-\frac{1}{4\pi}\frac{2}{k_0^2}\left(\frac{\partial^2}{\partial\rho^2} + \frac{1}{\rho}\frac{\partial}{\partial\rho}\right)\frac{\partial\eta}{\partial x_3} \qquad \text{C-66}$$

where

$$\eta = \int_0^\infty \frac{e^{\gamma_0(x_3+x_3')}}{\gamma_0}\,J_0(\lambda\rho)\,d\lambda \qquad \text{C-67}$$

since $\gamma_1 \sim |\lambda|$ in the quasistatic range.

η is known as the Foster integral (Foster (1931)) and has the solution

$$\eta = \frac{j\pi}{2}\,J_0\left(\frac{k_0}{2}\left(R_1 + (x_3+x_3')\right)\right)H_0^1\left(\frac{k_0}{2}\left(R_1 - (x_3+x_3')\right)\right) \qquad \text{C-68}$$

where $(x_3+x_3') \leq 0$

Combining the three terms

$$L_4 = \frac{e^{jk_0R_1}}{4\pi R_1}\left[1 + \frac{2}{k_0^2}\left(\frac{\rho^2}{R_1^2}\left(\frac{3}{R_1^2} - \frac{3jk_0}{R_1} - k_0^2\right) + 2\left(jk_0 - \frac{1}{R_1}\right)\frac{1}{R_1}\right)\right]$$

$$+ \frac{j}{4k_0^2}\left[J_0(k_0P_+)\,H_0^1(k_0P_-)\left(\frac{k_0^2(x_3+x_3')}{2R_1^2}\left(2 - \frac{\rho^2}{R_1^2}\right)\right)\right.$$

$$+ J_1(k_0P_+)\,H_0^1(k_0P_-)\,\frac{k_0}{R_1^2}\left(\frac{1}{2} - \frac{P_+}{R_1} - \frac{1}{2}\left(2 - \frac{\rho^2}{R_1^2}\right) + \frac{\rho^2}{2R_1P_+} - \frac{k_0^2\rho^2P_+}{R_1}\right) \qquad \text{C-69}$$

$$- J_0(k_0P_+)\,H_1^1(k_0P_-)\,\frac{k_0}{R_1^2}\left(\frac{1}{2} - \frac{P_-}{R_1} - \frac{1}{2}\left(2 - \frac{\rho^2}{R_1^2}\right) + \frac{\rho^2}{2R_1P_-} - \frac{k_0^2\rho^2P_-}{R_1}\right)$$

$$\left. + J_1(k_0P_+)\,H_1^1(k_0P_-)\,\frac{k_0^2(x_3+x_3')\rho^2}{2R_1^4}\right]$$

where

$$P_+ = R_1 + (x_1+x_1') \qquad \text{C-70}$$

$$P_- = R_1 - (x_1+x_1')$$

C-8 Integral L_5

The integral L_5 is modified to a Hankel transform using the same steps as used for L_3.

$$L_5 = \frac{1}{4\pi}\int_0^\infty \left(1 - \frac{\varepsilon_1}{\varepsilon_0}\frac{\gamma_0}{\gamma_1}\right)\frac{e^{\gamma_0(x_3+x_3')}}{2\gamma_0}\,\lambda J_0(\lambda\rho)\,d\lambda \qquad \text{C-71}$$

As mentioned in section C-4, the second term is negligible in the quasistatic approximation. L_5 is then given by

$$L_5 = \frac{e^{jk_0R_1}}{4\pi R_1} \qquad \text{C-72}$$

where $R_1 = (\rho^2 + (x_3+x_3')^2)^{1/2}$. The second term is readily shown to be $< \frac{\varepsilon_1}{\varepsilon_0}\,\frac{1}{\rho}$ and is negligible in comparison to C-72.

C-9 Integral L_6

The Hankel transform of L_6 is

$$L_6 = \frac{1}{4\pi}\int_0^\infty \frac{R_{01} - \gamma_{01}}{\lambda^2}\,\frac{e^{\gamma_0(x_3+x_3')}}{\gamma_0}\,\lambda J_0(\lambda\rho)\,d\lambda \qquad \text{C-73}$$

The reflection coefficient combination becomes

$$\frac{R_{01} - \gamma_{01}}{\lambda^2} = -\frac{2}{k_0^2} + \frac{2\gamma_0}{k_0^2\lambda} \qquad \text{C-74}$$

in the quasistatic approximation range. L_G is then

$$L_G = \frac{1}{4\pi}\int_0^\infty \left(-\frac{z}{k_0^2} + \frac{z\gamma_0}{\lambda k_0^2}\right)\frac{e^{\gamma_0(x_3+x_3')}}{\gamma_0}\,\lambda J_0(\lambda\rho)\,d\lambda \qquad \text{C-75}$$

The first term is given by

$$-\frac{1}{4\pi}\frac{z}{k_0^2}\int_0^\infty \frac{e^{\gamma_0(x_3+x_3')}}{\gamma_0}\,\lambda J_0(\lambda\rho)\,d\lambda = -\frac{z}{k_0^2}\frac{e^{jk_0R_1}}{4\pi R_1}$$

where $R_1 = (\rho^2 + (x_3+x_3')^2)^{1/2}$. The second term is given in terms of the Foster integral discussed in section C-7 and is

$$\frac{1}{2\pi k_0^2}\frac{\partial \mathcal{H}}{\partial x_3} \qquad \text{C-76}$$

The solution for L_G is

$$L_G = -\frac{z}{k_0^2}\frac{e^{jk_0R_1}}{4\pi R_1} - \frac{j}{4k_0^2}\left[\frac{k_0P_+}{R_1}J_1(k_0P_+)H_0^1(k_0P_-) - \frac{k_0P_-}{R_1}J_0(k_0P_-)H_1^1(k_0P_+)\right] \qquad \text{C-77}$$

where $P_\pm$ are given by C-70.

APPENDIX D

NUMERICAL EVALUATION OF SINGULAR INTEGRALS

In the numerical analysis of the scattering problems in the body of the thesis, it was necessary to evaluate numerically integrals with singular integrands. The most singular integrals to be evaluated had the general form

$$I(x_1, x_2) = \iint_A \varphi(x_1', x_2')\, g(x_1, x_1', x_2, x_2')\, dx_1' dx_2' \qquad \text{D-1}$$

where

$$g(x_1, x_1', x_2, x_2') = 1/\rho \qquad \text{D-2}$$

or

$$g(x_1, x_1', x_2, x_2') = H_0^1(\lambda\rho) \qquad \text{D-3}$$

$$\rho = \left((x_1 - x_1')^2 + (x_2 - x_2')^2\right)^{1/2}$$

where $\varphi(x_1', x_2')$ is analytic in A and $(x_1, x_2) \in A$. For the Hankel function form of g, the behaviour of the integrand is that of a logarithmic singularity near $(x_1', x_2') = (x_1, x_2)$. Since this is less singular than $1/\rho$, evaluation of the $1/\rho$ integrand automatically assures evaluation of the integral with the logarithmically singular kernel.

The point of this Appendix is to illustrate that these integrals can be evaluated numerically by integrating directly over the singular point by subdividing the integration region around the singularity. Near the singular point $(x_1', x_2') = (x_1, x_2)$, A was subdivided into four rectangular regions A_i, i = 1, 4 plus the remaining region A_5. This is illustrated in Fig. D-1 (a). D-1 then becomes

$$I = \sum_{i=1}^{5} \iint_{A_i} \varphi(x_1', x_2')\, g(x_1, x_1', x_2, x_2')\, dx_1' dx_2' = \sum_{i=1}^{5} I_i \qquad \text{D-4}$$

The numerical integration was carried out using a Gaussian quadrature algorithm. The extrapolatory nature of the Gaussian quadrature was used

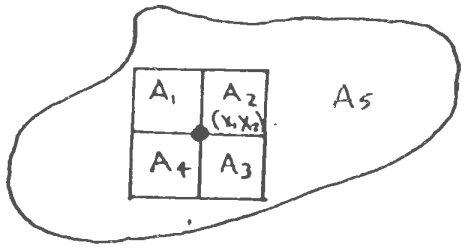

Fig. D-1(a) Sketch of subdivision of area A about singular point (x_1, x_2)

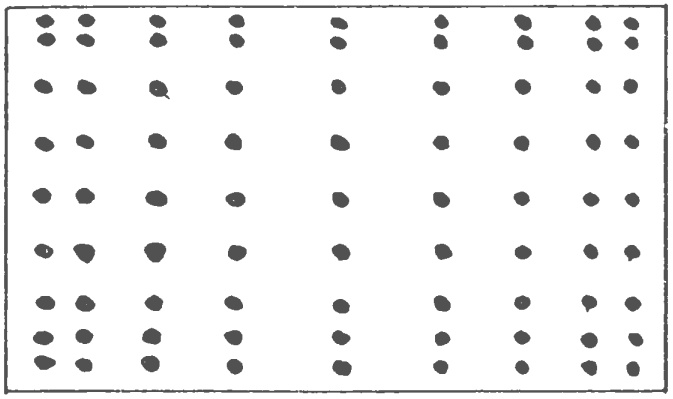

Fig. D-1(b) Two dimensional Gaussian quadrature mesh on rectangle.

to evaluate the integrals A_i, $i = 1,4$ as accurately as desired by increasing the degree of the quadrature.

Each integral in the singular region is given by a weighted sum of the form

$$I_i(x_1,x_3) \simeq \sum_r \sum_s W_r^p W_s^q \varphi(x_{1,r}^p, x_{2,s}^q) g(x_1, x_{1,r}^p, x_2, x_{2,s}^q) \qquad D\text{-}5$$

where W_i^N and X_i^N are the weights and nodes for Gaussian quadrature of degree N as given by Abramowitz and Stegun (1965) or Davis and Rabinowitz (1967). A sketch of the distribution of points in a rectangular region is shown in Fig. D-1(b). Since no node point lies at the singular point, (i.e. at a corner) the numerical integral tends to underestimate the true value of the integral. In order to test the accuracy and reliability of this quadrature technique, simple integrals which could be evaluated analytically were computed numerically using this scheme. One of these integrals is given here to demonstrate the results.

The trial integral was

$$I(0,0) = \int_0^\epsilon \int_0^\epsilon \frac{1}{(x_1'^2 + x_2'^2)^{1/2}} dx_1' dx_2' = 1.7627\epsilon \qquad D\text{-}6$$

which is just the original integral over A_i with φ = constant where A_i is a square with sides of length ϵ. The numerical values obtained for this integral with $\epsilon = 1$ for N varying from 2 to 20 are listed in Table D-1. They agree very closely with the theoretical value of D-6. For N = 2 the error (surprisingly) is only an underestimation of about 7%. As N increases, the error drops below 1% when $N > 6$. For the higher order quadratures, where $N \simeq 20$, the error drops below 1:1000.

This integration technique was always used to integrate directly over the singular points in the integrand. In all cases where the integral could not be checked analytically, convergence of the integrals similar to that observed in Table D-1 was found. The same agreement was found for integrals with the logarithmic singularity.

Table D-1 Tabulation of Numerical Quadrature Test Results

QUADRATURE NUMBER	INTEGRAL
2	1.673E 00
3	1.722E 00
4	1.739E 00
5	1.747E 00
6	1.752E 00
7	1.755E 00
8	1.757E 00
9	1.758E 00
10	1.759E 00
11	1.759E 00
12	1.760E 00
13	1.760E 00
14	1.760E 00
15	1.761E 00
16	1.761E 00
17	1.761E 00
18	1.761E 00
19	1.762E 00
20	1.762E 00

APPENDIX E

INDUCTIVE RESPONSE OF A CIRCULAR LOOP

The electromagnetic response of a small loop in a slowly time varying field is derived quite easily. If the loop has an internal resistance, R, and self-inductance L, then the current flow as a function of time in the loop satisfies the differential equation

$$R\, i(t) + L \frac{d\, i(t)}{d t} = V \qquad \text{E-1}$$

where

$$V = \oint \bar{E} \cdot d\bar{l} = -\frac{\partial}{\partial t} \iint \bar{B} \cdot d\bar{A} = \frac{d\varphi}{dt} \qquad \text{E-2}$$

Next, the Fourier transform pair

$$F(\omega) = \int_{-\infty}^{\infty} f(t)\, e^{j\omega t}\, dt \qquad \text{E-3}$$

$$f(t) = \frac{1}{2\pi} \int_{-\infty}^{\infty} F(\omega)\, e^{-j\omega t}\, d\omega \qquad \text{E-4}$$

are used to transform equation E-1 to the frequency domain. The transformation yields

$$(R - j\omega L)\, I(\omega) = -j\omega\, \Phi(\omega) \qquad \text{E-5}$$

or

$$I(\omega) = \frac{-j\omega}{R - j\omega L}\, \Phi(\omega)$$

The transfer function for the loop is simply

$$F(\omega) = \frac{-j\omega}{R - j\omega L} = -\frac{j\omega}{R} \frac{1}{(1 - j\omega/\omega_0)} \qquad \omega_0 = \frac{R}{L} \qquad \text{E-6}$$

The transfer function as a function of frequency is sketched in Fig. E-1 (a).

The impulse response function is given by

$$f(t) = \frac{1}{2\pi} \int_{-\infty}^{\infty} -\frac{j\omega}{R} \frac{e^{-j\omega t}}{\left(1 - j\frac{\omega}{\omega_0}\right)}\, d\omega \qquad \text{E-7}$$

This integral can be evaluated readily by contour integration using the contours sketched below for $t < 0$ and $t > 0$. The result is simply

$$f(t) \equiv 0 \qquad t < 0$$

$$\left.\begin{aligned} &= -2\pi j \sum \text{Residues} \\ &= -\frac{1}{L}\,\frac{e^{-t/\tau}}{\tau} \end{aligned}\right\} \quad t \geq 0 \qquad \tau = \frac{1}{\omega_0} = \frac{L}{R} \tag{E-8}$$

The impulse response of the loop is a simple exponential decay with decay constant $\tau = L/R$. The impulse response is sketched in Fig. E-1 (b). These results are presented in order to facilitate demonstration of some of the results derived in chapter 7.

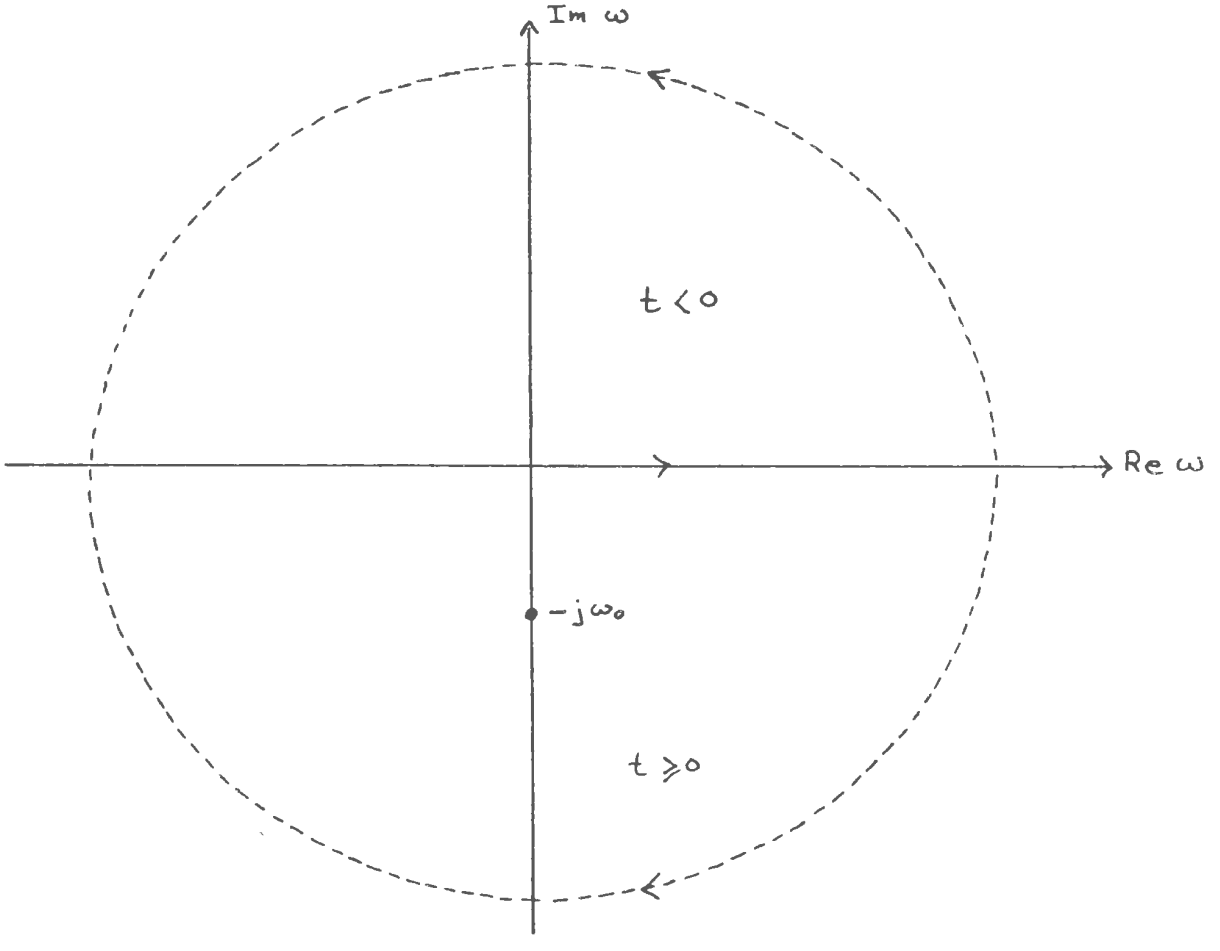

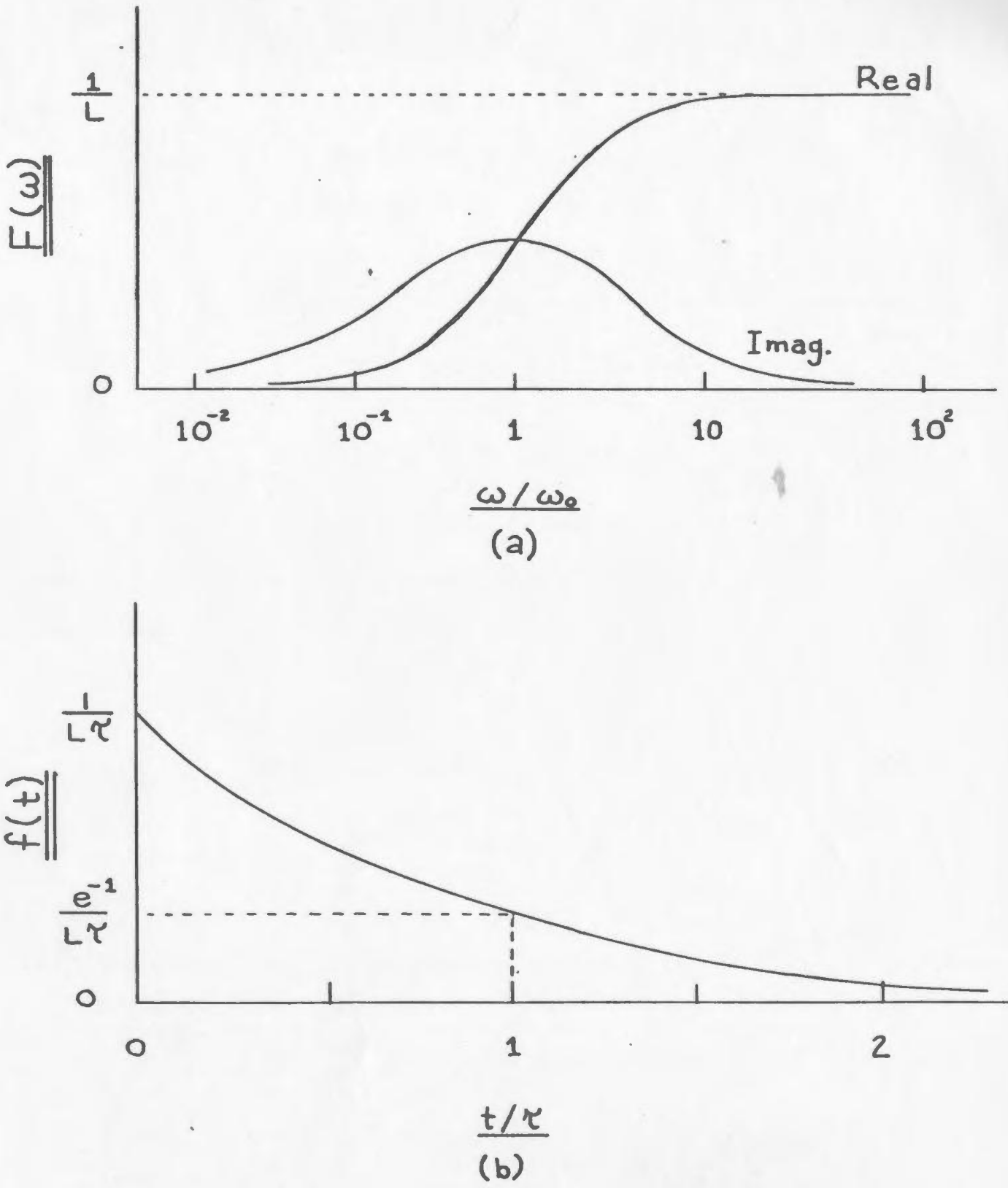

Fig. E-1 Sketch of circular loop inductive response transfer function and impulse response.

APPENDIX F

GREEN'S FUNCTIONS FOR STATIC EM PROBLEMS

F-1 Background

This appendix gives a brief summary and derivation of the Green's functions used in many geophysical problems when the electromagnetic fields are static in time. The Green's functions of interest in the thesis are those for the vector and scalar Poisson equation in an infinite region and for the scalar Poisson equation in a semi-infinite region with homogeneous Neumann boundary conditions at the surface.

F-2 Scalar Poisson Equation: Infinite Medium

The basic equation for all static electromagnetic problems in an infinite region is the scalar Poisson equation

$$\nabla^2 \Phi = -q \qquad \text{F-1}$$

The Green's function in three dimensions satisfies

$$\nabla_3^2 g(r,r') = -\delta_3(|\bar{r}-\bar{r}'|) \qquad \text{F-2}$$

where

$$\bar{r} = \sum x_i \hat{e}_i \qquad \text{F-3}$$

and $(\hat{e}_1, \hat{e}_2, \hat{e}_3)$ and (x_1, x_2, x_3) are the unit vectors and the coordinates of a cartesian coordinate system. In three dimensions $\delta_3(|\bar{r}-\bar{r}'|)$ is given by

$$\delta_3(|\bar{r}-\bar{r}'|) = \frac{\delta^+(|\bar{r}-\bar{r}'|)}{4\pi|\bar{r}-\bar{r}'|^2} \qquad \text{F-4}$$

For simplicity, $\bar{r}'$ is set to be the origin. Then

$$\frac{1}{r^2}\frac{\partial}{\partial r} r^2 \frac{\partial}{\partial r} g_3(r,0) = -\frac{\delta^+(r)}{4\pi r^2} \qquad \text{F-5}$$

Integrating twice w.r.t. r yields

$$g(r,r') = \frac{1}{4\pi|\bar{r}-\bar{r}'|} \qquad \text{F-6}$$

the familiar Green's function for the Poisson equation.

In some geophysical problems, it is convenient to think of the source being extended infinitely far into one direction with no spatial variation in its properties in this dimension. The source is then a line source. In this case, equation F-1 becomes independent of one coordinate. In the following analysis, the source is assumed infinitely long in the $\hat{e}_2$ direction and independent of x_2. F-2 becomes

$$\nabla^2 g_2(\bar{\rho},\bar{\rho}') = -\delta_2(|\bar{\rho}-\bar{\rho}'|) \qquad \text{F-7}$$

where

$$\bar{\rho} = x_1\hat{e}_1 + x_3\hat{e}_3$$

Incorporating the two dimensional delta function definition, F-7 becomes

$$\frac{1}{\rho}\frac{\partial}{\partial\rho}\,\rho\,\frac{\partial}{\partial\rho}\,g_2(\bar{\rho},\bar{\rho}') = -\frac{\delta^+(|\bar{\rho}-\bar{\rho}'|)}{2\pi\,|\bar{\rho}-\bar{\rho}'|} \qquad \text{F-8}$$

Integrating twice w.r.t. ρ yields

$$g_2(\bar{\rho},\bar{\rho}') = -\frac{1}{\pi}\ln|\bar{\rho}-\bar{\rho}'| \qquad \text{F-9}$$

F-3 Vector Poisson Equation: Infinite Region

The vector Poisson equation occurs in magnetostatic problems when the magnetic fields are generated by static current flow.

$$\nabla^2\bar{H} = -\nabla\times\bar{J}_s \qquad \text{F-10}$$

The corresponding Green's dyadic in three dimensions satisfies

$$\nabla_3^2\,\tilde{G}_3(\bar{r},\bar{r}') = -\delta_3(|\bar{r}-\bar{r}'|)\,\tilde{I} \qquad \text{F-11}$$

where $\tilde{I}$ is the unitary dyadic. F-11 can be solved by expressing $\tilde{G}_3$ in its cartesian components and solving for each component independently with the result

$$\tilde{G}_3(\bar{r},\bar{r}') = \frac{1}{4\pi|\bar{r}-\bar{r}'|}\,\tilde{I} \qquad \text{F-12}$$

Combining F-10 and F-12 yields the integral form of Ampere's law

$$\bar{H}(\bar{r}) = \frac{1}{4\pi} \int \frac{\bar{\nabla}' \times \bar{J}(r')}{R} \, d^3 r' \qquad \text{F-13}$$

F-4 Scalar Poisson Equation: Semi-Infinite Region

The solution of the scalar Poisson equation in a half-space with a homogeneous Neumann boundary condition on the surface is the basic equation for considering geophysical conduction problems. The half-space is used to simulate the Earth. The basic equations are

$$\nabla^2 \Phi = -q \qquad x_3 > 0 \qquad \text{F-14}$$

with

$$\frac{\partial \Phi}{\partial x_3} = 0 \qquad x_3 = 0 \qquad \text{F-15}$$

where Φ exists in the half-space $-\infty < x_1, x_2 < \infty$ and $x_3 \geq 0$. The Green's function satisfies

$$\nabla^2 g_3(r, r') = -\delta_3(|\bar{r} - \bar{r}'|) \qquad \text{F-16}$$

$$\frac{\partial}{\partial x_3} g_3(r, r') = 0 \qquad x_3 = 0 \qquad \text{F-17}$$

The solution is found by combining F-3 and F-4 with the method of images to yield

$$g_3(r r') = \frac{1}{4\pi R} + \frac{1}{4\pi R_1} \qquad \text{F-18}$$

where

$$R = |\bar{r} - \bar{r}'|$$
$$R_1 = \left((x_1 - x_1')^2 + (x_2 - x_2')^2 + (x_3 + x_3')^2\right)^{1/2} \qquad \text{F-19}$$

A similar analysis for two dimensional source fields yields

$$g_2(\rho,\rho') = -\frac{1}{\pi}\ln P - \frac{1}{\pi}\ln P_1 \qquad \text{F-20}$$

$$P = \left((x_1-x_1')^2 + (x_3-x_3')^2\right)^{1/2} \qquad \text{F-21}$$

$$P_1 = \left((x_1-x_1')^2 + (x_3+x_3')^2\right)^{1/2}$$

F-5 Summary

This short discussion of the Green's functions summarizes the more important static Green's functions required in most static electric and magnetic problems in geophysical analysis. The derivations of these results can be found in any standard text on electromagnetic theory or applied mathematics. More complex problems such as static conduction in an N-layered medium can be solved in a similar manner to the time-varying case of Appendix A.

BIBLIOGRAPHY

Annan, A.P., 1970, Radio Interferometry Depth Sounding, M.Sc. Thesis University of Toronto.

Annan, A.P., 1973, Radio Interferometry Depth Sounding: Part I - Theoretical Discussion, Geophysics, 38, 557-580.

Abramowitz, M. and I.A. Stegun, 1965, Handbook of Mathematical Functions, Dover Publications.

Banos, A., 1962, Dipole Radiation in the Presence of a Conducting Half-Space, Pergamon Press.

Brekhovskikh, L.M., 1960, Waves in Layered Media, New York, Academic Press.

Coggon, J.H., 1971, Electromagnetic and electrical modeling by the finite element method: Geophysics, 36, No. 1, 132-155.

Davis, P.J. and P. Rabinowitz, 1967, Numerical Integration, Blaisdell.

D'Erceville, I., and G. Kunetz, 1962, The effect of a fault on the earth's natural electromagnetic field: Geophysics 27, No. 5, 651-668.

Dieter, K., N.R. Paterson and F.S. Grant, 1969, IP and resistivity type curves for three-dimensional bodies: Geophysics, 34, No. 4, 615-632.

Duff, G.F.D. and D. Naylor, 1966, Differential Equations of Applied Mathematics, John Wiley and Sons.

Farstad, A.J., 1970, Surface Impedance Measurements for Geophysical Prospecting, M.Sc. Thesis, University of Colorado.

Foster, R.M., 1931, Mutual Impedence of grounded wires lying on the surface of the Earth; Bell System Technical Journal, X, 408-419.

Frischknecht, F.C., 1967, Fields about an oscillating magnetic dipole over a two-layer earth: Colo. School of Mines Quart., V. 62, No. 1

Garbacz, R.J. and R.H. Turpin, 1971, A generalized expansion for radiated and scattered fields: Trans. IEEE, AP-19, No. 3, 348-358.

Grant, F.S. and G.F. West, 1965, Interpretation Theory in Applied Geophysics, McGraw-Hill

Green, C.D., 1969, Integral Equation Methods, Nelson.

Greenfield, R.J., 1971, The electromagnetic response of a conducting disk for use in AFMAG interpretation. Geophysics, 36, 723.

Greenstadt, J., 1960, The determination of the characteristic roots of a matrix by the Jacobi method: in Mathematical Methods for Digital Computers, edited by A. Ralston and H.S. Wilf, vol. I and II, 1960, 1967, Wiley, New York.

Harrington, R.F. and J.R. Mautz, 1971, Theory of characteristic modes for conducting bodies: Trans. IEEE, AP-19, No. 5,622-628.

Harrington, R.F. and J.R. Mautz, 1971, Computation of characteristic modes for conducting bodies: Trans. IEEE, AP-19, No. 5,629-639.

Hayes, J.G., 1970, Numerical Approximation to Functions and Data, Athlone Press.

Hildebrand, F.B., 1956, Introduction to Numerical Analysis, McGraw-Hill

Hohmann, G.W., 1971, Electromagnetic scattering by conductors in the earth near a line source of current: Geophysics, 36, No. 1, 101-131.

Hohmann, G.W., 1969, Electromagnetic Scattering by Two-dimensional Inhomogeneities in the Earth, Ph.D. Thesis, University of California, Berkley.

Isaacson, E. and H.B. Keller, 1966, Analysis of Numerical Methods, John Wiley and Sons.

Jackson, J.D., 1962, Classical Electrodynamics, John Wiley and Sons.

Jones, F.W. and A.T. Price, 1969, The Perturbations of Alternating Geomagnetic Fields by Conductivity Anomalies: Geophys. J.R. Astr. Soc. 20, 317-334.

Keller, G.V., 1971, Natural - field and controlled - source methods in electromagnetic exploration: Geoexploration, 9, 99-147.

Kim, J.R., 1971, Computer-aided analysis of a finite arbitrarily shaped dielectric antenna: Trans. IEEE, AP-19, No. 3, 444.

Kline, M. and I.W. Kay, 1965, Electromagnetic Theory and Geometrical Optics, Interscience Publishers.

Kopal, Z., 1961, Numerical Analysis, Chapman and Hall.

Lamontagne, Y., 1970, Model Studies of the Electromagnetic Method: University of Toronto, M.A. Sc. Thesis.

Lamontagne, Y. and G.F. West, 1971, EM response of a rectangular thin plate: Geophysics, 36, No. 6, 1204-1222.

Landau, L.D. and E.M. Lifshitz, 1960, Electrodynamics of Continuous Media, Pergamon Press.

Mikhlin, S.G., 1964, Variational Methods in Mathematical Physics, A Pergamon Press Book, MacMillan Co.

Morse, P.M. and H. Feshbach, 1953, Methods of Theoretical Physics, Pts. I and II, McGraw-Hill.

Nehari, Z., 1961, Introduction to Complex Analysis, Allyn and Bacon, Inc., Boston.

Ott, H., 1941, Reflexion and Brechung von Kugelwellen: Effekte Q. Ordnung: Ann. Physik, v. 41, 443-466.

Parry, J.R. and S.H. Ward, 1971, Electromagnetic scattering from cylinders of arbitrary cross-section in a conductive half-space: Geophysics, 36, No. 1, 67-100.

Reitz, J.R. and F.J. Milford, 1960, Foundations of Electromagnetic Theory, Addison-Wesley.

Sommerfeld, A., 1949, Partial Differential Equations in Physics: New York, Academic Press.

Swift, C.M. 1967, A Magnetotelluric Investigation of an Electrical Conductivity Anomaly in the Southwestern United States, MIT Ph.D. Thesis.

Swift, C.M., 1971, Theoretical magnetotelluric and TURAM response from two-dimensional inhomogeneities: Geophysics, 36, No. 1, 38-52.

Wait, J.R., 1959, editor, Overvoltage Research and Geophysical Applications, Pergamon Press, New York.

Wait, J.R., 1962, Electromagnetic Waves in Stratified Media, Pergamon Press, (Revised edition, 1970).

Ward, S.H., 1967, Electromagnetic theory for geophysical applications: Mining Geophysics, 2, Society of Exploration Geophysicists.

Watson, G.M., 1952, A Treatise on the Theory of Bessel Functions: University Press, Cambridge.

Watts, R.D., 1972, Magnetotelluric Fields over Round Structures, University of Toronto, Ph.D. Thesis.

Weaver, J.T., 1963, The electromagnetic field within a discontinuous conductor with reference to geomagnetic micropulsations near a coastline: Canadian Journal of Physics, vol. 41, 484-495.

Wright, J.A., 1969, The magnetotelluric and geomagnetic response of two-dimensional structures: Geophysikalische Arbeiten sowie Mitteilungen aus Meteorologie und Astrophysik, GAMMA 7, 102 S, Institut fur Geophysik und Meteorologie der Technischen Universitat Braunschweig.